

**Investigating and Treating Severe Bladder
Malformations in the T30H Mouse Model**

Natalie Jane Milmoe

UCL

**A thesis submitted in fulfilment of the requirement for
the degree of Doctor of Philosophy**

I, Natalie Jane Milmo confirm that the work presented in this thesis is my own. Where information has been derived from other sources, I confirm that this has been indicated in the thesis.

Acknowledgements

I would like to thank Professor Paul Winyard for giving me the opportunity to carry out this research even though I spelled kidney and my own name wrong on my cover letter and CV. I am eternally grateful that you (hopefully) didn't notice, and for all the support, encouragement and advice you've given over the last 4 years. Thank you to Professor Rob Harvey for his early work on the project and to Dr Ahad Rahim for all the advice on the knock-down studies.

Thank you to everyone in the nephro lab throughout my time at ICH, Dr David Long for his invaluable advice and to Maria and Karen for knowing everything – literally nothing in the lab would get done without you. The ultrasound data which has been so invaluable for my project I couldn't have done without Dr Daniel Stuckey, to whom I am very grateful. Elisa, Sara, Jen, Nuria, Jennie, Laura, Alex (Todd), Alex (Lalayiannis), Kevin, Will, Gideon, Saif and Lauren – thank you for making the last four years so enjoyable and for all the help along the way. And of course, to thank you so much to my fave annoying medical student, who turned out to be not so annoying, is one of the best friends I could have, and I couldn't have done any of this without, thanks Daniyal.

Thank you to my mother for her support while living her best life in the south of France after the thankless task of bringing me up and yelling at me to do my homework for 14 years.

I also couldn't have done this without my friends and family. Thank you to Elliot, Javi and Steffi for all the chat, wine and picking up off the floor over the years. Family Pethybridge, Julia, Gordon and Ella, thank you for your endless enthusiasm, support and delicious food. Thanks Henry for suffering through all my most recent grammar mistakes. Thank you to Lea Rowing Club and all the amazing people who make up the rowing community for providing an essential source of procrastination.

And Ben, I would have given up a long time ago without your kindness, patience and humour. Thank you for getting me through my PhD, I really couldn't have done it without you.

Abstract

Obstructive uropathies account for 20% of paediatric end-stage renal failure. Renal damage often occurs before correction of obstruction is possible. There are few *in vivo* models to study obstruction. However, the symptoms of urinary obstructive flow are recapitulated in the T30H mouse model, providing a powerful tool for investigating disease.

The work presented in this thesis has three aims. The first aim was to characterise the model; T30H mice have a balanced, heritable translocation between chromosomes 2 and 11. They die soon after birth with large non-emptying bladders and hydronephrosis, despite absence of anatomical obstruction. Using ultrasound, phenotypic onset is at E16, whereupon the bladder becomes grossly distended due to lack of detrusor smooth muscle. The kidneys are adversely affected by obstruction, but all other organs are normal.

The second aim was to find the underlying genetic cause of the phenotype. I have discovered the translocation point causing the phenotype. It does not span recognised genes, but is upstream of Myocardin (*MYOCD*), a master regulator of smooth muscle. Changes to splice variant expression of *MYOCD* could cause the phenotype.

The third aim was manipulation of the phenotype using gene therapy. To investigate the role of *Myocd* in the mouse bladder, I isolated smooth muscle cells from wild-type bladders at E14, then transduced them with lentivirus containing *Myocd* shRNA. Knock-down reduces cell growth, consistent with the T30H phenotype. I have also established methodology which in future could be used to deliver antenatal gene therapy to T30H mice to rescue the phenotype.

I hypothesise that specific *Myocd* splice variants are essential for bladder smooth muscle development. In T30H mice their expression is disrupted, creating a disease phenotype. Understanding smooth muscle regulation will better our knowledge of urinary tract development and enable us to develop therapies for treating smooth muscle complications arising from obstructive uropathies.

Impact statement

Congenital anomalies of the kidney and urinary tract are one of the leading causes of end-stage renal failure in children. Bladder malformations in the form of lower urinary tract obstruction fall under this group of disorders. They are a phenotypically and genetically diverse group for which we have limited options for treatment. Treatment is often in the form of surgery which does not always restore function; patients can be left with problems with establishing continence and have persistent urinary tract infections throughout life. This creates a huge cost to both healthcare systems and emotionally for families affected.

New treatment options are desperately needed. One of the ways in which we can generate novel therapies is by using animal models. The T30H mouse model has a balanced translocation causing a bladder defect which was generated through chemical mutagenesis experiments many years ago. It has never previously been characterised genetically or phenotypically. This thesis establishes the mouse as a functional model for obstructive uropathy with onset of symptoms during gestation, mirroring human obstructive disorders. It also confirms both the location of the translocation and the gene affected – myocardin (*MYOCD*).

MYOCD is a master regulator of smooth muscle expression and is vitally important for proper bladder development. The translocation lies in a putative regulatory region for this gene. The disruption caused by the translocation alters the splice variants of *Myocd* which are expressed, therefore creating the smooth muscle phenotype in the T30H mouse. Humans have also been found with lower urinary tract obstructions with mutations to *MYOCD*. This establishes *MYOCD* as a potential target for gene therapies. Developing a methodology for high-frequency ultrasound guided injection of a viral vector to upregulate *Myocd* as a gene therapy for lower urinary tract obstructions has been explored in this thesis, and an innovation grant has been awarded to further develop this methodology, paving the way for future therapies.

The advanced capabilities of high-frequency ultrasound provide a powerful tool for investigating congenital defects. This methodology would likely provide useful insight

into other disease models during development and would also help to reduce the number of animals required to investigate developmental defects, providing a route for more ethical scientific investigation.

Collectively, this thesis presents a rationale for the prenatal therapy of a congenital disorder, using a previously unexploited animal model. This provides a platform for the reversal of diseases which otherwise have no cure.

Contents

List of Figures	11
Abbreviations.....	13
1 Introduction	17
1.1 Anatomy and Development of the Urinary Tract	17
1.1.1 Brief overview of kidney development.....	20
1.1.2 Anatomy and development of the bladder	22
1.1.3 Components of the Bladder.....	23
1.1.4 Myocardin	32
1.1.5 Human and Mouse Bladder Comparison.....	38
1.1.6 Summary	40
1.2 Developmental Disorders of the Lower Urinary Tract.....	41
1.2.1 Posterior Urethral Valves.....	41
1.2.2 Urethral Atresia.....	44
1.2.3 Prune Belly Syndrome.....	45
1.2.4 Gene Therapy.....	47
1.2.5 Summary	53
1.3 Models of Lower Urinary Tract Obstruction	54
1.3.1 Sheep models.....	54
1.3.2 Rodent obstruction models	57
1.3.3 Megabladder mouse	58
1.3.4 <i>In Vitro</i> Models.....	61
1.3.5 Summary	64
1.4 T30H mouse model	65
1.4.1 Chromosome FISH.....	70
1.4.2 Comparative Genomic Hybridisation Study.....	70
1.4.3 Summary	73
2 Hypothesis & Objectives	74
3 Materials	76
3.1 Mice	76
3.1.1 T30H Mice	76
3.1.2 Brachypody Mice	77
3.1.3 CD1 Mice	77
3.2 Immunohistochemistry.....	77
3.2.1 Histology	77

3.2.2	Western Blots.....	78
3.2.3	Antibodies	79
3.3	Microscopes	82
3.4	Ultrasound Scanning	82
3.5	Whole-Genome Sequencing	84
3.6	Polymerase Chain Reaction	84
3.7	Cell Culture.....	87
3.8	Biodistribution Study	87
4	Methods.....	88
4.1	Colony maintenance	88
4.2	Genetic Analysis.....	91
4.2.1	DNA Extraction.....	91
4.2.2	DNA and RNA Quantification	91
4.2.3	Whole-Genome Sequencing	91
4.2.4	PCR – Genotyping.....	92
4.2.5	Gel Electrophoresis	93
4.2.6	RNA Extraction	93
4.2.7	cDNA Generation	94
4.2.8	Reverse Transcription PCR.....	95
4.2.9	Quantitative PCR.....	96
4.3	Histological Analysis.....	98
4.3.1	Tissue Fixation.....	98
4.3.2	Tissue Embedding	98
4.3.3	Sectioning.....	99
4.3.4	PAS staining.....	99
4.3.5	Immunohistochemistry.....	99
4.4	Microscopy.....	102
4.4.1	Blinded Scoring of Gut Morphology.....	103
4.5	Ultrasound Scanning	103
4.6	Manipulation of Myocardin Expression	105
4.6.1	Cell culture – whole organ culture.....	105
4.6.2	Cell culture – dissociated cell culture	106
4.7	Western Blot	107
4.7.1	Protein Extraction	107
4.7.2	Protein Quantification.....	108

4.7.3	Western Blotting	109
4.8	Bladder Vector Biodistribution Study	110
4.9	Statistical Analysis	111
5	Results	113
5.1	Identifying the T30H Translocation Point	113
5.1.1	Whole-Genome Sequencing	113
5.1.2	Confirmation by PCR	117
5.1.3	Reverse transcriptase PCR for genes in close proximity	122
5.1.4	Reverse Transcriptase PCR for splice variants	124
5.1.5	Q-PCR for splice variants	129
5.1.6	Summary	131
5.2	Phenotyping the T30H Moue	132
5.2.1	PAS Staining	133
5.2.2	Alpha smooth muscle actin expression	135
5.2.3	Calponin Expression	143
5.2.4	Uroplakin 3a Expression	143
5.2.5	Myocardin Expression	151
5.2.6	Ultrasound Scanning	153
5.2.7	Summary	158
5.3	<i>In Vitro</i> Manipulation	159
5.3.1	Whole organ culture	159
5.3.2	Organoid Culture	165
5.3.3	Dissociated bladder culture	165
5.3.4	Avenues for <i>in vivo</i> gene therapy	170
5.3.5	Summary	176
6	Discussion	177
6.1	Characterising the T30H Mouse Genetics	177
6.1.1	Chromosomal translocations – mapping the breakpoint	177
6.1.2	Genetic context of the chromosome breakpoint	180
6.1.3	Mechanisms for differential splice expression	183
6.1.4	Correcting the malformation and finding the enhancer	185
6.2	Characterisation of the T30H mouse Phenotype	187
6.2.1	Why is the T30H mouse a valid model	191
6.3	<i>In Vitro</i> Manipulation	196
6.4	Future work	203

6.4.1	Rescue of the Phenotype	203
6.4.2	Development of a conditional knockout model	203
6.4.3	Discovering the Myocardin Enhancer	205
6.5	Thesis Summary	207
References	209
Appendix	247

List of Figures

Figure 1: Anatomy of the Urinary Tract.....	19
Figure 2: Kidney Developmental Stages.....	21
Figure 3: Bladder and Bladder Wall Anatomy.....	24
Figure 4: Bladder Developmental Stages and Associated Morphogen Gradients.....	30
Figure 5: Myocardin Signalling Pathway.....	33
Figure 6: Alternate Splice Variants of Myocardin.....	35
Figure 7: Signalling Pathway for Smooth Muscle Expression	37
Figure 8: Congenital Disorders of the Lower Urinary Tract.....	42
Figure 9: Examples of Animal Models of Lower Urinary Tract Obstruction.....	55
Figure 10: Karyotyping T30H Mouse Chromosomes.....	67
Figure 11: T30H Mouse P1 Urinary Tract.....	68
Figure 12: GDF5 Control Mouse Morphology.....	69
Figure 13: Chromosome FISH Strategy.....	71
Figure 14: Comparative Genomic Hybridisation Study Results.....	72
Figure 15: Table Detailing Primary Antibodies Used.....	81
Figure 16: Table Detailing Microscopes and Objectives Used.....	83
Figure 17: Table Detailing all Primers Used In PCR Reactions.....	86
Figure 18: Breeding Outcomes for T30H Heterozygous Mice.....	90
Figure 19: Viral Vectors and Titres Used for Biodistribution Study.....	112
Figure 20: Tablet View of the Translocation on Chromosome 2.....	115
Figure 21: Tablet View of the Translocation on Chromosome 11.....	116
Figure 22: PCR Strategy to Confirm the Translocation Point.....	118
Figure 23: Genetic Sequence of the T30H Translocation Point.....	119
Figure 24: Graph Showing the Distance Between Flanking Genes and the Translocation points.....	121
Figure 25: RT-PCRs for Translocation Flanking Genes.....	123
Figure 26: RT-PCR for Alternative Splice Variants of Myocardin Exon 2a.....	127
Figure 27: RT-PCR for Alternative Splice Variants of Myocardin Exon 10a.....	128

Figure 28: Quantitative PCR for Myocardin Exons 2a and 10a.....	130
Figure 29: PAS Staining of P1 T30H and Wild-Type Kidneys.....	134
Figure 30: Timeline of α SMA Staining in Wild-Type Mice.....	137
Figure 31: α SMA Staining in T30H Mice and Wild-Types.....	138
Figure 32: α SMA Staining of T30H Kidneys.....	139
Figure 33: α SMA Staining of P1 Bladders in T30H and Wild-Type Mice.....	140
Figure 34: α SMA Staining of T30H Gut.....	141
Figure 35: α SMA Staining of E16 Bladders in T30H and Wild-Type Mice.....	142
Figure 36: Timeline of Calponin Staining in Wild-Type Mice.....	144
Figure 37: Calponin Staining in P1 T30H Mouse Bladder.....	145
Figure 38: Calponin Staining in E16 T30H Mouse Bladder.....	146
Figure 39: Timeline of Uroplakin 3a Staining in Wild-Type Mice.....	147
Figure 40: Uroplakin 3a Staining at Timepoints of Interest in Wild-Type Mice.....	148
Figure 41: Uroplakin 3a Staining in P1 T30H and Wild-Type Mice.....	149
Figure 42: Uroplakin 3s Staining in E16 T30H and Wild-Type Mice.....	150
Figure 43: Myocardin Staining in T30H and Wild-Type Mice.....	152
Figure 44: Ultrasound Scans of T30H and Wild-Type Mouse Bladders.....	155
Figure 45: Volumetric Measurements for the Bladder of Wild-Type and T30H Mice During Development.....	157
Figure 46: Whole Bladder Culture Strategy and Growth in Culture.....	160
Figure 47: Strategies for Bladder Culture.....	164
Figure 48: Lentivirus Dosage Cell Culture Growth Results.....	167
Figure 49: Dissociated Cell Culture Western Blotting and Growth Results.....	169
Figure 50: Biodistribution Samples AAV1 and AAV2.....	172
Figure 51: Biodistribution Samples AAV6 and AAV7.....	173
Figure 52: Biodistribution Samples AAV8 and AAV9.....	174
Figure 53: Biodistribution Samples Adeno and Lenti.....	175
Figure 54: Table of Smooth Muscle Genes of Interest & their Genomic Locations.....	189

Abbreviations

AAV – Adeno Associated Virus

Ahcy – Adenosylhomocysteinase

ASIP – Agouti Signalling Protein

α SMA – Alpha Smooth Muscle Actin

Bp – Base Pair

BMP – Bone Morphogenic Protein

BSA – Bovine Serum Albumin

CAKUT – Congenital Anomalies of the Kidney and Urinary Tract

CArG - CC(A/T)6GG DNA sequence

CDH – Cadherin

cDNA – complementary DNA

CKD – Chronic Kidney Disease

CNN - Calponin

CRISPR - Clustered Regularly Interspaced Short Palindromic Repeats

DAB – Diamino benzidine

DNA – Deoxyribose Nucleic Acid

DNAHC9 – Dynein Heavy Chain 9

dNTP – Deoxyribonucleotide triphosphate

DMEM – Dulbecco's Modified Eagle Medium

E – e.g. E14 embryonic day

ERK – Extracellular Signal Regulated Kinase

ERT2 – Estrogen Receptor T2

FBS – Fetal Bovine Serum

FGF – Fibroblast growth factor

FISH – Fluorescence In Situ Hybridisation

GAPDH - Glyceraldehyde 3-phosphate dehydrogenase

GDF5 – Growth Differentiation Factor 5

GFP – Green Fluorescent Protein

Gli (1,2,3) – Glioma associated oncogene

gRNA – Guide RNA

GSK3 – Glycogen Synthesis Kinase 3

HDR – Homology Directed Repair

HRP – Horseradish peroxidase

ITS – Insulin Transferrin Selenium

KB – Kilobase

KLF4 – Kruppel like factor 4

KRT5 – Keratin 5

LP – Lamina Propria

LUTO – Lower Urinary Tract Obstruction

M – Molar

Map2k4 - Mitogen-Activated Protein Kinase Kinase 4

MEF2 – Myocyte Enhancer Factor 2

MiR – MicroRNA

Mgb – Megabladder

MOI – Multiplicity of Infection

MRTF – Myocardin Related Transcription Factor

Myocd – Myocardin

P – e.g. P1 postnatal day

PAS – Periodic Acid Schiff's

PBS – Phosphate Buffered Saline

PBS – Prune Belly Syndrome

PBS-T – PBS TWEEN

PCR – Polymerase Chain Reaction

PFA – Paraformaldehyde

Ptc – Patched

PUV – Posterior Urethral Valves

qPCR – quantitative Polymerase Chain Reaction

RNA – Ribonucleic Acid

RNase – ribonuclease

Rpm – revolutions per minute

RT-PCR – reverse transcription polymerase chain reaction

Shh – Sonic Hedgehog

shRNA – Short hairpin RNA

SM-MHC – Smooth Muscle Myosin Heavy Chain

Smo – Smoothened

SRF – Serum Response Factor

TAE – Tris Acetate EDTA

TEM – triethylenemelamine

TGF – Transforming Growth Factor

TUNEL – Terminal Deoxynucleotidyl Transferase dUTP Nick End Labelling

Up3a – Uroplakin 3a

URP – Urotensin Related Protein

US – ultrasound

UTI – Urinary Tract Infection

UTO – Urinary Tract Obstruction

WHP – Woodchuck Hepatitis Virus

Wnt – Wingless

WT – Wild-Type

1 Introduction

1.1 Anatomy and Development of the Urinary Tract

The urinary system, in both humans and mice, consists of the kidneys, the ureters, the bladder and the urethra (**Figure 1a**). The kidney's primary function is to filter waste products from the blood and convert them into urine. The kidneys also perform diverse other processes essential to homeostasis. They regulate pH balance, osmolarity and blood pressure as well as secreting and maintaining the level of various hormones. These hormones control hypoxia response, production of red blood cells and absorption of calcium (Carlson, 1994).

The functional unit of the kidney is the nephron (**Figure 1c**); they are found within the parenchyma of the kidney (**Figure 1b**). The nephron is composed of the renal corpuscle, containing the glomerulus and its surrounding Bowman's capsule, and the renal tubule. The renal corpuscle is the site of blood plasma filtration, which occurs between the capillaries and the glomerulus. The waste products from the blood diffuse from the capillaries into the glomerulus, and then are passed into the renal tubules for concentration to conserve water.

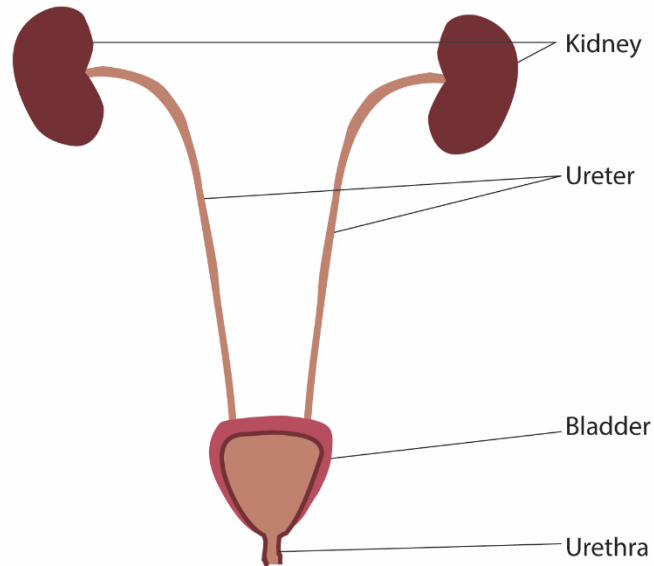
Renal tubules have accompanying peritubular capillaries which run alongside the ascending and descending components of the renal tubule, and these capillaries take away water that is reabsorbed. The renal tubules consist of several components. The first section into which the glomerular fluid is passed for concentration is the proximal convoluted tubule, which is distinguished by its brush borders, which increase the surface area for better absorption. This is followed by the loop of Henle, which has ascending and descending sections of differing permeability. These differences in permeability along with electrolyte pumps create different concentration gradients of urea, a waste product of protein metabolism, in the medulla. This then forces water from the glomerular fluid through osmosis, creating highly concentrated urine for excretion. The ascending loop of Henle is impermeable to water, and so the high concentration of the filtrate is maintained. On passing through the loop of Henle, the concentrated filtrate then enters the distal convoluted tubule. The distal convoluted tubule contains many ion transport channels and is

involved in maintaining blood pH; it absorbs or releases various ions to balance pH dependent on the presence or absence of various hormones.

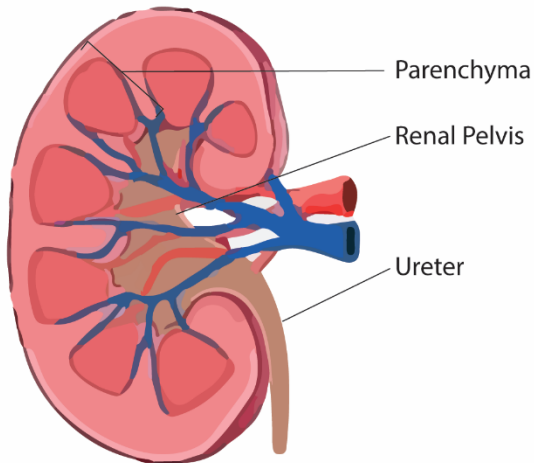
The filtered urine then passes into the renal pelvis of the kidney (**Figure 1b**), which is a collection of collecting ducts which extends into the ureter. It extends from the ureter and is anchored in the renal parenchyma by connective tissue and smooth muscle. Urine passes from the renal pelvis into the ureters, tubes whose walls contain smooth muscle, which pass urine down into the bladder. The ureters enter the bladder in an area called the trigone, and at this entry point the smooth muscle of the bladder and the ureters intersect to form the ureterovesical valves which prevent reflux of urine back into the kidney (Carlson, 1994).

The bladder is a muscular sac which can expand to store urine, allowing urination to be infrequent and under voluntary control after continence is gained during infancy. It is an organ capable of storage capacity because of its smooth muscle wall, which can stretch to increase capacity and contract to expel urine. Upon urination, urine is passed from the bladder into the urethra. The urethra is a tube which connects the bladder to the urinary meatus and allows urine to exit the body. The urethral sphincter, which allows urine to enter the urethra, is composed of striated muscle as well as smooth muscle. This striated muscle in addition to the detrusor smooth muscle of the bladder allows urination to be voluntary once continence has been gained (Churchill et al, 1987).

a. The Renal Tract



b. The Kidney



c. The Nephron

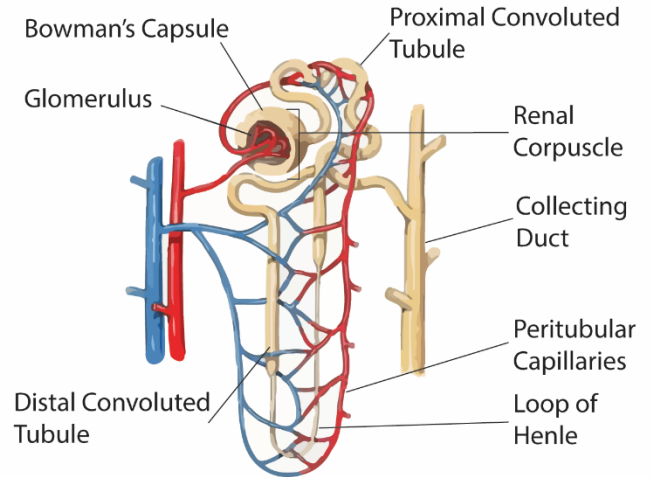


Figure 1. Anatomy of the urinary tract. The urinary tract consists of the kidneys, ureters, bladder and urethra (a). The kidney (b) filters waste products from the blood and converts them into urine, which is stored in the bladder before being expelled from the body. Filtration is carried out by the nephron (c), the functional unit of the kidney.

1.1.1 Brief overview of kidney development

The renal system arises from the intermediate mesoderm and can be broadly classified into three morphological stages: the pronephros, the mesonephros and the metanephros (**Figure 2**). These stages follow evolutionary development. The pronephros is the final excretory organ in the simplest vertebrates, the mesonephros is present in fish and amphibians, and the metanephros is present in amniotes. (Seldin et al, 1992)

The pronephros arises in day 22 of human gestation, and connects laterally with the pronephric ducts, which descend towards the cloaca, as the urogenital sinus has not yet fully formed. *Lim1* expressing-cells are indicative of kidney specification, and in embryos where Pax2 and Pax8 are knocked out the embryo does not form a pronephros and does not seem capable of the mesenchymal-epithelial transitions required for kidney development (Bouchard et al, 2002).

As the pronephric ducts extend towards the cloaca, they induce adjacent intermediate mesoderm to form additional sets of tubules, which become the mesonephros. The continuation of the pronephric duct becomes the mesonephric or Wolffian duct. By the end of the fourth week of gestation the Wolffian ducts attach to the cloaca. In the fifth week of development at the site of attachment the Wolffian duct forms an outgrowth called the ureteric bud. It then begins to grow into the intermediate mesoderm and will go on to form the metanephros, which will form the adult kidney. The remains of the pronephros and the mesonephros go on to be reabsorbed through apoptosis or become integrated into the male genital system: specifically, the tube that connects the testes to the ejaculatory ducts, which connect to the urethra (Carlson, 1999).

	Pronephros	Mesonephros	Metanephros
Human	Day 22	4 - 8 Weeks	8 Weeks - Birth
Mouse	E8	E9	E10

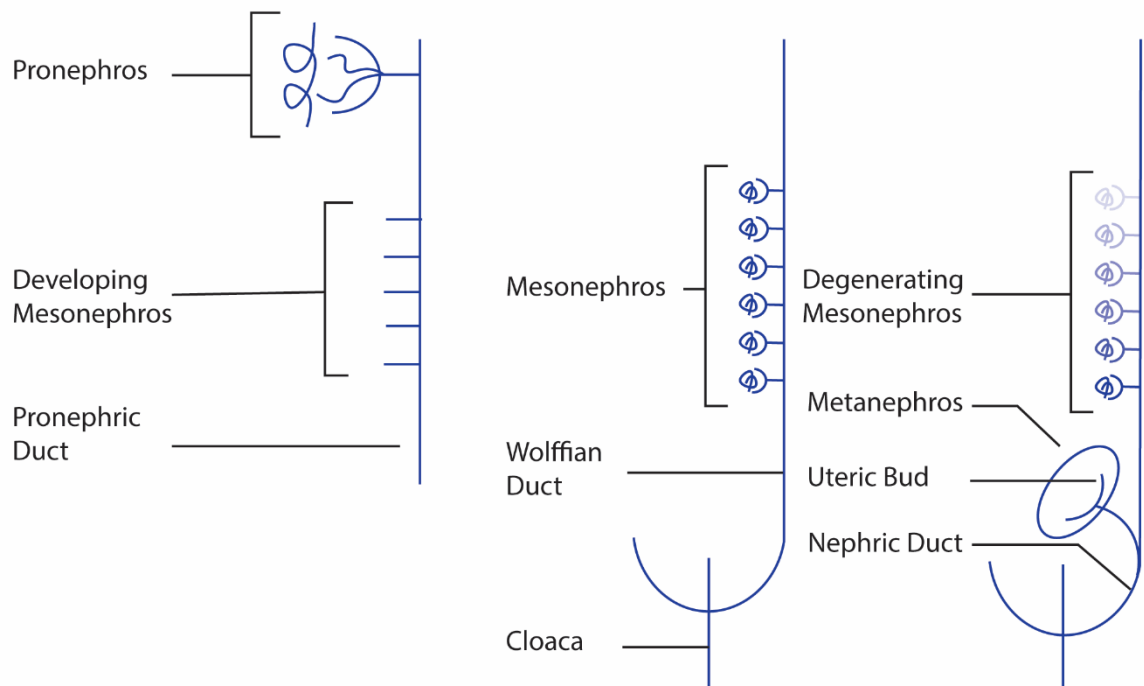


Figure 2. The three morphological stages of kidney development are the pronephros, the mesonephros and the metanephros. They arise at day 22, 4-8 weeks, and from 8 weeks to birth in human gestation. In mice these stages occur at embryonic day 8, 9 and then 10. The metanephros continues to grow to become the adult kidney. The pronephros and mesonephros, early embryonic structures, are reabsorbed or are integrated into the male genital system during the rest of development.

1.1.2 Anatomy and development of the bladder

There are two embryological lineages responsible for the development of the urinary tract. While the upper urinary system, composed of the ureters and the kidneys, derives entirely from the epithelial Wolffian duct, the lower urinary tract is separately derived from the cells of the endodermally derived cloaca.

The development of the lower urinary tract – the bladder and the urethra – initiates with the division of the cloaca into the rectum and the urogenital sinus in the sixth and seventh weeks of human gestation. In mice this occurs between E10.5 and E12.5. The urogenital sinus is an embryonic structure which is the precursor to the bladder; it is initially an epithelial tube to which the Wolffian ducts are attached via the common nephric duct. The area of this attachment in the posterior of the early bladder is called the urogenital sinus ridge, and it is an important signalling centre for ureter attachment and remodelling (Shapiro et al, 2000).

The area above the urogenital sinus ridge elongates and expands as development continues, and will become the urinary bladder, whereas the area below it will become the urethra (Georgas et al, 2015). In humans the urinary bladder and urethra are observable from around 7 weeks of gestation onwards (Cao et al, 2008). The area where the ureters and the urethra meet in the bladder is called the trigone, and at this site the layers of tissue become much thinner and have less smooth muscle than the rest of the bladder, particularly the bladder fundus, or dome. Throughout development the bladder dome increases in size and grows a thick smooth muscle wall.

Anatomically, the fully developed bladder is divided into the dome, neck and the trigone (Figure 3). The dome is the muscular portion of the bladder in which urine collects and can expand to increase capacity. The bladder neck is the area between the entry point of the ureters and the opening of the urethra. It is formed at the base of the trigone surrounding the urethra. The trigone is an area of the bladder with reduced smooth muscle compared to the dome and is the point where the ureters and urethra insert, with all three insertion points forming a triangle (Cao et al, 2008).

1.1.3 Components of the Bladder

In the fully developed bladder, there are three layers of tissue, the urothelium, the lamina propria and the smooth muscle layer, all of which are vital to proper bladder function (**Figure 3**).

Also integral to proper function are the nerves of the bladder and the bladder vasculature. Voluntary urination is controlled by three sets of nerves emanating from the spinal cord. The pelvic parasympathetic nerves connect the bladder and urethra to the spine, the lumbar sympathetic nerves are found in the bladder and connect the bladder base to the urethra, and the pudendal nerves are found in the urethral sphincter. Sensory neurons which innervate the smooth muscle of the bladder wall send signals to the central nervous system monitoring the level of bladder distension. When the bladder is voided, parasympathetic nerves which innervate the bladder detrusor smooth muscle layer contribute to controlling the release of urine by exiting muscarinic receptors in these cells. The internal urethral sphincter then relaxes; this is not under voluntary control. Finally, the external urethral sphincter relaxes, which is under voluntary control (Yoshimura et al, 2003).

In terms of the vasculature, the main blood supply to the bladder is derived from the internal iliac vessels – specifically the superior vesicle arteries. The bladder also has extensive microvasculature in order to supply oxygen to the cells of the detrusor smooth muscle wall. The bladder microvasculature is specialised to allow constant supply of blood despite the deformation of the tissue due to the expansion of the bladder to accommodate storage of urine. When the bladder is empty the vessels have a coiled morphology which then allows them to ‘uncoil’ when the bladder is distended. Connecting vessels between arterioles and the capillary network are also arranged perpendicularly to the bladder wall; this means that they are exposed to less stress when the bladder expands. There are also higher levels of arterial sphincters per capillary sphincter present to allow tighter control over blood flow into the bladder (Hossler et al, 2013).

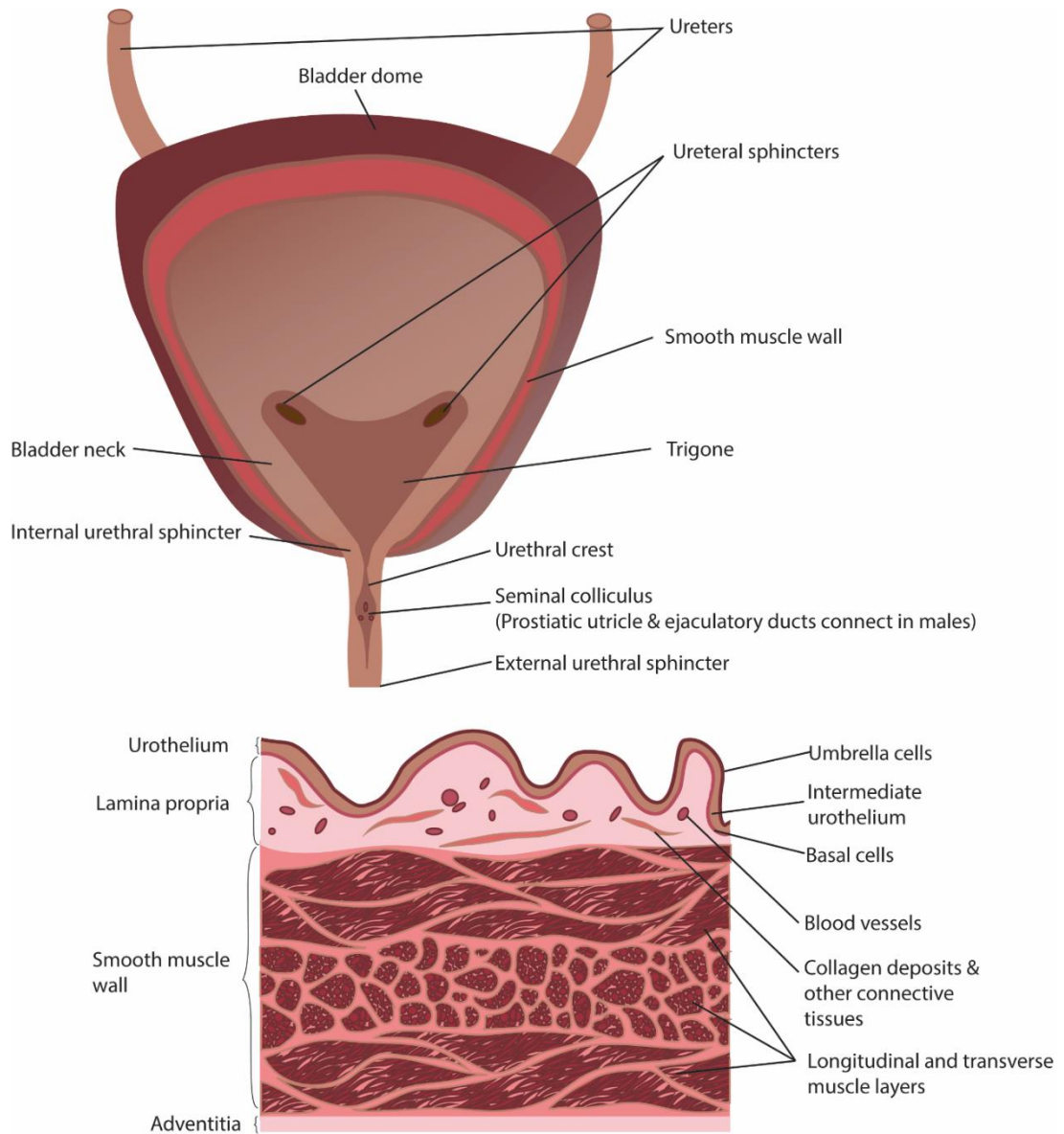


Figure 3. The bladder can be divided into the dome, neck and the trigone. The dome is the most muscular portion of the bladder and can expand to store urine. The ureters and the urethra connect within the bladder neck to form the trigone. In the cross section of the bladder wall, three distinct layers are present: the urothelium, the lamina propria and the smooth muscle wall. The adventitia is also present, and is the outermost layer of connecting tissue which covers the bladder.

1.1.3.1 Urothelium

The urothelium is a watertight layer which protects the rest of the tissue from the urine stored in the bladder. It also lines the renal pelvis, the ureters and the posterior urethra. The urothelial cells form important feedback mechanisms for mechanical and chemical changes to the bladder; this is mediated by neurons lying adjacent to the urothelial membrane (Hicks, 1975).

The urothelium is formed of three cell types which segregate to three different layers: the basal cells, attached to the basement membrane, intermediate cells, and umbrella cells, at the apex of the tissue. The umbrella cells are highly plastic, and their morphology can deform and stretch so the bladder can expand to store urine. They possess a unique cell membrane integral to the barrier function of the epithelium; they have asymmetric unit membranes, so called because they are double the thickness of the inner membrane, composed of intercalating plaques connected by hinge regions (Khandelwal et al, 2009). These membranes contain uroplakins. These proteins, along with others, such as occludins and claudins, form hexagonal plaques which create a water-tight seal and prevent damage occurring to the tissue of the renal system by the toxic components found in urine (Birder et al, 2013). In mice, uroplakin expression begins at E13, in some parts of the urothelium, with all urothelial cells expressing uroplakin from E14 onwards (Zhou et al, 2010).

The dramatic expansion of the bladder to store urine while maintaining barrier function, and then subsequent contraction upon voiding, is highly dependent on the membrane plasticity of umbrella cells. It is hypothesised that these cells undergo stretch mediated endocytosis and exocytosis in order to regulate the size of the cell membrane, in addition to folding and unfolding of the mucosal surface (Truschel et al, 2002).

There are 4 different types of uroplakin protein, which heterodimerise with each other; these heterodimers then associate to form hexagonal structures which bind together to form plaques. Uroplakin 1a binds to uroplakin 2, and uroplakin 1b binds

to uroplakin 3. These uroplakin heterodimers are not specifically expressed in different areas of the bladder, as Liang *et al.* (2017) found uroplakin 3 in all urothelial plaques. Uroplakin 3 has multiple isoforms, with uroplakin 3a being the dominant one and the most studied (Matuszewski *et al.*, 2016).

The urothelium not only has a barrier function but is also an important signalling centre for the bladder in the maintenance of continence and a proper voiding pattern (Apodaca *et al.*, 2007). Urothelial cells possess many surface receptors and ion channels which respond to mechanical signalling. Stimulation of these receptors induces ATP release from the urothelium which is then received by nerve cells of the urothelium or the lamina propria (Birder *et al.*, 2012).

Terminally differentiated umbrella cells are derived from the basal and intermediate cells of the urothelium, and expression of uroplakin is generally considered to be a marker for urothelial differentiation. Cells of the basal layer of the epithelium express cytokeratin 5 and can be induced to express uroplakins in response to disease (Schäfer *et al.*, 2017). Terminally differentiated cells are relatively long-lived; other less terminally differentiated cells of the basal and intermediate layers of the urothelium can regenerate very quickly on injury to the tissue, reforming a robust, impermeable protective layer (Lee 2011).

1.1.3.2 Lamina Propria

The lamina propria lies between the urothelium and the detrusor muscle of the bladder. It is composed of an extracellular matrix and a diverse range of cell types, including a vascular and lymphatic network. There are variances in the thickness of the lamina propria in different regions of the bladder, with the trigone having a thinner lamina propria layer, and the bladder dome having the greatest thickness (Paner *et al.*, 2007). The lamina propria must undergo constant remodelling as the bladder fills and empties. In order to undergo this remodelling cells of the lamina propria express many adhesion molecules such as laminins, fibronectins, glycans and glycoproteins. In the empty bladder these cells form a loose, non-structured arrangement, but as the bladder fills the cells of the lamina propria change

orientation so that they lie parallel to the urothelium, aiding in maintain the structural integrity of the bladder (Andersson et al, 2014).

The lamina propria also contains afferent nerves thought to be vital for sensory signalling in the bladder to aid micturition. The greatest quantity of these nerves is found in the bladder neck, where they form an intricate network of nerves close to the urothelial lining (Gosling et al, 1974).

The development of the bladder mesenchyme, containing both the lamina propria and the smooth muscle layer below it, is dependent on sonic hedgehog (*Shh*) signalling and its downstream receptors for proper development. Fibroblast growth factors (*fgfs*) are involved in negative feedback loops for *Shh* in the development of several organs (Morales et al, 2016). In embryos where *Fgfr2* is knocked out, there is reduced smooth muscle, but increased growth of the lamina propria, and in particular the collagen element of the tissue. This shows the importance of the feedback mechanisms in the different tissue types in the bladder and their role in development (Ikeda et al, 2017).

1.1.3.3 Smooth Muscle

Smooth muscle cells are located in multiple areas of the body, predominantly in organ walls and the walls of vessels. They differ from the other muscular tissue types of the body, cardiac and skeletal muscle, in that they lack striated banding patterns. Their contraction is also not under voluntary control. Smooth muscle cells have a greater ability to be able to stretch and still maintain the ability to contract, unlike skeletal muscle (Michel, 2016).

Bladder smooth muscle cells have two functional phenotypes: either a contractile phenotype – elongated cells with a high level of contraction related proteins – or a synthetic phenotype, where cells exhibit high levels of proliferation, migration and excretion of extracellular matrix. This allows smooth muscle tissue to be highly responsive to both physiological changes and disease, and they retain this plasticity in adults as well as during development (Owens et al, 2004).

Smooth muscle is a vitally important layer in the bladder due to its ability to expand to store urine at low pressure in order to protect the kidneys, and to prompt micturition under voluntary control. Contraction and relaxation of the detrusor smooth muscle of the bladder is dependent, as with all other muscle tissues, on interactions between actin and myosin. In the bladder there is a higher actin to myosin ratio compared with vascular smooth muscle (Uvelius, 1980). Bladder smooth muscle contraction is dependent on calcium ion levels, which enter smooth muscle cells on stimulation of the cells by motor neurons. These calcium ions activate calmodulin, a calcium ion binder, which in turn activates myosin, a contractile protein (Fry et al, 2002). When muscle contraction needs to be inhibited, caldesmon and calponin compete for calcium ions and inhibit myosin when they are taken up (Deng et al, 2007).

Different myosin isoforms are specific to different muscle tissue types; in smooth muscle cells, smooth muscle myosin heavy chain (SM-MHC) is specific. *SM-MHC* itself has four different isoforms, which are present at different developmental stages, and can be found in different ratios between visceral and vascular smooth muscle. Expression in the bladder is essential for proper voiding, and in disease where the structure of the bladder changes, like lower urinary tract obstruction, the expression ratios of *SM-MHC* isoforms change, further altering the functional contractility of the bladder. If *SM-MHC* is knocked out, then smooth muscle cannot develop properly, resulting in a very thin-walled, non-functional bladder (Li et al, 2018).

Myosin binds to actin in order to initiate muscle contraction. Actins are highly conserved across species, and as with myosin, different subtypes are specific to different muscle types. Smooth muscle-specific actins are alpha smooth muscle actin (α SMA), gamma smooth muscle actin (γ SMA), as well as beta and gamma cytoplasmic actins. α SMA is more prevalent in vascular smooth muscle and γ SMA is more prevalent in organ smooth muscle. The presence of both, however, is essential in both organs and vessels (Vandekerckhove et al, 1978). α SMA is present at the very earliest stages of smooth muscle cell differentiation in the bladder, and γ SMA is then expressed as the cells mature. When α Sma is knocked out, the bladder loses its ability

to generate the same levels of force required to void the bladder (Zimmerman et al, 2004).

The differentiation of smooth muscle tissue from the primitive mesenchyme of the early bladder is dependent upon signals from the bladder epithelium (**Figure 4**). This process of mesenchymal muscle differentiation is present in multiple organ systems, including the gut, and when mesenchyme is transplanted between different tissues, epithelium from other organ systems – for example, the gut, the stomach and the uterus – can initiate the development of smooth muscle in bladder mesenchyme (DiSandro et al, 1998). This is also not specific to embryological age of the tissue, as even adult epithelium can induce differentiation (Cao et al, 2008).

The Shh signalling pathway is essential for this transition and therefore smooth muscle formation. Shh is involved in many systems during development, and knockouts are embryonic lethal (Chiang et al, 1996). In the renal system when Shh is attenuated there is a severe reduction in the smooth muscle level in all organs of the – including the ureters, urethra and the bladder (Yucel et al, 2004).

When Shh is expressed, it binds to Patched (Ptc), repressing it, and as a result releases smoothed (Smo) inhibition. This allows a signalling cascade to initiate which results in Gli transcription factors (Gli1, Gli2 and Gli3) being expressed. These then target Shh-dependent pathways such as the Wnt and BMP signalling pathways (Shiroyanagi et al, 2007, Haraguchi et al, 2007).

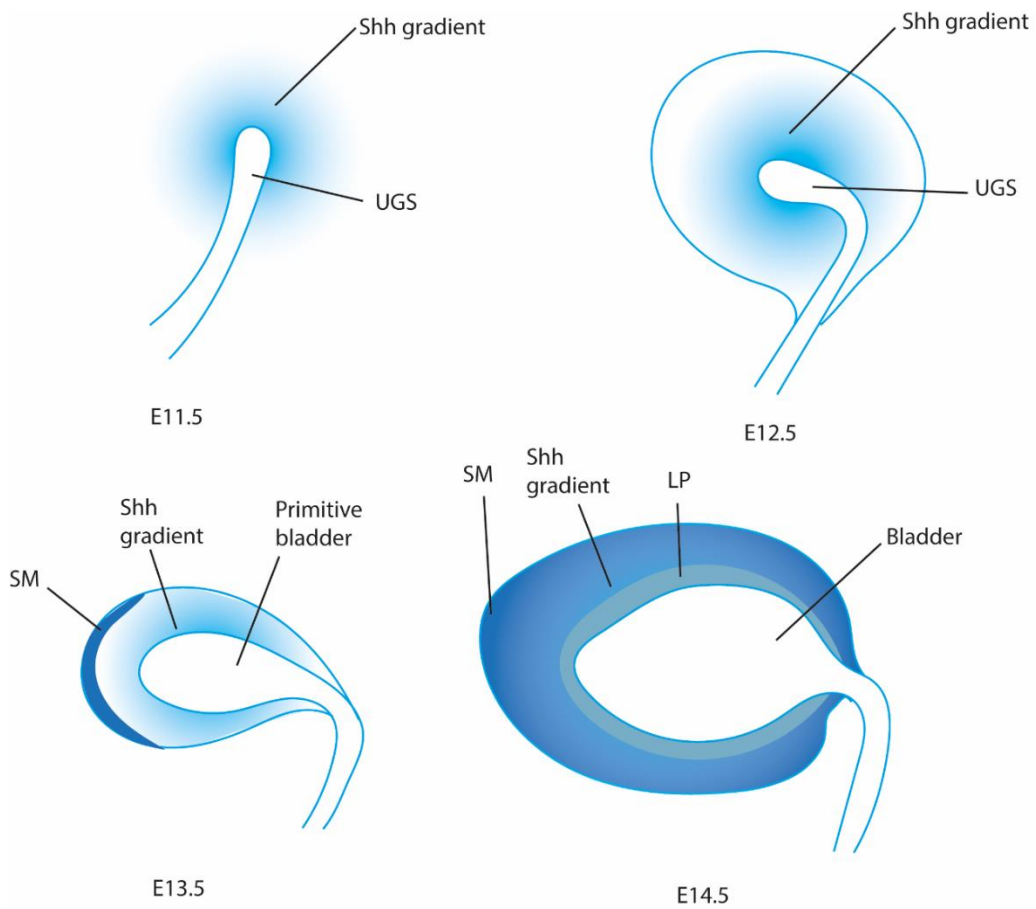


Figure 4. The development of smooth muscle in the bladder is initiated by sonic hedgehog signalling (Shh). Shh forms a concentration gradient which is strongest at the urothelium. The entire bladder mesenchyme is capable of differentiating into smooth muscle, but only the layers further from the urothelium do so. The differentiation of smooth muscle begins in a layer furthest from the urothelium at E13.5 in the mouse. Shh - sonic hedgehog, UGS - urogenital sinus, SM - smooth muscle, LP - lamina propria

In mice, Shh signalling begins in the urogenital sinus from E11.5, which increases at E12.5 until smooth muscle begins to form at E13.5, after which the level of Shh expression decreases in the urothelium. Whilst the entire bladder mesenchyme can differentiate into smooth muscle, only the layer of tissue furthest from the epithelium differentiates into smooth muscle, and the layer closest to the epithelium goes on to form the lamina propria. This is because Shh forms a concentration gradient in bladder tissue, with different levels of expression inducing differentiation of different tissues; high levels of *Shh* expression close to the urothelium are inhibited from forming smooth muscle, whereas in the outer mesenchyme furthest from the epithelium where Shh is low smooth muscle cells are able to differentiate (Cao et al, 2008). Shh concentration gradients as a mechanism for cellular patterning and differentiation is not exclusive to the bladder and can also be seen in the neural tube – an embryonic structure which later forms the brain and spinal cord (Ericson et al, 1995).

Gli1 expression prior to the initiation of smooth muscle expression in the bladder is spread throughout the mesenchyme. In mice this is at E12. Gestation progresses and the expression of this marker becomes increasingly restricted to the inner mesenchyme adjacent to the urothelium by E16. Conversely, *Gli3* expression is not detected at E12, but as development continues it is found solely in the outer mesenchyme of the bladder. This inner mesenchyme will go on to become the lamina propria, and the outer mesenchyme will become the smooth muscle layer (DeSouza et al, 2013).

Gli2 enters the nucleus in mesenchymal cells and initiates upregulation of *BMP4*, which then goes on to activate SMAD proteins, predominantly SMAD2 and 3. This activation allows SMAD proteins to move into the nucleus of the cell and activate transcription of smooth muscle control genes such as myocardin (*MYOCD*) (Tasian et al, 2010). GLI proteins also target the WNT signalling pathway, particularly *Wnt2*, which is an activator of *Klf4*, which inhibits *Myocd*. This inhibition is turned off during smooth muscle cell differentiation by small signalling molecules called microRNAs, in this case MiR-199a-5p (Hashemi Gheinani et al, 2015).

Smooth muscle begins to develop in the bladder at the 12th week of gestation in humans, at E13 in mice, and is initially characterised as mesenchymal compaction prior to the expression of smooth muscle-specific markers. Smooth muscle cells begin to develop on the outer layer of the mesenchyme and then progress towards the lamina propria. The developmental stage of the smooth muscle layer in the bladder can be ascertained by its expression profile. Early smooth muscle expresses α SMA, intermediate smooth muscle expresses calponin, and mature smooth muscle expresses *SM-MHC* (Miano et al, 1994).

1.1.4 Myocardin

The activation of expression of smooth muscle genes is mediated by transcription factors such as MYOCD (Chen et al, 2002). When it is heterodimerised with SRF, which is ubiquitously expressed, *MYOCD* is a master regulator of CArG box-mediated smooth muscle gene expression (**Figure 5**) (Yoshida et al, 2003). SRF has a highly conserved MADS box which is used for DNA binding onto CArG boxes to initiate transcription (Chang et al, 2003). Almost all smooth muscle genes have a CArG box in their regulatory regions, and SRF binds to these CArG boxes to initiate transcription (Li et al, 2005). *Myocd* induces smooth muscle cells to develop a contractile phenotype, initiating expression of multiple smooth muscle markers and promoting terminal differentiation into these cell types by activating transcription of *CDKN1A*, a cell cycle inhibitor (Kimura et al, 2010).

If *Myocd* is knocked out it is embryonic lethal, with embryos dying at E10.5 of gestation due to heart and vessel deformations (Li et al, 2003). *Myocd* not only activates transcription of smooth muscle genes *in vivo* but can also activate transcription in cell lines (Yoshida et al, 2003).

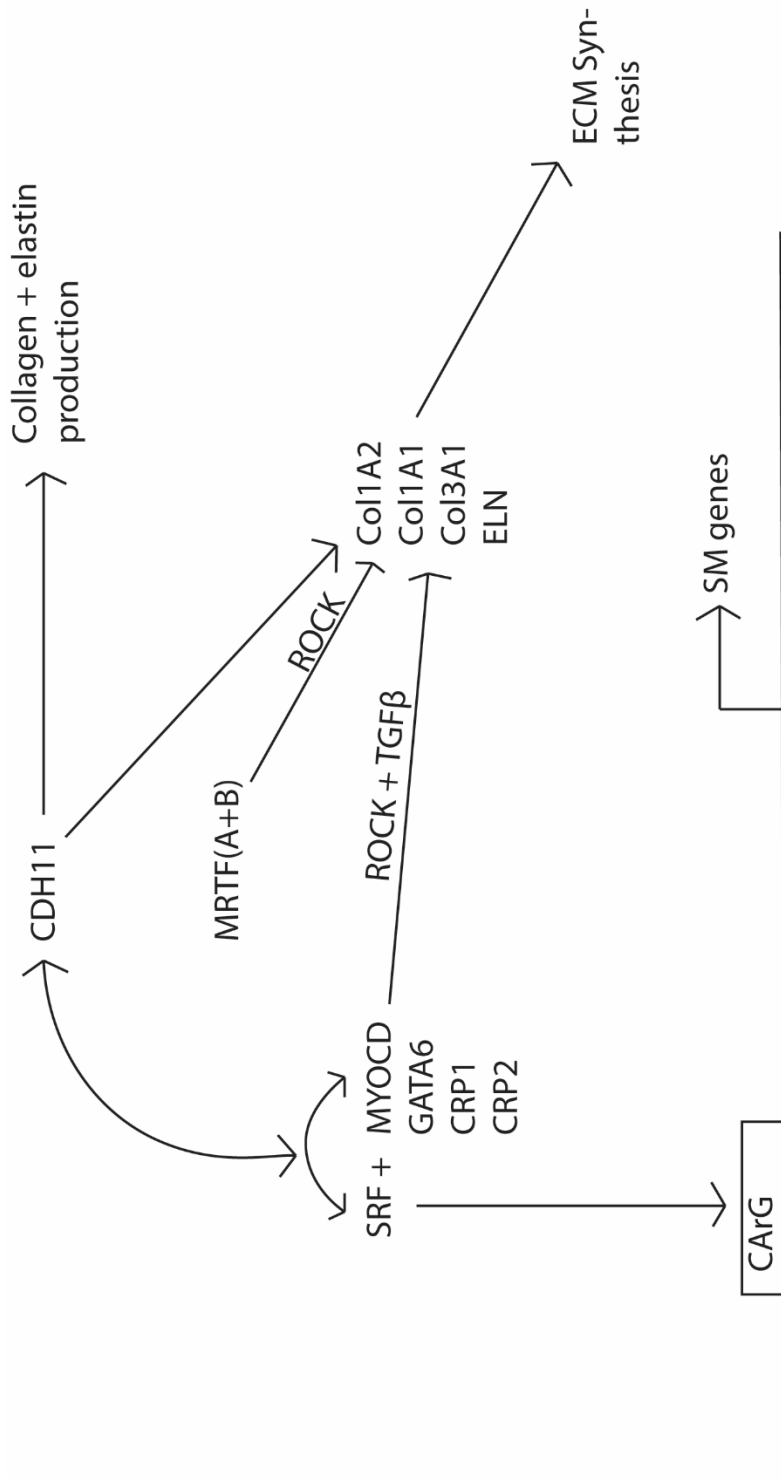


Figure 5. Myocardin (MYOCD) can act in addition to co-factors to induce expression of smooth muscle genes during development. It can also induce the expression of collagens and elastins to generate extracellular matrix. This process is accelerated in response to injury and can create scarring in the tissue.

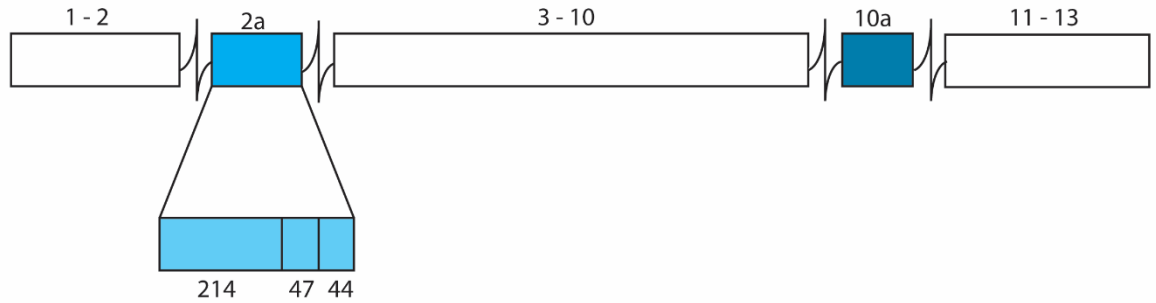
Myocd was first discovered in the heart, using in silico profiling, and described as an 807 amino acid protein; further investigation uncovered an additional 128 terminal protein residues. It is expressed in the bladder, but also the vessels and the gut, and is capable of making undifferentiated embryonic stem cells express smooth muscle-specific markers (Wang et al, 2001, Du et al, 2003).

Myocd has 15 exons, several of which undergo alternative splicing, four of which centre around the inclusion or exclusion of exons 2a and 10a (**Figure 6**). *Myocd* without the inclusion of either exon 2a or 10a and *Myocd* with only exon 10a included are expressed primarily in cardiac smooth muscle cells but can also be expressed in other smooth muscle cells. The inclusion of exon 10a incorporates an MEF2 binding domain, as well as an ERK1/2 phosphorylation site and a GSK3 phosphorylation domain, allowing tighter post-translational regulation of proteins with exon 10a incorporated. Adding GSK3 inhibitors to smooth muscle cells in culture has a similar effect to blocking *Myocd10a* expression, suggesting this post-translational phosphorylation is key to *Myocd10a* function (Ilagan et al, 2011).

Exon 2a is expressed more highly in smooth muscle cells. Its transcription creates a premature stop codon, which causes translation to skip to an alternative start codon in exon 4. *Myocd* including exon 2a can be expressed either with or without exon 10a, of which the former is the more abundant (Imamura et al, 2010).

In mice exon 2a is 305 base pairs long and contains three different domains, of 214, 44 and 47 base pairs. Of these domains, either the 214 base pair splice variant or the 44 base pair splice variant can be expressed. When either variant of exon 2a expressed, an MEF2 binding domain is lost, and a variety of different phosphorylation sites are both lost and gained depending on whether *Myocd214* or *Myocd44* are expressed. The loss of the MEF2 domain could aid the protein's ability to bind to SRF and increase its ability to promote smooth muscle gene expression (Creemers et al, 2006). Both variants of *Myocd* with exon 2a included are more highly expressed in the bladder than any other organ, especially for the 44 base pair variant of exon 2a. These splice variants of *Myocd* have also been found in human bladder samples, and the sequence of *Myocd* is highly conserved between species (Saha et al, 2009).

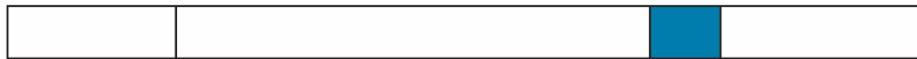
Figure 5



Variant 1



Variant 2



Variant 3



Variant 4



Myocardin expression level



Figure 6. Myocardin contains 13 exons in both mice and humans. Two of these exons, 2a and 10a, undergo alternative splicing to produce 4 different splice variants of the gene. Exon 2a can undergo further alternate splicing, expressing either a 214bp fragment or a 44bp fragment. The expression level of the four myocardin splice variants differs from organ to organ, exon 10a is more commonly included in the heart, and exon 2a is more commonly included in the bladder.

Myocd is also required for maintenance of the bladder postnatally. When *Myocd* expression is reduced bladder capacity is reduced, as *Myocd* is required for the expression of connexin 43. Connexin 43 is an important molecule in cell adhesion in the bladder (Imamura et al, 2013). When it is knocked out postnatally, embryos die six months after knockdown with deformations to the great arteries and other smooth muscle tissues including the bladder (Huang et al, 2015).

Other members of the MYOCD transcription factor family of proteins have similar function to MYOCD in smooth muscle cells. There are two other genes in the *Myocd* family called myocardin related transcription factors-1 and -2 (MRTF1/2), which have similar function to *Myocd*, but cannot fully compensate for *Myocd* being knocked out, in either the heart or other smooth muscle tissues (Hoofnagle et al, 2011).

GATA6 is a transcription factor that also heterodimerises with SRF in order to bind to CArG boxes to activate smooth muscle genes and has been shown to activate *α Sma* (Kanematsu et al, 2007). GATA6 only activates smooth muscle expression via SRF in the bladder and arteries, and not in other organs containing smooth muscle. In organs such as the heart and the gut, which also contain smooth muscle, GATA6 must act together with GATA4 to activate gene expression (Morrisey et al, 1996).

Molecules involved in cell-cell adhesion are also integral to smooth muscle cell differentiation (**Figure 7**). Cadherin 11 (CDH11) is a cell adhesion molecule that also regulates the production of extracellular matrix components. It forms a positive feedback mechanism with *Myocd*. CDH11 mediated activation of phosphorylated SMAD2 and 3 is required for MYOCD expression, and MYOCD in turn regulates CArG box mediated expression of elastin and collagen. MYOCD also forms a positive feedback mechanism to promote further expression of CDH11 (Row et al, 2016).

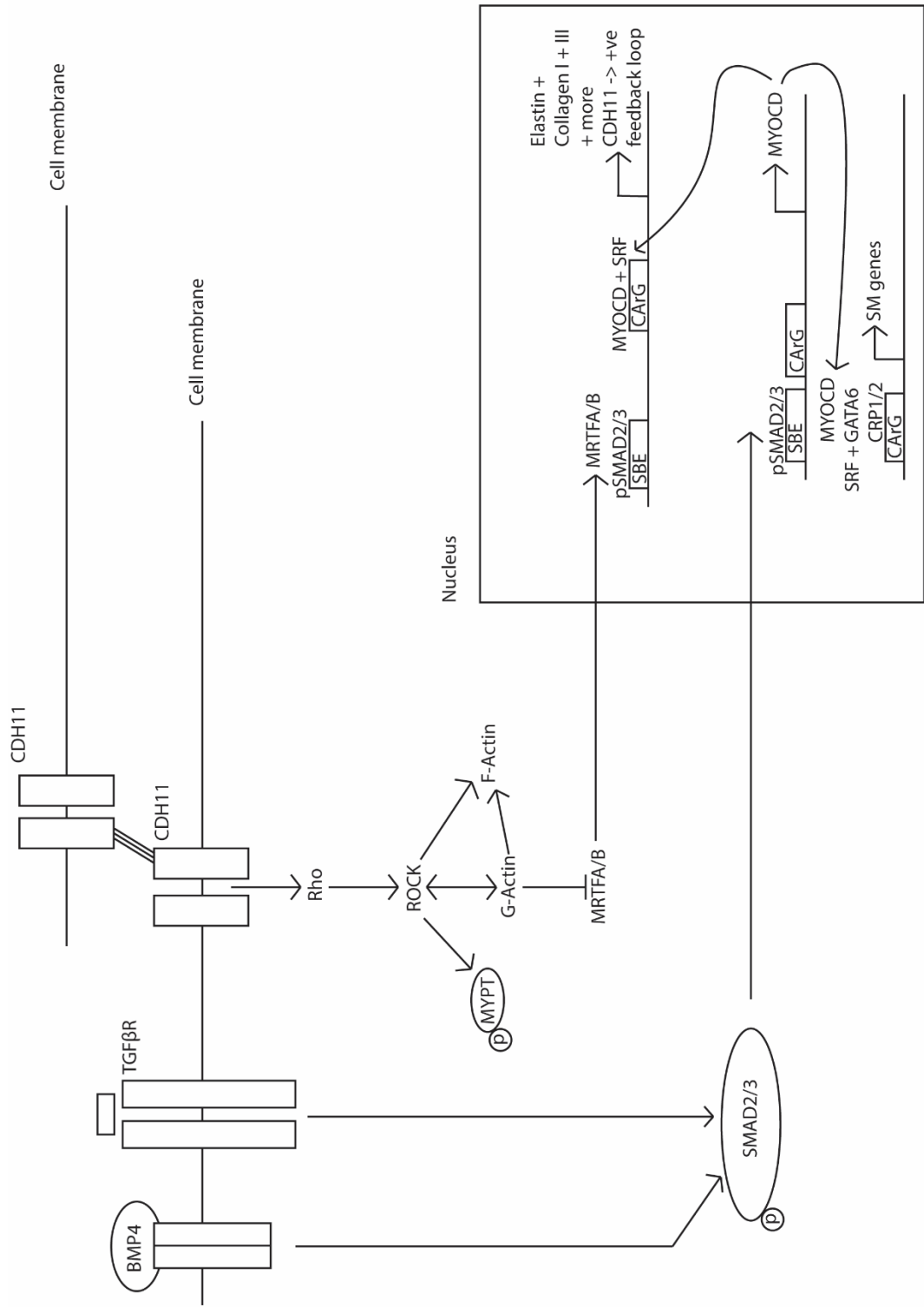


Figure 7. Signalling network required for activation of smooth muscle gene expression. Myocardin (MYOCD) is a master regulator of smooth muscle expression when heterodimerised with SRF. Activation of this signalling complex is dependent on multiple intra- and extracellular signalling pathways.

1.1.4.1 Conditional Myocardin Knockout Mouse Model

Huang *et al.* (2008) have used a smooth muscle cell restricted inducible knock-out mouse model of Myocd to show that the gene is not only required for development of smooth muscle tissue, but also maintenance of the tissue in adult mice. Tamoxifen-inducible SMMHC-CreERT2/MyocdF/F were generated to delete exon 8, which results in a protein that is unable to bind to SRF and then induce smooth muscle gene expression. When 6-week-old mutant mice were treated with tamoxifen, 80% of mice had died within 6 months, and no mice survived beyond 10 months. In mice which had died, the arterial structure was grossly malformed, and there were also gastrointestinal and urinary tract malformations. In particular in the bladder there was an almost complete lack of smooth muscle and mice presented with a hyperextended, non-emptying bladder. Postnatal knock-out of Myocd leads to autophagy of smooth muscle cells, which leads to apoptosis and degradation of smooth muscle tissue.

1.1.5 Human and Mouse Bladder Comparison

The mouse is an extremely widely used animal model to investigate both development and disease in humans. The mouse makes an excellent model because of the many genetic and physiological similarities between mice and humans (Perlman, 2016). However, this is not true for every characteristic shared between the two species. The organisation of the bladder wall is similar among the majority of terrestrial mammals, although there are some differences between the relative thicknesses of various layers (De Sessa, 1995).

When comparing human and mouse bladders, the structure of the two organs is largely the same, although there are some key differences. In humans, after continence is gained in childhood, bladder voiding occurs to empty the bladder at socially acceptable times and locations. In mice, however, micturition is an important part of mouse behaviour and communication, and male mice will void urine throughout their cage as a way of expressing social dominance (Hill et al, 2018). This involves partial voiding through time rather than complete bladder voiding in humans, an important difference in voiding pattern and bladder function between

the two species. This has led to there being some question over whether the bladder acts as a true storage organ for urine in mice (Yang et al, 2014). There are also some differences to the molecules present in the urothelium, while they are broadly similar, uroplakin expression in humans is more associated with the level of cellular differentiation than in the mouse (Wu et al, 2009). The bladder also lies in a different position in humans compared to mice in that humans are bipedal, and that mice are quadrupeds. This can create some physiological differences when modelling disease in mice (De Sessa, 1995).

While there are several differences between the human and mouse bladder there are still many factors which make mice an excellent model for studying bladder development and disease. Comparative studies investigating the similarities between the interstitial cells of the bladder in the two species find that they are broadly similar, although enough differences are present that translating research in mice into humans should still bear in mind the difference between the two species (Gevaert et al, 2017). A single cell transcriptomic map of both the human and the mouse bladder has also been generated to compare the similarities and differences between the two species (Yu et al, 2019). Bladder cell transcriptomes cluster to form highly similar clusters of gene expression between humans and mice, indicating that many of the signalling molecules are evolutionarily conserved between species (Yu et al, 2019).

The mouse is an animal model which has been widely used in the past to study both development and disease in the bladder (Kitta et al, 2018). There are some differences between the bladders of the two species, but this is outweighed by the similarities between them, along with the ease of genetic manipulation, short gestation and lifespan, ease of husbandry and relative inexpensiveness of mice.

1.1.6 Summary

The urinary system is formed of the kidneys, ureters, bladder and the urethra. It has diverse roles in maintaining the body's homeostasis and in the excretion of waste products from the body through the production of urine. The bladder allows for the storage and voluntary voiding of urine once continence is gained in infancy in humans. The tissue is comprised of three layers, the urothelium, the lamina propria and the detrusor smooth muscle, all are vitally important for function.

Urinary tract development is complex and relies on the cohesive signalling of multiple gene expression pathways. *Myocd* is particularly important for the formation of the smooth muscle layer of the bladder. It heterodimerises with SRF to bind to the regulatory areas of smooth muscle genes, thereby regulating their activation. *Myocd* is essential to proper smooth muscle development, maintenance and function in the bladder.

1.2 Developmental Disorders of the Lower Urinary Tract

Congenital anomalies of the kidney and urinary tract (CAKUT) are estimated to account for between 20 and 30% of anomalies detected prenatally (Nicolaou et al, 2015). They are a diverse group of disorders in terms of etiology and phenotype. CAKUT are the leading cause of end-stage renal failure in children; the genetic and molecular basis, however, are poorly understood, limiting genetic counselling and treatment options for patients and families (Rasouly et al, 2013). Three of the most common disorders where lower urinary tract obstruction is present are Posterior urethral valves, urethral atresia and prune belly syndrome (**Figure 8**).

1.2.1 Posterior Urethral Valves

Posterior Urethral Valves (PUV) are by far the most common form of developmental lower urinary tract obstruction. They occur in between 1 in 3000 and 1 in 8000 live births. In around two thirds of cases PUV are detected during fetal ultrasound after discovering the presence of antenatal hydronephrosis. They are the most common single defined cause of paediatric end-stage renal failure.

PUV occurs only in males, and there is no real female equivalent. They were defined by Stephens (1955) as being due to abnormal fusion of the Wolffian duct with the urogenital sinus early in development, at around week 4 of gestation in humans. The valves occur between the internal urethral sphincter and the seminal colliculus. They actually present as a continuous membrane of fibrous connective tissue, surrounded by transitional epithelium. Early dissections resulted in the misidentification of the structures as valves as opposed to a membrane (Krishnan et al, 2006).

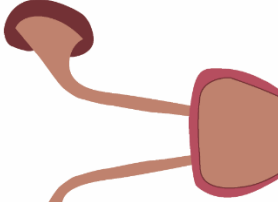
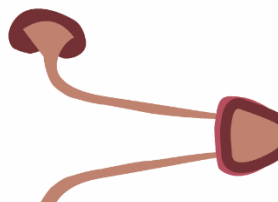
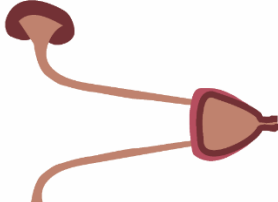
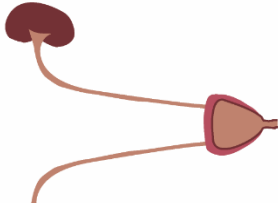
 <p>Normal</p>	 <p>Posterior Urethral Valves</p>	 <p>Urethral Atresia</p>	 <p>Prune Belly Syndrome</p>
Symptoms	Antenatal hydronephrosis and thickening of the bladder wall with extensive fibrosis caused by a membrane in the urethra which prevents the voiding of urine.	Failure of the urethra to form properly leaving no way for urine to be voided. Also results in oligohydramnios which is the greatest threat to life	Variable phenotype but generally a lack or deficiency of muscle in the abdominal wall, cryptorchidism, and a range of urinary tract abnormalities such as megacystis, hydronephrosis, and renal dysplasia
Incidence	1 in 3000-8000	Very rare	3-4 in 100,000
Genes Involved	CD59, TCP11L1, CSTF3, among others	Unknown, rarity a barrier to discovering culpable genes - postulated some of the same genes as in PBS	Myocardin, HNF1 β , BMPR1B, STIM1, NOG

Figure 8. The three most common causes of lower urinary tract obstructions are posterior urethral valves, urethral atresia and prune belly syndrome. These three disorders have diverse genetic etiology but share a kidney phenotype, hydronephrosis, fibrosis and reduced nephron number, with varying degrees of severity. Many children with these disorders will progress to end stage renal failure.

The cause of PUV is not always known case by case. The initiation of ureteric bud formation, elongation of the Wolffian duct and insertion into the correct area of the urogenital sinus is a complex process developmentally and involves many genes. A study by Chiaramonte *et al.* (2016) identifies several cases where multiple members of the same family are affected with PUV or symptoms relating to PUV, suggesting that there is an important genetic element to developing PUV. Genes identified in families, however, are often specific to that family and are rarely seen in other cases of PUV. For example, in one family the mother and two sons have a duplication of the short arm of chromosome 11, implicating the genes CD59, TCP11L1 and CSTF3 (Chiaramonte *et al.*, 2016). In another family chromosome 1 is the area identified as being affected in whole-genome hybridisation studies, but the genes affected are not identified (Weber *et al.*, 2005).

PUV may be identified either *in utero* or after birth. Via ultrasound PUV can be diagnosed with the following symptoms: enlarged and overextended bladder, deficiency in amniotic fluid levels, or abnormalities to the kidneys such as hydronephrosis (Eckoldt *et al.*, 2004). Holmdahl *et al.* (1998) show that up to 45% of patients will experience reduced kidney function before reaching adulthood, and often also have problems with incontinence and repeated urinary tract infections (UTI).

Treatment is initially to relieve the fluid build-up in the bladder, this can be done *either in utero* or after birth, and the stage at which it is carried out is usually dependent on the severity of symptoms in the patient. Prenatal intervention is in the form of a vesicoamniotic shunt in order to drain the bladder. The benefits to this treatment are in improving the pulmonary prognosis for the fetus (McLorie *et al.*, 2001). Holmes *et al.* (2001) found that prenatal draining of the bladder does not actually improve renal function, and is associated with higher risk of mortality, so there is some debate over whether vesicoamniotic shunts should be used. This is despite the improvement in lung function they can provide by introducing more circulating amniotic fluid into the amniotic sac from the drained bladder.

After birth, the obstruction is removed via surgery, but according to Bilgutay *et al.* (2016), around 20% of patients still have chronic kidney disease (CKD) two years post removal of obstruction, requiring transplantation. The most striking element of the bladder phenotype is the thickening of the smooth muscle wall, which impedes the functionality of the bladder – the muscle wall is thick has extensive fibrosis and is unable to dilate fully or allow proper voiding. In many children bladder augmentation is required in order to restore functionality to the bladder and improve patient continence (Freedman et al, 1999).

1.2.2 Urethral Atresia

Whereas in cases of PUV there is partial obstruction of the urethra, in urethral atresia there is complete obstruction. Urethral atresia is much rarer than PUV; the symptoms are similar to those seen in patients with valves, but are much more severe (Gonzalez et al, 2001). Precise frequencies of the disorder are difficult to calculate, as the disorder is so severe that pregnancies are often terminated. Most reported cases are in males. In order to survive after birth, patients must be treated *in utero* with a vesicoamniotic shunt in order to alleviate the oligohydramnios that occurs. This is important, as the most likely cause of death for these children is due to the consequences of their poor pulmonary function (Freedman et al, 1999).

Poor pulmonary function in children with urethral atresia and other forms of lower urinary tract obstruction occur as part of Potter's syndrome, which is caused by oligohydramnios *in utero*. Oligohydramnios is a deficiency of amniotic fluid during pregnancy (Rabie et al, 2017). It has multiple causes but one of the more common is urinary tract obstruction; amniotic fluid which is ingested by the fetus cannot be excreted as urine if there is an obstruction at any point in the urinary tract, resulting in less amniotic fluid surrounding the fetus. The features of Potter's syndrome are reduced pulmonary development, specific facial features, and potentially eye and heart defects (Miyahara et al, 2016).

1.2.3 Prune Belly Syndrome

Prune Belly Syndrome (PBS) has highly variable phenotype but can generally be characterised as a lack or deficiency of muscle in the abdominal wall, cryptorchidism, and a range of urinary tract abnormalities such as megacystis, hydroureteronephrosis, and renal dysplasia (Woodard, 1985). It is a very rare condition predominantly affecting boys, with an incidence of around 3-4 in 100,000 live births, although it may be slightly more common than these figures indicate, as parents often abort affected fetuses due to the severity of the condition (Seidel et al, 2015).

The etiology of PBS is predominantly unknown, and there are cases of both familial PBS and isolated cases where there is no previous family history. There are two hypotheses for the defects underlying PBS: the mesodermal defect hypothesis and the urethral obstruction malformation complex hypothesis. Both of these situations probably occur in different cases, as PBS can have either physical or functional obstruction of the bladder (Woolf et al, 2019).

The urethral obstruction malformation complex hypothesis postulates that the atrophy of the abdominal muscle wall is due to the extreme extension of the bladder and other components of the urinary tract, which would also impede the descent of the testes in boys. This hyperextension is thought to be caused by a transient blockage or obstruction of the urethra (Samal and Rathod, 2015).

The mesodermal defect hypothesis states that during development, interactions between the intermediate and the lateral plate mesoderm – the developmental origin of the abdominal wall as well as the urogenital sinus ridge – fail to coordinate properly resulting in the multisystem defect seen in PBS (Straub and Spranger, 1981).

There is an association between chromosomal rearrangements and PBS. This often involves many genes, which would be expected for a complex and multisystem disorder. PBS has been linked to chromosome deletion syndrome 17q12 (Granberg et al, 2012), trisomy 21 (Amacker et al, 1986) and deletions in the long arm of

chromosome 6 (Fryns et al, 1991). No single gene is common to all cases of PBS, but several are reported to be prevalent in multiple cases.

HNF1 β is a transcription factor involved in mesodermal development and its expression is present throughout multiple organ systems and has been identified in multiple cases of PBS where the gene has been deleted or otherwise altered (Granberg et al, 2012). Boghossian *et al.* in 2018 carried out a study to identify pathogenic copy variants in PBS cases, and identified the genes *BMPR1B*, *STIM1*, *NOG* and *MYOCD*. Both *BMPR1B* and *NOG* are transcription factors involved in the BMP signalling family, which is extremely important in mesodermal patterning during development, as well as skeletal muscle cell differentiation (Danesh et al, 2009, Costamagna et al, 2016). *STIM1* also has a role in skeletal muscle differentiation (Stiber et al, 2008), and *MYOCD* is a master regulator of smooth muscle expression and is expressed in both the bladder and the ureters as earlier described (Caubit et al, 2008).

Treatment options for PBS vary according to the symptoms present in each patient but most children with the syndrome undergo corrective surgery. The most common is to correct undescended testes, but patients also usually undergo some form of abdominoplasty to reconstruct the abdominal defect caused by improper muscle development. Nearly half of patients will require vesicostomy, to create an alternate outlet for the bladder to drain. Ureteral reimplantation using the bladder wall as an alternate valve to prevent reflux into the kidneys is also common. Around 20% of patients will also require kidney transplants (Seidel et al, 2015).

1.2.4 Gene Therapy

Gene therapy is a methodology where nucleic acids are introduced into a cell in order to correct or compensate for a genetic fault or abnormality within the genotype of the cell. This can be in the form of replacement of a gene that is faulty or lacking, or suppression of a gene which is expressed and is creating harm. The earliest gene therapy studies involved orphan diseases where there were few alternative treatments, such as Leber's congenital amaurosis and X-Linked Severe Combined Immunodeficiency, among others (Sharif et al, 2017, Cavazzana et al, 2016). Increasingly, gene therapy is being considered as an option for more widespread diseases such as cancer and heart diseases rather than only rarer heritable disorders (Matkar et al, 2017).

Several gene therapies are currently approved for use in treating human diseases, and the majority of those in clinical trials are targeted towards cancer treatments (Lam et al, 2013). Another example which has been met with clinical success is gene therapy of the retina. Retinal dystrophies caused by mutations to the gene RPE65 have been successfully treated using an AAV gene therapy restoring the full function of the gene (Bainbridge et al, 2008). This either maintained or improved visual function in patients with a disease which normally results in a debilitating loss of sight, with few reported side effects (Bainbridge et al, 2008). Follow up studies on the same patients in subsequent years reported still few adverse side effects but in many cases the improvements to retinal sensitivity were either modest or were only transient (Bainbridge et al, 2015). Studies in animal which has informed dosage and the expected improvements in retinal function did not completely correlate with the effects observed in humans (Bainbridge et al, 2015). This demonstrates that there is still some way to go in the refinement of these gene therapies and the care which must be taken when directly extrapolating results from animal models into humans

Gene therapy still faces many obstacles to being accepted into widely used medical practise. Some initial trials in humans resulted in vector-related leukaemia in some patients (Cavazzana et al, 2016). This has meant that one of the most important factors in gene therapy design is the safety of the treatment. Advances in vector

generation in recent years has made significant strides in both the safety and the efficacy of gene therapies.

The route of delivery of the gene therapy into target cells varies between each disease being treated. Ideally a treatment would simply be injected intravenously into the patient and the vector would only act on diseased tissue or be safe enough that incorporation into non-target cells would not harm the patient. However, for the treatment to be as safe as possible, therapy is often introduced directly into diseased tissue of interest, for example into a tumour or specific organ. This can sometimes introduce complications, for example when designing therapies for cystic fibrosis patients, a vector must be able to penetrate the thick mucus and scar tissue caused by the disease (Yan et al, 2019).

For this reason, vector design is extremely important in gene therapy. The ideal vector must be non-toxic, must not produce an immune reaction, be highly efficient, so as few vector particles as possible need to be administered, and must be specific to its target tissue to limit spread (Matkar et al, 2016). Vectors can be either viral or non-viral. Non-viral vectors are regularly synthesised in the form of plasmid DNA. These vectors are increasingly attractive because they are less likely to provoke an immune reaction, as they are often packaged in liposomes or polymers (Zylberberg et al, 2017). Plasmid DNA is also not incorporated into the DNA of the cell and is instead transcribed straight from the plasmid, a safer alternative to incorporation of the DNA into the cell. Problems associated with the delivery of very large genes are also not found in non-viral vectors as the limit imposed by the size of a viral vector is not an issue. However, non-viral vectors are associated with lower transfection efficiency, early degradation and non-specificity.

Viral vectors are more established in the field. The three most common vector types are adenoviruses, adeno-associated viruses and lentiviruses. In all viral vectors the wild-type viral DNA is altered to both load the desired nucleic acid cassette and to remove the virus's ability to replicate. Adenoviruses are double-stranded DNA viruses with a genome of around 30kb (Crystal, 2014). In nature they are non-threatening viruses which infect host epithelial tissues, although they can cause

problems in immune compromised individuals. Their DNA does not integrate into that of the target cell. This can be an advantage if only a single dose of the therapy is required, for example to promote blood vessel growth to a specific site. It also presents an advantage in that not integrating into host DNA means that there is less of a carcinogenic risk with the vector. However, if long term treatment is required or if there is rapid cell turnover in the treated tissue multiple doses of the therapy would be required. Although adenoviruses have extremely good transduction efficiency, their ubiquity introduces a problem, as by adulthood most humans have some level of immunity to them. This can cause the virus to be ineffective but can also have the side effect of producing a harmful inflammatory reaction in patients. This further presents them as a good vector for single hit treatments where long-term administration of the gene is not required, but less useful for long term conditions (Crystal, 2014).

Lentiviruses are also used as vectors for gene therapy. Lentiviruses are a type of retrovirus, with a single stranded genome. They integrate their DNA into that of the host chromosome. They can also target both dividing and non-dividing cells, and once integrated, DNA is passed on to daughter cells. This makes lentiviral vectors excellent for long term therapeutics but are not as safe as vectors which do not integrate into the host DNA (Anguela et al, 2018). This is because the random insertion has the potential to lead to activation of oncogenes, causing cancer. Because of the potential dangers of injecting lentivirus *in vivo*, most current uses of lentivirus in patient trials are for use in *ex vivo* treatments where the virus is used to treat induced hematopoietic or other stem cells from the patient (Anguela et al, 2018). These are then re-administered to the patient. This has been successfully used in to treat adults with β -thalassemia (Cavazzana-Calvo et al, 2010).

Adeno-associated virus (AAV) vectors are increasingly popular choice of vector. In nature they infect humans and primates but produce minimal immune reactions. They have a single stranded genome and can package sequence up to 5kb (Naso et al, 2017). Multiple serotypes of AAV exist, and different serotypes can be utilised depending on the vector target. This is because AAV enters the cell through

interactions with carbohydrates found on the cell membrane, or through cell membrane surface receptors. As this differs from cell to cell different serotypes will preferentially target some cell types over others. This is particularly useful if a specific cell type or organ system must be targeted by the vector. For example, AAV8 targets the liver well, whereas AAV1 and AAV9 target muscle cells well (Wang et al, 2014, Kattenhorn et al, 2016).

1.2.4.1 *In Utero* Gene Therapy

Single gene disorders which are present from birth make attractive targets for gene therapy and are often the easiest to target as a single gene locus is culpable for the disease. However, the later a disease is treated the more damage is done to the body by the disease. This may present the patient with secondary disease caused by their condition throughout life even if the faulty gene is treated. A neat solution to this problem would be to treat the disease *in utero* before secondary complications have a chance to develop (Witt et al, 2017). The immune system of the fetus is also not fully mature, which presents a significant advantage for vector delivery in that less of the vector can be used to achieve the same result if the immune system does not prevent the virus from reaching cells (Chauhan et al, 2004). The fetus itself is also of a smaller size which means less viral particles would be required to reach all the cells of a specific organ or tissue. Progenitor cells are also more prevalent in the fetus and targeting these cells would negate the need to then treat the patient with subsequent injections throughout life (Witt et al, 2017).

The earliest animal models of *in utero* gene therapy were in sheep and mice (Coutelle et al, 1995). And were initially faced with problems in creating specificity in the vector. Good results in terms of the vector only targeting cells of interest were obtained in the sheep lung, but this was carried out using an invasive surgical technique which would not be appropriate in humans (Coutelle et al, 1995). The lack of specificity also created a concern in that the vector may reach the gonads and the gene therapy may reach the germ cells of the patient where it could be passed on. The difficulties have steadily been surmounted with more sophisticated vector technologies and more refined ultrasound imaging. Many current *in utero* gene

therapy strategies deliver the gene therapy through ultrasound guided injection. This was successfully carried out in mice with neurodegenerative disease caused by GBA, which in humans can be lethal in childhood. (Massaro et al, 2018). Intracranial injections of AAV to restore GBA expression restored function and allowed treated mice to live for 18 weeks where they would usually die soon after birth (Massaro et al, 2018). In humans this disease is treated in its milder forms by enzyme replacement therapy. This is not possible in more severe cases of the disease in children because the enzyme replacement therapy cannot cross the blood brain barrier. Treatment using gene therapy offers a solution to this problem as AAV vectors can cross this barrier (Eblan et al, 2005).

Haemophilia is another disorder which has shown promising results for *in utero* gene therapy (Pearson et al, 2013). Current treatments require multiple transfusions and are both time consuming and expensive. Injected gene therapy in the form of a lentiviral based vector into E15.5 fetal mice resulted in the mice still expressing the therapeutic protein over a year after injection with no immune response to either the introduced protein or the lentivirus (Waddington et al, 2004). As one of the most common developmental diseases, Duchenne's muscular dystrophy is a popular target for the development of gene therapies. It is also a promising target for *in utero* therapies because of the difficulties in targeting the many cells affected by the disorder. In the fetus there are both fewer cells in total because the body is smaller and more progenitor cells to target. One of the early barriers to development of these treatments is that the mutated gene, dystrophin, is very large. This introduced problems in that it was then difficult to find an appropriate vector which would be able to package the gene. This can be overcome by using high capacity adenoviral vectors (Reay et al, 2008), and because the injection is carried out *in utero* the normal problems associated with immune activation when injecting adenovirus would not be an issue (Reay et al, 2008). However, this still results in low levels of gene transfer to the muscles because of the large number of cells which need to be reached, even *in utero*.

There are still several barriers to overcome before *in utero* gene therapy can become accepted practise in treating human disease. This is both in the practicality of the treatment and in terms of ethical considerations. For gene therapy in the fetus to go ahead there must be a clear rationale for there being a greater benefit to treatment *in utero* as opposed to after birth, and for it to both be safe for the mother and for the developing fetus. There is now a large body of work demonstrating both effectiveness and safety *in utero* in a large variety of animal models (Almeida-Porada et al, 2019) as well as evidence in small children who have successfully been treated using gene therapy (Mendell et al, 2017). Stem cell therapies have also been successfully administered *in utero* to treat various diseases. This is where donor cells are grafted into the fetus, most successfully to treat X-linked severe combined immunodeficiency through implantation of paternal bone marrow. Introducing this tissue *in utero* reduces the risk of graft rejection as well as treating the disorder before birth and symptoms of the disease become a problem (Flake et al, 1996). *In utero* gene therapy in humans is probably not far away from being a reality. However, the safety of the mother of the fetus must first be insured, as well as the event of germline integration of the vector eliminated. This will require further refinement to therapeutic techniques as well as vector design. In terms of ethical concerns, it must also be considered that gene therapies may not completely resolve the disease being treated and may result in the birth of children who will present with morbidities throughout life, where otherwise a pregnancy may have been terminated. This would result in an extreme burden to the families involved as well as potential suffering for the child receiving treatment, so full and informed counselling must be provided for patients before it would be possible for trials to go ahead in humans (Almeida-Porada et al, 2019).

1.2.5 Summary

Congenital disorders of the lower urinary tract are one of the leading causes of end-stage renal failure in children. The three commonest diseases are posterior urethral valves, urethral atresia and prune belly syndrome. These three disorders primarily affect boys. They can have diverse phenotypes and genetic etiology but share the fact that the bladder is either non-emptying due to physical or functional obstruction, and that the kidneys have reduced functionality due to reflux of urine.

Treatment options are limited to surgery, which does not resolve all the symptoms of these disorders (Clark et al, 2003). Patients can have complications throughout life with problems such as incontinence and repeated urinary tract infections and will often require kidney transplants. This creates an enormous economic burden on healthcare systems, as well as the emotional burden on families. Both a greater understanding of the etiology of these diseases in addition to novel treatment options are required going forward. A treatment option which may be used in the future for these diseases is *in utero* gene therapy utilising viral vectors. It has been used successfully in multiple animal models to treat various diseases and may be applied to lower urinary tract malformations in the future. Lower urinary tract malformations are an inviting target for gene therapy, as early intervention may save damage to the kidneys, which is the main cause of problems for patients later in life. A valuable tool for investigating these diseases and their possible treatments is the use of animal models.

1.3 Models of Lower Urinary Tract Obstruction

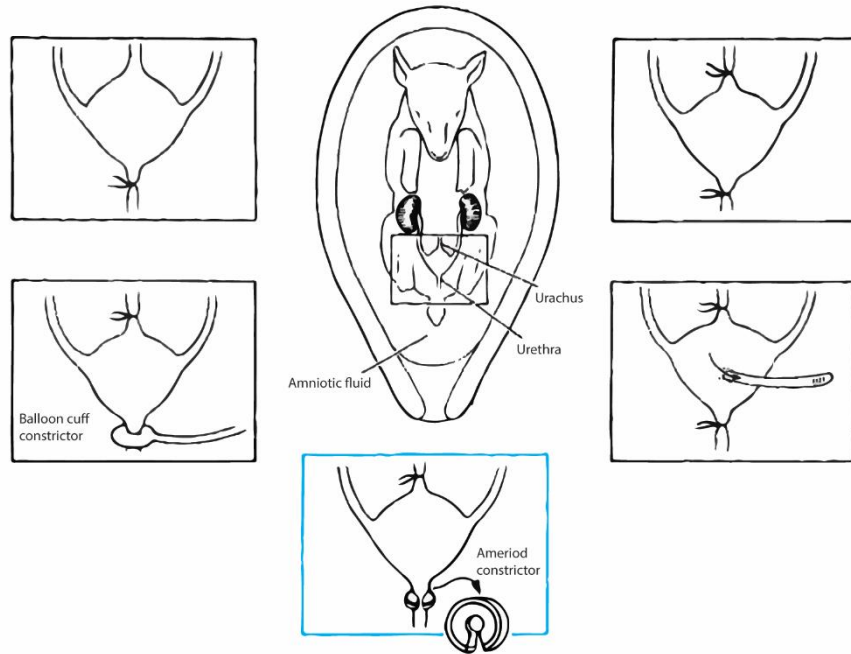
Animal models are a useful tool for both bettering our understanding of human diseases and investigating new treatments for disease. The animal models for lower urinary tract obstructions, however, are relatively poorly developed. The first models were induced obstruction models in large animals, which then progressed into surgically induced obstruction models in rodents. Only relatively recently have genetic animal models been generated for modelling lower urinary tract obstructions.

1.3.1 Sheep models

The earliest models for lower urinary tract obstruction were created in sheep through the generation of a surgical obstruction *in utero*. *In utero* there are two outlets for urine to exit from the bladder. The first and most obvious is the ureter, the second is an embryonic structure called the allantois. This outlet closes during gestation, and its fibrous remnants are referred to as the urachus. Patent urachus is where the urachus remains open due to disruption of its closure and urine continues to drain through this outlet.

Several methods for generating lower urinary tract obstruction in sheep have been tested (**Figure 9a**). If the urethra was ligated prior to the closure of the allantois, the embryos developed patent urachus and urine simply drained through it, resulting in no obstruction symptoms. This highlights the importance of the urachus in providing protection from obstruction. If both the urethra and urachus were blocked, then obstruction symptoms were much more severe and resulted in very high mortality *in utero* (Harrison et al, 1982). The best method for creating surgical obstruction which recapitulates human lower urinary tract obstructions was ligating the urachus and then gradually closing the urethra with a constriction device with slowly closes during gestation. Fetal lambs with induced obstruction using this method present with megacystis, hydroureter, hydronephrosis and pulmonary hypoplasia, all of which are common symptoms of children with lower urinary tract obstructions. Ovine gestation is around 150 days, and obstruction procedures were typically carried out between 90 and 110 days of gestation (Harrison et al, 1983).

a



b

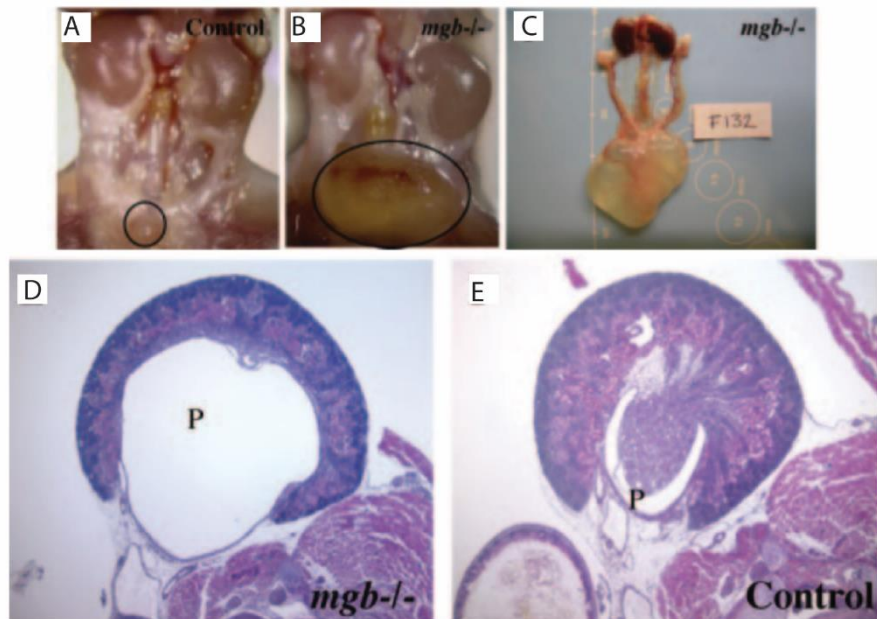


Figure 9a. One of the first successful models for lower urinary tract obstruction was in the sheep. Several surgical methods were used to initiate obstruction but the most similar to the disease phenotype in humans was generated by tying off the urachus and then using an ameriod constrictor to slowly close of the urethra. Figure adapted from Harrison et al, 1983. 9b. The megabladder mouse model is a genetic model of lower urinary tract obstruction. Compared with a wild type mouse (A) the megabladder mouse has a grossly extended bladder (B and C) in addition to hydronephrosis of the kidneys. This can be more easily seen using histology (D) the renal pelvis is extremely enlarged compared to the wild type (E). Figure adapted from Singh et al, 2007.

In experiments to relieve obstruction in the fetal lamb model, fetal cystostomy was carried out and the condition of these lambs was markedly improved compared with lambs where the obstruction was not relieved. All the lambs where the obstruction was not relieved died due to poorly developed lungs, in addition to the defects to the kidney and bladder (Harrison et al, 1982). The hypothesis is then that obstructions should be relieved when possible in human cases of disease. While this does improve the symptoms of oligohydramnios in humans, it does not improve outcome for regaining renal function; children still have problems with gaining continence which can persist throughout life (Bilgutay et al, 2017).

The histology of the renal dysplasia present in the fetally obstructed lambs was very similar to that seen in humans with obstruction; symptoms include disorganisation of tubular structures and fibrosis (Glick et al, 1983). The obstruction must be initiated early in development however, as initial experiments inducing late stage obstruction failed to create renal dysplasia (Tanago, 1972). There is an increase in size of the bladder, but also an increase in cell death in the smooth muscle and lamina propria layers, consistent with the remodelling which takes place during hyperplasia (Thiruchelvam et al, 2003).

Sheep models can also be used to compare the temporal effects of obstruction. The initial obstruction models used by Harrison *et al.* (1983) were severe in comparison with humans with lower urinary tract obstruction; the kidney phenotype is more similar to prune belly syndrome than it is to posterior urethral valves, which is a much more common disease. In a study where fetal lambs are only obstructed for either 9 or 30 days the size of the bladder increased with both lengths of obstruction time; the bladder structure was very different. With a longer obstruction period there is a much thicker smooth muscle wall layer with much higher collagen content. The bladders obstructed for 9 days had a thicker smooth muscle wall but unchanged contractility levels; some of the kidneys in these animals were also cystic (Farrugia et al, 2006).

Sheep models are useful tools for generating artificial obstruction models, but they also have a number of limitations. They are extremely expensive animal models to

use, and our understanding of the genetics and the laboratory reagents, such as antibodies, that are available for use in sheep is not as well developed as those for more widely used animal models such as rodents, rabbits and chicks. They also have an extremely long gestational period compared with mice. The model that is created also does not perfectly mirror all the characteristics of lower urinary tract obstructions in humans, particularly in response to the relief of the obstruction.

1.3.2 Rodent obstruction models

Surgically induced obstruction models have been created in rodents such as guinea pigs, rats and mice. Due to the small size of all these animals however, it is not possible to carry out surgical obstructions *in utero*, so they must be carried out after birth. In mice kidney development carries on until 7-10 days after birth, unlike in humans where kidney development finishes by week 34, so obstructions could still be carried out and an effect be seen on the developing kidney, but the animals are still too small for the procedure to be easily carried out.

When obstructions are created in adult rodents, some similar phenotypes can be seen to human lower urinary tract obstructions. In guinea pigs when a surgical obstruction is created there is an increase in fibrosis in the bladder and a reduction in the number of nerves innervating the muscle layer (Williams et al, 1993). In another study guinea pigs are also used to measure changes in glycogen content in the bladder muscle wall after obstruction, in order to use this measure as a biomarker of how well the bladder recovers after the obstruction is relieved. With increased bladder function there are increased glycogen levels (de Jonge et al, 2008).

Mice also show similar phenotypes to humans with lower urinary tract obstruction. When mice are obstructed at 6 weeks old, as with other studies, bladder weight increases, as does collagen deposition in the smooth muscle layer. The bladder's contractile ability *in vitro* is also reduced (Iguchi et al, 2016).

Many induced obstruction models in the literature are performed on adult mice and then used to model prostatic hyperplasia – which causes partial bladder outlet obstruction, but in humans only affects adult men later in life. Some of the symptoms

of congenital urinary tract obstruction and prostatic hyperplasia are similar; there is hypertrophy of the smooth muscle cells of the bladder wall, and an increase in bladder size, increased inflammation of the bladder wall (Michishita et al, 2015). Animal models of this kind of obstruction are usually generated in rats, and these models can be very useful in both investigating the immune and inflammatory response to obstruction, and in ascertaining how membrane receptors change in response to obstruction (Zeng et al, 2015). These models can be used to learn a great deal about obstruction and can be used to infer the responses that might be present in patients with congenital urinary tract obstructions, however, because the obstruction has been performed in adult mice and is being used to model a disease which typically arises in old age in humans, they cannot be used as models of lower urinary tract obstructions in children.

Surgically induced obstruction models in small mammals are useful as they are much cheaper and have more reproducible results than large animals such as sheep. The tools available with which to study the animals are much more sophisticated, yet there are limitations in that the animals small size prevents surgery during early development. This means that it is impossible to be able to truly study the development of both the bladder and the kidney properly during obstruction using an induced model in rodents.

1.3.3 Megabladder mouse

One of the only genetic mouse models of lower urinary tract obstruction is the megabladder mouse model (**Figure 9b**). It was first reported by Singh *et al.* in 2007, and is caused by the transgene MLR19, a bovine sodium myoinositol co-transporter gene which can be induced to cause translocations through an α A-crystallin/ α B-crystallin promoter. This transgene inserts into chromosome 16 and causes about 1 megabase of DNA to be translocated to chromosome 11. Mice homozygous for this translocation present with a grossly enlarged bladder *in utero*, hydronephrosis, hydroureter and renal failure. All other organ systems are normal and mice which are heterozygous for the translocation show no disease phenotype. The insertion point of the translocation on chromosome 11 is around 500kb upstream of *Myocd*, which

could be the cause of the phenotype observed through disruption of long-range enhancers (McHugh, 2014).

Phenotype onset is at E15, and the bladder presents with a severely reduced smooth muscle wall and disorganisation of the lamina propria; the urothelium, however, appears normal. At E15 the level of smooth muscle expression is severely reduced, with small areas of differentiated smooth muscle interspaced with areas of undifferentiated mesenchyme; on staining PTCH deposition was normal, but SRF was absent, showing that the disruption to the signalling pathway is downstream of *Patched*. There are also greatly increased levels of apoptosis in the presumptive smooth muscle cell layer of megabladder mice compared to wild-type controls.

Expression profiling analysis was carried out for chromosomes 16 and 11, and several genes were found to be overexpressed in megabladder mice compared to wild-types. Of these genes, *Urp* showed a four-fold increase. When smooth muscle cells in culture were treated with URP it resulted in a decrease in cell growth. Expression profiling also identified over 50 dysregulated genes which are downstream targets of the *Myocd-Srf* signalling pathway, showing the extent to which normal smooth muscle growth is affected. *Myocd* and *Srf* themselves were downregulated; other smooth muscle regulatory pathway genes, such as *Gata6*, were upregulated, suggesting that compensatory mechanisms may be activated. No change was found in *Shh*, *Ptch*, *Smo* or *Gli* genes, suggesting that the genes affected by the translocation are downstream of these factors (Singh et al, 2008).

In the megabladder mouse kidney the renal pelvis is largely distended, and the parenchyma is compressed. The extent of the renal injury is directly related to the extent of hydronephrosis; the extent of hydronephrosis is variable between animals. Markers present in diseased kidneys such as α SMA and TGF- β 1, both indicators of fibrosis and increased collagen deposition, show the extent of renal damage on staining and closely resemble the expression pattern seen in paediatric hydronephrosis (Ingraham et al, 2010). One of the first signs of hydronephrosis in megabladder kidneys is increased expression of uroplakins in the renal pelvis; this could be a protective mechanism for the kidney as the renal pelvis expands and the

membrane becomes more impermeable in order to store urine and prevent it from backflowing into the kidney. There also appears to be a 'pop off' mechanism which mimics that seen in humans with lower urinary tract obstruction, in that one of the kidneys will have much more severe hydronephrosis than the other, and the urothelium will remodel so that the renal pelvis in this kidney acts as an additional area for urine storage in a presumed effort to prevent further damage to the kidneys (Becknell et al, 2013).

As a response to the hydronephrosis present in the megabladder mouse model, the kidney reacts in several ways to ameliorate the deleterious effects of impaired urine drainage out of the organ. This involves three mechanisms. Firstly, TGF β 1-mediated fibrosis in the kidney, evidenced by increased α SMA expression and increased collagen deposition. Secondly, increased retinoic acid signalling, which delays kidney maturation and allows the organ to maintain a more plastic, developmental phenotype to better respond to disease. Finally, increased steroid hormone metabolism to decrease the inflammatory response in the kidney (McHugh, 2014). While these mechanisms help to retain some kidney function, they do not totally stop the progress of the disease and particularly the increased collagen deposition and fibrosis can cause problems for kidney function later in life.

The urothelium of both the bladder and the renal pelvis is heavily remodelled during disease progression in megabladder mice. MiR-205 is a specific regulator of epithelial remodelling and is found at higher levels with increasing disease severity in megabladder mice; it can also be found in the most severely dilated tubules of the kidney itself, which does not occur in wild-type controls (Wilhide et al, 2016). The cells of the urothelium also increase in number and the intensity of uroplakin expression increases. If uroplakin 1b is knocked out then the severity of the phenotype is greatly increased (Jackson et al, 2018).

After birth male mice do not live beyond four to six weeks of age and die from renal insufficiency; female megabladder homozygous mice have much slower disease progression and can live for up to a year and breed. Male mice can be rescued by diverting the urine by performing a cutaneous vesicostomy, which prevents further

damage to the kidneys (Carpenter et al, 2012). The more severe phenotype in male mice could be due to the longer urethra. Studies have also found, however, that the kidneys of male mice differentially express sexually dimorphic transcripts, indicating that the kidney takes on a more 'female' expression profile in response to disease. These transcripts are significantly centred around steroid hormone metabolism, indicating that a female transcriptome provides more protection from the adverse effects of inflammation during renal pathogenesis (Becknell et al, 2013, McHugh, 2014).

Megabladder mice have also been crossed with *Myocd* knock-out mice. *Myocd* knock-out is embryonic lethal, but heterozygotes are normal and can breed. Megabladder homozygotes which are also heterozygote *Myocd* knock-outs still retain the megabladder phenotype but in addition have patent ductus arteriosus. The ductus arteriosus is an embryological structure which connects the main pulmonary artery and the proximal descending aorta and allows the lungs to be bypassed by the majority of the blood *in utero*. Normally this duct closes at birth, and McHugh (2014) postulates that this failure to close with the additive effect of *Myocd* heterozygous knockout as well as megabladder homozygous genotype is because the cells contributing to the ductus arteriosus share a *Myocd* regulatory pathway.

1.3.4 *In Vitro* Models

Many *In vitro* models of the bladder as a whole or of its individual components have been generated both to investigate its development and disease.

Whole bladders from adult rabbits and rodents can be grown *ex vivo* to model cancer cell invasion (Estrada et al, 2006). Segments of human bladders taken from cancer biopsies have also been grown to model cancer development (Knowles et al, 1980). In terms of embryonic development mouse bladders have been used to model the effects of vascular endothelial growth factor on the developing bladder (Burgu et al, 2006, Burgu et al, 2007). These models can work well to model the bladder in development and disease but are limited in that they cannot completely mimic the environment of the bladder *in vivo*. The explants can only be grown for a limited amount of time before deformation to the membrane they are grown on occurs, and

if larger tissues are grown this also risks cells at the core of the tissue becoming hypoxic (Burgu et al, 2006, Fry, 2004). They also do not incorporate the distension and contraction of bladder tissue which occurs *in vivo* as part of bladder filling and voiding (Liaw et al, 2018). It is also difficult to effectively administer treatments to whole organ cultures as cells at the centre of the organ are less likely to receive therapies administered to culture medium.

To overcome this problem cells can be dissociated, then reaggreated and grown as organoid cultures. These have proven extremely useful in bladder cancer research. Historically there has been a paucity of culture models for bladder cancer, and three-dimensional urothelial cultures have been used as a model system from specific cancers taken from patient biopsies. In the future these could be used for testing therapies which would be specific to the tumour biopsied (Mullenders et al, 2019, Lee et al, 2018). Other strategies have also been pursued, such as organ on a chip technology, which could also be used for large scale testing of drugs or other therapies (Vasyutin et al, 2019). These organoid models present a significant advantage in that they maintain the cell to cell interactions integral to the bladder in both health and disease (Yoshida et al, 2016).

It is technically challenging to achieve similarity to the *in vivo* environment in the bladder *in vitro* as a whole organ. To surmount this problem, and to model specific structures in more detail, separate components of the bladder are often grown *in vitro*. Bladder physiology has long been modelled using explant cultures, which can be used to measure contractility and the changes to the bladder's ability to contract given various treatments (Fry, 2004, Malysz, 2014). This is generally carried out using rodent tissue. As with whole organ culture, the growth of these bladder explants can be limited by larger sized tissues becoming hypoxic, so culture is generally only short term. However, this is balanced by the cells' ability to better maintain their normal phenotype when grown as explants rather than as dissociated cells. When grown as explants bladder smooth muscle cells are better able to maintain their contractile phenotype and their generation of extracellular matrix is also more similar to that found *in vivo* (Wang et al, 2012).

As well as *ex vivo* culture models of bladder smooth muscle there are also many culture systems for the urothelium. The urothelium is a multilayer structure where cellular signalling between urothelial layers is essential for function, so there is considerable benefit to growing these cells as a three-dimensional structure. While these cells can be grown in culture as a monolayer, cells grown in this manner may not necessarily recapitulate the functional phenotype of urothelial cells (Turner et al, 2008). They can also be grown as multilayer structures, and present with considerably more similarity to the permeability and electrical resistance of the urothelium *in vivo* (Cross et al, 2005). This ability for the urothelium to grow *in vitro* in a multilayer structure with more similarity to the way that the cells would behave *in vivo* demonstrates that the urothelium may in some circumstances be able to self-organise to form the pseudostratified layers essential for urothelial function. This is apparent when the urothelium is grown as an organoid culture in the presence of urine, as it would *in vivo* (Horsley et al, 2018, Bouhout et al, 2015). These organoid models have many applications for studying disease, such as bladder cancers or urinary tract infections (Horsley et al, 2018, Mullenders et al, 2019).

While many of these *in vitro* models make extremely useful tools for investigating disease, less *in vitro* models are used to understand development, or the diseases associated with affecting children. While some of the diseases that have already been investigated using organ or organoid models can present in children, research is often in adult tissue, either from rodent samples or from adult human biopsies. Part of this is due to the availability of material. Human biopsies are much more readily obtained from adults and the small size of fetal or early postnatal rodent tissue makes culture of whole organs and generation of organoids technically challenging. Some studies have used fetal tissue however (Burgu et al, 2006), and further research into this area will be vital for treating bladder disease in children as equivalence between adult and child tissues cannot be assumed.

1.3.5 Summary

Currently the only available animal models for lower urinary tract obstruction are inducible surgical models, the megabladder mouse model and conditional knock-out models. *In vitro* models of both the whole bladder and its constituent parts have also been developed.

Surgical models are a useful resource and some of the first experimental obstruction models were created in these animals. However, they are easiest to perform in sheep and other large animals, which makes them prohibitively expensive and highly time-consuming owing to longer gestational periods than those in mice.

The megabladder mouse model is a genetic model of functional lower urinary tract obstruction. It accurately recapitulates the kidney phenotype seen in humans with obstruction and is a powerful tool for both investigating the progression of renal disease and in the search for future therapies.

Inducible knock-out models will be a valuable resource in the future as our ability to genetically manipulate mouse genetics improves. However, there is currently no way to selectively knock-out *Myocd* or other genes of interest in smooth muscle exclusive to the urinary tract. Going forward, more animal models are required in order to properly investigate lower urinary tract obstructions and inform future therapies. This is true especially as the disorders urinary tract obstruction models hope to mimic are genetically and phenotypically diverse, so more animal models will greatly benefit our understanding of disease progression.

1.4 T30H mouse model

The T(2:11)30H homozygote mouse model (T30H mouse) was generated through triethylenemelamine (TEM) mutagenesis experiments. TEM inducible mutagenesis creates translocations in the gametes of treated mice (Cattanach, 1957). The T30H mouse has a balanced, heritable translocation between chromosomes 2 and 11, and was originally created in experiments designed to investigate the role of maternal and paternal imprinting in mice (Cattanach et al, 1985). The chromosomes involved were recognised as being chromosomes 2 and 11 through unpublished chromosomal condensation studies previously carried out at Harwell when the mice were first produced (**Figure 10**); however, this is technically difficult to perform for mouse chromosomes, so is not a valid genotyping tool in most laboratories due to the technical difficulty. The skill has been lost in most laboratories due to the widespread use and ease of genotyping using PCR.

T30H heterozygote mice present as normal, with no detectable defects to any organs systems and mice achieve normal life spans. T30H homozygotes die soon after birth with a highly distended bladder and severe hydronephrosis to both kidneys (**Figure 11**). All other organs systems are normal, including other systems with smooth muscle tissue, such as the gastrointestinal system and the circulatory system.

Only the chromosomes involved in the translocation and not the actual chromosome break points were known prior to the beginning of my PhD project, so in previous work on the mouse model there was no way of carrying out a diagnostic PCR on affected animals to ascertain genotype. Therefore, breeders at Harwell crossed the T30H mouse strain with mice containing a deletion to the gene *Gdf5*, a gene on chromosome 2 close to the translocation which causes brachypody in affected individuals (**Figure 12**). Offspring of T30H mice crossed with brachypody mice must bear two intact and untranslocated versions of chromosome 2 and therefore must be wild-types; this provides an easy way to tell which mice in a colony do not bear a translocation and should not be bred from. The brachypody mice selected by breeders at Harwell to cross with T30H mice also have a different coat colour to make it easier to tell which mice wild-type from a very young age.

T30H mice are an extremely useful model for lower urinary tract obstructions, as the kidney phenotype is similar to that seen in humans with cases of lower urinary tract obstruction. Previously, the mouse model has not been extensively studied and its potential as a disease model has not been fully taken advantage of. In order to use the animal model to its fullest potential, the model needs to be characterised and the genetic source of the defect discovered as part of this PhD.

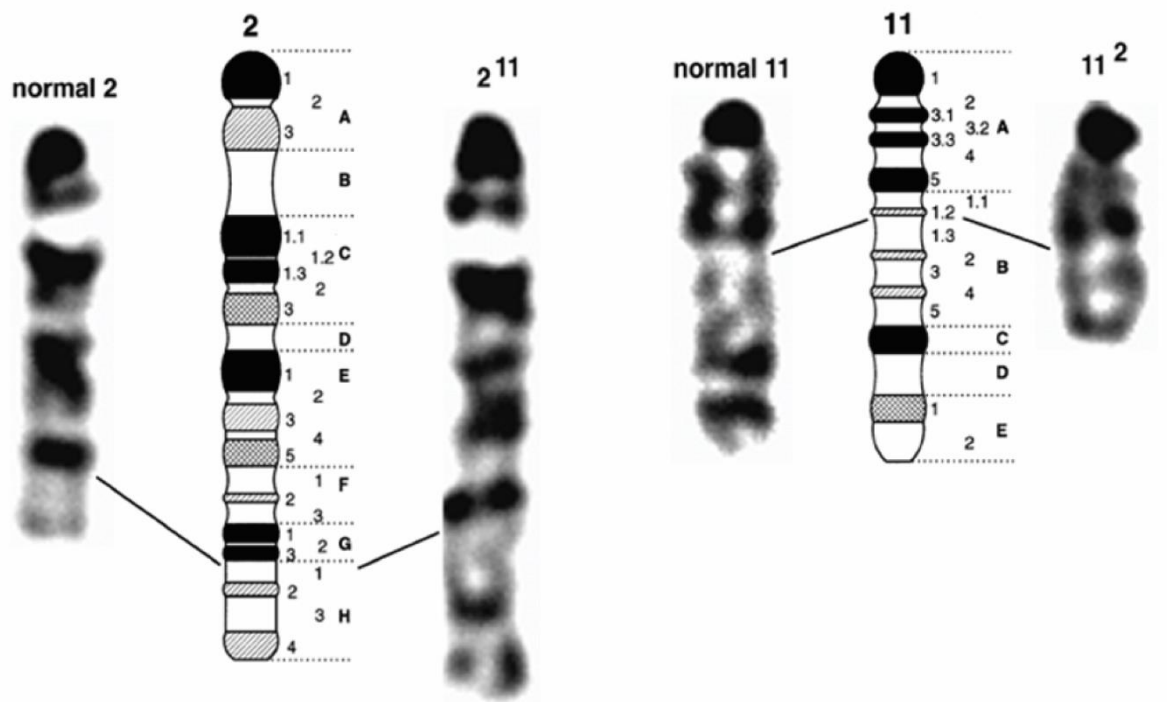
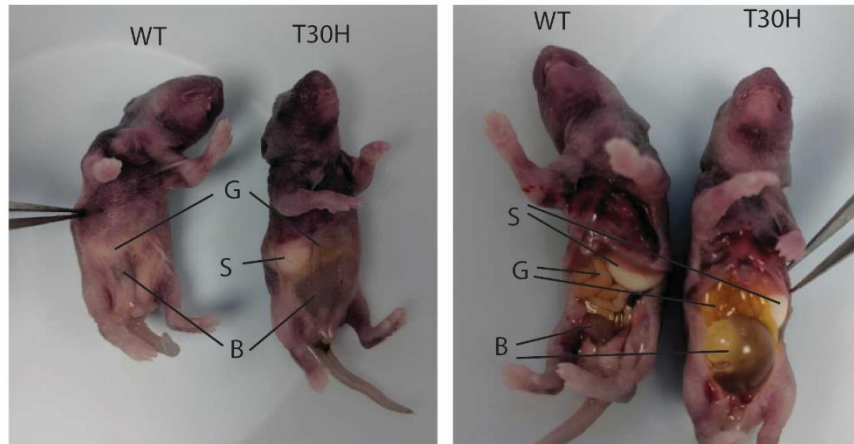


Figure 10. Karyotyping is a rarely used form of genotyping because of its technical difficulty. Early investigations into the T30H mouse model used karyotyping to find the chromosomes between which the translocation has taken place. The translocation has taken place between chromosome 2 and 11, making chromosome 2 longer and chromosome 11 noticeably shorter. This technique can also be used to ascertain approximate translocation points according to banding pattern, although this does not give precise locations. Karyotyping experiments carried out by Ted Evans and Colin Beechey.

A



B

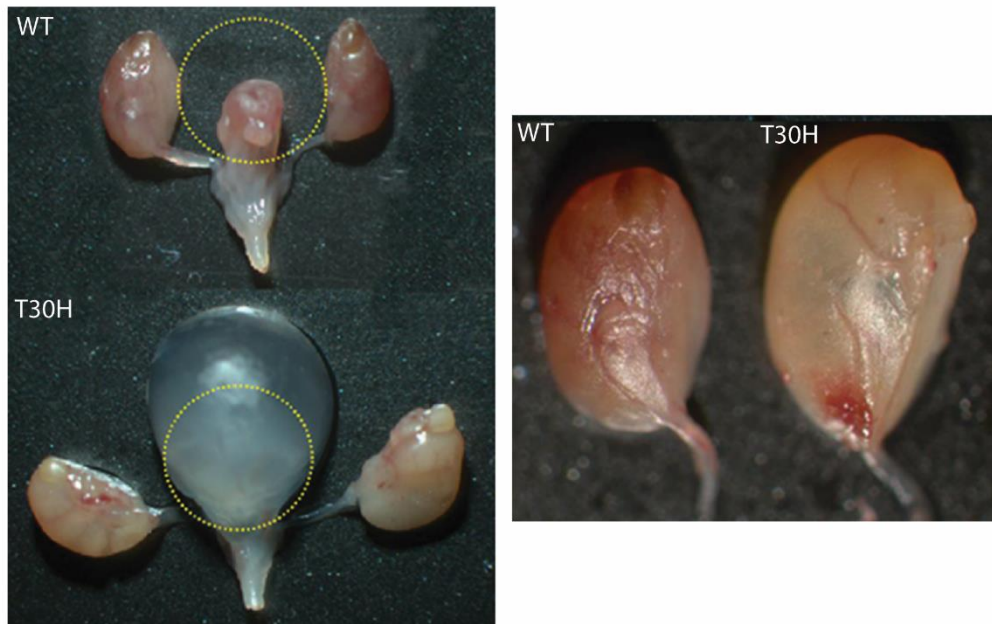


Figure 11A. T30H mice (left of all images) are usually relatively easily diagnosable from birth - the enlarged bladder can be easily seen through the thin abdominal skin and is a quick way to ascertain whether new-born pups have the mutation or not. When the pups are culled and then dissected the bladder in T30H mice takes up much of the abdominal cavity and has a very thin wall. B. When the urinary tract has been dissected out the bladder of T30H mice is much larger than that of a wild type littermate. Yellow circles are of the same size to offer context of the size difference between the two bladders. The hydronephrosis of the kidneys which can be seen upon sectioning can also be seen after the kidneys have been dissected - the kidneys are larger than those from wild type mice and fluid build-up can be seen as the kidneys are paler and more transparent in the T30H mouse.

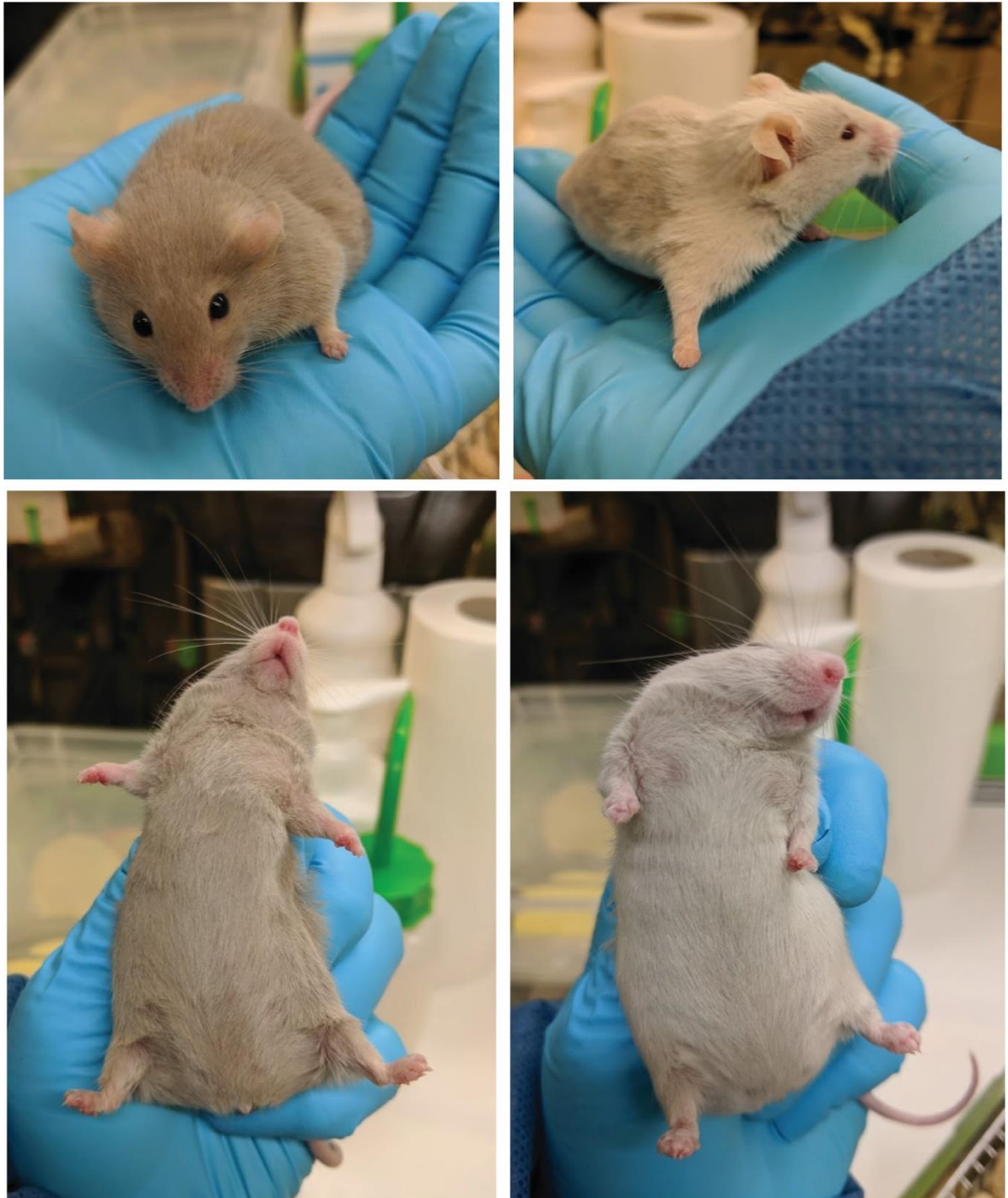


Figure 12. Two examples of brachypody mice, the mice have shortened limbs and digits and also have a different coat colour to heterozygotes. Both of these characteristics can be easily discerned from around P3 or 4, making it easy to work out which mice in a litter do not contain a translocation and should not be bred from.

1.4.1 Chromosome FISH

Prior to the commencement of my PhD project, previous lab members, (David Monk and Phillip Stainer) had carried out chromosome fluorescence in situ hybridisation (FISH) studies (**Figure 13**). This involved using fluorescently labelled tags to make one end of chromosome 2 or 11, and then sequentially marking the opposite end of the chromosome with another tag, which is 'walked' down to meet the other chromosome. In the case of T30H mice the tag will switch to labelling the other chromosome after the translocation point. This confirmed the location of the translocation and narrowed down the area in which the exact position of the translocation must be. It confirmed the location down to a region of about 1 megabase on both chromosomes 2 and 11.

1.4.2 Comparative Genomic Hybridisation Study

A comparative genomic hybridisation study was also carried out (**Figure 14**). This was funded by Kirk McHugh of Ohio State College of Medicine, samples were supplied by our lab and then sent for commercial analysis by Kirk McHugh. Comparative genomic hybridisation is a technique used to analyse the number of copy variants between two related samples. When translocations take place, they are often in areas with a high number of repetitive DNA elements (Kasai et al, 2018), so analysing areas of high copy number is a good way of finding presumptive regions for chromosome translocation points. Although several sites were found, subsequent PCRs to attempt to confirm them as translocation sites failed to generate any positive results.

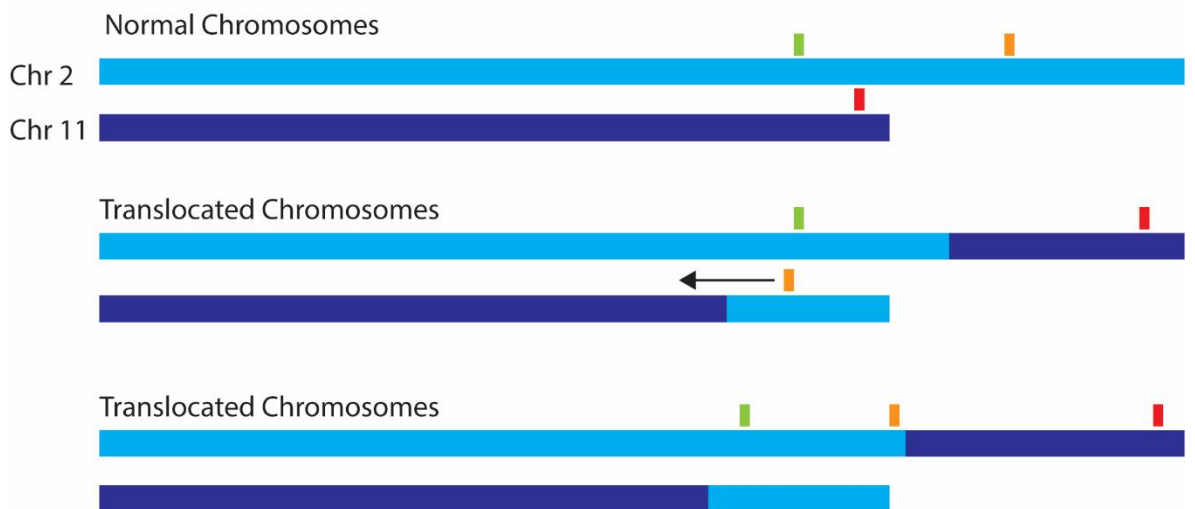
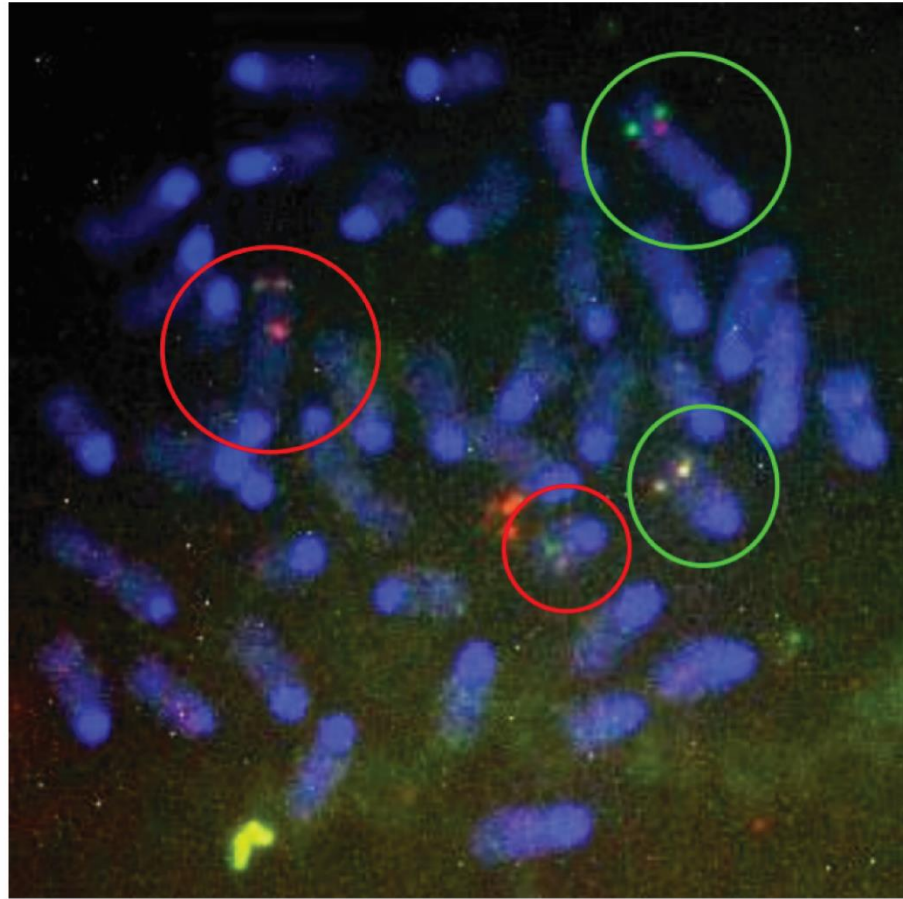


Figure 13. Chromosome FISH (Fluorescence in situ hybridisation) was initially used to narrow down a prospective area in which the translocation has taken place. Fluorescent probes are bound at different locations on translocated chromosomes. Two of the probes (Green and red in the example above) are fixed, one on the end of one of the translocated chromosomes and one much further down the other chromosome. The third probe is moved down the arm of the chromosome upstream of the translocation point. As the probe crosses the translocation point then all three fluorescent probes will be on the same chromosomes when imaged. The stretch of DNA between the two probes before and after this point will contain the region in which the translocation point can be found. Chromosome FISH experiments carried out by David Monk and Phillip Stanier.

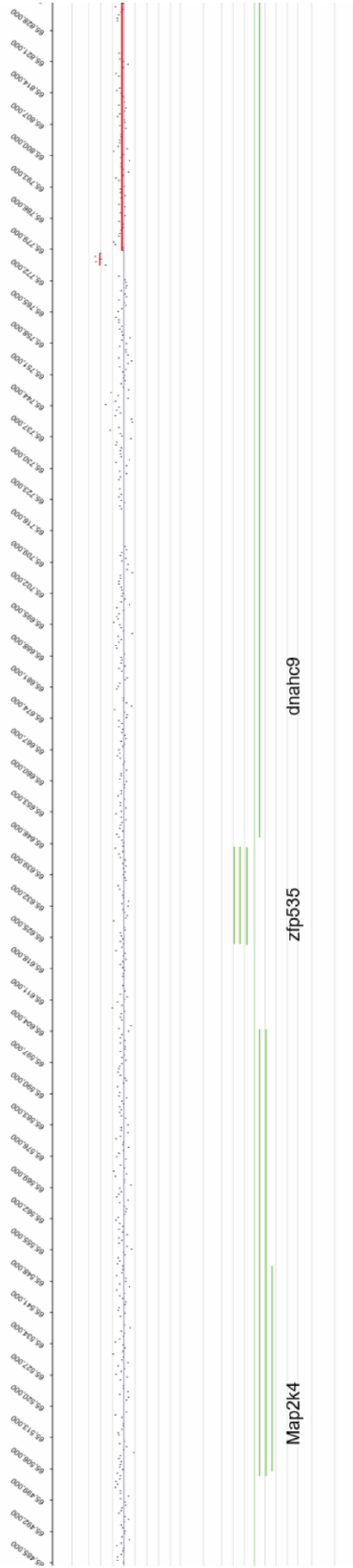


Figure 14. A comparative genomic hybridisation study was carried out to find locations in the T30H mouse genome where there are duplications. Areas where there are higher levels of duplication than normal are indicative of translocations having taken place. There was a prospective area identified within the gene Dnahc9 but carrying out PCRs along this area of the genome did not provide any positive results in terms of the location of the translocation. Funding provided for CGH study by Kirk McHugh.

1.4.3 Summary

The T30H mouse model was first generated in TEM chemical mutagenesis experiments. It has a balanced translocation between chromosomes 2 and 11. Prior to the commencement of my PhD the T30H mouse was not well characterised and had not been used to its full potential as a model for congenital lower urinary tract obstruction.

The mouse presents with a grossly extended bladder and severe hydronephrosis of both kidneys: mice die soon after birth from renal failure. The translocation point responsible for the disease was narrowed down to a presumptive region of around 1 megabase on chromosome 11 and 2, using data from karyotyping, chromosome FISH and comparative genomic hybridisation. More precise information relating to the location of the translocation point had not been found. There was also no genotyping method, further complicating the characterisation of T30H homozygotes as there was no sure way to differentiate between them and wild-type mice aside from observation of the phenotype.

2 Hypothesis & Objectives

The T30H mouse model was generated many years ago and has been put forward as a possible mouse model of lower urinary tract obstruction. Lower urinary tract obstructions have few available treatments and are generally associated with poor outcomes for patients. The lack of treatment options means that patients are often left with debilitating symptoms throughout life, creating a huge burden for patients and their families, as well as healthcare systems. There are currently few animal models both to investigate the progression of these diseases and possible treatment options for them.

The T30H mouse has previously not been utilised to its fullest extent as an animal model of lower urinary tract obstructions, and prior to my studentship it was not known whether the mouse would in fact be an appropriate model for lower urinary tract obstructions. The T30H mouse had not been fully phenotypically characterised, and the genetic cause of the obstructive phenotype had not been uncovered.

I hypothesise that the T30H mouse models human lower urinary tract obstructions well and can be used to both investigate the genetic cause of these disorders and to investigate possible treatments for them. In order to interrogate this hypothesis my thesis has three main aims:

1. The first aim was to find the underlying genetic cause of the phenotype. Without this knowledge it was impossible to genotype the mice, making the mouse model extremely impractical. Knowledge of the genetic cause of the genotype is also necessary to investigate the genetic cause of the lower urinary tract obstruction phenotype in the mice and then to compare this with humans with the disorder.
2. The second aim was to characterise the model; T30H mice have a balanced, heritable translocation between chromosomes 2 and 11. They die soon after birth with large non-emptying bladders and hydronephrosis, despite absence of anatomical obstruction. However, changes to protein expression levels had not been fully examined through histology, and because of the lack of ability to genotype the mice it was not known how the disorder develops *in utero*.

3. The third aim was manipulation of the phenotype using gene therapy. If the genetic cause of the phenotype can be found, then the manipulation of this gene may restore function to the bladder.

3 Materials

3.1 Mice

All studies involving mice were approved by both the Home Office and the Institute of Child Health Animal Welfare committee and procedures were carried out under Home Office license PE52D8C09. In order to comply with the 3Rs (replacement, reduction, refinement), non-invasive methods, such as ultrasound scanning, were used wherever possible. Ultrasound scanning also reduces the number of animals used by identifying the number of mutants carried by a pregnant female. In another effort to minimise the number of animals culled, all wild-type mice that were generated through mating which were not of the required genotype were offered to the biological services unit for use in handling and schedule 1 training.

3.1.1 T30H Mice

T30H mice were originally generated from a male which had received TEM (triethlenemelamine) mated to a wild-type female in specific locus imprinting experiments performed at Oak Ridge National Laboratory (Roane County, Tennessee, USA). This caused a translocation between chromosomes 2 and 11. T30H mice used in this project were obtained from MRC Harwell Institute (Oxfordshire, UK), the colony was generated from frozen zygotes which were then implanted into pseudopregnant wild-type mice by staff at MRC Harwell. Heterozygotes are maintained as breeding pairs. Mice were maintained on a JU.CBA-c⁺ background. In order to boost the number of heterozygotes, however, T30H heterozygote males were also outcrossed against CD1 females. The translocations were maintained as confirmed by genotyping PCR. The T30H homozygote phenotype is passed on in an autosomal recessive fashion, both sets of chromosomes 2 and 11 must be translocated in order for there to be a phenotype. Suspected T30H homozygous mice were culled at birth using schedule 1 methods (cervical dislocation) to minimise suffering.

3.1.2 Brachypody Mice

Brachypody mice were used to cross with T30H mice in order to identify mice with no translocation. These mice contain a mutation to the gene *Gdf5*, this induces shortening of the limb bones, specifically the metacarpals, metatarsals, and basal and middle phalanges. This is visible from birth (**Figure 12**). The brachypody mice supplied by Harwell had also been bred with a different coat colour to the T30H mice in order to further distinguish them from mice bearing the translocation.

3.1.3 CD1 Mice

A wild-type outbred mouse strain, which can become inbred over time, CD1 (Charles River Laboratories, Harlow, UK), was used for all generation of primary tissue culture samples and wild-type control samples. For embryonic samples females with timed pregnancies were sacrificed at E14 for primary cell culture and at relevant timepoints for wild-type control samples. Bladders and other relevant organs were then dissected and used in further experiments.

3.2 Immunohistochemistry

3.2.1 Histology

All histology samples used in this project were fixed using formalin, embedded in paraffin wax and then sectioned and stained using DAB (3,3'-Diaminobenzidine) or immunofluorescence staining. Detailed protocols for these methods can be found in **section 4.3**.

Paraffin wax, periodic acid, Schiff's reagent, Mayer's hematoxylin solution, sodium citrate tribasic dehydrate, Phosphate buffered saline (PBS), TWEEN 20, SIGMAFAST™ 3,3'-Diaminobenzidine (DAB) tablets, Sudan black B powder and formalin were purchased from Sigma-Aldrich (Merck).

Other reagents were purchased from the following companies: ethanol 100% AR from KimiaUK, Histo-Clear and HistoMount from National Diagnostics, hydrochloric acid from Scientific Laboratory Supplies (SLS), Dako pen (hydrophobic pen) and EnVision+ system HRP labelled polymer anti-rabbit from Dako, hydrogen peroxide

from VWR, Bovine serum albumin (BSA) from Fisher Scientific (Thermo Fisher Scientific), aqueous mounting solution SlowFade gold from Invitrogen (Thermo Fisher Scientific), Superfrost plus microscope slides and microscope coverslips from Thermo Fisher Scientific.

Sections were cut from embedded tissues using a microtome, model HM 330 supplied by Microm and serviced by Optech microscopes Ltd.

3.2.2 Western Blots

Western blotting is a technique which can be used to identify protein expression of tissues or cell cultures. In this project protein was extracted from cultured cells, measured using a BCA assay, and then proteins stained for using several primary antibodies (**Figure 15**). Staining was measured by detection of the level of oxidation generated in an applied substrate to the blot by an HRP-conjugated (horseradish peroxidase) secondary antibody. A detailed protocol for this method can be found in **section 4.7**.

Trizma base, glycine, phosphate buffered saline (PBS), TWEEN 20, Ponceau S solution, sodium orthovanadate, phenylmethylsulfonyl fluoride (PMSF), cOmplete™ protease inhibitor cocktail and 2-mercaptoethanol were purchased from Sigma-Aldrich. 4x Laemmli sample buffer, mini protean TGX precast gel 4-15% 10 well comb (50µl/well), transblot turbo transfer pack mini format 0.2µm PVDF and precision plus protein westernC standards were purchased from Bio Rad.

Other reagents were purchased from the following companies: Pierce BCA (bicinchoninic acid assay) protein assay kit and SuperSigna west dura extended duration substrate, 96 well plates for BCA assays from Corning, sodium dodecyl sulfate (SDS) from Invitrogen (now Thermo Fisher), Bovine Serum Albumin (BSA) and RIPA lysis and extraction buffer from Thermo Fisher, stripping solution from Merck Millipore, Marvel dried semi skimmed milk from Premier Foods and X100 autoradiography film hyperfilm ECL from GE Healthcare.

Values for the BCA assay were obtained using Biotek synergy HT plate reader. Gels were run using a Bio-Rad PowerPac Basic or PowerPac 200, and Bio-Rad Mini-

PROTEAN Tetra System. Western blots were transferred using Trans-Blot Turbo Transfer system transfer pack purchased from Bio-Rad.

3.2.3 Antibodies

3.2.3.1 Primary antibodies

The following primary antibodies were used in this thesis. All antibodies are unconjugated, all information can also be found in **Figure 15**:

Calponin (Sigma Aldrich C2687) used for immunohistochemistry. Monoclonal antibody produced in mouse against human uterus smooth muscle extract.

Green Fluorescent Protein (GFP) (Abcam ab13970) used in immunohistochemistry and western blotting. Polyclonal antibody produced in chicken against full length GFP protein.

Keratin 5 (KRT5) (BioLegend 905901) used for immunohistochemistry. Polyclonal antibody produced in chicken against a peptide sequence derived from the C-terminus of mouse keratin 5 protein.

KI67 (Abcam ab15580) used for immunohistochemistry. Polyclonal antibody produced in rabbit against human amino acids 1200-1300.

Laminin (Sigma Aldrich L9393) used for immunohistochemistry. Affinity isolated polyclonal antibody produced in rabbit against basement membrane of Engleberth Holm-Swarm (EHS) mouse sarcoma.

Myocardin (Santa Cruz SC21559) used for immunohistochemistry. Polyclonal antibody produced in goat reactive against rat and mouse Myocd.

Myocardin (Sigma Aldrich SAB4200539) used for immunohistochemistry and western blotting. Polyclonal antibody produced in rabbit against a synthetic peptide corresponding to the internal sequence of human MYOCD that is conserved in mouse and rat.

S100 (Dako Z0311) used for immunohistochemistry. Polyclonal antibody produced in rabbit, immunogen isolated against cow brain.

Serum Response Factor (SRF) (Santa Cruz SC25290) used for immunohistochemistry. Monoclonal antibody produced in mouse raised against amino acids 209-508 of SRF of human origin

Smooth muscle alpha actin (Dako M0851) mouse anti human was used for both western blotting and immunohistochemistry. It is specific to the N-terminal synthetic decapeptide of smooth muscle alpha actin.

Smooth muscle myosin heavy chain (Dako M3558) used for immunohistochemistry. Monoclonal antibody produced in mouse against human uterine tissue.

Uroplakin IIIa (Abcam AB82173) used for immunohistochemistry. Polyclonal antibody produced in rabbit against the human C terminus of uroplakin IIIa from amino acid 250 onwards.

Antibody	Company	Product code	Species raised in	Application & concentration used
Calponin	Sigma-Aldrich	C2687	Mouse	IHC, 1:150
GAPDH	Sigma-Aldrich	G9545	Rabbit	Western, 1:10,000
Green Fluorescent Protein	Abcam	ab13970	Chicken	IHC, 1:200
Keratin 5	BioLegend	905901	Chicken	IHC, 1:200
KI67	Abcam	ab15580	Rabbit	IHC, 1:200
Laminin	Sigma-Aldrich	L9393	Rabbit	IHC, 1:100
Myocardin	Santa Cruz	SC21559	Goat	IHC, 1:100
Myocardin	Sigma-Aldrich	SAB4200539	Rabbit	IHC, 1:200, western, 1:1000
S100	Dako	Z0311	Rabbit	IHC, 1:200
Serum Response Factor	Santa Cruz	SC25290	Rabbit	IHC, 1:50
Smooth muscle alpha actin	Dako	M0851	Mouse	IHC, 1:200, western, 1:10,000
Smooth muscle myosin heavy chain	Dako	M3558	Mouse	IHC, 1:100
Uroplakin 3a	Abcam	AB82173	Rabbit	IHC, 1:200

Figure 15. Table lists all antibodies used in this thesis, including the company the antibodies were purchased from, the product code, animal the antibody was raised in and the application the antibody was used for and at what concentration.

3.2.3.2 Secondary antibodies

The following secondary antibodies were used: polyclonal goat anti rabbit HRP (P0448), polyclonal rabbit anti mouse HRP (P0260), polyclonal rabbit anti rat HRP (P0450), polyclonal rabbit anti goat HRP (P0160), rabbit pAb to chicken IgY (HRP) (ab97140), Alexa Fluor 594 goat anti mouse IgG (A11005), Alexa Fluor 594 donkey anti rabbit IgG (A21207), Alexa Fluor 488 goat anti mouse IgG (A11001) and Alexa Fluor 488 goat anti chicken IgG (A11039). All HRP conjugated antibodies were purchased from Dako, apart from rabbit pAb to chicken IgY (HRP), which was purchased from Abcam. All fluorescent secondary antibodies were purchased from ThermoFisher Scientific.

3.3 Microscopes

Microscopes used were Zeiss Axioplan and Olympus IX71. Cameras used for each microscope were Zeiss AxioCam HRC rev3 camera and Hamamatsu Orca R2 camera respectively. The objectives used in both microscopes are detailed in **Figure 16**.

Images were saved and exported as TIF files and were then labelled and analysed using ImageJ. Figures were compiled using Adobe Illustrator.

3.4 Ultrasound Scanning

T30H mice with timed pregnancies were scanned using a VisualSonics Vevo 2100 imaging station ultrasound scanner (FUJIFILM VisualSonics Inc). Mice were sedated using an isoflurane/O₂ mix, and then secured to a heated stage to retain body temperature. Isoflurane percentage for induction of anaesthesia was 5%, and then was maintained at 1-2%, with a flow rate of 0.5-1L/min. Hair was removed from the abdomen using depilatory cream (Veet, Reckitt Benckiser), and then pups were located and scanned using a VisualSonics MS-550 probe for image acquisition. This probe has a central frequency of 40 MHz, axial resolution of 40 mm, lateral resolution of 90 mm, image depth of 15 mm, and image width of 14 mm. Ultrasound gel was purchased from Anagel (Surbiton, Surrey, UK). A detailed methodology for ultrasound scanning can be found in **section 4.5**.

Microscope	Objective	Magnification	Numerical Aperture
Zeiss Axioplan	Plan-NEOFLUAR	5	0.15
Zeiss Axioplan	Plan-NEOFLUAR	10	0.3
Zeiss Axioplan	Plan-NEOFLUAR	20	0.5
Zeiss Axioplan	Plan-NEOFLUAR	40	0.75
Olympus IX71	Olympus LUCPlanFLN	10	0.3
Olympus IX71	Olympus LUCPlan FLN with correction collar	20	0.45
Olympus IX71	Olympus LUCPlan FLN with correction collar	40	0.6

Figure 16. Two microscopes were used for all images in this thesis, the details of the objectives, magnification and numerical aperture are all detailed above.

3.5 Whole-Genome Sequencing

DNA extraction was carried out using a kit purchased from Thermo Scientific (GeneJET genomic DNA purification kit). The tissue used for sequencing was from phenotype confirmed T30H homozygote brain tissue.

Preparation of the DNA library and all sequencing reactions were carried out by Dr Deborah Hughes at the UCL Institute of Neurology. Sequencing was carried out using an Illumina HiSeq 3000 (Illumina, inc. San Diego, California, USA). Library preparation kits and sequencing reagents were purchased from Illumina by Dr Hughes.

3.6 Polymerase Chain Reaction

The polymerase chain reaction (PCR) can be used to amplify primer-specific sections of DNA. This can be used as a genotyping method but can also be used to ascertain gene expression levels when it is performed using a cDNA library generated from RNA. Detailed protocols for these methods can be found in **section 4.2**.

AccuPrime Pfx SuperMix, ultrapure agarose, SYBR green SuperMix and SYBR safe were purchased from Invitrogen. *RNAlater*, EDTA, Trizma base and acetic acid were purchased from Sigma Aldrich. iScript cDNA synthesis kit and iScript reverse transcription SuperMix for RT-qPCR were both purchased from Bio-Rad. The RNeasy plus mini kit was purchased from Qiagen and the first strand DNA synthesis kit and GeneJET genomic DNA purification kit were purchased from Thermo Scientific. The Monarch DNA Gel Extraction Kit and gel loading dye, purple (6X) were purchased from New England Biosciences. SyGreen mix Lo-ROX was purchased from PCR Biosystems.

Quantification of DNA and RNA was carried out using a NanoDrop ND-1000 Spectrophotometer. Imaging of gels was carried out using Gel Doc EZ Imager purchased from Bio-Rad. The CFX96 Real-Time system C1000 touch thermal cycler for running qPCRs was also purchased from Bio-Rad. Genotyping PCRs and RT-PCRs were run using a MasterCycler ep gradient S purchased from Eppendorf. Sequencing of PCR products was carried out by SourceBioscience.

Primers were purchased from either Sigma Aldrich or Eurofins; DNA sequences are detailed in **Figure 17**. For reverse transcriptase PCR three sets of primer pairs were designed for each experiment using Primer3 software (ELIXIR), unless primers were ordered based on work carried out by other research groups. For each new primer pair used a gradient PCR was carried out using a positive control cDNA specific to the gene expression being tested.

Primer name	Company	Forward primer	Reverse primer	Annealing temperature (°C)
Ahcy	Sigma Aldrich	TGTGTGCAGACTGTACCT	AGCAGAAATGGCCTCACTCT	56.2
ASIP	Eurofins	CCAGTTGTCTTGTCTCGAC-CA	CTTTCTTTCAGCCAGGC-CAAC	60
Brachypody	Sigma Aldrich	AGGAATGTCTTTAGGTGGCC	ACTCCCCAAACTCCTCACTC	56.2
GAPDH	Eurofins	AGTCCATGCCATCACTGC-CACCCA	TCCACCACCCTGTTGCTG-TAGCCG	Any
GFP	Sigma Aldrich	AAGGGCATCGACTTCAAGG	TGCTTGTGCGCCATGATAT-AG	Any
Map2k4	Sigma Aldrich	ATCAGTGGACAGCTTGTG-GA	CAGAGCGGACATCAT-ACCCT	58.3
MY1Fa	Eurofins	ATGACACTCCTGGGGTCT-GAACAC	n/a used in combination with MY5R	58.3
MY214	Sigma Aldrich	GGATGGAAGAGAAGAG-GAAAGGAAC	CCCAGAAACCCCACTCAA-GG	52.5
MY44	Sigma Aldrich	n/a used in combination with MY214	CAGTAAGTATGTGGCTGAT-GTAGC	52.5
MY5R	Eurofins	n/a used in combination with MY1Fa	TCACGGAAGAATCCATCGGC	58.3
Myo10aqPCR	Sigma Aldrich	TGCTGTGTTGAATCCTTAGGC	GGCAATGCTTACTTCTGG-GT	54.3
Myo10aRT	Sigma Aldrich	ACCCAACAACCATTACT-TCCTGGC	CGGCTGGCATTCTCCACT-TTCAA	54.3
Myocd	Eurofins	CAAAAGCAAGGAAGGATG-GGT	TCCACCAAAGGCCT-TATTGCT	60
NonAgouti	Sigma Aldrich	GAGCTGATGCGGAGTA-GAGT	CGGTGAAGAAGCACAG-GAAG	52.5
Normal T30	Sigma Aldrich	GCTGTCCTTTTGGGGTTACA	CTGGCCAGGAATGTCT-TTAG	56.2
SRY	Sigma Aldrich	TTGTCTAGAGAGCATG-GAGGGCCATGTCAA	CCACTCCTCTGTGACACT-TTAGCCTCTCGA	60

Figure 17. All primers used in this thesis, for genotyping, reverse transcriptase PCRs and quantitative PCRs, in alphabetical order.

3.7 Cell Culture

Cell culture was used in this project as a way to facilitate the manipulation of the smooth muscle phenotype of the bladder *in vitro*, specifically by attempting to alter *Myocd* expression. Several methodologies were used for cell culture, all of which are detailed in **section 4.6**.

DPBS, Advanced DMEM/F12 reduced serum media, ITS (insulin, transferrin, selenium), fetal bovine serum, L methionine, penicillin streptomycin and trypsin EDTA were purchased from Gibco. Cell culture flasks were purchased from Corning and Falcon. Cell scrapers were purchased from VWR. Chamber slides were purchased from Thermo Fisher. Cell culture inserts were purchased from Merck Millipore. *Myocd* mouse shRNA lentiviral particles were purchased from OriGene along with associated scrambled controls.

All cells used were primary embryonic cells derived from the bladder. This tissue was collected from CD1 mice with timed pregnancies.

3.8 Biodistribution Study

Adeno-associated virus, adeno, and lentivirus were provided by Dr Simon Waddington at the UCL Institute of Women's Health (Karda et al, 2014). Viral variants were injected into CD1 mice, also by Dr Simon Waddington. Both male and female mice were used.

4 Methods

4.1 Colony maintenance

Prior to the commencement of my project a colony of T30H mice was ordered from Harwell. I then maintained and expanded the colony. Offspring that survive to birth had one of three possible genotypes, wild-type, T30H heterozygote or T30H Homozygote, in a 1:4:1 ratio. Including offspring that die *in utero*, the ratio was 1:4:1:10. The ratio group of 10 were those embryos which had unbalanced chromosomal translocations, which is incompatible to life. These embryos die *in utero* and are reabsorbed (**Figure 18**). This results in just over 60% (62.5%) of embryos being re-absorbed *in utero*. Due to this, the T30H heterozygotes can be described as sub-fertile due to the translocation. This resulted in very low litter numbers, with the maximum size observed being 5, and the minimum being 1. A litter size of 2 was the norm.

Prior to the development of a genotyping method for T30H mice by PCR, the inclusion of a deletion within *Gdf5* on non-translocated chromosome 2 was used to differentiate wild-type mice. This gene is close to the putative translocation point – if the translocation is lost then this allows it to be easily detected as no more mice will be born with brachypody (**Figure 12**). This deletion causes homozygotes with both versions of the mutated gene to develop brachypody – a shortening of the limb bones. T30H mice were outcrossed against these mice. Wild-type progeny with two copies of an intact, non-translocated chromosome 2 were homozygous for the *Gdf5* mutation, resulting in these mice having shortened limbs and digits (**Figure 12**). If mice only had one copy of this knock-out then they had a normal limb phenotype, meaning that wild-type mice had shortened limbs and T30H heterozygotes and T30H homozygote mice had normal limbs because they had at least one copy of the intact *Gdf5* gene.

In order to increase numbers of breeding heterozygotes, heterozygote males were also bred with wild-type brachypody females from the same genetic background. In these cases, half of the offspring were wild-types and half were T30H heterozygotes and could be used for breeding. The litter numbers for this genetic background were

still relatively low, however, in part because half of the fertilised eggs had unbalanced chromosome numbers and were reabsorbed *in utero*. Prior to the development of a genotyping method it was not possible to outcross T30H heterozygotes with an outbred strain of mice with higher litter numbers to increase the pool of heterozygotes. This was because without the brachypody phenotype it would have been impossible to tell the difference between wild-type and heterozygote animals.

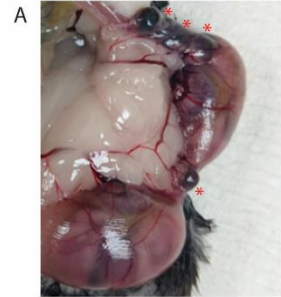
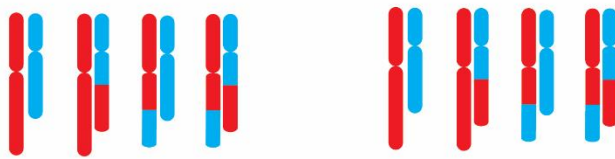
After a genotyping method was designed, T30H heterozygote males were outcrossed with CD1 female mice. Offspring were genotyped and wild-types culled. When heterozygotes from these crosses were then bred together, they still produced T30H mice with identical phenotype to non-outcrossed offspring. This was confirmed by genotyping by PCR, phenotype confirmation by dissection, and histology. Litter sizes increased slightly, with the average size being 3-4 as opposed to 2.

It was also much easier to breed a greater number of heterozygotes, as heterozygote males could be bred with CD1 females to give litters half of which were wild-type and half of which were heterozygotes. These could be litters of up to 15, so larger numbers could be generated quickly. Potential loss of the translocation was an issue but was monitored by the genotyping of every animal born. This was also consolidated by every six months sending off the purified PCR product from genotyping the heterozygous mice to be sequenced. This ensured that the translocation point was retained with the same sequence. The phenotype has been retained through all breeding generations thus far.

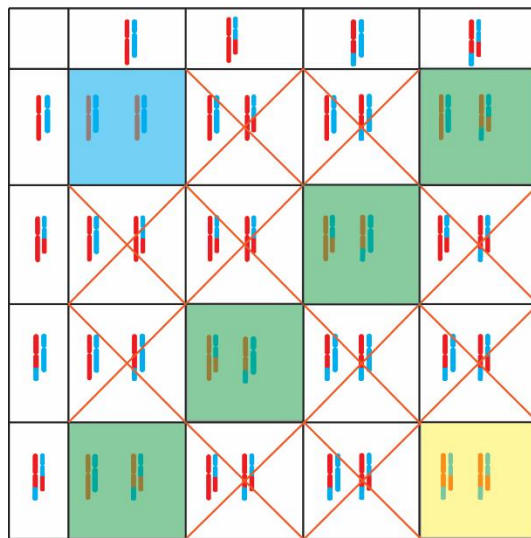
Heterozygote parent chromosome 2 and 11 genotypes



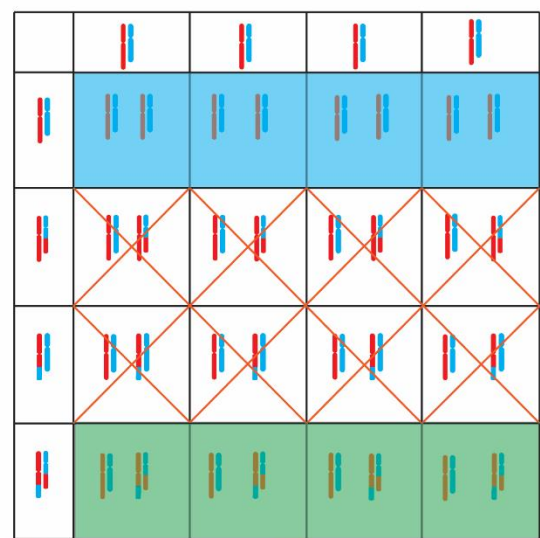
Possible parent gametes



T30H het x T30H het



T30H het x wild type



Unbalanced translocation
 Wild type
 T30H heterozygote
 T30H homozygote

Figure 18. T30H heterozygous mice are maintained as breeding stock. They can either be bred together to generate both T30H homozygotes and heterozygotes, as well as offspring not bearing the translocation at all. Some of the offspring do not receive a pair of balanced chromosomes, this results in the loss of genes and makes these pups non-viable and they are re-absorbed in utero. An example of this is in the image above (A), with reabsorbed pups marked with a *. This is in the ratio 10:4:1:1, unbalanced translocations: heterozygotes: no translocation: homozygotes. Heterozygous mice can also be bred with wild type mice to generate more heterozygotes quickly to increase breeding stocks of heterozygotes. Half of pups have unbalanced translocations; a quarter have no translocation and a quarter are heterozygotes.

4.2 Genetic Analysis

4.2.1 DNA Extraction

DNA was extracted for genotyping animals. In the case of T30H homozygous mice the tail was taken from culled pups for DNA extraction after the mice were culled on observation of the T30H phenotype. When a new litter was born ear-clips were taken from mice before weaning in order to discern wild-type mice from heterozygotes.

DNA was purified from tissue samples using a genomic DNA purification kit. DNA Extraction was carried out according the manufacturer's protocol. The tissue samples were left to digest overnight in a digestion solution with proteinase K added in order to break down the cellular components of the tissue and release the DNA from the nucleus of the cells. RNA was then removed from the sample by incubating it with RNase. The lysate was then mixed in a 1:1 ratio with 70% ethanol and the DNA bound to a silica membrane through centrifugation at $\geq 8000g$ for one minute. Impurities were then removed by further centrifugation $\geq 8000g$ with washing buffers for one minute at a time. The DNA was then eluted through centrifugation at $\geq 8000g$ using elution buffer and then used in further protocols.

4.2.2 DNA and RNA Quantification

The concentration of DNA and RNA was determined by using a NanoDrop ND-1000 Spectrophotometer. The quality of the nucleotides was assessed by using the $oD260/oD280$ ratio, with the highest purity for DNA at a ratio of 1.8 and for RNA at 2.0.

4.2.3 Whole-Genome Sequencing

Whole-genome sequencing was carried out using DNA extracted from T30H mouse brain. It was then transferred to the UCL Institute of Neurology where whole-genome sequencing was carried out by Dr Deborah Hughes. From the genomic DNA sent to the Institute of neurology a DNA library was produced through PCR-free synthesis. It was then sequenced using an Illumina HiSeq 3000 also at the Institute of Neurology.

Once the DNA library was prepared, the genome was sequenced through clonal amplification of adaptor ligated DNA fragments, followed by massive parallel sequencing. This was carried out by cyclical reversible termination, where DNA templates were sequenced through sequential rounds of base incorporation, imaging and then cleavage. This reversible termination was carried out by fluorescently labelled reversible terminators which were added with the incorporation of each dNTP, imaged and then cleaved. The imaging step determined which base had been added. Once the genome had been sequenced reads were visualised using Tablet software (developed by the James Hutton Institute).

To confirm the area identified by the software was the translocation point the area was cloned on plasmids. The DNA was then excised from these plasmids and then sent off for sequencing. Primers were then designed surrounding the translocation point and used to test T30H homozygous mice, heterozygous and wild-type mice as a second way of determining that the translocation point was in the area identified.

4.2.4 PCR – Genotyping

Genotyping PCRs were carried out using 1µl of template DNA (between 10pg and 200ng) in addition to 1µl of each primer to give a working solution of 200nM. These were used with 20µl AccuPrime Pfx SuperMix (Invitrogen). This mix contains DNA polymerase which is antibody bound at room temperature and is only activated in the denaturation step of PCR cycling. The SuperMix contains 22U/mL of Thermococcus species KOD thermostable polymerase complexed with anti-KOD antibodies, 66mM Tris-SO₄ (pH 8.4), 30.8mM (NH₄)₂SO₄, 11mM KCl, 1.1mM MgSO₄, 330µM dNTPs, AccuPrime proteins, and stabilizers.

Other PCRs were carried out using iTaq polymerase purchased from Bio-Rad, where PCR reagents are supplied individually in order to modify the protocol as required to adapt to different primers. In these reactions 2.5µl of 10X iTaq buffer was used to give a working solution of 1X, as well as 0.75µl of MgCl₂ (1.5mM working concentration), 0.5µl of dNTP mix (200µM of each nucleotide), 0.125µl of iTaq polymerase (1.25U), 1 µl each of the forward and reverse primer (concentration

between 100nM and 500nM) and between 5 and 10µg of DNA template. This mix was then made up to 25µl with sterile, nucleotide free water.

PCRs were carried out on a thermocycler with the following protocol: heat activation of primers for 1 minute at 95°C followed by 30 cycles of denaturing for 1 minute at 95°C, annealing for 1 minute at a variable temperature and elongation for 1 minute at 68°C, this was then followed by a further elongation period at the end of these cycles for 7 minutes at 72°C.

The annealing step was variable and was dependent on the sequence composition of the primers used. Details on the individual annealing temperatures for each primer pair can be found in **Figure 17**. For the T30H genotyping PCR using primers ASIP and Myocd the annealing temperature was 60°C. For the sex determination PCR using SRY primers the annealing temperature was also 60°C.

4.2.5 Gel Electrophoresis

PCR products were visualised using gel electrophoresis. 1% agarose gels were used in all experiments. These gels were made by heating agarose with 1xTAE buffer in a microwave until it was dissolved, and then adding 4µl of SYBR Safe per 100ml to this solution to allow visualisation of DNA. The solution was then poured into a gel mould with a comb inserted to allow addition of DNA. Once the gel was set it was removed from the mould and inserted into an electrophoresis tank filled with 1xTAE buffer.

To run the PCR product, 1µl of gel loading dye was mixed with 10µl of PCR product and then loaded into the wells of the gel. The gel was then run at 100 volts for 30 minutes. After this the bands were visualised, and images recorded by using the Gel Doc EZ imager. A DNA ladder was used to estimate band length.

4.2.6 RNA Extraction

RNA was extracted from tissue in order to ascertain gene expression levels. If RNA was not immediately extracted from tissues, it was preserved in *RNAlater* and frozen at -80°C to prevent degradation through RNase activity. RNA was extracted from either fresh or defrosted tissue using an RNA extraction kit. Using this kit cells were lysed using a lysis buffer and then silica membranes were used to bind RNA and wash

away impurities using centrifugation at $\geq 8000g$. RNA was dissolved from the membrane using RNase free water and then eluted, again through centrifugation at $\geq 8000g$. It was then either frozen and stored at -80°C or used immediately in downstream protocols.

4.2.7 cDNA Generation

Complementary DNA (cDNA) was be synthesised from single-stranded RNA using the enzyme reverse transcriptase. This was then used as a template for reverse transcription PCR (RT-PCR) or quantitative PCR (qPCR). Generation of cDNA was carried out using cDNA synthesis kits. These kits contained a polymerase, random primers to initiate amplification and dNTPs, in addition to an RNase inhibitor to stop RNA degradation.

Two kits were used for generation of cDNA. The iScript cDNA synthesis kit (BioRad) uses $4\mu\text{l}$ of 5x iScript reaction mix, which contains oligo(dT) and random hexamer primers. These reactions also used $1\mu\text{l}$ of iScript reverse transcriptase pre-blended with RNase inhibitors. RNA template was then added to give between 100fg and $1\mu\text{g}$ of RNA total, then the rest of the reaction volume was made up with RNase free water to total $20\mu\text{l}$.

The reaction mix was then incubated in a thermal cycler with the following reaction times and temperatures: 5 minutes at 25°C as a priming step, followed by 20 minutes at 46°C to allow reverse transcription, followed by 1 minute at 95°C to inactivate the reverse transcriptase, the cycler then held at 4°C until the reaction mix was removed from the cycler.

This kit was optimised to produce cDNA $<1\text{kb}$ in length. Where longer cDNA products were required the first strand cDNA synthesis kit was used instead. This kit takes advantage of a different form of reverse transcriptase, M-MuLV reverse transcriptase, to produce longer stretches of cDNA, up to 9kb .

The first step in this kit degrades any contaminating DNA. Up to $1\mu\text{g}$ of RNA was incubated for 30 minutes at 37°C with $1\mu\text{l}$ of 10x reaction buffer with MgCl_2 and $1\mu\text{l}$ of RNase from DNase I. RNase free water was also added to make the reaction mix

up to 10 μ l. 1 μ l 50mM EDTA was then added and incubated at 65°C for 10 minutes. This prepared RNA was then used in the cDNA synthesis protocol.

For this protocol, between 0.1 and 5 μ g of RNA was used. To this template 1 μ l of either oligo(dT)₁₈ or random primers were added. Oligo(dT)₁₈ primers initiate synthesis from the poly(A) tail of the mRNA template and random primers initiate at random throughout all RNA included in a sample. This resulted in more diverse cDNA generated which can lead to less sensitive and specific RT-PCR results. Therefore, in all protocols where first strand cDNA synthesis was used oligo(dT)₁₈ primers were used.

To the RNA template and primer mix water was added to make the mix up to 11 μ l. After this 4 μ l of 5x reaction buffer, 1 μ l of 20U/ μ l RiboLock RNase inhibitor, 2 μ l of 10mM dNTP mix and 2 μ l of M-MuLV Reverse Transcriptase at 20U/ μ l concentration were added. This gives a total volume of 20 μ l.

This mix was then transferred to a thermal cycler. For oligo(dT)₁₈ primers there should be an initial step of 60 minutes at 37°C; for random primers this should be changed to 5 minutes at 25°C followed by 60 minutes at 37°C. In both cases the reaction was terminated by heating the mix to 70°C for 5 minutes. The synthesised cDNA was then either used immediately in downstream protocols or stored at -20°C for short term storage or -80°C for longer term storage.

4.2.8 Reverse Transcription PCR

Reverse transcription PCR was used to ascertain whether a gene was being expressed and, if specific primers were used, which splice variants of the gene were being expressed. This was done by using the cDNA generated from RNA from tissue or cultured cells at a specific timepoints of interest.

After cDNA was generated a PCR was carried out using primers specific to genes of interest. Initially a gradient PCR was carried out to ascertain the correct annealing temperature for each primer using a positive control sample. The optimum annealing temperature for Nonagouti and My44 was 52.5°C, for Myo10aRT was 54.3°C, for Ahcy at 56.2 and for Map2k4 was 58.3°C. Primers for GAPDH, a housekeeping gene,

were run as a control for all samples. The primers for this gene worked well at all temperatures tested. The annealing temperatures for all these primers can also be referred to in **Figure 17**.

PCRs were visualised using gel electrophoresis, all RT-PCR reactions were visualised using 1% agarose gels as described previously. A DNA ladder was used to estimate band size and ensure the expected band size was being amplified by the reaction.

4.2.9 Quantitative PCR

Quantitative PCR (qPCR) allows a quantifiable method of gene expression. To prepare a qPCR a master mix was made up for each experiment. Each reaction required 20 μ l of master mix. For 20 μ l of master mix, 10 μ l of SYBR green was added (supplied in 2X concentration, working solution must be 1X), as well as 0.5 μ l of reverse primer, 0.5 μ l of forward primer (working concentration for both primers was 0.2 μ M) and 8 μ l of nuclease free water. This was then scaled up for the number of reactions which were carried out on each plate. Once this was made up 19 μ l of master mix was added to each well of a 96 well qPCR plate. To this 1 μ l of cDNA was added.

Three sets of primers were used, Myo10a forward and reverse, My44 forward and reverse and GAPDH forward and reverse as a control. All samples were run in duplicate and negative controls with omitted cDNA were also used.

Plates were then added to a qPCR thermal cycler, with the following protocol: 95°C for 3 minutes, followed by 95°C for 30 seconds, primer specific temperature for 30 seconds, 72°C for 30 seconds. These three steps were cycled 45 times. The variable temperature was found by running a gradient PCR using a positive control cDNA where expression was expected. This was followed by the generation of a melt curve where the plate was incubated at 65°C for 15 seconds and then 95°C for 15 seconds. The melt curve was used to confirm that there was only one PCR product being generated by the generation of a single peak in the curve. Files were then exported as excel files for analysis.

Double delta Ct analysis was used to analyse qPCR data. The expression of the gene being tested was compared to a housekeeping gene, GAPGH for all samples. For all

experiments, the tested experimental value (TE) was taken from the raw PCR data as well as the GAPDH control value (HE). A control value is needed to obtain relative expression against for each data set, so the sample tissue with the lowest relative expression from the raw data was used for this value in each data set, both for the gene being tested (TC) and the housekeeping gene control (HC).

The difference between TE and HE (TE-HE) and TC and HC (TC-HC) were then calculated. These values were defined as the delta Ct values for both experimental (ΔCTE) and the comparative samples with the lowest expression in the data set (ΔCTC). The difference between these two values for each sample was then calculated to give the value $\Delta\Delta\text{Ct}$. All calculations were in logarithm base 2, so to normalise this data the $2^{-\Delta\Delta\text{Ct}}$ value was calculated to obtain the expression fold change for the data. The standard deviation for these values were then calculate and the data plotted on a bar chart.

4.3 Histological Analysis

4.3.1 Tissue Fixation

Tissue samples selected for immunohistochemical analysis were dissected out from mice culled according to schedule 1 methods of euthanasia (schedule 1 of the Animals (Scientific Procedures) Act 1986). Tissues were fixed in order to preserve the tissue's morphology and prevent the tissue from decaying. Fixation also increases a tissue's rigidity allowing thin sections to be cut. Fixation was carried out by immersion in neutral buffered 10% formalin. The length of time for fixation to take place was dependent on the size of the tissue. This could be as little as an hour at room temperature to several days at 4°C. After fixation in formalin tissues were washed in 70% ethanol to remove remaining fixative and then immersed in 70% ethanol for storage.

Cells grown in chamber slides were washed with PBS and then fixed in ice cold methanol for 5 minutes at 4°C. Cells were then washed again using PBS and then kept at 4°C with 0.05% sodium azide in PBS before using in further protocols.

4.3.2 Tissue Embedding

Embedding is a process which clears and dehydrates tissue and allows for long-term storage. Fixed tissues were dehydrated using increasing concentrations of ethanol in a dilution series. Tissues were submerged in 70% ethanol for an hour, followed by 80%, 90% and 100%, also each for an hour, although this was increased to two hours for larger tissues.

The tissue was then transferred to a clearing agent, HistoClear for an hour, and then transferred into 1:1 HistoClear to paraffin wax. After this it was transferred into paraffin wax for an hour twice before setting in a cassette with fresh wax. For larger tissues such as whole embryos or whole P1 mice the incubation times for all solutions were increased to two hours. These embedded tissues can be stored long-term and sectioned.

4.3.3 Sectioning

Sections of 5µm thickness were cut from paraffin embedded tissues using a microtome. Sections were then transferred to a water bath to heat and straighten out the sections before transferring them to a superfrost plus slide. These were then transferred to a 30°C oven and left to dry and adhere to the slides overnight.

4.3.4 PAS staining

Periodic acid Schiff (PAS) staining can be used to stain sugars in tissues. The periodic acid hydrolyses diols in glucose to create an aldehyde, and then the Schiff reagent reacts with this to give a pink stain. This is useful in the kidney because it can be used to differentiate the brush borders of proximal tubule which are high in sugar (Longley et al, 1954).

Cut sections were dewaxed by submersion in Histo-Clear twice for 5 minutes each time. They were then rehydrated by submerging in 100% ethanol twice and 70% ethanol once for 5 minutes each time. Slides were then placed in periodic acid for 5 minutes on a shaker. Slides were then washed in tap water twice for 5 minutes each before being placed in Schiff reagent for 15 minutes on a shaker.

Slides were then washed twice in tap water again before counterstaining with Mayer's haematoxylin, a nuclear stain which colours the nucleus in cells purple, for one minute. Slides were then washed in tap water again for 5 minutes before being dehydrated again back up the dilution series of ethanol, by washing in 70% ethanol for 5 minutes, followed by twice in 100% ethanol and twice in Histo-Clear, each for 5 minutes. Slides were then mounted by covering with HistoMount followed by a coverslip. HistoMount was allowed to set overnight at room temperature before imaging slides.

4.3.5 Immunohistochemistry

Specific antigens were stained for using immunohistochemistry and then visualised using either light or fluorescence microscopy depending on the technique used. This technique uses antibodies generated against an antigen of interest in a known host.

Antibodies against this host could then be targeted by secondary antibodies as an amplification step.

Antibodies when first ordered were checked against positive controls (usually suggested in the product information) where the tissue was available. A gradient of dilutions was also set up to test which was the best concentration of antibody to use. Four dilutions were normally used, 1:50, 1:100, 1:500, 1:1000. If at all concentrations the antibody did not produce good staining an alternate antigen retrieval method was used (rather than citrate buffer), usually by incubation with proteinase K or trypsin.

The secondary antibodies used were conjugated to either the enzyme horseradish peroxidase (HRP) or to fluorophores. In the case of HRP when 3,3'-Diaminobenzidine (DAB) was added to the slide the DAB reacts to form a brown precipitate which was visualised using light microscopy. In the case of secondary fluorophores, these were visualised because they emit light when excited by different lasers. Different fluorophores had different emission spectra, allowing multiple antigens to be targeted and visualised in a single sample.

The protocols for staining with DAB or with fluorescent secondaries were similar but differ in some respects.

4.3.5.1 DAB Staining

5µm slides cut from paraffin embedded sections were dewaxed and rehydrated using Histo-Clear and dilutions of ethanol using the protocol described previously for PAS staining. The process of fixation can mask epitopes through the creation of crosslinks, so tissue was treated to expose these epitopes. There are multiple techniques which can be used for antigen retrieval but with all antibodies used in this thesis antigen retrieval by microwaving in citrate buffer was used. Citrate buffer was made using 10mM sodium citrate, tribasic, dehydrate, dissolved in 1L of water, followed by adding 22ml 0.2M hydrochloric acid. The buffer was first heated using a microwave for 10 minutes, and then the slides added and then microwaved for 15 minutes.

Slides were left to cool down to room temperature and then washed in distilled water.

In order to use horseradish peroxidase endogenous peroxidases must first be quenched to prevent background staining. This was done using 1.5% hydrogen peroxide diluted in PBS, incubating slides for 10 minutes and then washing in distilled water. Sections were then drawn around using hydrophobic pen and then washed in PBS-TWEEN.

To further prevent background staining slides were then incubated in blocking buffer. Blocking buffer was made up from 10% FCS, 2% BSA and 0.1% TWEEN in PBS. Slides were incubated for 1 hour at room temperature in a humidified chamber. During this incubation primary antibodies were diluted in block, this dilution was specific for each antibody (α SMA 1:200, Calponin 1:100, GFP 1:1000, Krt5 1:100, Laminin 1:50, Myocardin 1:200, S100 1:50, SRF 1:50, SMMH 1:50, Uroplakin 3a 1:200). After blocking the primary antibody was applied and then incubated at 4°C overnight.

The next day primary antibody was washed off in PBS-TWEEN, and then secondary HRP conjugated antibody applied at 1:300 concentration, diluted in block. This secondary antibody must be raised against the host animal used to produce the primary antibody used. For example, if an antibody was being used which was raised in rabbit then the secondary antibody must be anti-rabbit. The sections were incubated in the secondary antibody for 30 minutes at room temperature. They were then washed off in PBS-TWEEN before incubation in EnVision for a further 30 minutes to amplify the signal; this was then washed off in PBS.

The DAB used was stored in solid form in 2 different tablets which are then dissolved when the reagent is used. This is in order to keep the molecule stable. The two DAB tablets were dissolved in 5ml of distilled water as per the manufacturer's instructions. DAB was then applied to slides and colour development observed under a microscope. Time for the colour to develop was recorded and used to stain all slides in the specific assay. The time for colour development to occur varied between 20 seconds and 10 minutes. Slides were then washed in distilled water. Slides were then

counterstained in Mayer's hematoxylin for 1 minute to counterstain nuclei. They were then washed in distilled water again for five minutes.

After this, sections were dehydrated in increasing dilutions of ethanol and then in HistoClear and then were finally mounted using HistoMount and a coverslip using the same protocol as PAS staining.

4.3.5.2 Fluorescent Staining

Staining using fluorescent antibodies uses the same protocol on the first day as for DAB staining, but the hydrogen peroxide step was omitted as HRP was not used in a fluorescent staining protocol.

On the second day the primary antibody was washed off using PBS, and then secondary antibody diluted in block is applied at 1:300 dilution and then incubated in the dark for an hour at room temperature. The secondary antibody was washed off using PBS and then incubated in sudan black for 10 minutes in order to block autofluorescence. This was then washed off in PBS; slides were then dipped in distilled water and then mounted using aqueous mounting solution and a coverslip. Coverslips were sealed using clear nail varnish. Slides were stored at 4°C and imaged as soon as possible as fluorescently conjugated antibodies fade over time.

4.3.5.3 Negative Controls

Negative controls were used for all staining methods to ensure that staining observed is specific to the antigens of interest, and that there is no background staining. Negative controls were generated by omitting primary antibody for both fluorescent and DAB immunohistochemistry. The primary antibody step was replaced with the same volume of blocking buffer; with the same length of incubation.

4.4 Microscopy

Two microscopes were used for various aspects of my thesis. An Olympus IX71 was used to monitor cells while they were in culture and to ascertain whether GFP was expressed in lentiviral knock-down experiments. A Zeiss Axioplan was used to image all sectioned slides. This microscope uses a halogen lamp for brightfield imaging. It

was also used for epifluorescence imaging, using fully automated 4 colour fluorescence with a mercury arc, HBO lamp. Images were taken using a Hamamatsu Flash 4 camera, the objectives used were 5x/0.16 10x/0.45 20x/0.8 40x/1.3 63x/1.4. The software used to set up and take images was developed by Zeiss, image capture was sequential. Images were captured as single optical sections, and when fluorescence was used laser power and gain were standardised between samples after initial set up using positive controls. Once images were captured, they were exported for analysis using ImageJ (developed by NIH).

4.4.1 Blinded Scoring of Gut Morphology

To establish whether or not T30H mice had any differences to their gut morphology compared to wild-type mice three representative images of the small intestine were taken at 20x magnification of three T30H and three wild-type samples, all at P1. All samples had been stained with α SMA using DAB to visualise the antibody. Images were then compiled in a Microsoft Word document and each sample given a number from 1 to 6. Three participants (Daniyal Jafree, Saif Malik, Lauren Russell) were then asked to blind score whether they thought that the samples they had been provided with were any different to the samples from mouse 6, which they had been told was a wild-type mouse. An example score sheet can be found in the Appendix, and the genotypes of the mice are as follows: mouse 1, T30H, mouse 2, WT, mouse 3, T30H, mouse 4, T30H, mouse 5, WT. Mouse 6 was the wild-type mouse participants were asked to compare against.

4.5 Ultrasound Scanning

In order to capture developmental timepoints in T30H development I transferred T30H mice with timed pregnancies to the Centre for Advanced Biomedical Imaging (CABI) and scanned these mice using an ultrasound scanner. Mice were scanned at E14, E15, E16 and E18. Each mouse was scanned no more than three times in a given pregnancy.

Mice were sedated using an isoflurane/O₂ mix, and then secured to a heated stage to retain body temperature. Isoflurane percentage for induction of anaesthesia was

5%, and then was maintained at 1-2%, with a flow rate of 0.5-1L/min. Heart rate was monitored by the heated stage in the areas where the front and hind legs were secured. Body temperature was monitored using a rectal thermometer. Hair was then removed from the abdomen using depilatory cream.

Pups were first located, counted and their orientation recorded using the ultrasound probe. The bladder was then found in each embryo and individual pictures were taken for reference of both the bladder and kidneys, if the kidneys were visible. The probe was then centred on the bladder and a three-dimensional scan was taken through the whole organ. The volume of the bladder was then calculated using the VisualSonics software of the imaging station.

Once images were acquired mice were allowed to regain consciousness in a recovery room before being returned to the main area of the animal house. If embryonic samples were required mice were culled using schedule 1 methods (cervical dislocation) and the embryos dissected for use in further protocols.

4.6 Manipulation of Myocardin Expression

In order to further investigate *Myocd* expression the *Myocd* phenotype was manipulated using cell culture. Initially whole organ culture was attempted, but then changed to dissociated cell culture.

4.6.1 Cell culture – whole organ culture

For whole organ culture embryos were dissected from timed pregnancies in CD1 (wild-type) mice at E14. The bladders from these mice were then dissected out using a dissecting microscope. Bladders were then placed into sterile serum-free media while the remaining bladders were dissected.

Serum-free DMEM F12 was added to six well tissue culture plates; a tissue culture insert was then placed into each well. Up to four bladders were added to each insert, with at least 0.5cm gap between each bladder. Bladders were then grown in a 37°C humidified tissue culture incubator. Bladders were fixed at various timepoints in order to measure growth in culture. This organ culture methodology was developed by Burgu *et al.* (2006).

4.6.1.1 Quantification of Bladder Muscle Wall Thickness

In order to ascertain whether the bladders had grown in whole organ culture, bladders were fixed and sectioned. Fresh, uncultured bladders and bladders from day 2, day 3 and day 4 of culture were used. Every third slide was then stained for α SMA using DAB staining to stain the smooth muscle wall of the bladder brown. These slides were then imaged using the Zeiss Axioplan microscope at the same magnification. ImageJ was then used to draw a cross roughly through the centre of each bladder, and the length of the brown area measured by the intersecting arms of the cross measured in each bladder, to give 4 total measurements for wall thickness for each section of the bladder. Values were then exported into Microsoft Excel. Three bladders from each condition were analysed, and the mean bladder wall thickness of each individual bladder was calculated, and then further combined to give a mean bladder wall thickness for each timepoint. The standard deviation was also calculated for each individual bladder and for each collated timepoint.

4.6.2 Cell culture – dissociated cell culture

For dissociated cell culture cells were obtained from the bladders of embryos from timed CD1 mouse pregnancies. Mice were culled using schedule 1 methods and the embryos dissected out at embryonic day 14 of gestation. The bladders were then dissected from embryos using a dissecting microscope and placed into dissociated bladder culture media. This was comprised of advanced DMEM/F12, 20% fetal bovine serum, ITS, methionine and penicillin streptomycin. Once all bladders were dissected, organs were placed into a 10cm tissue culture dish under the dissecting microscope with 1ml of dissociated culture media. Bladders were then cut into small pieces using syringe needles.

After this, bladders were spun down at 200g for 5 minutes, and then transferred into trypsin for 4 minutes in a water bath at 37°C. After this the tissue was collected by pipetting – after the trypsinisation step all tissue clumps together – and then then transferred into pre-warmed dissociated culture media for 10 minutes at 37°C. The tissue was then dissociated into single cells by repeated pipetting. Cells were then counted using a hemocytometer and then plated at a density of 1×10^5 cells per cm^2 . Cells were split in a 1:1 ratio when they reached 70% confluence.

Myocd was knocked down in these dissociated cells using short hairpin RNA (shRNA) packaged in a lentiviral vector. This lentiviral vector, along with the scrambled control vector, was purchased from OriGene. The viral particles used induced cells to express green fluorescent protein (GFP) to distinguish whether cells had been successfully transduced. GFP expression was driven by an independent cytomegalovirus (CMV) promoter not linked to shRNA reading frame, ensuring that GFP was always expressed when the virus is transduced. Initially, the most important thing to find out was the correct multiplicity of infection (MOI) for the protocol. Lentivirus can have deleterious effects on cells, causing apoptosis, if they are dosed with too many viral particles per cell, however, enough viral particles must still infect the cells to be able to give a high level of the cell population with *Myocd* knock-down. One control population was set up with no virus treatment, and then another two populations were set up with 1MOI of *Myocd* knock-down virus, and another with 10MOI knock-

down of the virus. Another control 2 control populations were set up using 1MOI and 10MOI using a scrambled control lentiviral vector, which produced a random, non-specific DNA code instead of a targeted knock-down. This scrambled control ensured that any changes observed in treated cells are caused by the knock-down of *Myocd* and not simply as a side effect of viral treatment.

Cells were transfected with lentivirus on the day of their dissociation. After 5 days they were examined under a microscope to ascertain whether transduction had been successful. This can be gauged by whether any cells glow green, meaning they were expressing green fluorescent protein (GFP). In the samples which had been dosed at 1MOI no green cells were observed, whereas fluorescence was observed with the 10MOI treatment. Ideally a 100MOI treatment would also have been used to ascertain the dosage which would have resulted in the most cells undergoing successful transduction. However, I was limited by the amount of scrambled control virus purchased from the company and did not have sufficient scrambled control virus to perform a 100MOI test dose. As there appeared to be minimal difference in cell growth comparing 10MOI scrambled control with 1MOI scrambled control and the untreated sample 10MOI dosage was used going forward.

Once cells had regained 70% confluence after three passages, they were collected for western blotting to assess how lentiviral knock-down had affected protein expression.

4.7 Western Blot

Western blotting is a methodology for assessing whether protein has been expressed or not. Protein was extracted from cells and then denatured and run on a gel using electrophoresis to separate them by size. They were then transferred to a membrane; an antibody was used to probe for the protein and allows it to be imaged through visualisation of the HRP conjugated to the secondary antibody

4.7.1 Protein Extraction

Pierce Lysis buffer was used to extract protein from cells. This buffer was prepared in advance using cOmplete EDTA-free protease inhibitor cocktail at 40µl per ml in

distilled water, plus 10µl per ml of PMSF at stock concentration of 10mg/ml (phenylmethylsulfonyl fluoride, another protease inhibitor) and 10µl per ml of sodium orthovanadate at stock concentration of 100mM, which is also a protease inhibitor. This solution was then placed on ice.

Culture medium was removed from cells and then the adherent cells washed with ice cold PBS. 1ml of the lysis buffer was added to each T25 tissue culture flask, and this was then placed on ice for 10 minutes, with periodic tilting to wash the lysis buffer over cells. After this incubation cells were then removed from the flask using a cell scraper, and then transferred to an Eppendorf tube on ice. Lysis was then completed by shearing through a 26-gauge syringe needle.

The Eppendorf tube was then transferred to a centrifuge and spun at 13,000g for 10 minutes to pellet out cell debris. The supernatant containing the protein was then removed for further protocols or stored at -20°C.

4.7.2 Protein Quantification

Before a western blot was carried out protein was first quantified so that a direct comparison could be made when running a western blot. This was done by comparing extracted protein to a stock solution of BSA. BCA (bicinchoninic acid) exhibits colour change from green to purple proportionally to the level of protein it is exposed to.

First a dilution series was set up by adding 50µl of BSA at 2mg/ml in an Eppendorf tube labelled 2000. Six further Eppendorf tubes were then set up with 60µl of distilled water, labelled 1000, 500, 250, 125, 62.5 and 0. 60µl of BSA was added to the first tube, mixed and then transferred into the tube marker 500, mixed, and then 60µl was transferred to the next tube, and so on down the dilution series.

Protein samples which were to be measured were diluted 1:4 with distilled water to make a 5 times dilution. 10µl of the diluted sample was then transferred to a 96 well plate, and then 10µl of each of the standards was also transferred in duplicate.

BCA reagent was then be made up by adding one-part reagent A to reagent B. 190µl of the prepared BCA reagent was added to each sample well. This was then incubated at 37°C for 30 minutes. Absorbance was then measured at 562nm and recorded. The values for the dilution gradient were then plotted on a graph and a line of best fit calculated. The equation for this line was used to calculate the concentration of the protein samples from their absorbance values.

4.7.3 Western Blotting

The day before the western blot was started blocking buffer was made up from 5% non-fat milk in PBS in addition to 0.1% TWEEN and 0.1% BSA. Stock 10x running buffer was also prepared in advance from 30g tris base plus 144g glycine and 10g of SDS in 1L of distilled water.

Before blotting the proteins were first denatured. Between 15 and 30µg of protein were used per sample. To denature the protein 10% β-mercaptoethanol and 4x Laemmli sample buffer were dissolved with the protein and then heated at 95°C for 10 minutes.

Precast gels were removed from their packaging and placed inside the running tank. The 10x glycine running buffer was diluted to 1x running buffer with distilled water and then used to fill the gel running tank. The sample was loaded inside the gel columns along with protein ladder. The gel was then run for an hour at 100v.

While the gel was running, the primary antibody was prepared in blocking buffer. The level of dilution in blocking buffer was dependent on the antibody, MYOCD is at 1:1000, αSMA 1:10,000, GAPDH at 1:10,000.

After the gel had finished running it was transferred onto PVDF membranes using a trans blot turbo transfer system. In this process the protein was transferred from the gel onto a membrane, which was then used for imaging. After transfer, the membrane was washed twice for 5 minutes in PBS-TWEEN (PBS-T). It was then blocked for an hour at room temperature to prevent background staining. After blocking, the membrane was washed 6 times for 5 minutes each in PBS-T. It was then probed with primary antibody overnight at 4°C.

The next day the primary antibody was removed and stored for further use – typically this could be reused up to five times before the antibody dilution loses efficiency. The membrane was then washed 6 times in PBS-T to wash off any antibody that had not properly bound. While the washing took place, the secondary antibody was prepared by diluting in blocking buffer. This used HRP conjugated antibodies against the host species of the primary antibody used, in a dilution of 1:1000. After the washing step was completed, the membrane was probed with secondary antibody for an hour at room temperature. Secondary antibody can be reused, so after this incubation it was stored at 4°C and reused in the same way as primary antibody could be, up to a maximum of five times.

Improperly bound secondary antibody was then removed by washing 6 times for 5 minutes each time. To visualise the HRP secondary the membrane was then incubated with Pierce EBL western blot substrate for 1 minute. Excess liquid was shaken from the membrane and then placed inside a development cassette. This was then taken to the dark room and the membrane within the cassette was exposed to ECL x-ray film – initially for one minute but if this was not sufficient to produce bands on the x-ray film then test 5 and 10 minutes. The maximum reaction time was 1 hour.

4.8 Bladder Vector Biodistribution Study

In order to manipulate *Myocd* expression in T30H mice in the future, the optimal vector for transfection must be identified. To do this a biodistribution study was carried out by collaborators at the Institute of Women's Health (Simon Waddington, Jo Ng). This study aimed to identify to which location various viral vectors preferentially targeted, and specifically which vectors best targeted the bladder. CD1 mice were injected in the retino-orbital region with an expression vector or control at P1 and then the paw tattooed in order to identify which mouse pup had been injected with which construct. Each of the vectors contained a ubiquitous promoter (CMV), as well as GFP as a tag to identify where the vector has successfully transduced. The vectors also contained WPRE, which was the Posttranscriptional Regulatory Element – in this case it was taken from woodchuck hepatitis virus. It was a DNA sequence used in the 3' UTR region of a mammalian expression cassette.

When it was transcribed it created a tertiary structure which improves the stability of mRNA; this in turn increases the likelihood that the gene delivered by the vector will be transcribed. The vectors and viral titres which were injected are detailed in **figure 19**.

The mice were then culled at postnatal day 35 and the bladders dissected. One bladder from each injection sample was frozen in RNA later, and all other bladders were fixed for sectioning and imaging.

4.9 Statistical Analysis

Statistical analysis was carried out for any data sets with sufficient technical replicates (≥ 3). First data was established as following a normal distribution. A p value was generated for each data set using a Shapiro Wilk test, if the p value is greater than 0.05 the it can be accepted that the distribution of the data is normal. Next an unpaired t test was used to ascertain whether the mean of data sets of interest was significantly different. 99% confidence intervals were used to determine whether any two means were statistically different to each other. It was only accepted that they were significantly different if $p \leq 0.01$.

Viral vector	Viral titre (vg/ml)	Volume injected
AAV9.CMV.GFP.WPRE	1.8×10^{13}	20 μ l
AAV8.CMV.GFP.WPRE	1.1×10^{13}	20 μ l
AAV7.CMV.GFP.WPRE	1.8×10^{13}	20 μ l
AAV6.CMV.GFP.WPRE	1.4×10^{13}	20 μ l
AAV5.CMV.GFP.WPRE	1.8×10^{13}	20 μ l
AAV2.CMV.GFP.WPRE	1.3×10^{13}	20 μ l
AAV1.CMV.GFP.WPRE	1.9×10^{13}	20 μ l
Ad. CMV.GFP.WPRE	3.3×10^{12}	20 μ l
Lenti CMV.GFP.WPRE	1.13×10^9	20 μ l

Figure 19. Vector types along with viral titre and the volume injected into each pup in the biodistribution study. vg/ml - viral genomes per millilitre.

5 Results

5.1 Identifying the T30H Translocation Point

One of the most important initial aims for my thesis was to uncover the location of the translocation point in T30H mice, which would pave the way towards identifying the genes responsible. The T30H mouse model has long been postulated as a model for lower urinary tract obstruction; but without the knowledge of the genetics behind the phenotype it would be impossible to conclusively identify affected pups. Additionally, this makes it impossible to target therapies to correct the phenotype. The location of the chromosome translocation would also allow the model to be more directly relatable to human disease if it was found that humans shared mutations to the gene which caused the T30H mouse model. Prior to the commencement of my project the translocation points were known to be between chromosomes 2 and 11, within an approximate area of around 1mb narrowed down following results generated by previous members of my laboratory (Chapter 1.4). A precise location for the translocation was not known.

5.1.1 Whole-Genome Sequencing

The strategy I decided to use to locate the translocation point was whole-genome sequencing. This had never been pursued previously because of prohibitive cost when the technology first became available. With the advent of next-generation sequencing it was possible to sequence the entire genome of a T30H mouse relatively rapidly and with less expense.

DNA samples from the head and limbs of a confirmed T30H mouse were extracted. These regions were selected for DNA extraction as other organs were retained for use in histology or RNA extraction. The tissue was obtained from a T30H mouse confirmed through observing the extended bladder and kidney hydronephrosis from sectioning. The DNA extracted from these samples was then sent for sequencing.

Sequencing was then carried out by high-throughput sequencing using an Illumina HiSeq 3000. This involves production of a DNA library through PCR-free synthesis. Once the library is prepared, the genome is sequenced through clonal amplification

of adaptor-ligated DNA fragments, followed by massive parallel sequencing. This is carried out by cyclical reversible termination, sequencing DNA templates by sequential rounds of base incorporation, imaging and then cleavage. This reversible termination is carried out by fluorescently labelled reversible terminators which are added with the incorporation of each dNTP, imaged and then cleaved. The imaging step determines which base has been added (Bentley et al, 2008).

Once the data set for the genome had been accumulated, a software program called Tablet was used to analyse the genome. Tablet is a viewer for next-generation sequencing assemblies. A prospective area for the translocation point on chromosome 11 was already known from the chromosome FISH studies carried out by David Monk and Phillip Stainer. This area was around 1Mb in length and stretched from just upstream of *Myocd* to an area upstream of *dnahc9*. The prospective area was brought up as a display on Tablet, and from there the contig alignment examined. Tablet can display all the read pairs in a given contig. In cases where a translocation is present, the read pairs will not match to the same contig. This is because the forward read will begin on one chromosome, but then sequencing from the other end of the read will be in a different chromosome and matching to a different contig. Tablet highlights these mismatched reads in yellow, making them easy to find, and narrowing down the translocation point to a very small area (**Figure 20, Figure 21**).

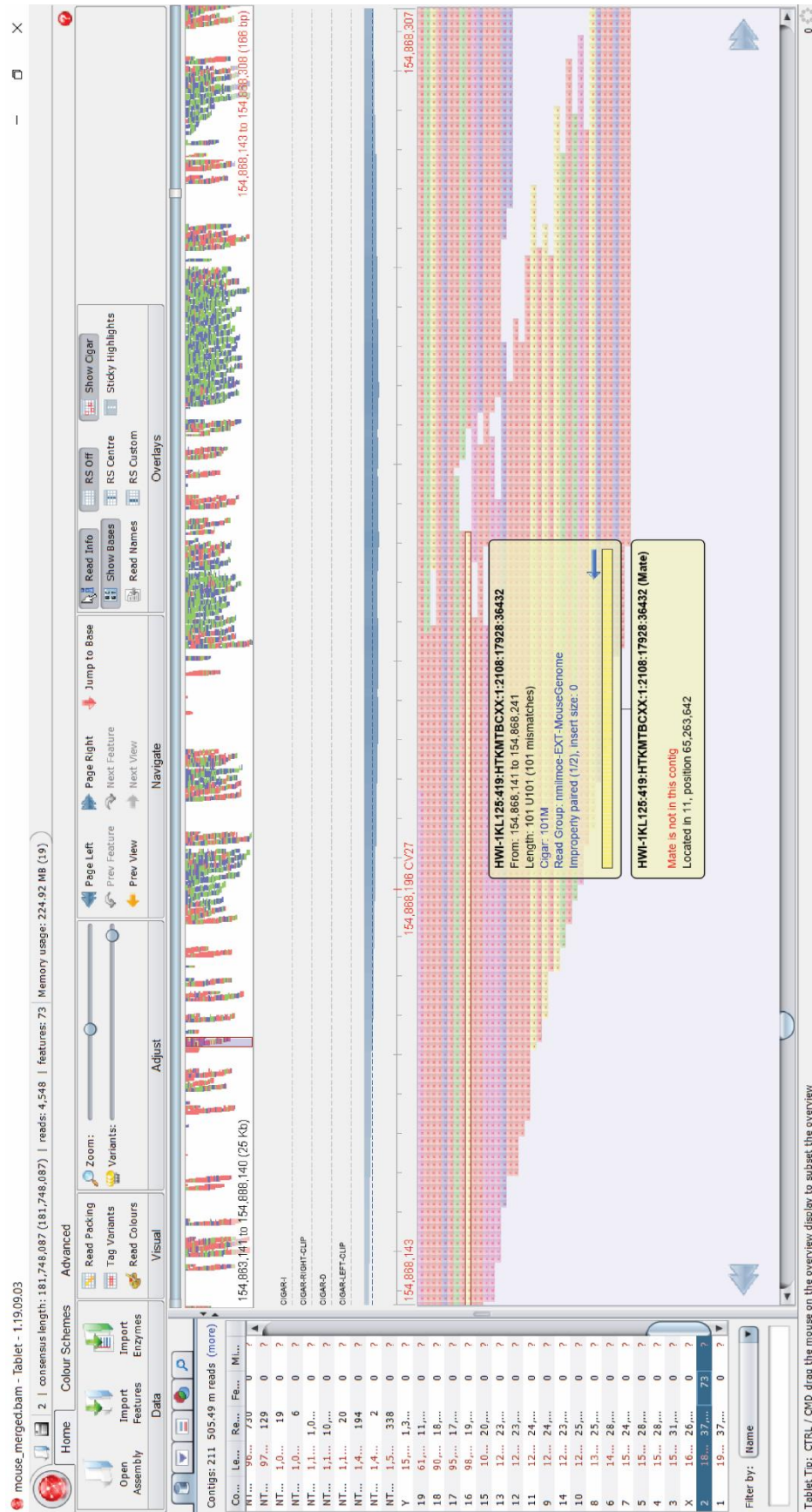


Figure 20. Screenshot of the location of the translocation point on chromosome 2 using genome browser software Tablet. Tablet has viewing settings which marks paired reads, mismatched reads with no partner, and mismatched reads with a partner in a different contig. It can also indicate which contig a mismatched read partner can be found in, which is invaluable for identifying translocation points. All reads highlighted in yellow indicate reads where the pair is not in the same contig but can be found on a different chromosome.

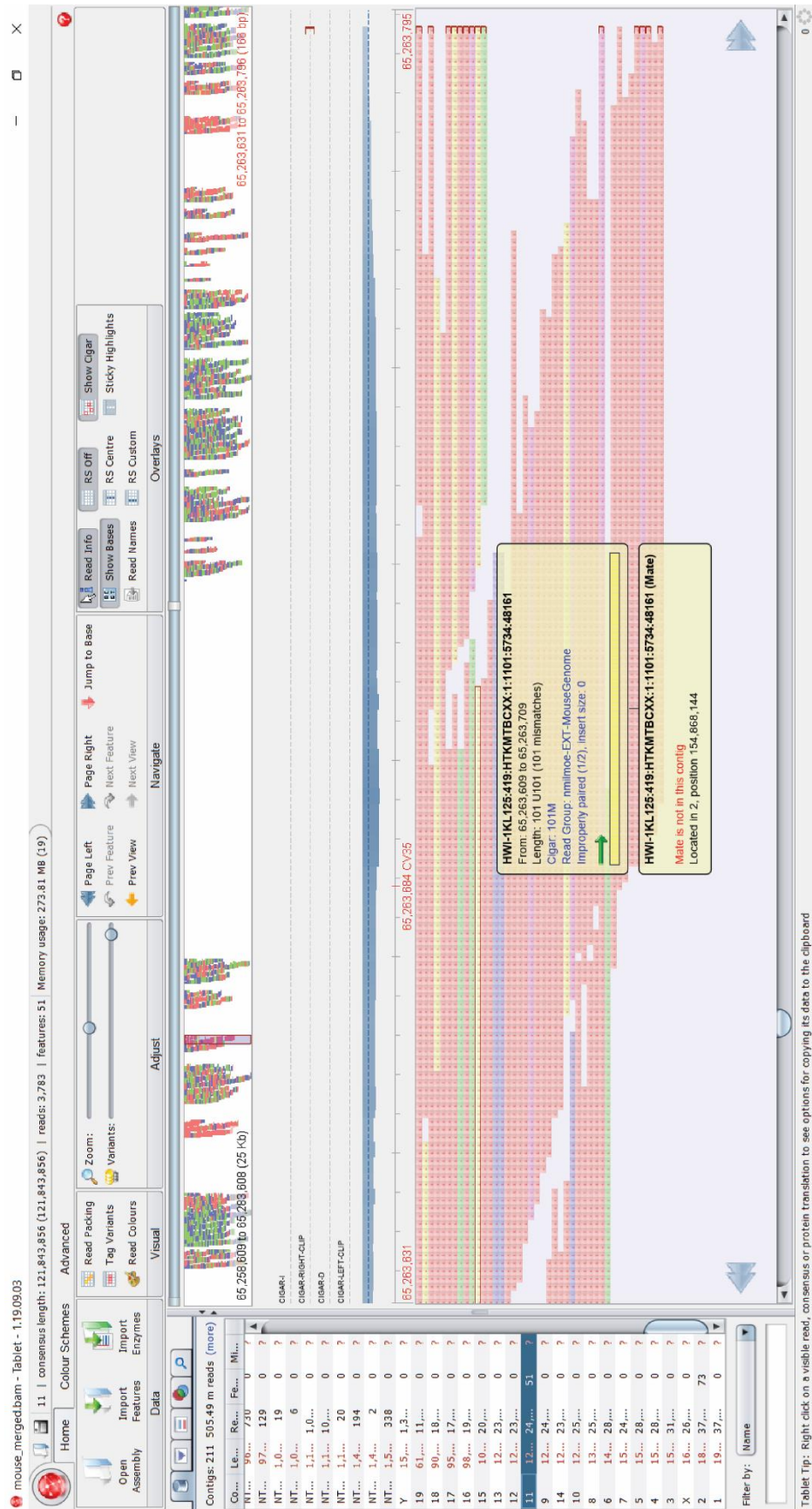


Figure 21. Screengrab of the location of the translocation point on chromosome 11. This was located by searching for the location of the read pair not in the same config as the read on chromosome 2. This mismatched read and all other reads around it which are highlighted in yellow had a mismatched read with the pair not found in the config. They have corresponding pairs on chromosome 2.

This area was found in the T30H samples on both chromosome 11 and chromosome 2. There was also a region of interest on chromosome 2 from chromosome FISH studies, but this had not previously been focused on because of the presence of *Myocd* on chromosome 11. Both translocation points were within the presumptive regions from the chromosome FISH studies. The area highlighted by the genomic hybridisation study, however, was not near the region identified by Tablet on chromosome 11. This implies that the genome hybridisation study was either picking up an anomalous result or was a small area of repeat regions unrelated to the translocation point. The sequencing results, however, are not infallible, if the translocation point had fallen within repeat regions then there was the potential for the sequencing results to be incorrect. Further confirmation of the sequencing results using PCR were required to confirm whether or not these results were accurate.

5.1.2 Confirmation by PCR

The translocation point identified by Tablet was confirmed using PCR. Primers were designed flanking the translocation points on chromosomes 2 and 11 (**Figure 22**). Four runs per sample were used to confirm the translocation point. In one lane both sets of chromosome 2 primers were used, and in another both sets of chromosome 11 primers were used. In the other two lanes the primers were swapped; these would be used to identify whether the translocation point was present. In one run both set of forward primers from chromosomes 2 and 11 were used, and then in the final lane both sets of reverse primers were used. This is because the DNA strands have been reversed during the translocation.

Carrying out this PCR strategy using T30H, T30H heterozygote and wild-type samples confirmed that the area the primers were flanking was the correct prospective area for the translocation point (**Figure 22**). This was then confirmed by extracting the PCR product from the gel and amplifying it. The amplified PCR product was then sequenced by Source Bioscience. The exact sequence location for the translocation point was then determined (**Figure 23**).

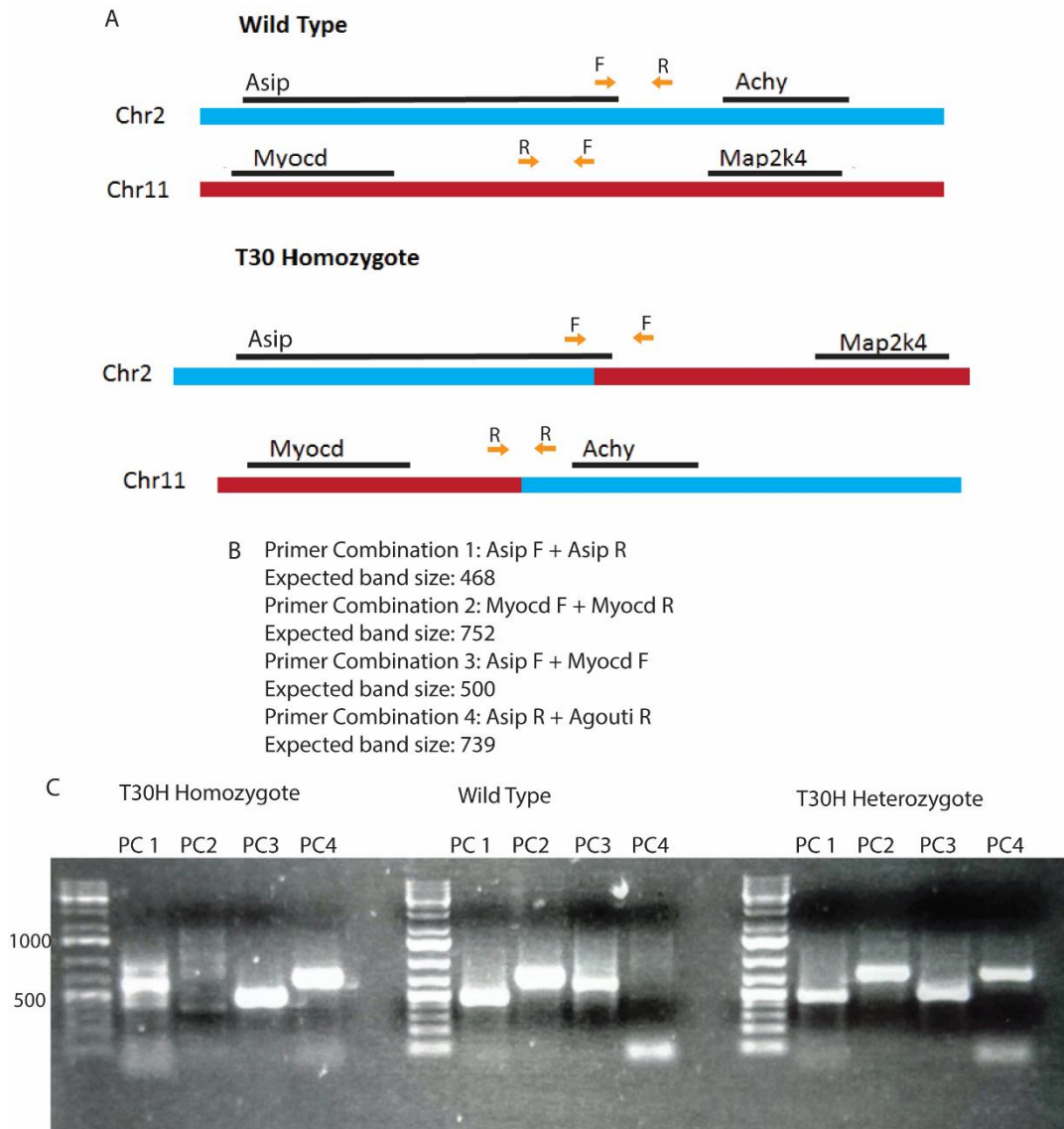


Figure 22. A - PCR strategy to confirm the location of the translocation breakpoint. Primers were designed flanking the two translocation regions. These could be swapped to amplify bands of intact chromosomes as well as translocated ones. Genes surrounding the translocated regions are also indicated. B - All primer combinations used along with their corresponding expected band sizes. C - The PCR confirmed that the region identified was in fact the translocated region. This primer combination was also then used for all genotyping going forward. Two non-specific bands are amplified in this PCR. PC1 in T30H homozygotes is non-specific as is PC3 in heterozygotes. This was confirmed by sending purified DNA from these reactions for sequencing. To ensure the phenotype was not lost, every six months the DNA amplified from the translocated region from a heterozygous mouse was sent for sequencing. N=8 sent for sequencing.

Breakpoint 1

```
CCAGTTGTCTTGTCTCGACCATACAAATTTATTATTCTTTGTCTAGAGAA
TATAAAAGCATCGTGCTTTGGGCACTTCTTCAGACTTTATGCTCTTGTGA
AGATCCCCATATACACGGAAATTTAATAAAACTTTATGCTCTTTCTCTTA
TTAATCAGTTCTTATAACAATGAATATGGGTTCTTAGATCCAGCCAAAGAG
CCCACATAAGAATAAGAGGGGAGACGAGAGGACCCCCCCCCCACTCACA
TAATTGGAAAGTGATGAAGTCACGTATGTCCAACCACAGATCTGACATTG
AGCTTCACTGTCCTACCTACTTTATACAAAGAACTGTATGAGAA CATA CA
TGGTACAGACACACAGACAAAACACTCATATATATAAAATATGTGGATTT
TTAAAAAATCTGCCAAGTATGGTGGCACATGTTTGTAATCCCATACAAGA
TGGAAATAGAAATATCCTGGGGGTCTGCTGGCCAGCTGGCCCGACTACTT
GGTGAGTTCTAGGCTAATGAGAAAGCTTATCTGAAAAATTATCATGATGA
TGATAATGAGTACCTGAGGAACAACATGTGAGGTTTTCTCTGGTCTATA
ACAAATACAGAATGTATATTTTTTATCATACATAGTTTAGACATTAATTC
CTCTAAATATATGTTTTTCTTTTTACCAATTACAGTGTTGGTTCACAGA
GTAAATTAGCTAGAATGGACCCATCCTTCCTTGCTTTTG
```

Breakpoint 2

```
TCCACCAAAGGCCTTATTGCTGTTTCTCTGTTGATTATTTAGCTGTGTTT
CCGAGAGTCTATCTACGAGTAAGAGATTGTCAAGAAAGAACCCTTCTACT
GATTAGGTGTTGAGGGGTTGGGTACCAGCTCAGTCAGTAAAGCACTTGCC
TGGAAAATATCAGGACATGAATTTTATCCCCAGAGCCCATGTCAAAAAGT
GCCAAGTGTGGGGAACCAGAGACATGGTTCAGAGGTTAAGAGCATTGGCT
GCTCTTACAGAGGACTTGGGTTTCTGTTGGTTAGCACCCACGTTGTGGCTC
ACAGTCACCTGTAAACAACAGTTCTAGAGGACTGATGCTTTATTCTGACCT
CCAGGAGGTCATCTTTCTGATGAGAAGAGTCTCTGTGAGCAATTAAGAA
CAATGAGGTAAGTGAACAATGTCCATGGCATTGAATTTAAGAGCAGAGTGG
GATTCAAAAGGGAGAGCATCCTCTTTGGGTTGGCCTGGCTGAAAGAAAG
```

Chr 11

Chr 2

Extra sequence

Figure 23. The exact genetic sequence of the translocation points on both chromosome 2 and 11. On breakpoint 2 there is also some additional sequence DNA. Initial sequencing n = 1, subsequent sequencing of PCR product to confirm that the translocation had not been lost, n=8.

5.1.2.1 Location on Chromosome 2

On chromosome 2 the translocation point falls approximately 7.5KB within the 3' UTR region of the *nonagouti* gene (**Figure 24**). This gene is primarily expressed in the integumentary system, specifically the hair follicles. It controls pigment distribution in the hair follicle, with different variants of the gene determining coat colour. Knockouts of the gene in mice become obese and can be used as a model for type II diabetes (Klebig et al, 1995, Yen et al, 1994). Apart from kidney disease induced by type II diabetes there is no renal phenotype associated with *agouti* mutations.

The translocation is also close to the gene *Ahcy* – approximately 15KB downstream. *Ahcy* is a highly conserved gene expressed widely throughout the body in diverse organ systems (Kusakabe et al, 2015). Gene knockouts have a disease phenotype in relation to ageing and mortality and the skeletal system. In humans, mutations to the orthologous gene cause hypermethionemia, a metabolic disorder. There is no renal system phenotype associated with knockouts of the gene.

The translocation point is also nearly a megabase (~990KB) away from *Gdf5*, the gene historically used before the genotyping PCR was developed to determine whether pups born bore translocated chromosomes for not.

5.1.2.2 Location on Chromosome 11

The translocation point on chromosome 11 falls in a less gene-rich area close to the smooth muscle gene regulator, *Myocd* (**Figure 24**). As described previously, this gene is directly involved with activation of smooth muscle expression through cofactor binding with serum response factor (SRF) which then in turn binds to CArG boxes in the regulatory areas of smooth muscle genes.

The only other gene close to the translocation point is *Map2k4*. Knockout mice bearing this gene do not exhibit any renal associated phenotypes. Knockouts have disease phenotypes related to ageing and mortality, liver function and growth.

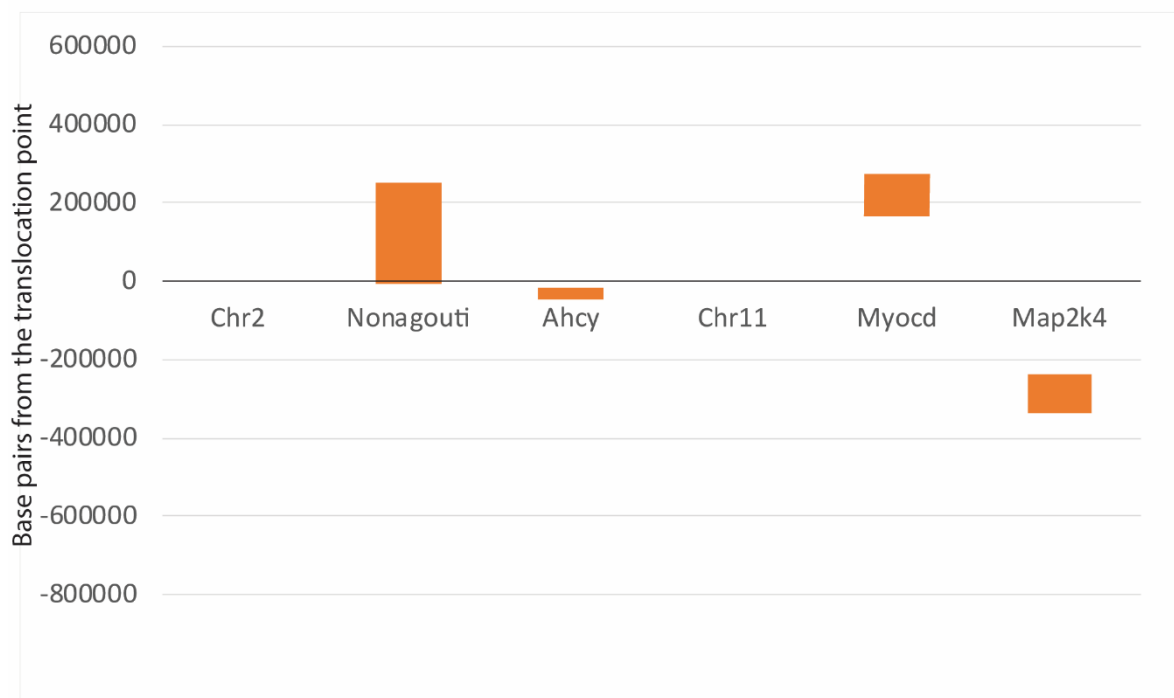


Figure 24. The distance in base pairs that each of the flanking genes lies from the translocation point on chromosomes 2 and 11. The translocation intersects the 3 prime end of Nonagouti, and is furthest away from the gene most likely to be implicated in the phenotype, Myocardin (Myocd). This gene does, however, have postulated long range enhancer regions residing in the area of the translocation point on chromosome 11.

The most likely of the genes to cause the T30H phenotype in both regions is *Myocd*, which is around 180kb away from the translocation point. Despite it being the gene furthest away from the translocation point of the four flanking genes its role as a master regulator of smooth muscle expression provides compelling evidence for its involvement with the phenotype. Other animal models where *Myocd* expression is altered also show a similar phenotype to that seen in T30H mice (Huang et al, 2015, McHugh, 2014). Further studies into the genetics behind the T30H mouse model concentrated on investigating the role of *Myocd* in creating the T30H mouse phenotype.

5.1.3 Reverse transcriptase PCR for genes in close proximity

Assuming that *Myocd* is the gene involved in generating the phenotype of the mouse model because of its role in development is not sufficient to be able to draw any firm conclusions. Other genes surrounding the translocation point must be tested and ruled out to ensure that the translocation is not altering their expression and that they are also not contributing to the phenotype.

Primers were designed for nonagouti, *Ahcy* and *Map2k4* and then tested on positive controls from wild-type mice on a temperature gradient to find the optimal annealing temperature (**Figure 25**). The samples used for positive controls were based on the tissues which were noted as having the highest expression from the mouse ENCODE consortium (Yue et al, 2014). Nonagouti was tested using testes tissue samples, *Ahcy* was tested using liver samples and *Map2k4* was tested using brain samples. Three sets of primer pairs were ordered for each gene and the one which showed the clearest expression in gradient PCRs was used to test T30H and wild-type mouse samples for changes to expression.

The primers were then tested in the T30H mice using a panel of tissue samples consisting of the bladder, kidney, gut, liver, heart and lung samples. The same organ panel was tested in wild-type mice for comparison. There was also a housekeeping gene control (*Gapdh*) for all these tissue samples.

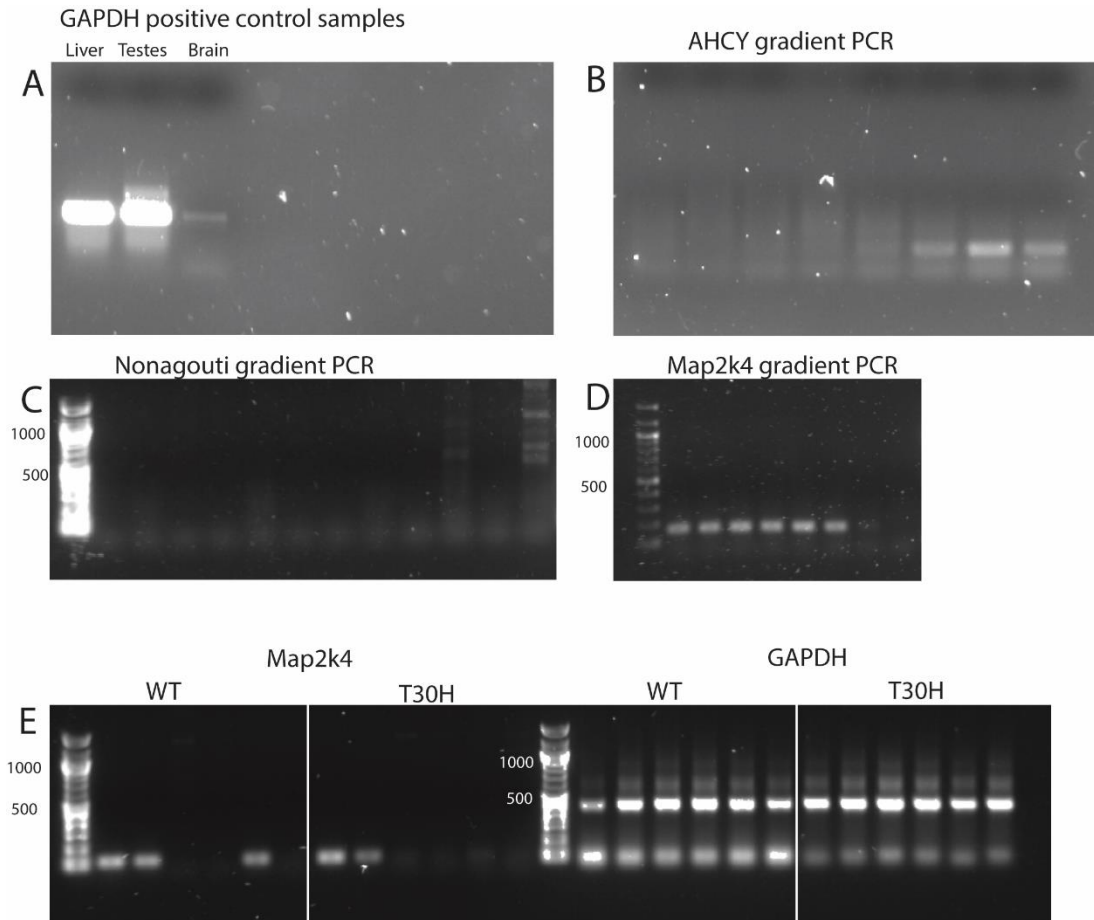


Figure 25. RT PCR of genes flanking the translocation point. A. GAPDH PCR of the three positive control sample tissues selected to perform a gradient PCR on the three primers. Tissues are adult liver, testes and brain, all taken from adult mice. B. Gradient PCR for AHCY tested on adult liver cDNA. Predicted PCR product size - 111bp C. Gradient PCR for Nonagouti tested on testes cDNA. Predicted PCR product size 624bp. D. Gradient PCR for Map2k4 using brain cDNA. predictedPCR product size 118bp. E. RT-PCR of Map2k4 tested on bladder, kidney, gut, liver, heart and lung tissue from P1 T30H and WT P1 mice, as well as GAPDH RT-PCR for the same samples. N=2.

In almost all samples there were no differences in expression between wild-type and T30H mice. There were no positive results from any of the nonagouti or *Achy* samples in either T30H or wild-type mice, after observing bands of the expected lengths in positive control tissues using a gradient PCR. *Map2k4* was expressed in the kidney and bladder in both samples. In the heart there was a defined band in the wild-type mice but a very faintly defined band in the T30H mice. This could indicate a difference in expression, but no difference was seen in heart samples in histology.

5.1.4 Reverse Transcriptase PCR for splice variants

I then examined the expression of *Myocd* in the same tissue panel used to gauge the expression of translocation-flanking genes. Ascertaining *Myocd* expression is made difficult by the fact that the gene undergoes alternative splicing depending on in which organ it is expressed in. *Myocd* has four different splice variants, which are differentially expressed in different organ systems (Imamura et al, 2010). It has been suggested that there are bladder-specific *Myocd* splice variants that are essential to normal bladder detrusor smooth muscle development (Saha et al, 2009).

Once the location of the translocation point was found it was important to understand both whether *Myocd* was the gene responsible for the phenotype, and the mechanism behind the development of the phenotype. Understanding the differential expression of the *Myocd* gene in T30H homozygous mice compared to controls is key to understanding whether alternative splicing in the bladder is essential for smooth muscle growth.

A RT-PCR strategy was used which had previously been developed to investigate gene expression in Mgb mice (Saha et al, 2009). It amplifies two different sections of cDNA, which determine whether or not a long or a short form of exon 2a have been included when *Myocd* is transcribed. Exon 2a can be split into three parts – a 214bp section, a 47bp spacer section, and a 44bp section. The 214bp section can be expressed alone or in addition to the 44bp section. Both variants introduce a premature stop codon, truncating the final protein.

Exon 2a was used as opposed to 10a because it has been suggested in previous studies that exon 2a is more important to smooth muscle expression in the bladder, whereas alternate exon 10a expression is more important in the heart (Imamura et al, 2010). Exon 2a has an in-frame stop codon, which then causes translation from an alternate start codon in exon 3, causing the expression of a truncated protein. In wild-type mice, the shorter, truncated protein is reported by the literature to be more prevalent in the bladder than any other organ, although there is also expression in the heart and other organs containing smooth muscle.

In the PCR strategy used, 6 organs (bladder, kidney, gut, liver, heart and lung) were analysed from P1 T30H homozygote and wild-type mice. In the wild-type mice, the longer form of the gene with the addition of 241bp plus 44bp exon 2a is most widely expressed in the bladder (**Figure 26**). In all other organs the shorter 214bp exon 2a is more highly expressed, especially in the heart. In the T30H homozygous mouse samples however, in the bladder sample there is increased expression of the shorter version of the splice variant containing exon 2a, and in all other organs there appears to be a global decrease in the expression of both splice variants. This suggests that the expression of *Myocd* is widely disrupted in T30H homozygous mice.

In the gut and liver there is a larger band present. In the paper reporting the PCR strategy this band is also observed and the authors describe it as being non-specific (Saha et al, 2009). To ensure this was true, the PCR product was excised from the gel, DNA purified and then sequenced by the company Source Bioscience. This amplified DNA was non-specific as had been previously reported.

The difficulty with carrying out RT-PCRs using T30H homozygous bladder tissue is in the extent of the malformation of the organ. Because the smooth muscle wall layer is so reduced there may only be very few bladder smooth muscle cells within the tissue sample used to extract RNA. This could mean that the *Myocd* expression in these samples may not be from bladder smooth muscle cells at all but could be due to vascular smooth muscle cells of the bladder. However, the differences in expression of *Myocd* in all other organs sampled still suggests that there is a difference in *Myocd* expression in T30H homozygous mice.

I also carried out RT-PCR to test for the presence of exon 10a in wild-type and T30H mice (**Figure 27**). In wild-type mice it has been reported that this exon is most heavily involved with heart development and muscle maintenance (Imamura et al, 2010). In the wild-type test samples, the tissues with the highest expression are the heart and the bladder. There is no expression observable in the gut and the liver. In the T30H mouse samples there is increased expression in the heart, bladder and the lung. There is also an additional band of exon 10a expression in the kidney. This could imply a compensatory level of expression of exon 10a to respond to the differences in expression to exon 2a.

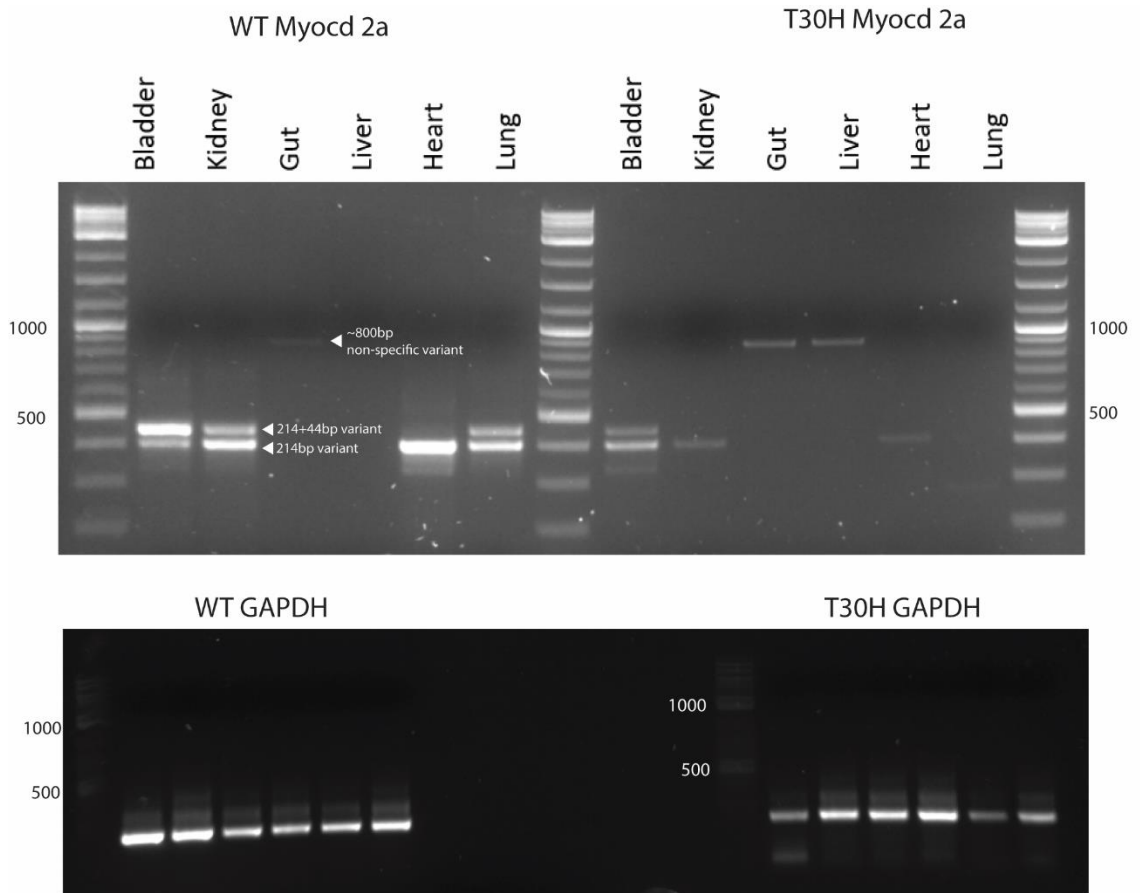


Figure 26. Reverse Transcriptase - PCR to ascertain the expression of exon 2a isoforms in myocardin. Six organs were taken from P1 T30H homozygous and wild type mice. In the wild type mice the longer form of the gene with the addition of exon 2a is most widely expressed in the bladder, the reverse is true for the heart, where only the shorter variation is present. In the T30H homozygous mouse samples however, in the bladder sample there is increased expression of the shorter splice variant of exon 2a, and in all organs there appears to be a global decrease in expression. This suggests that the expression of myocardin is widely disrupted in T30H homozygous mice. A positive control for the presence of GAPDH, a housekeeping gene, was also run for all organ samples in T30H and wild type mice. Although every care was taken to ensure an equal amount of cDNA was loaded there are some discrepancies in the T30H GAPDH control blot. This could mean that the corresponding myocardin 2a blot may not represent accurate expression. Typical blot, n=5.

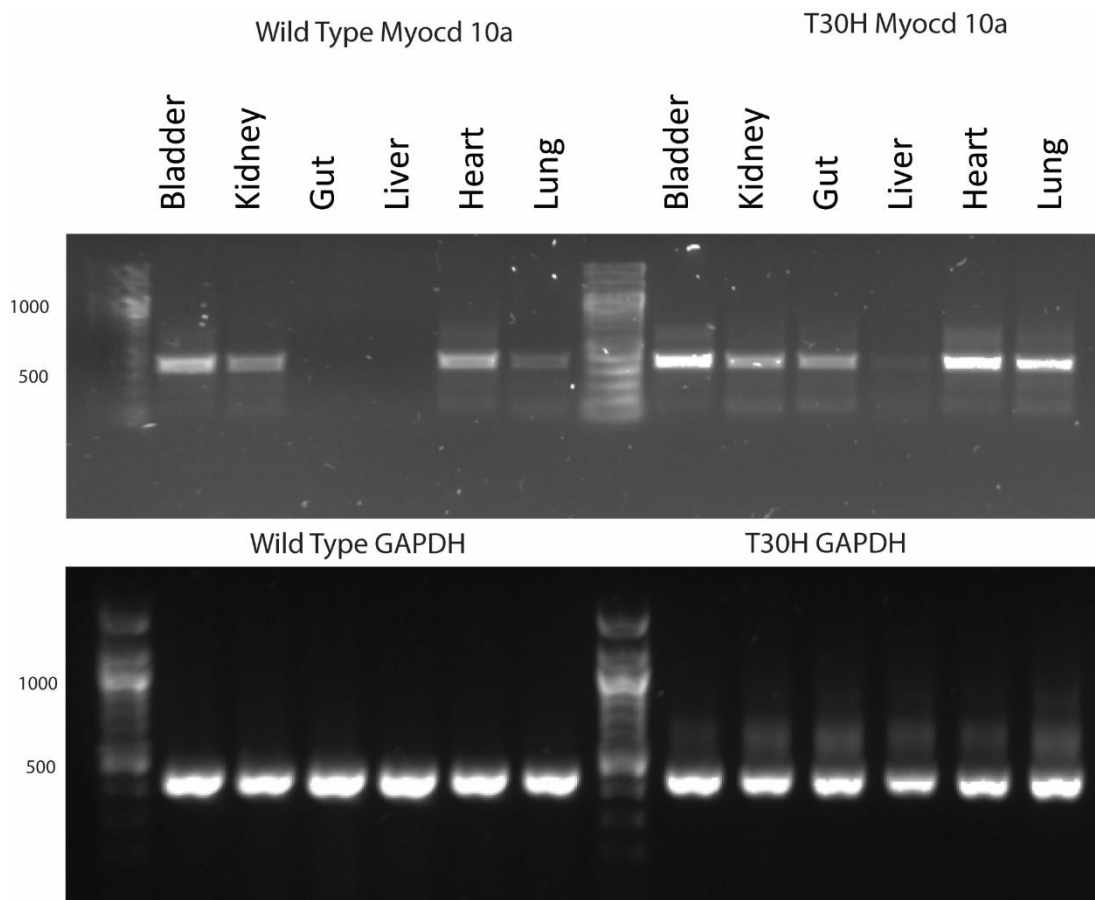


Figure 27. Reverse transcriptase PCR to detect whether exon 10a is expressed or not, as well as GAPDH controls, in both wild type and T30H mice. In wild type mice the most expression is in the bladder and the heart, with some additional expression in the kidney and the lung. This is consistent with findings in the literature. In T30H mice there appears to be increased expression in the bladder, as well as in the heart and in the lung. There is also an additional band of exon 10a expression in the gut sample. Typical blot, n=3.

5.1.5 Q-PCR for splice variants

I have also carried out quantitative PCR experiments for the expression of exons 2a and 10a in both T30H and wild-type mice (**Figure 28**). The expression of these splice variants of *Myocd* were standardised against the expression of *GAPDH*, a housekeeping gene. Assays have been graphed separately for each exon and for wild-types and T30H samples, this is because of the very high expression in some samples. They have also been graphed together on a separate plot using logarithmic scaling in order to compare all samples.

In wild-type mice, the organ in which exon 2a was most highly expressed is the heart. Expression in all other organs is relatively similar, apart from the bladder, which is slightly lower. Exon 10a, in contrast, has the highest expression by a very large margin in the bladder, followed by the heart and with negligible expression in all other organs tested. The error, however, is the highest in the samples with the highest expression for the respective expression in each organ.

In T30H mice exon 2a is most highly expressed in the heart, followed by the bladder. Expression in all other organs is lower. The relative expression of exon 2a of *Myocd* in all organs is higher than in the wild-type controls. In the bladder this is much higher.

Myocd exon 10a is also differentially expressed in T30H mice. The highest relative expression is still in the bladder, but it is much lower than that of the wild-type. The next highest level of expression is in the heart and then the gut, but these are still relatively low. Again, in the heart the expression of exon 10a is lower compared to the wild-type.

This would suggest that mice bearing the translocation have differential expression of *Myocd* splice variants. Gaining samples from the bladder in T30H mice, however, is difficult because there is so little bladder tissue present. *Myocd* expression in the bladder sample could have a large contribution from the vessels present in the bladder simply because there is so little bladder smooth muscle tissue.

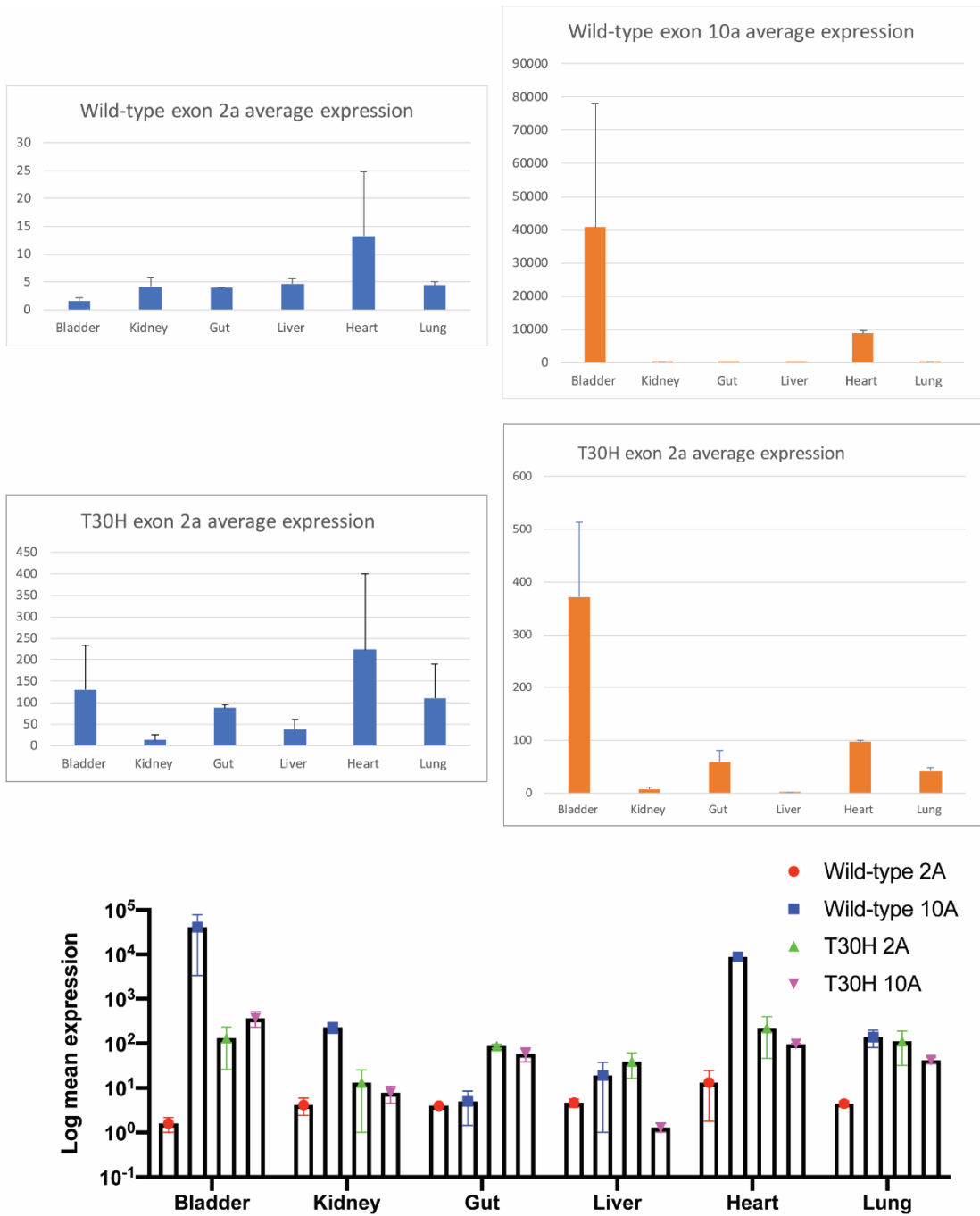


Figure 28. Quantitative PCR results for the relative expression levels of myocardin exon 2a and exon 10a, in both wild-type and T30H mice. Expression is displayed in separate graphs because of the disparity in the level of expression of exon 10a in the bladder compared to all other samples. The relative expression is also displayed on a collated graph with data converted to a logarithmic scale in order to display all samples on the same axis. N=2 for all data sets.

5.1.6 Summary

Uncovering the precise sequence of the area of the translocation point was necessary to properly genotype T30H mice, uncover the genes which might be involved in the phenotype, and to find targets for future therapies. The translocation point found using next generation sequencing and is in the 3-prime region of the gene Nonagouti on chromosome 2, and around 180kb away from the translocation point. The gene most likely to be responsible for the genotype is *Myocd*. I have investigated whether this is truly the case by carrying out reverse transcriptase PCRs and quantitative PCRs for the expression of different splice variants of *Myocd*. The expression of both exon 2a and exon 10a is altered in T30H mice compared to wild-types, and there appears to be a global decrease in *Myocd* expression in T30H mice. This could be the cause of the smooth muscle bladder phenotype observable in T30H mice.

5.2 Phenotyping the T30H Mouse

Prior to the commencement of my project, the T30H mouse had not been fully characterised, nor the histology fully explored. Previously this had been difficult because of the inability to genotype the mice, but once the translocation had been found it became possible to be certain of which mice were homozygotes. I carried out this characterisation initially by fixing, embedding, sectioning and then staining T30H mouse tissue samples, and then comparing them with T30 heterozygotes and with unrelated wild-type mouse samples.

This involved examining structural defects in the urinary tract, as well as using a number of markers to detect changes to protein expression in mutant mice. Other organs were also investigated to establish whether the mice only had urinary tract abnormalities; ensuring no other organ systems were affected.

Samples were initially taken at P1 – this was in order to avoid culling as few T30H breeding heterozygotes as possible as small litter numbers made maintaining colony stocks difficult. T30H mice die soon after birth, and death due to renal failure can only be avoided by manually assisting bladder voiding, therefore, all suspected T30H mice were culled at birth and then genotype was confirmed by PCR. At the commencement of the project, genotyping was unavailable, and so the majority of samples were also taken at birth to be sure of the phenotype and to retain breeding females.

Markers used for phenotyping and investigating bladder and kidney defects in the T30H mice were specific to smooth muscle, and to other bladder specific markers, such as those found in the urothelium.

5.2.1 PAS Staining

Initially, PAS staining with counterstain in Mayer's haematoxylin was used in order to identify the gross structural defects present in the T30H mouse model. PAS staining is also particularly useful to identify the morphology of the kidney because it stains the brush borders of the proximal tubules pink. It was primarily used to identify the defects in kidney development.

Examining the kidney in this way, it was possible to identify the extensive hydronephrosis present in T30H mice. P1 kidneys were examined in T30H mice (**Figure 29**). Hydronephrosis was present in P1 samples, and in some sections distension of both the proximal and distal tubules as well as the glomerulus was also present; this indicates extensive retention of urine in the kidney. Distension of the ureters was also observed in some samples.

*

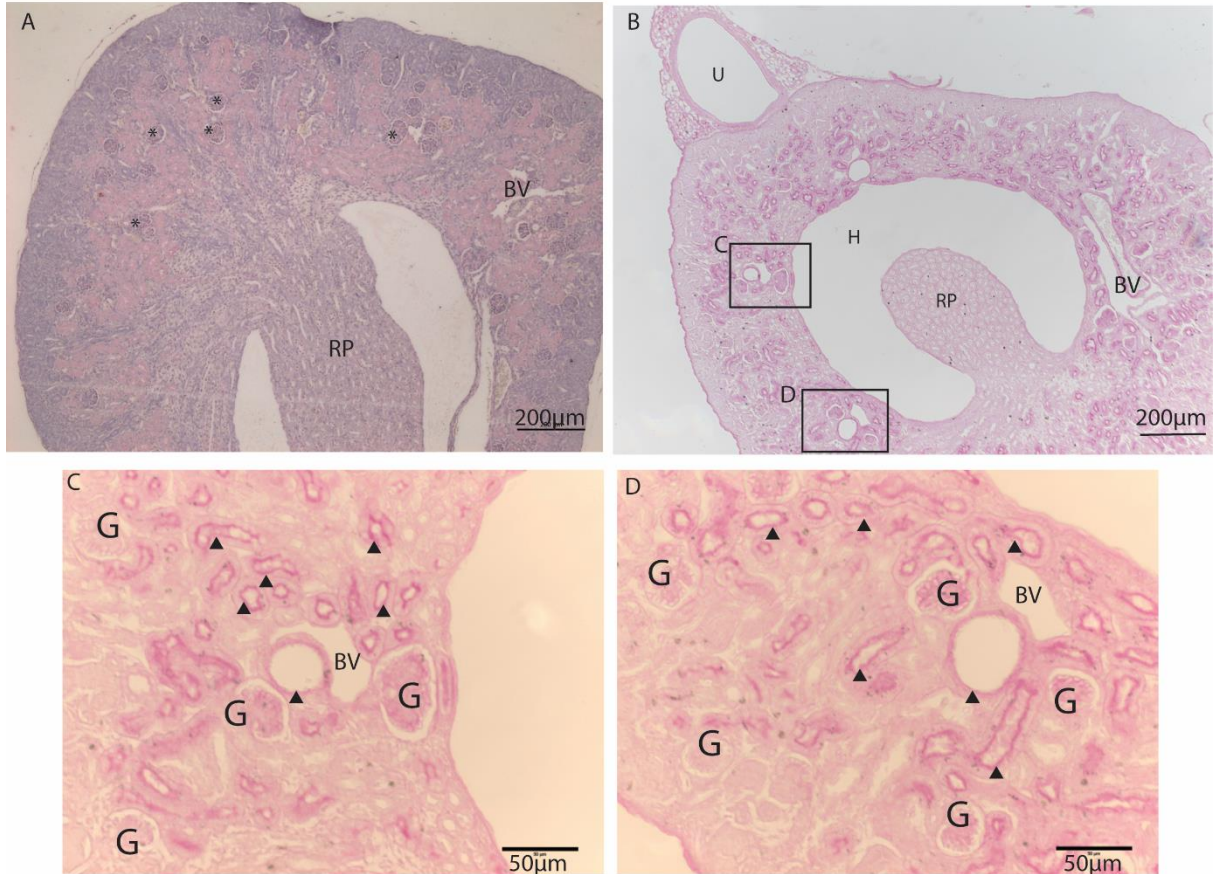


Figure 29. PAS stained images of T30H and wild-type kidneys at P1. A. Wild-type P1 kidney stained using PAS staining. glomeruli are marked with *. B. T30H kidney stained using PAS staining, hydronephrosis (H) is observable surrounding the renal pelvis (RP) as a larger gap surrounding the renal pelvis than is observable in the wild-type kidney. Some nephrons also show distension of the tubules. Examples shown at higher power in C and D. C & D. There is evidence of distension of some proximal and distal tubules, in addition to the glomeruli. Representative images of n=3 kidneys. RP - renal pelvis, H - hydronephrosis, G - glomerulus, * - glomerulus, ▲ - proximal tubule, BV - blood vessel, U - ureter.

5.2.2 Alpha smooth muscle actin expression

α SMA is a marker of smooth muscle cells. I used α SMA staining to examine the structural abnormalities to the kidneys and bladder. In normal mice the marker begins to be expressed at E13, and then as development progresses the proportion of smooth muscle cells present in the bladder increases (**Figure 30**). In the bladder of T30H mice the proportion of α SMA positive cells in the bladder is severely reduced compared to wild-types, and only a thin line is visible, if the protein is expressed at all (**Figure 31, Figure 33**). α SMA is one of the major constituents of the detrusor smooth muscle wall in the bladder and is required for contraction of the muscular wall which allows bladder emptying (Zimmerman et al, 2004). It is also present in the gut (**Figure 34**), but no differences were observed between wild-type mice and T30H homozygotes in this tissue.

The bladder of T30H mice also showed severely reduced structure generally. In wild-type mice the bladder typically has a thick muscle wall in order to retain and release urine, as well as defined layers of lamina propria and urothelium. In P1 T30H mice this muscle wall is almost completely absent, and in large areas it is reduced to only a few cells thick. The other layers of the bladder wall were also difficult to identify; the bladder is so distended that all remaining layers are also comprised of very few cells. At E16 this is also true, but to a slightly lesser extent, indicating that the bladder phenotype worsens in the later stages of development. The bladder of T30H mice is considerably reduced compared to the wild-type (**Figure 35**). The intensity of DAB staining is also reduced compared to the wild-type, also possibly indicating reduced α SMA expression.

In the kidney of T30H mice at P1 there is increased α SMA expression compared to wild-type kidneys at the same stage, particularly around the renal pelvis and collecting ducts (**Figure 32**). An increase in expression of α SMA indicates fibrosis and scarring in the kidney (Sun et al, 2016), which in this case could be due to the reflux of urine into the kidney from the bladder.

In other organs which normally express α SMA, such as the gut, there was no observable difference between T30H mice and wild- types. This was ascertained by

taking three representative images of the gut in three T30H mice and three wild-types stained with α SMA. These were then compiled into a document and sent to three other members of my research group for blind scoring (Daniyal Jafree, Saif Malik and Lauren Russell) (See Appendix for score sheet). Scoring was carried out by participants being told the final mouse sample in the series was wild-type and then asking participants to compare all other mouse samples to this wild-type sample. They were asked whether they thought each mouse's gut morphology was the same or different to the wild-type or whether they were not sure. All three participants found that two T30H of the mouse samples and the two wild-type samples were no different to the wild-type mouse they had been asked to compare against. In the final T30H mouse sample all three participants were not sure whether it was different or not to the wild-type sample, although one of the participants remarked that the sample preparation could have influenced this decision as they thought that the sample looked as though it may have dried out as it was being prepared.

In heart tissue the similarity between wild-type and T30H morphology was confirmed by imaging the whole organ. This was carried out by collaborators at CABI (Centre for Advanced Biomedical Imaging) (Claire Walshe). As she was developing a novel imaging technique utilising HREM (High-Resolution Episcopic Microscopy) (Weninger et al, 2018), I am not able to publish the images obtained using this imaging technique in this thesis. HREM involves imaging individual slices of the tissue and then reforming the tissue as a three-dimensional image. This allows visualisation of the tissue on multiple planes. However, I was able to share these images with an expert in heart development, Professor Peter Scambler. He determined that the hearts of both heterozygote and T30H mice at P1 were normal. Septation of ventricles, atrial and outflow tracts were all normal. The atrioventricular and semilunar valves were normal, and there was normal rotation and alignment of the great vessels with the ventricles. Coronary arteries formed and originate at normal ostia. This three-dimensional imaging technique was favoured over traditional histology because the heart is a complex, three-dimensional organ in which it is difficult to ascertain an idea of whether there are differences to the morphology of the organ by observing a single plane.

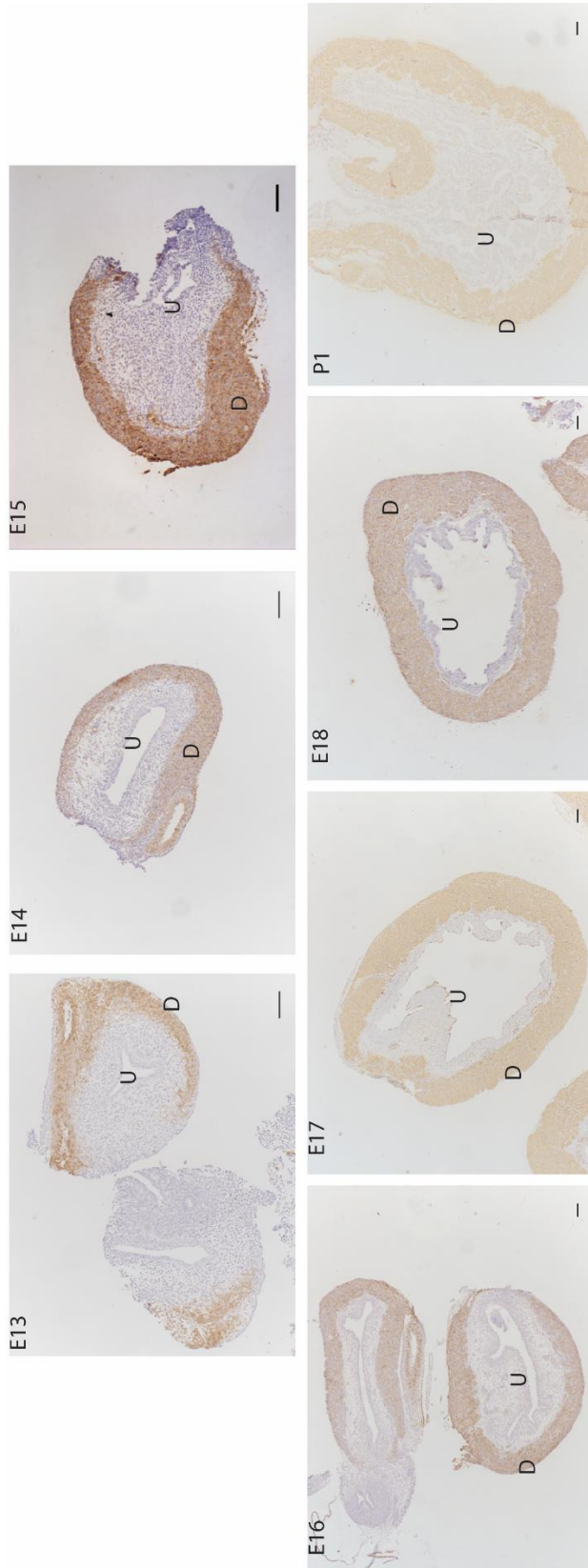


Figure 30. Timeline of bladder development in wild type mice starting from E13 and going through to birth (P1). All images are DAB stained with a smooth muscle actin. DAB staining appears brown/orange. In some sections this appears more yellow because the company supplying EnVision used for staining at the beginning of the project was no longer produced, forcing a slightly different protocol to be used. This more yellow staining still denotes positive α smooth muscle actin. Representative images, n=5. D - detrusor smooth muscle, U - urothelium. All scale bars are set to 100 μ m.

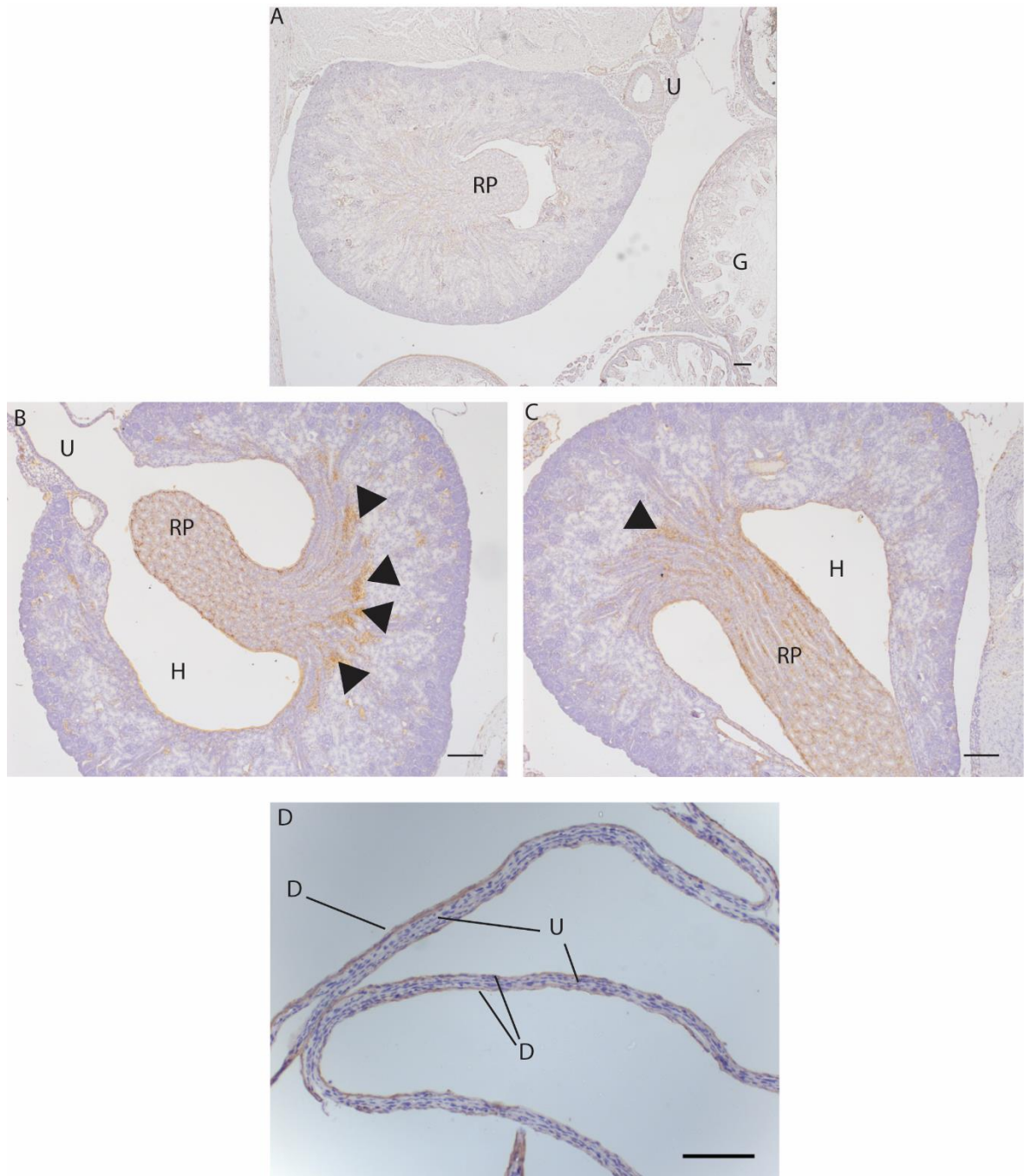


Figure 31. α smooth muscle actin stain of T30H kidney, and bladder histology. A is a wild-type control kidney also stained with α smooth muscle actin. B & C. T30H kidneys show extensive hydronephrosis (H) in addition to increased α smooth muscle actin staining in the renal pelvis (RP). Increased α smooth muscle actin expression in the kidneys indicates fibrosis, this is indicated with arrows. D. The bladder of T30H mice has extremely reduced smooth muscle cells. All scale bars shown are 100 μ m, representative images, n=3. D - detrusor smooth muscle wall, G - gut, H - hydronephrosis, RP - renal pelvis, U - ureters.

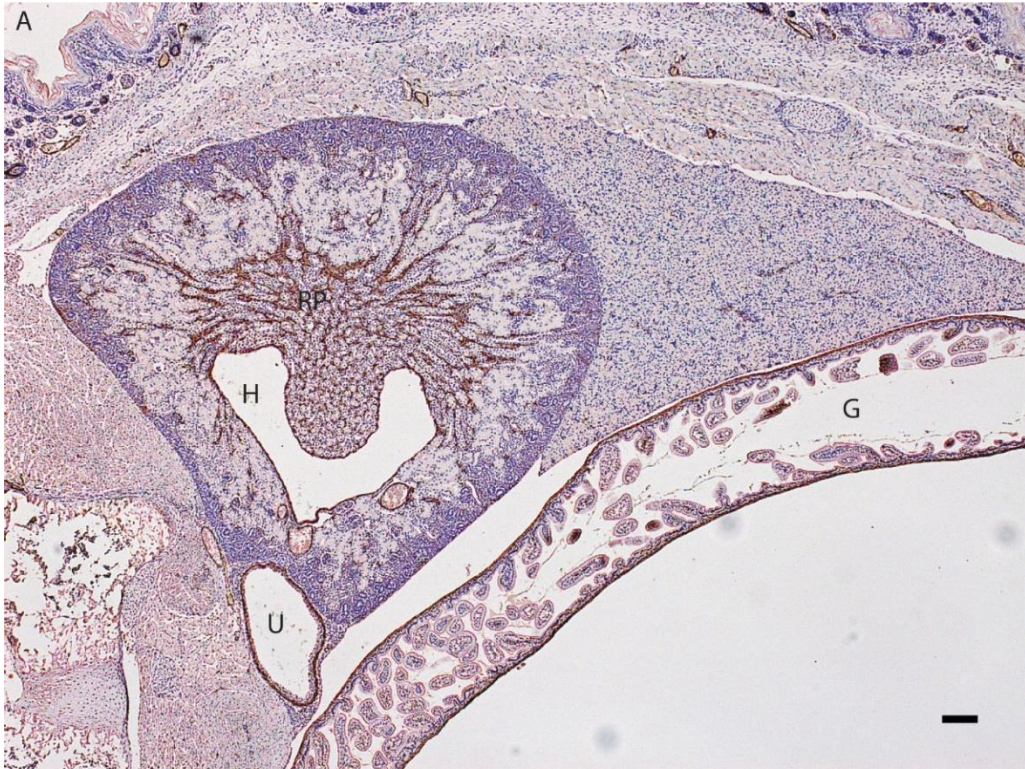


Figure 32. Images of T30H mouse kidney at P1. Both are stained with alpha smooth muscle actin. Both the hydronephrosis (H) and the fibrosis (▼) around the renal pelvis (RP) are very evident. The ureter (U) is also distended, but the gut (G) appears normal. Glomeruli are marked with an asterisk (*). All scale bars are set to 100µm, representative images, n=3. BV - blood vessel, G - gut, H - hydronephrosis, U - ureter.

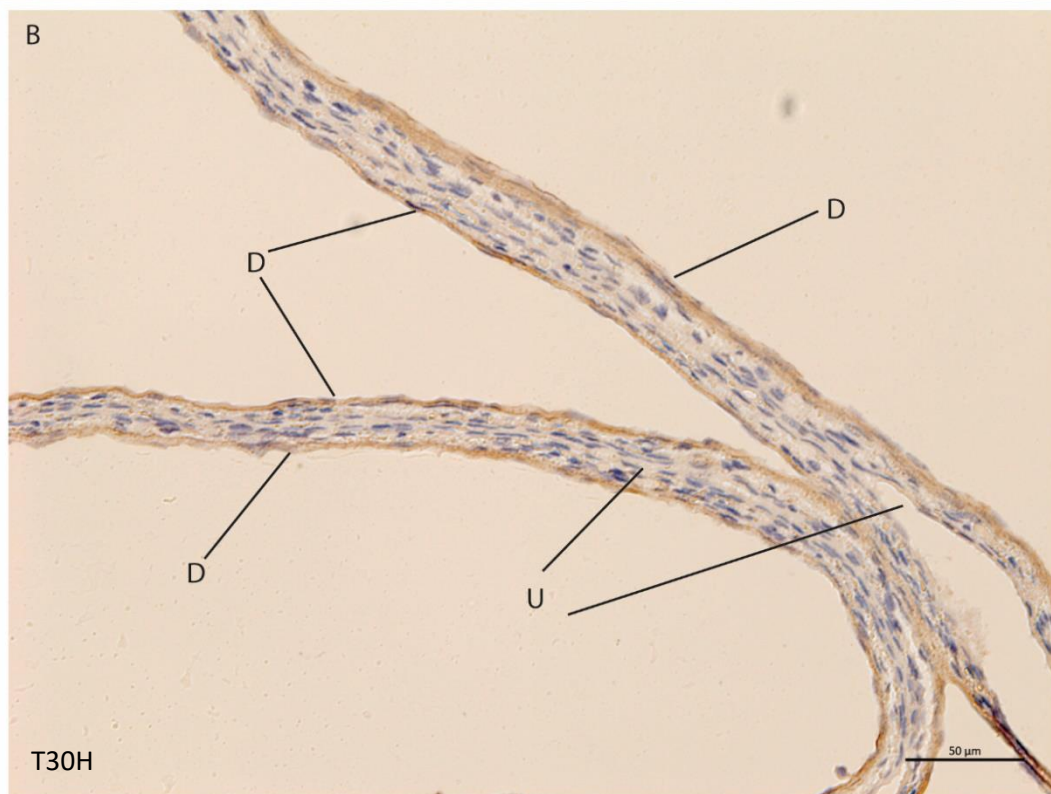
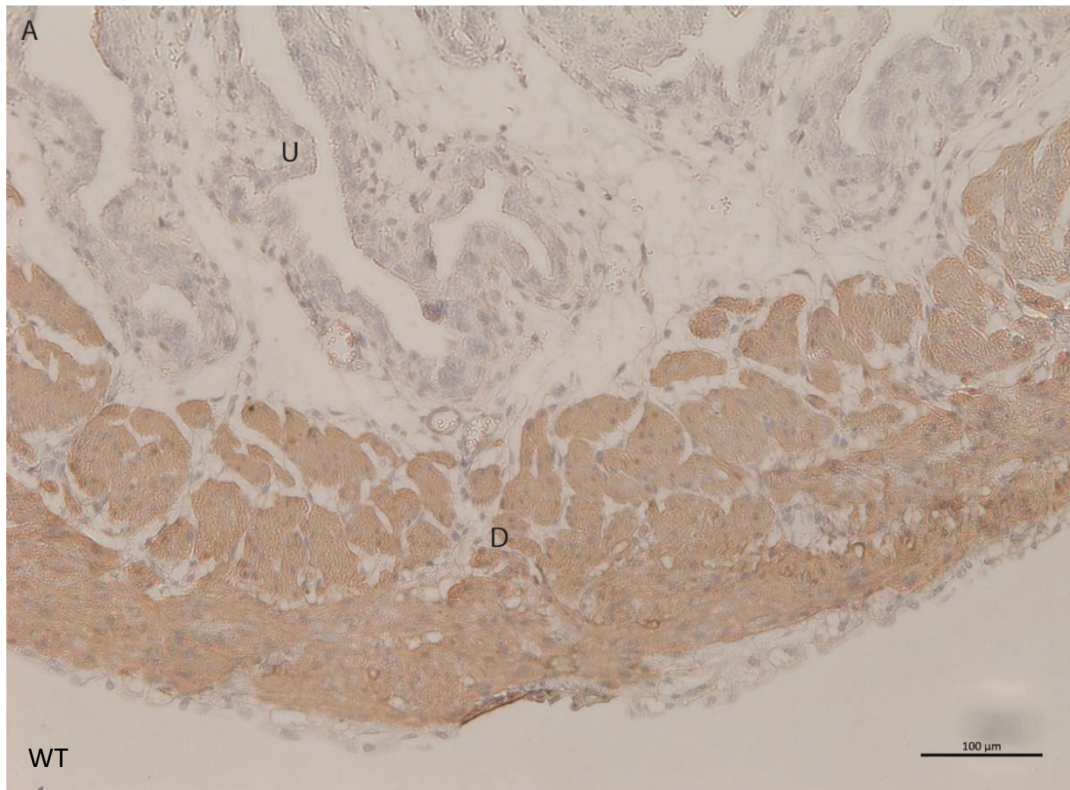


Figure 33. A. Wild-type control bladder stained with alpha smooth muscle actin. The smooth muscle wall is thick and well developed. B. The bladder of a T30H mouse, also stained with alpha smooth muscle actin. The bladder detrusor smooth muscle wall is reduced to only a few cells thick. Representative images, n=3. D - detrusor smooth muscle wall, U - urothelium.

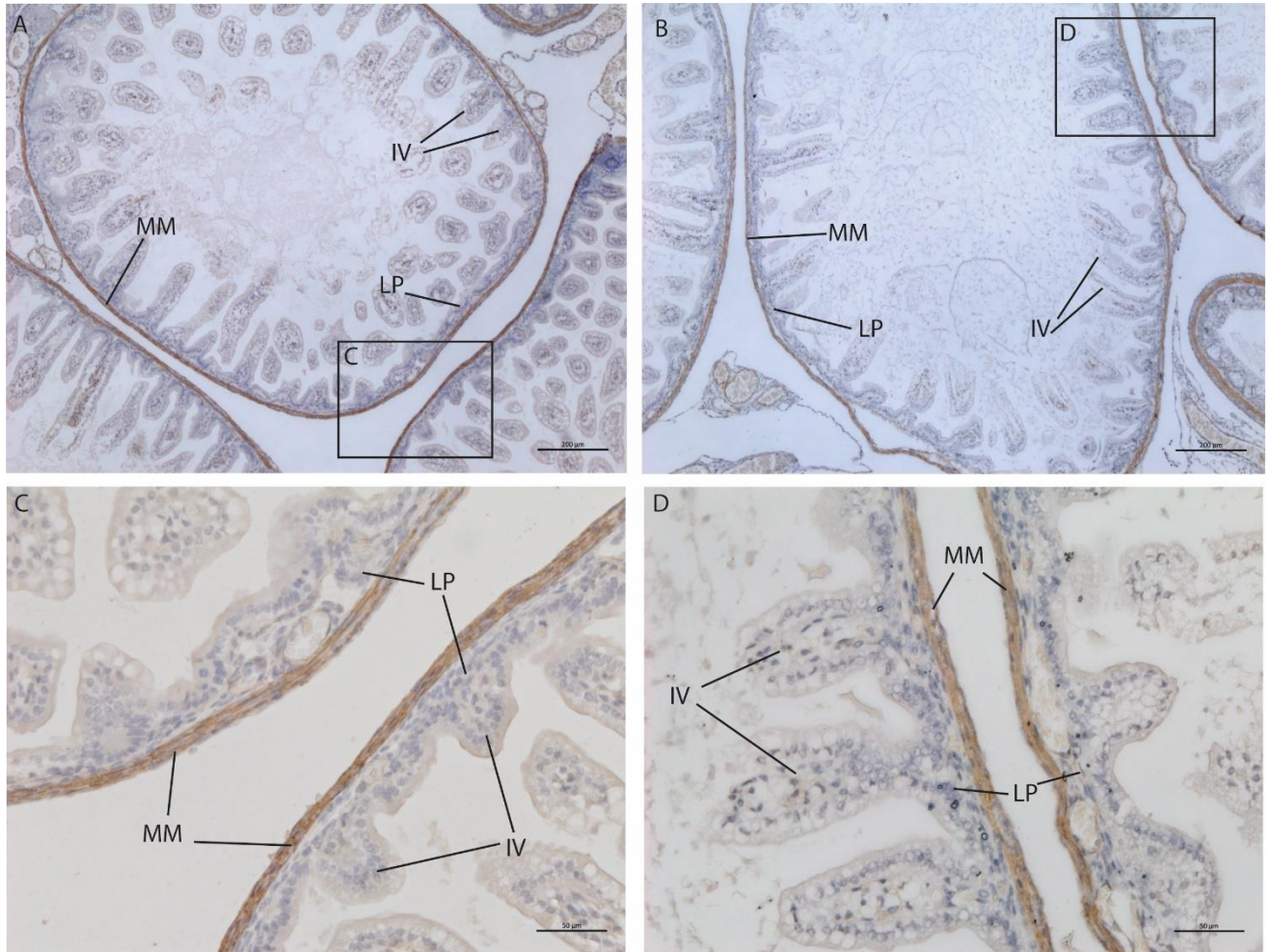


Figure 34. A. wild type P1 gut sample stained with alpha smooth muscle actin. B. compared to a T30H P1 gut sample also stained with alpha smooth muscle actin. No discernible difference is observed between the two. C. Wild-type and D. T30H mouse gut samples at higher magnification. Representative images, n=3. IV - intestinal villi, LP - lamina propria, MM - muscularis mucosae.

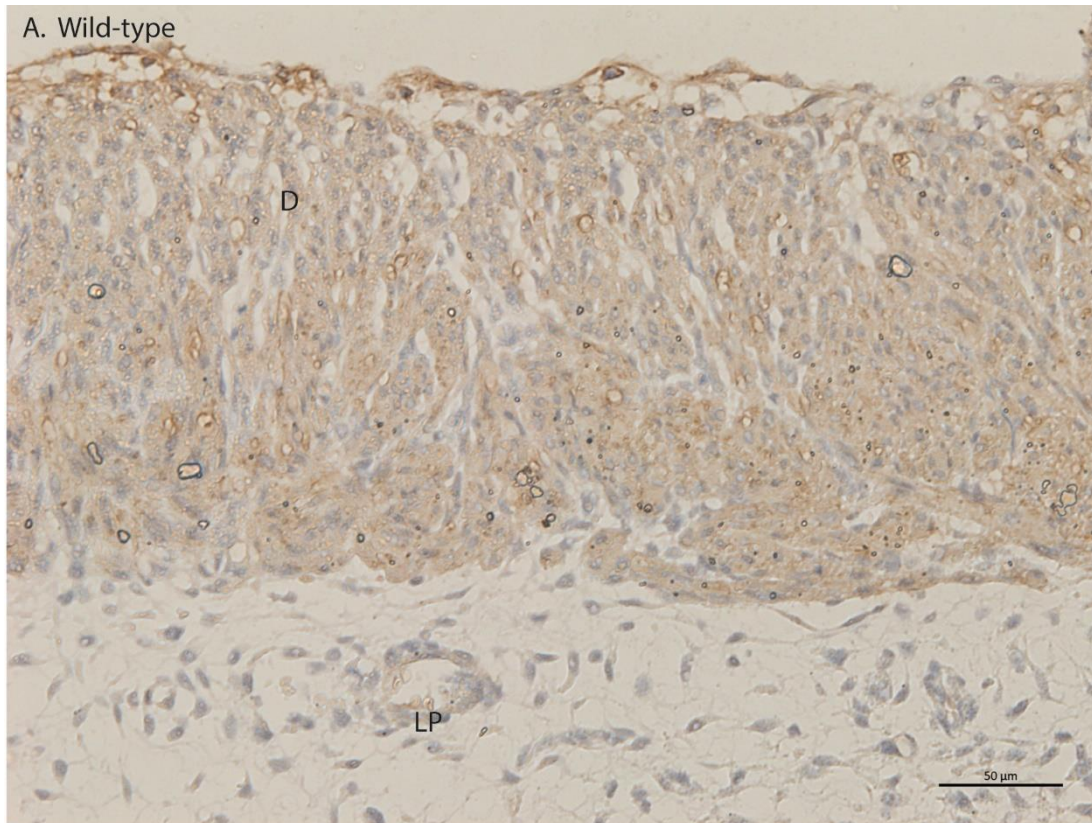


Figure 35. E16 alpha smooth muscle actin staining in the bladder of a T30H mouse compared to a wild-type. Image A shows a WT mouse bladder and Image B shows a T30H mouse bladder. WT sample representative of n=5, T30H n=1. D - detrusor smooth muscle wall, LP - lamina propria, U - urothelium. All scale bars set to 50 μ m.

5.2.3 Calponin Expression

Similar to α SMA, calponin also acts as a marker for smooth muscle cells, but only those that are active, so it can be used as a marker for mature smooth muscle cells. Throughout development staining for calponin is non-specific until E16-17. This implies that smooth muscle cells begin to mature and become fully functional at this stage (**Figure 36**). The expression pattern for calponin is close to that of α SMA in the T30H mouse samples (**Figure 37**). There is severely reduced proportion of calponin-positive staining cells in the smooth muscle wall of the bladder compared to that of T30 heterozygotes and wild-type mice. At E16 in wild-type mice there is minimal expression of calponin (**Figure 36, Figure 38**), this would indicate the smooth muscle cells present are not mature. This is also true for T30H mouse bladders at E16 (**Figure 38**), despite the gross morphological differences in the size of the smooth muscle wall at this point in development.

5.2.4 Uroplakin 3a Expression

Uroplakin 3a is a marker of the urothelium, where it forms urothelial plaques on umbrella cells to protect the tissue of the bladder from the harmful components of urine. Expression of uroplakins begins at E13, and their expression across the urothelium becomes fully established at E14 (**Figure 39, Figure 40**). The expression of uroplakin 3a in the urothelium of T30H mice at P1 is very similar to that seen in wild-type mice and in heterozygous mice at the same stage (**Figure 41**). It is also present in the ureters of T30H mice at similar levels to what is seen in wild-type mice at P1. This indicates that the defect present in T30H mice is primarily of the smooth muscle layer and not of the urothelium. Uroplakin 3a expression is also visible in the ureters of T30H mice, although they are distended compared to the wild-type (**Figure 41**). Earlier in development, at E16 there is uroplakin 3a expression in a similar pattern to that observed in wild-type mice at the same stage (**Figure 42**).

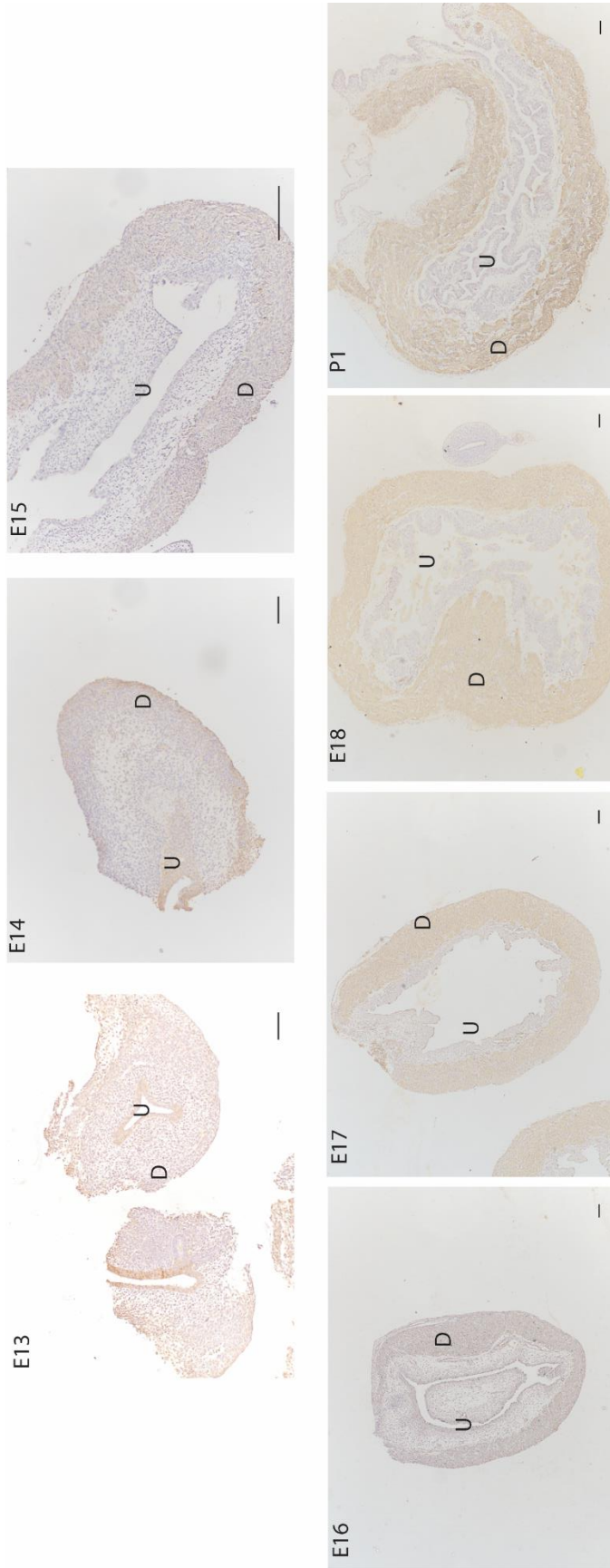


Figure 36. Calponin expression stained by DAB staining in wild type mice throughout development from E13 to birth (P1). All scale bars shown are 100µm, representative images, n=5. D - detrusor smooth muscle wall, U - ureter.



Figure 37. Calponin DAB staining in T30H mouse bladders at P1. Calponin is only present in mature muscle cells, of which there are a great deal less compared with wild type bladders (Figure 36). The two example bladders are from two different mice. All scale bars in images are set to 100 μ m, n=3. U - urothelium, D - detrusor smooth muscle.

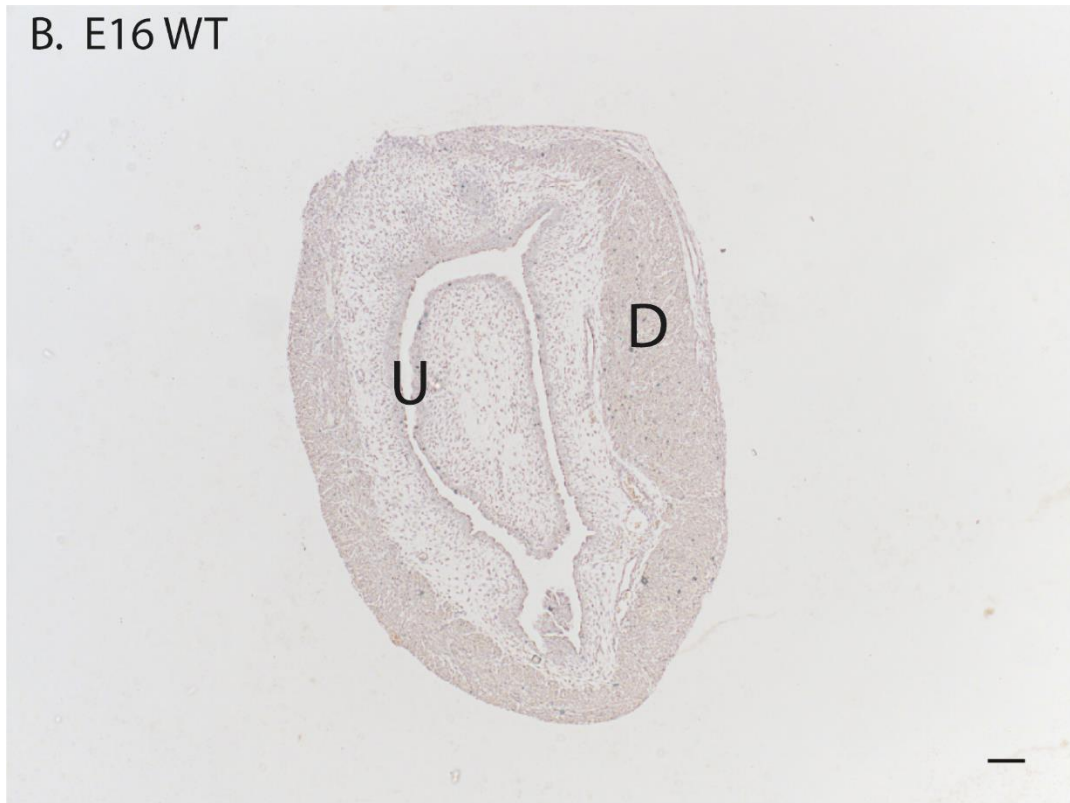


Figure 38. E16 calponin staining in T30H and wild-type bladders. In the wild-type sample the scale bar is set to 100 μ m, in the T30H sample the scale bar is set to 50 μ m. D- detrusor smooth muscle, U - urothelium.

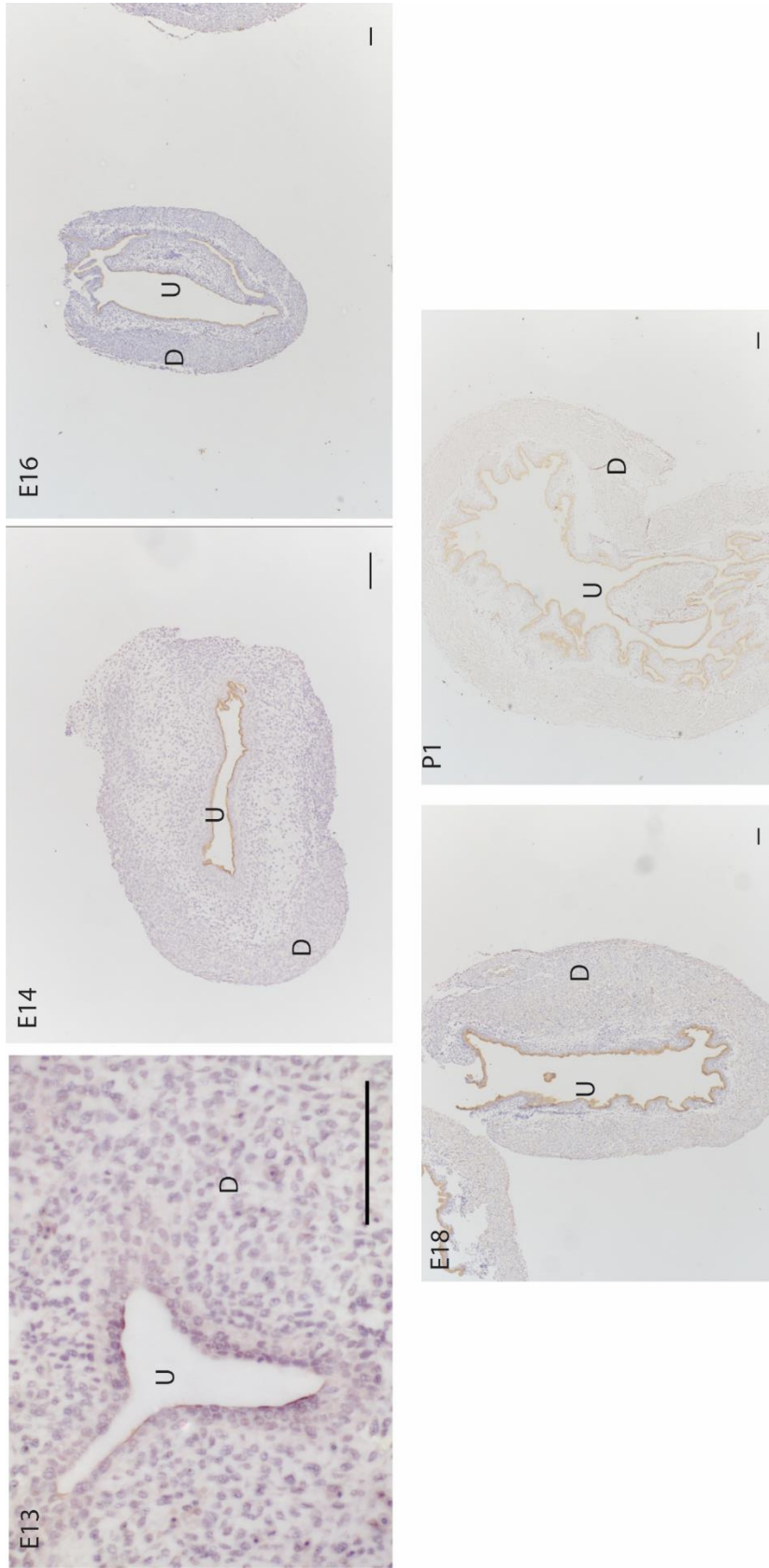


Figure 39. Uroplakin 3a DAB staining on wild type bladders throughout development. Uroplakin 3a starts to appear in the urothelium at E13 and is established around the entire urothelium by E14. This is then maintained through development up until birth. All scale bars in images are set to 100µm, representative images, n=5. D – detrusor smooth muscle wall, U – urothelium.

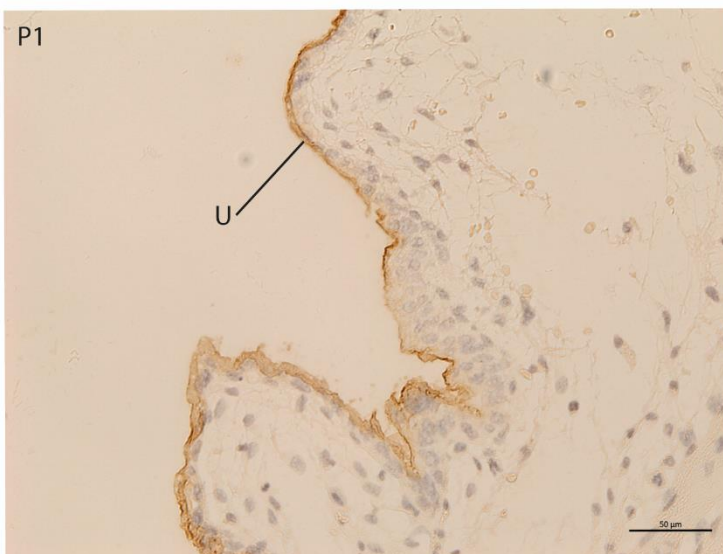
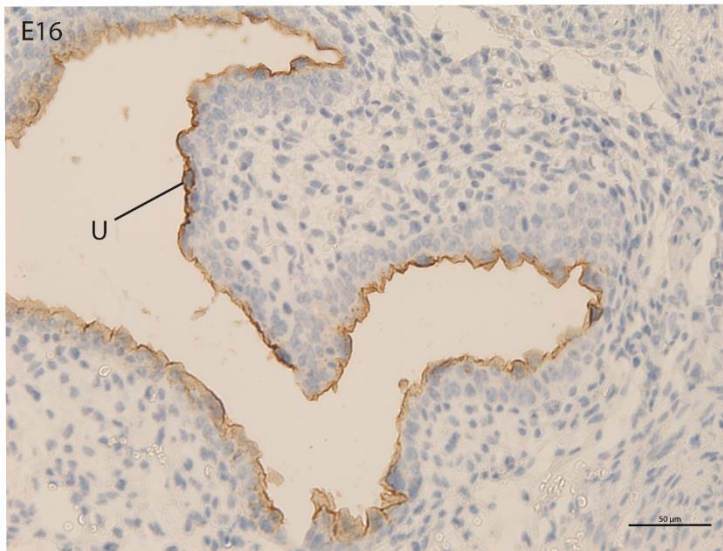
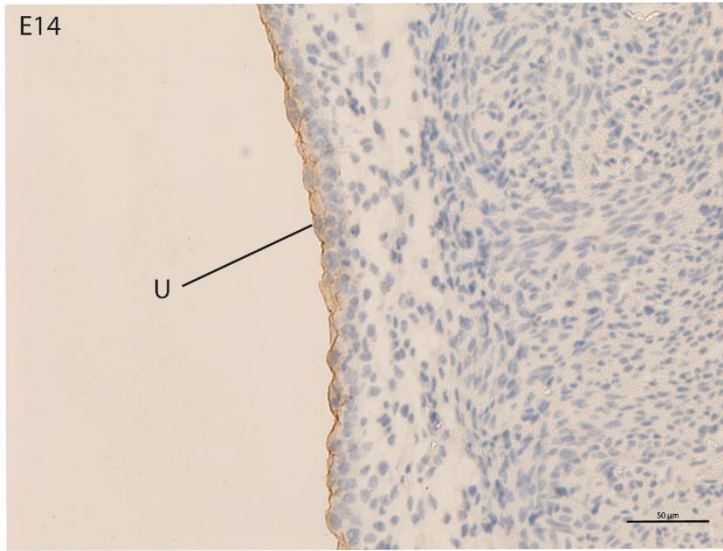


Figure 40. Higher power images of the urothelium at timepoints of interest, E14, E16 and P1. All are wild-type mice, representative samples, n=5. All scale bars set to 50μm. U - urothelium.

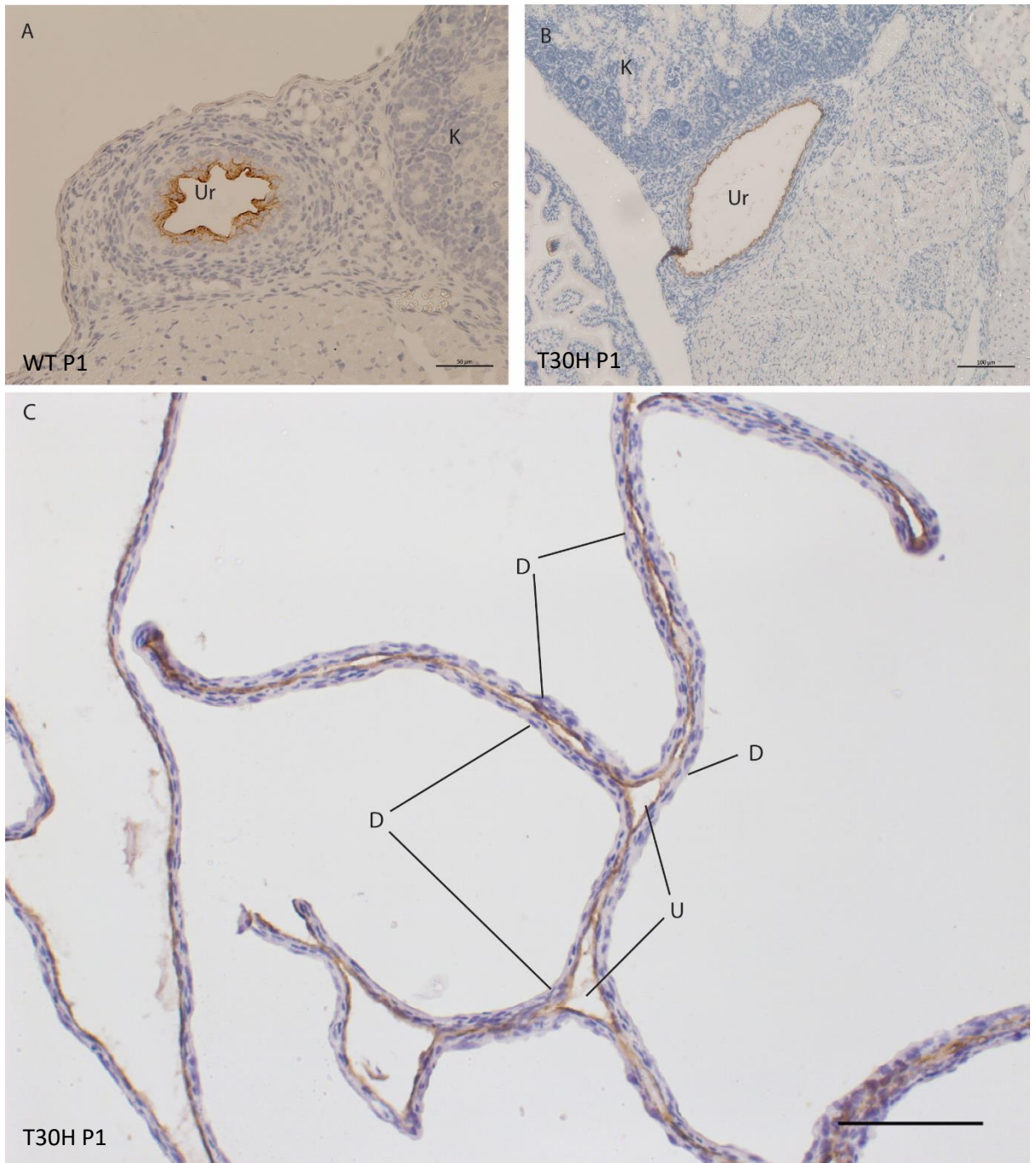


Figure 41. DAB stained Uroplakin 3a expression in a wild type P1 ureter (A) compared to a P1 ureter in a T30H mouse (B). The ureter of the T30H mouse is extremely distended, suggesting backflow of urine. C The bladder of a P1 T30H mouse, the bladder wall is extremely reduced compared to wild type bladders at the same stage, uroplakin 3a staining is still present (Figure 39 & 40). Scale bars for B and C are set to 100 μ m, Scale bar in A is set to 50 μ m. Representative samples, A n=2, B & C n=3. Ur - ureter, K - kidney, D - detrusor smooth muscle, U - urothelium.

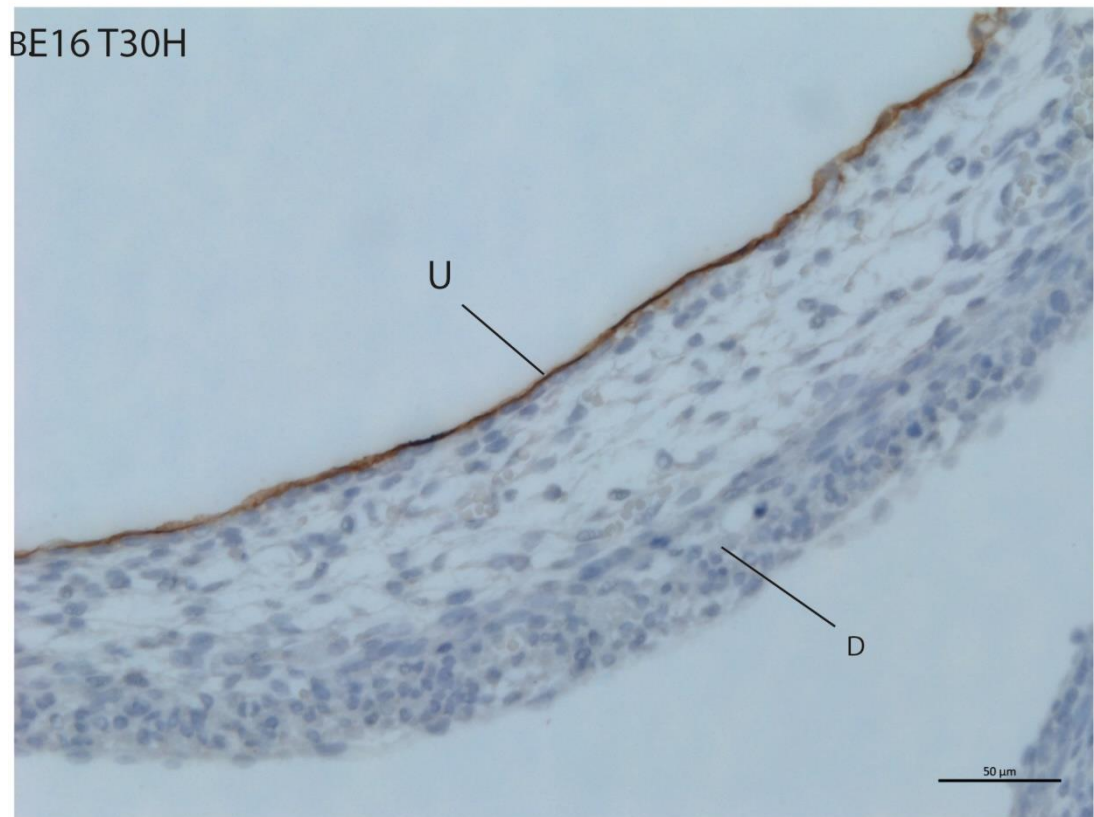
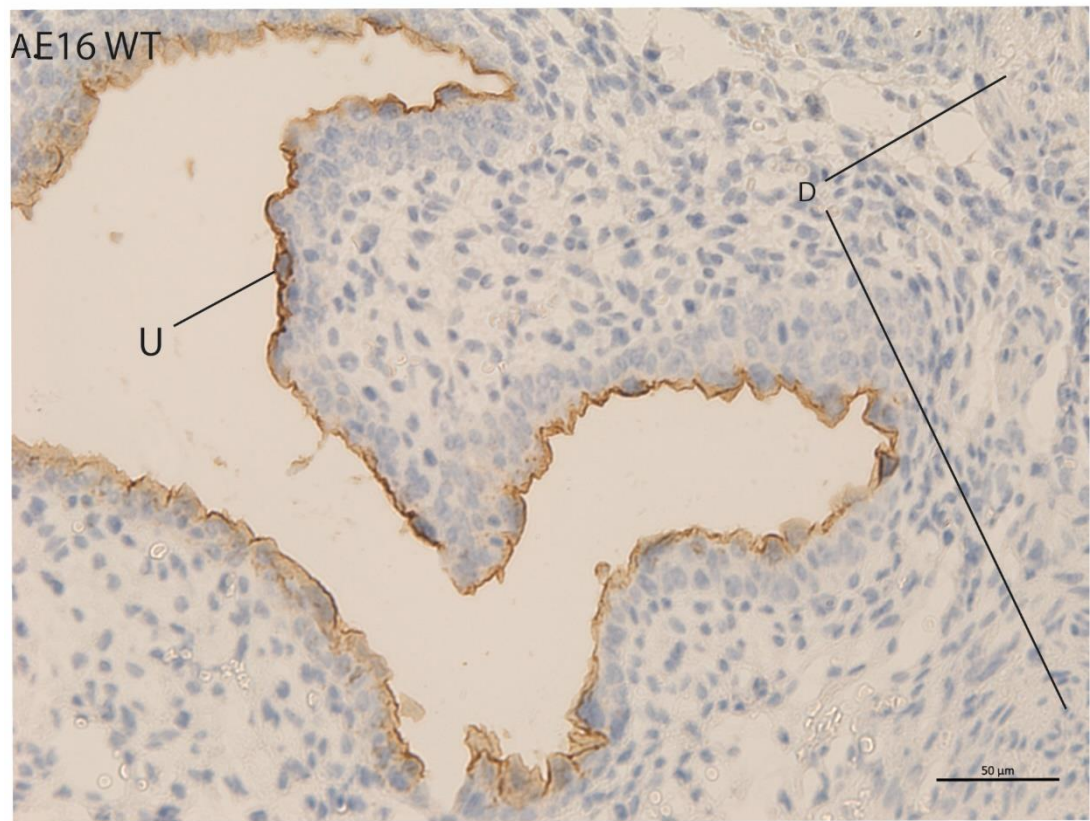


Figure 42. E16 Uroplakin 3a staining in the bladder of a T30H mouse compared to a wild-type. Image A shows a WT mouse bladder and Image B shows a T30H mouse bladder. WT sample representative of n=5, T30H n=1. D - detrusor smooth muscle wall, U - urothelium. All scale bars set to 50 μ m.

5.2.5 Myocardin Expression

MYOCD is a regulator of smooth muscle expression. Its expression in normal development is localised to organs which express both smooth muscle and cardiac muscle. Examining the expression of *MYOCD* by using antibodies is made difficult by the fact that the antibodies produced against *MYOCD* do not work well (Lyu et al, 2018). Nevertheless, a *MYOCD* antibody was used to ascertain whether there were any observable differences in expression between wild-type mice and T30H mice (**Figure 43**).

In both T30H mice and wild-types *Myocd* staining is very non-specific. Globally there appears to be more staining in the wild-type than in the T30H mice. These results, however, must be taken within the context of the limited reliability of the antibody used.

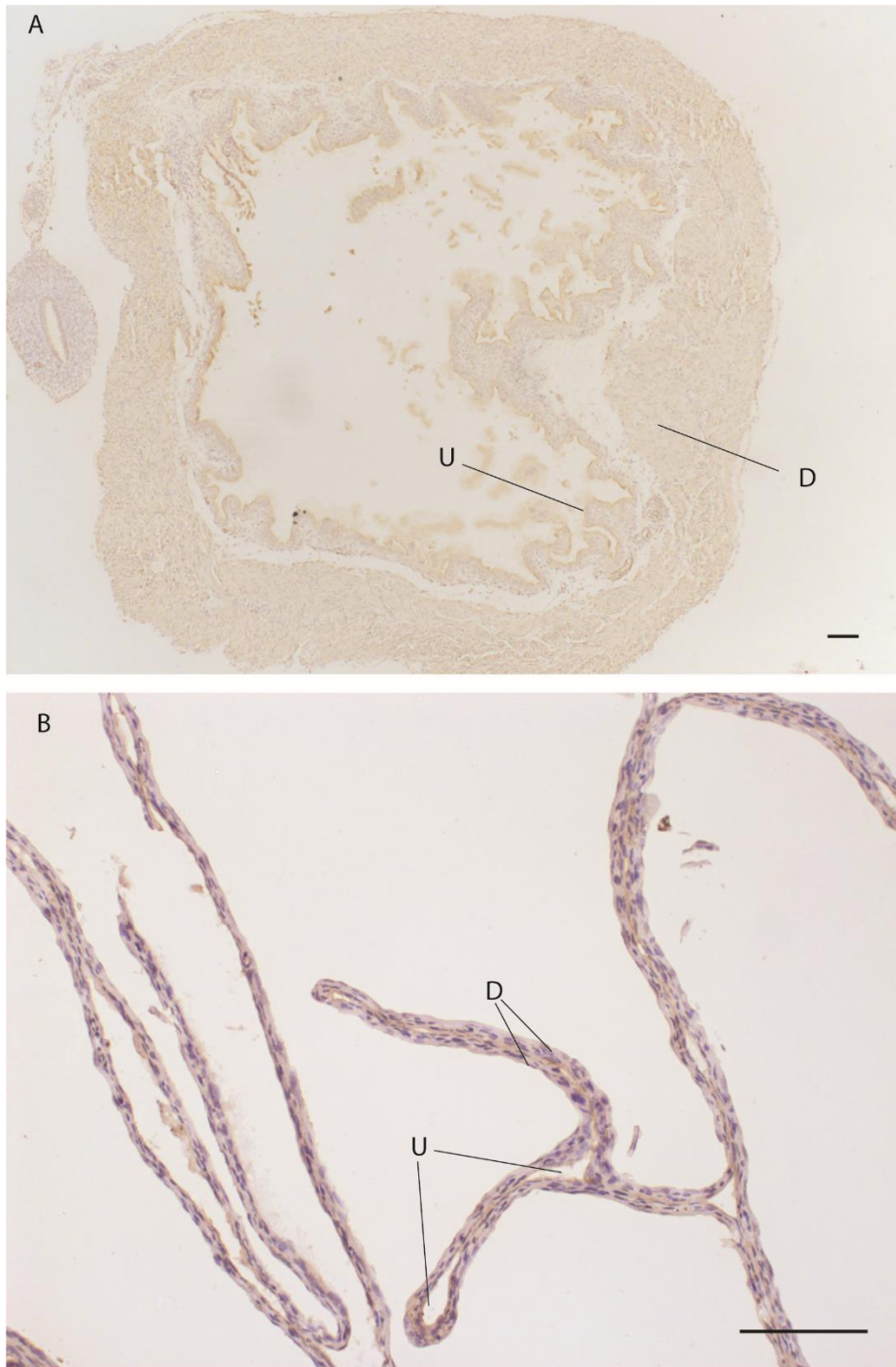


Figure 43. A an E18 wild-type mouse kidney stained with myocardin. The antibody is non-specific but does stain the smooth muscle wall. B A T30H P1 mouse bladder stained with myocardin. There is some staining present, and it could be reduced compared to the wild type, but it is impossible to draw decisive conclusions due to the unreliability of the antibody. All scale bars are set to 100 μ m. Wild-type representative of n=5, T30H representative of n=3.

5.2.6 Ultrasound Scanning

T30H mice are sub-fertile and the litter numbers are very small. This creates difficulties in having enough breeding animals to be able to sacrifice pregnant females in order to collect developmental timepoints. To get around this problem, we sent plugged T30H mice to the Centre for Advanced Biological Imaging (CABI) for high-frequency ultrasound scanning. This is a non-invasive technique that allows the whole fetus to be visualised *in utero*, and for measurements to be taken of the dimensions and morphology of the organs, without harm to the developing fetus or pregnant female.

Confirmed plugged T30H heterozygotes were initially scanned at E14, E16 and E18 of pregnancy (**Figure 44**). It is possible to compare individual fetuses as their position within the uterine horns changes minimally throughout gestation; this is also made easier by the low litter number of T30H mice. Once the pups were born, the entire litter was sacrificed and then genotyped and dissected, in order to ascertain which pups were T30H, heterozygotes or wild-types. To match up the genotypes of the litters to their phenotype *in utero*, either a pup's position in the uterine horn was noted throughout the pregnancy and compared to that when pregnant females were sacrificed, or the genotype was taken after the pups were born and the phenotype extrapolated from the genotyping results. The phenotype was so severe in homozygous pups that it was relatively easy to identify T30H mice *in utero* just from the size of the bladder.

Once identified from later observations or genotyping, at E14 T30H mice, heterozygotes and wild-type mice were indistinguishable using ultrasound; with no difference observable between T30H mouse organs and wild-type organs. Depending on the position of the fetus it was often not possible to obtain an image of the bladder in all pups at this stage due to the extremely small size of the bladder. The kidneys also do not start producing urine until after E14, which makes identification of the bladder even more difficult as it is not filled with fluid (Caubit et al, 2008).

At E15 and E16 there was a clear and identifiable phenotype in the T30H mice. The bladder was clearly enlarged and takes up much of the abdominal cavity.

Hydronephrosis was also identifiable in the kidney by E16, further confirming that the phenotype is well established by this point. In some examples, one kidney exhibited more hydronephrosis than another, indicating a 'pop off' mechanism is present in some T30H mice, similar to that seen in humans and other mouse models as a protective adaptation to obstruction (McHugh 2014, Rittenberg et al, 1988). Heterozygote mice were indistinguishable from wild-type littermates. The bladder was of a normal size and there was no evidence of hydronephrosis.

Again, at E18 the enlarged bladder phenotype was clearly evident in the T30H mice, and heterozygotes were indistinguishable from wild-type mice. Hydronephrosis of the kidneys was also present in T30H homozygotes. In most scans the kidney was not observable in wild-type mice. This is because the scanning method best identifies differences in fluid density between tissues, if no hydronephrosis is present in the kidneys then they are difficult to identify. They are also usually not present in the same plane of the ultrasound scan as the bladder in wild-type mice. This is in contrast to T30H mice, where the large increase in bladder volume means that the bladder can be found on the same plane as the kidneys as it takes up much of the abdominal cavity.

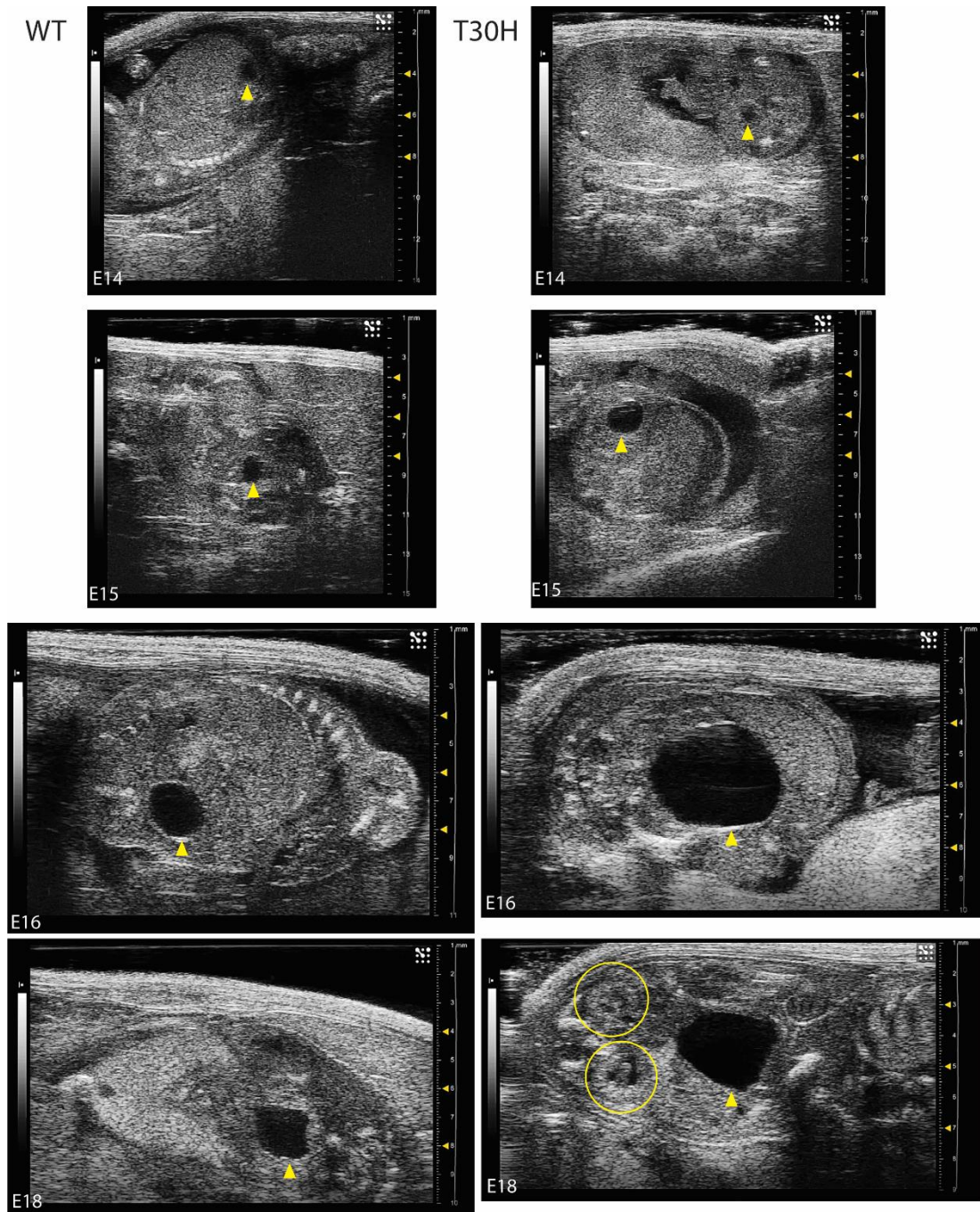


Figure 44. Images of T30H kidneys on the right compared to wild-type kidneys on the left. The bladder shows a marked increase in volume from E15 onwards in both wild-type and T30H mice, but this is much more extreme in the mutant mice. All bladders within images are marked with an arrow, and the kidneys exhibiting some hydronephrosis are shown circled in yellow at E18 on the T30H mouse. Images for both wild-types and T30H samples are not all of the same animal, as not all embryos had a bladder which was large enough to scan at E14, and some embryos were sacrificed mid-gestation for sample collection. WT n numbers: E14 - n=9, E15 - n=2, E16 - n=14, E18 - n=5; T30H n numbers: E14 - n=3, E15 - n=1, E15 - n=4, E18 - n=3.

5.2.6.1 Bladder Volume Quantification

Bladder volume can be quantified using ultrasound software (**Figure 45**). A three-dimensional scan can be made by centring on the middle of an object of interest, for example, the bladder, and then scanning through either side of the centred organ of interest. The ultrasound machine can then reconstruct these scans as whole images. The volume can then be calculated by the software by highlighting the beginning of a three-dimensional shape and then scanning through.

I quantified the volume of the bladders of T30H, heterozygote and wild-type littermates with no translocation. At E14 bladders were very rarely large enough to scan, in diseased and wild-type animals. At E15 again, it was difficult to scan, but some volumes were large enough to quantify, and in the T30H mice the bladder is noticeably larger. At E16 this difference increases even more, to just over 50 μ l. It seems to level off at this point, as the volume at E18 is still between 50 and 70 μ l. In the wild-type and heterozygous pups there is very little difference between the two groups. The bladder volume generally increases as the pups develop, apart from a sample where the volume decreases at one later time point. This could be because the bladder has recently voided and so has a smaller volume of urine. There is a large difference between the wild-type and heterozygous pups tested compared to the T30H mice, all wild-type or heterozygote mice have a maximum volume at E18 under 20 μ l.

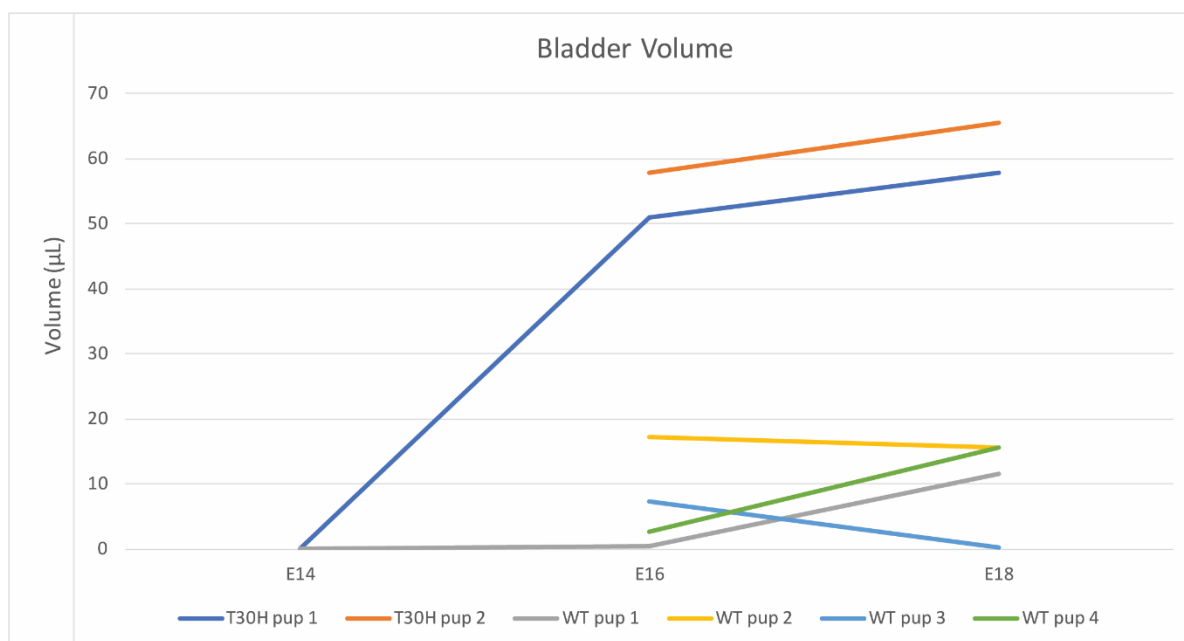


Figure 45. Volumetric measurements for T30H mice, heterozygotes and wild types. Not all timepoints are available for all mice, either because they were not scanned at all timepoints or the bladder was not identifiable. The different phenotypes were indistinguishable at E14. At E16 the T30H phenotype is first identifiable, and there is a very large difference between the T30H mice and wild types and heterozygotes. This continues at E18 but doesn't increase as much as it does between E14 and E16. WT - n=4, T30H - n=2

5.2.7 Summary

T30H mice can be characterised by their smooth muscle defect to the bladder. The smooth muscle wall is reduced to being only a few cells thick in homozygotes; this creates a functional lower urinary tract obstruction as the very thin muscle wall is not able to expel urine during development. This is confirmed by staining for markers of the smooth muscle layer. The urothelium of the T30H mice is normal, further indicating that the T30H mouse primarily has a defect exclusively to the smooth muscle layer. The kidneys of T30H mice also show signs a response to reflux due to obstruction. There is extensive hydronephrosis and the renal pelvis is distended. This reflux also extends into some of the nephrons. The kidneys of T30H mice also exhibit increased α SMA expression on staining which could indicate fibrosis of the kidney due to reflux. This kidney phenotype recapitulates that seen in human lower urinary tract obstructions such as PUV, urethral atresia and PBS. This indicates that the T30H mouse makes an excellent animal model of lower urinary tract obstruction. This was hypothesised at the beginning of the project and this evidence helps to confirm this hypothesis.

Other organs which express smooth muscle such as the gut are indistinguishable from wild-types using histology. T30H heterozygotes are also indistinguishable from wild-types using both histology and ultrasound.

T30H mice are sub-fertile, which results in very small litter numbers. To gain multiple timepoints for development in a single litter, high-frequency ultrasound scanning was used to identify the onset of the phenotype. T30H mice were indistinguishable from wild-type littermates at E14, and phenotype onset begins at E15 with the first production of urine.

5.3 *In Vitro* Manipulation

Once we knew the location of the translocation, and the most likely genes involved in causing the phenotype, potential avenues for gene therapy could be explored. I used culture of primary cells to further investigate the role of *Myocd* in bladder smooth muscle development. The aim was to initially knock-down *Myocd* expression in bladder cells in order to mimic the effects that the translocation would have *in vitro*. I then explored ways in which the phenotype could be rescued in the future by restoring *Myocd* expression to the bladder.

5.3.1 Whole organ culture

In order to develop a methodology to correct the mutation *in utero*, *Myocd* expression in the developing bladder was manipulated at first *in vitro* in order to refine experimental techniques, and to give an idea of the response to *Myocd* manipulation. For *in vitro* bladder culture all organs are collected from timed plugs in CD1 mice. Bladders are then collected at E14. This timepoint was chosen as it is the first timepoint at which the bladder can be easily isolated from surrounding tissues, and the first point in development where the bladder begins to have functionality in terms of both storing and passing urine. The smooth muscle is still yet to fully mature however; the smooth muscle cells are not yet organised into the mature blocks of contractile cells observed from E18 onwards. The bladders harvested at E14 then possess smooth muscle cells that are at a reasonably early stage in development and should give an accurate representation of the differentiation into mature smooth muscle cells in culture.

CD1 mice were used in these preliminary experiments as they produce very large litters, of between 8 and 20 pups, and the T30H mice were too rare. Once they were dissected, they were grown on millicell insert filters using F14 DMEM with ITS added (**Figure 46**). Historically in our lab serum was found to inhibit growth in whole organ culture, so this was omitted (Burgu et al, 2006).

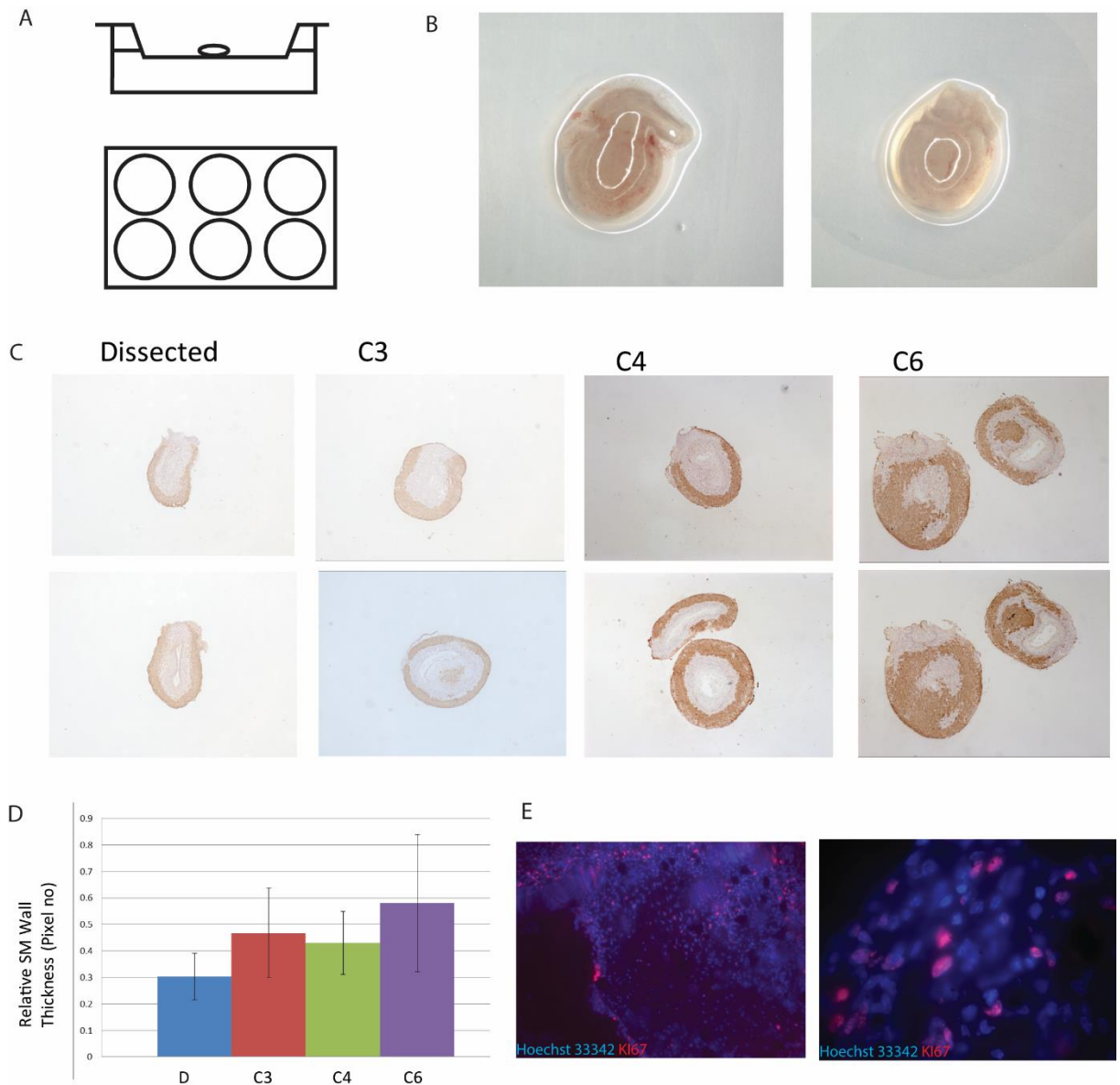


Figure 46. A. whole organ culture is carried out by placing the dissected organ onto a milicell insert placed on top of cell culture media. B. Images of dissected bladders while in cell culture immediately after dissection. White circles are reflections captured by the camera which could not be removed. C. Timeline of bladder growth in organ culture. All bladders are stained with smooth muscle alpha actin, and these are examples of images used for quantification of the thickness of the smooth muscle cell wall. D. The relative thickness of the smooth muscle cell wall. The greatest increase in growth was seen after 3 days in culture, after this the morphology of the bladder wall starts to become irregular as the organ flattens to the membrane. Although there appears to be an increasing trend for bladder wall thickness as the number of days in culture increases, these means were not statistically different from each other using an unpaired t test. N=3 bladders at each timepoint. E. sectioned bladders from whole organ culture at culture day 3, stained with a live cell dye and Ki67, a proliferative marker. The presence of Ki67 suggests that the change in the thickness of the smooth muscle wall is due at least in part to cell growth and not just to deformation of the organ to the membrane. Representative images of n=3 bladders after 4 days in culture.

Initially in order to measure the growth of the bladders, three bladders were analysed at day 2, 3 and then 6 of culture. They were fixed, embedded and then stained for α SMA in order to highlight the detrusor smooth muscle present (**Figure 47**). The bladders at each stage were then imaged to compare with control bladders taken, embedded and stained that had not been cultured. This was done so that the differences in the smooth muscle wall could be directly compared, as this would be the component of the bladder that would be manipulated in later experiments.

However, the thickness of the bladder wall is highly variable dependent on where in the bladder the section is taken. In the bladder dome the smooth muscle wall is at its thickest, and is the area of the tissue which has the most effect on the ability of the bladder to contract and expel urine. The smooth muscle layer is at its thinnest at the trigone, where the ureters and the urethra attach to the bladder. In an attempt to limit this variation and give as uniform a thickness to the smooth muscle wall as possible to aid analysis, the trigone was removed when the bladders were initially dissected.

Some variation was still present, however, and was a limitation on the culture method and its ability to accurately depict the changes taking place through time. It would also be a limitation in assessing any changes that therapy would induce. At later timepoints the bladder wall also becomes much more variable and begins to look abnormal. This shows that the longer the model is cultured, the further it diverges from what is seen *in vivo*. This could be because the longer the bladder is cultured, the more the tissue flattens to the cell culture insert. This could be to be closer to the culture media, and the flattening would also result in oxygen being able to dissolve into the tissue more easily, increasing cell viability.

Although there appears to be an upward trend in the thickness of the bladder smooth muscle wall the more days it is grown in culture, the mean bladder wall thicknesses at 3, 4 and 6 days of growth in culture were not statistically different from the mean bladder wall thickness of dissected E14 bladders. This was calculated using an unpaired t test, as the data distribution was normal. The P value for the data was greater than 0.05 so the null hypothesis that there was no difference between the

mean bladder wall thickness in any of the 4 data sets was accepted. This highlights a limitation in the culture method, as if the bladders do not grow enough during normal culture conditions to be statistically distinguishable from their dissected start point then it would be impossible to tell whether treating the bladders would have any effect on the thickness of the smooth muscle wall.

KI67 is a cellular marker for proliferation and is present during all active stages of the cell cycle but is not present in quiescent cells. It is therefore used as a marker for rapidly dividing cells, so the number of cells expressing KI67 can be used to establish the level of growth occurring in cultured cells. It was used to ensure that growth was actually taking place and that cells were viable. The presence of the marker in sectioned bladder tissue indicates that changes to the morphology of the cultured bladders were at least in part due to cell growth and not simply due to the culture conditions.

The method used here has also been used in the literature and has met with success in culturing bladder as well as other organs (Price et al, 2009, Anders et al, 2013). The culture technique is not ideal, however, as the bladders do not completely retain their original morphology as they flatten to the millicell insert. There is also a lack of circulating blood, and the muscle wall is not given the opportunity to fully extend and contract with a bladder voiding cycle as it would during embryonic development. Due to the very small size of the bladders on dissection (~500µm) it would be very difficult to create these conditions in culture.

The goal for refining the culture system was to be able to formulate a method for delivering gene therapy and testing its efficacy *in vitro*. I decided that along with the difficulties in quantifying bladder growth, it would have been very difficult to effectively deliver gene therapy to the organs in culture. The organs are grown on filters, meaning that not all surfaces would be in contact with the media containing the therapeutic vector. This would make transduction very inefficient. The vector could also be injected into the organs, but together with the small size of the bladders being a barrier, there would still be the problem of only very localised transduction as there is no blood flow. The methods of virus delivery would also not be similar

enough if virus was delivered to the cell culture medium below the insert. When therapy is delivered to fetal mice it would be injected straight into the bladder, and not into the tissue surrounding it, and would then be retained as the T30H mice do not void the bladder during gestation. This would not be possible to model in an organ culture model without a considerable amount of optimisation and testing. It was therefore decided in the interests of generating as much data as possible in the limited time of the project a simpler culture method would be required to assess therapeutic potential of *MYOCD*. Going forwards I used dissociated cell culture techniques in order to do this (**Figure 47**).

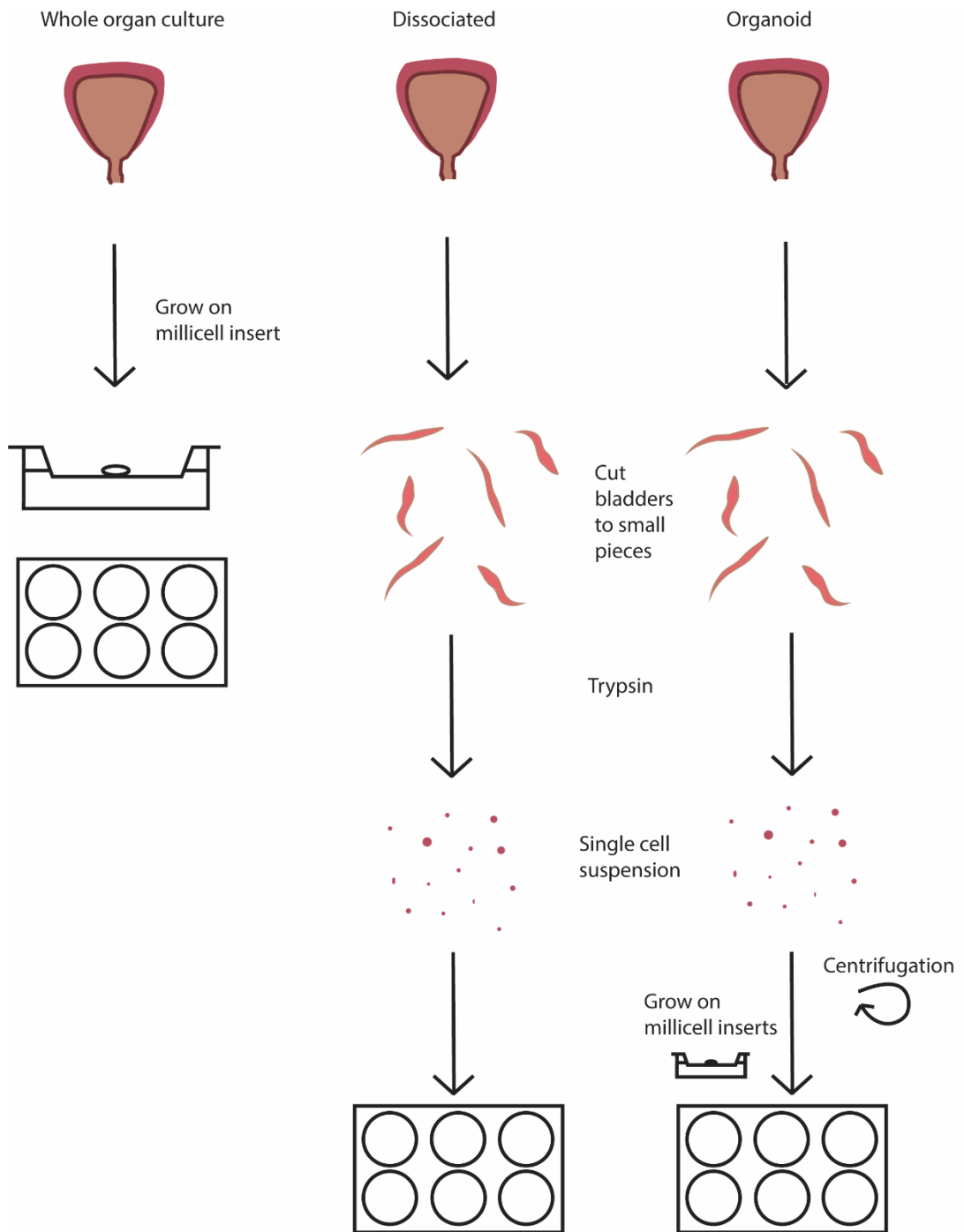


Figure 47. Schematic for the three types of bladder culture used in this project. Whole organ culture, dissociated cell culture and organoid culture.

5.3.2 Organoid Culture

Organoid culture involves the dissection of an organ, the separation of the organ into individual cells, and then reaggregation of the cells in a way to mimic the structure of the cells *in vivo*. One method of organoid culture is reassociation of these cells by centrifugation into a pellet which can then be grown in a similar way to the organ culture described above – at the air liquid interface on a cell culture insert (Unbekandt et al, 2010).

Organoids grown in this way show many similarities to the embryonic organs from which they are derived. They show some self-organising capacity and can be used to treat individual cells with a therapy so that there is a high level of therapy penetrance to the cells and they can then be reassembled into a semblance of the organ from which they were derived. Organoid growth and cell-cell interactions can then be observed. This technique has been used extensively in the kidney but has not been developed to the same extent in the bladder (Oxburgh et al, 2017).

Bladder organoids were generated from dissociated E14 bladder cells and grown on millicell inserts. While growth was observed, unfortunately all plates were infected before any data could be obtained from the bladder organoids. This methodology is technically complex and uses a large amount of starting tissue. A single litter of mouse embryos will only generate two organoids. Both in compliance with the principle of the three Rs in animal research and in the interests of finding a simple, easy to replicate culture method, dissociated culture was then used to test the effects of changing *MYOCD* expression instead.

5.3.3 Dissociated bladder culture

Dissociated bladder cell culture provides a more efficient system to be able to test gene therapy. Bladders were taken at E14 from timed plugs from wild-type female mice. Cells were dissociated by trypsinisation followed by disruption by repeat pipetting (**Figure 47**). Three different cell populations were grown in each assay. Two were used as controls, one was untransduced, and the other was transduced with a control virus containing scrambled DNA along with GFP to act as a maker of

successful transduction. This scrambled DNA control was used to ascertain the level of cell death due to transfection with the virus alone and not related to the gene knocked down. When viral titre delivered to cells is too high there is cell death, so the level of transduction must be optimised.

The third population of cells was the treated cell population. A lentiviral vector was added in order to knock-down *MYOCD* expression in the cultured smooth muscle cells. Four different variants of viral particle were used, each able to knock-down expression of different *MYOCD* splice isoforms. These were pooled and used in order to achieve as efficient knock-down as possible.

Cells were treated on the same day as collection from the embryos with lentivirus. Initially, two different concentrations of virus were used in order to find the optimal concentration of virus. Viral vectors are introduced to cells in relation to the number of infectious units per cell, as opposed to concentration within the culture medium. After dissociation cells were counted using a hemocytometer, and then the multiplicity of infection (MOI) was calculated. MOI is the number of viral particles per cell, so a MOI of 1 would mean that 1 viral particle per cell would be introduced to the cell culture medium. Two MOI doses were initially tested, 1MOI and 10MOI. These two concentrations were used in order to assess the optimal number of infectious units to treat to achieve a high percentage of transduction without affecting the viability of the cells. High viral titre decreases cell viability so there is a play off between high transduction and viability. Ideally a 100MOI concentration would also be tested to find the limits of the effect on cell viability. However, as the vector was not made in house a maximum MOI of 10 was used in order to conserve the vector and prevent the experiment from becoming prohibitively expensive. Successful transduction was assessed through GFP expression. No GFP expression was observed in either the 1MOI scrambled control treated cells or the 1MOI *Myocd* knock-down treated cells, whereas GFP expression was observed in the 10MOI treatments. As the cell growth did not appear to be different between the 1MOI treated scrambled control, 10MOI treated scrambled control and the untreated control cells a concentration of 10MOI was used going forwards (**Figure 48**).

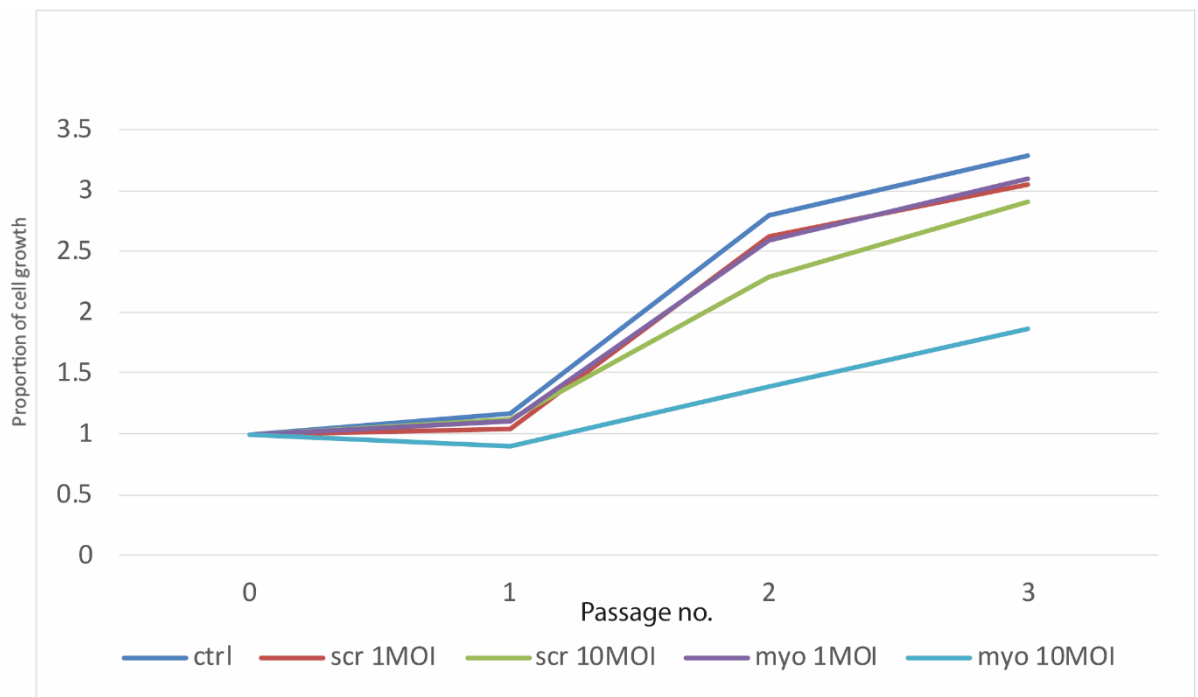


Figure 48. Five growth conditions were used to ascertain the correct MOI to dose the dissociated bladder cultures with in order to knock down myocardin expression. These conditions were untreated control (ctrl), Scrambled (scr) control 1 MOI, Scrambled control 10 MOI, Myocardin (myo) 1 MOI and Myocardin 10 MOI. The number of cells in each culture condition was counted using a haemocytometer while passaging the cells. There appeared to be little difference between the two scrambled control samples. It was not possible to statistically calculate whether this is true because this assay was only carried out once to preserve lentivirus. From observation, no cells in either scrambled or myocardin knock-down assays with 1MOI expressed GFP using a microscope. For this reason, and because there appeared to be little difference in growth between the scrambled 1MOI and 10MOI treatment, a dose of 10 MOI was used going forward.

Cells were harvested after they had regained 70% confluence after three passages to collect protein. Knock-down experiments were repeated in triplicate. In terms of cell growth, the control untransduced group exhibited the most growth. This was closely followed by the scrambled control (**Figure 49**). The *Myocd* knock-down population of cells grew the least of the three populations. This indicates that *Myocd* knock-down either results in cell death or inhibits cells from multiplying in culture.

Protein extracted from harvested cells was used in western blots in order to ascertain the level of knock-down of MYOCD and to also gauge the level of other associated proteins in the smooth muscle expression pathway. MYOCD was evident in both the control group and the scrambled control group, although it was slightly reduced in the scrambled control. This could have been because the virus may have had a deleterious effect on the cells given the scrambled control. This could have resulted in changes to their gene expression, in this case to *Myocd*. The band indicating the presence of MYOCD protein was absent in the knock-down group of cells, indicating very efficient knock-down. This was only true for the first of the three assays carried out; in the remaining two assays there was a decreased level of MYOCD in knock-down samples compared to controls, but not to the same extent as the first assay. This could be due to the fact that repeated freeze thaw cycles significantly decrease lentivirus viability. While every precaution was taken to prevent repeated freeze thawing, including aliquoting the stock of virus on arrival from the company it was ordered from, variances in freezer temperatures could have still contributed to this decreased viral efficiency. The level of different *Myocd* splice variants could not be ascertained through western blotting with the antibody used as the antibody is specific to an internal sequence of human *Myocd* specific to isoform 2, and so only produced one band on western blotting.

When the presence of the α smooth muscle protein was tested using western blotting there was shown to be a decrease in the *Myocd* knock-down sample compared to the two control samples, although there was still expression of the protein. GAPDH was used as a housekeeping protein control and was present to an equal extent in all samples tested.

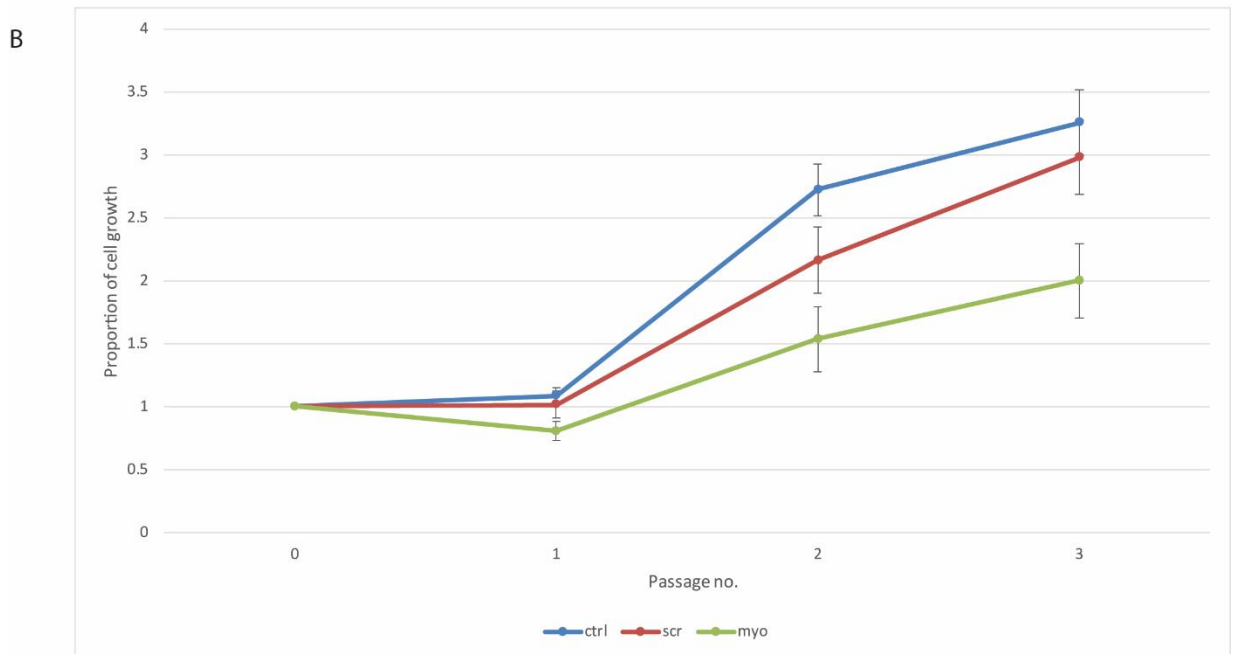
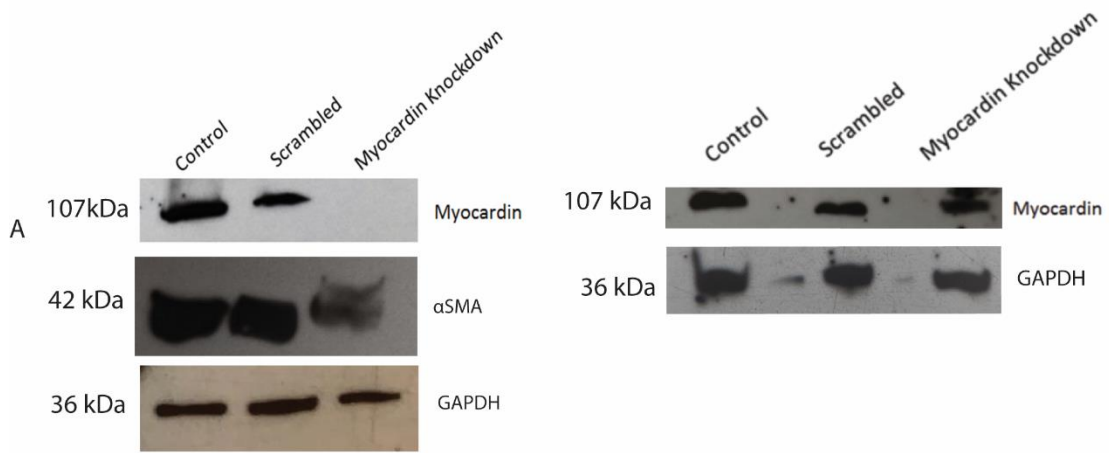


Figure 49. A. Western blots from protein collected from cells from the control, scrambled control and myocardin knockdown experiments. In the first assay (blots on left) knock-down was highly efficient, this level of knockdown was less efficient in further experiments (blots on right). Smooth muscle alpha actin protein expression was also reduced in the myocardin knockdown experiment in the first assay. B Average growth data from three repeats of the knockdown assay, including control and scrambled control. After cells had regained confluence after 3 passages the control and scrambled control populations were not significantly different ($p=0.2820$), whereas the myocardin knock-down treated cell population was significantly different to the untreated control ($p=0.0051$) Western blots, Myocd $n=2$, GAPDH $n=2$, α SMA $n=1$. Cell growth data, $n=3$ for each condition.

5.3.4 Avenues for *in vivo* gene therapy

The changes to *Myocd* splice isoform expression, driven by a cis-acting promotor region, which are then disrupted by the translocation in T30H mice is the most likely cause for the phenotype observed. Disruption of this promotor region may result in changes to the splice variants of *Myocd* expressed. Splice variant expression of *Myocd* appears to be organ specific (Saha et al, 2009). If the disruption to the promotor region changes the splice variants of *Myocd* present in the bladder then this could in turn lead to a disruption of growth of detrusor smooth muscle cells in the bladder wall. This could be either through increased cell death or through reduced cell growth. This leads to an insufficient number of detrusor smooth muscle cells for the bladder to be able to contract and void *in utero*. This results in a large, amuscular, non-emptying, distended bladder.

This hypothesis is supported by imaging and gene expression data collated in this thesis. After assessing the effects of *Myocd* knock-down on cultured primary embryonic bladder cells, the next step is to explore how the modulation of *Myocd* could be used as a gene therapy to rescue the T30H phenotype in the future. The T30H mouse models enlarged and non-emptying bladder is an ideal vehicle for the delivery of gene therapy *in utero*. Any treatment delivered would be held within the bladder by the fact that it is non-emptying, providing the therapy with close proximity to the target cells, and little chance to affect non-target tissue. This section describes possible avenues for the packaging vector used to deliver future gene therapies for the modulation of *Myocd in utero* to T30H mice.

5.3.4.1 Biodistribution study

The first step to developing a viable way of upregulating *Myocd in utero* is to find a reliable vector for delivery. Collaborators at the Institute of Women's Health have a great deal of experience in viral-based gene therapy and set up a biodistribution study in order to ascertain the efficiency of a variety of vectors in targeting cells (Mattar et al, 2015). Mice were injected by collaborators at the Institute of Women's Health in the retino-orbital region with a viral vector expressing only GFP and driven by a ubiquitous promotor at P1, and then their paws tattooed so that the specific

vector they had been injected with could be ascertained. Nine different vectors were tested. All vectors also included a post-transcriptional regulatory element from woodchuck hepatitis virus (WHP). This regulatory element creates a tertiary structure when transcribed which increases mRNA stability and the likelihood of expression of the gene delivered. There were at least two repeats of each injected vector. Animals were then sacrificed 35 days later, and the bladders collected. All bladders were fixed, embedded and then sectioned.

Initially I stained the bladders using DAB staining for GFP. AAV1 (adeno-associated virus 1), AAV2, AAV5, AAV6, AAV7, AAV8, AAV9, adenovirus and lentivirus were the constructs used. Of these constructs, the AAV1 and AAV9 vectors showed the most staining for GFP, although most of the vectors tested showed positive staining of the urothelium (**Figure 50, Figure 51, Figure 52, Figure 53**).

The lentivirus showed staining that was no different to the uninjected controls. On comparison with samples from other parts of the body though, this construct also showed no staining in the liver, which should have been the best targeted organ by the lentivirus, so it is possible that the virus provided was not functional. The liver can be used as a positive control for virus integration; lenti-, adeno- and adeno-associated viruses target a range of organs in the body but are most likely to be well-integrated into the liver than any other organ (Pfeifer et al, 2001).

It was of interest to establish which vector would target the smooth muscle of the bladder most effectively, as this is the tissue which would be targeted with future T30H mouse therapies. Several vectors showed GFP expression in various tissues of the bladder, but AAV1 and AAV9 showed the most GFP staining using DAB staining. Further tests would need to be carried out to test RNA expression of GFP before concrete conclusions could be made. From the data analysed so far AAV1 and AAV9 are the most promising vectors and should be the focus of future experiments.

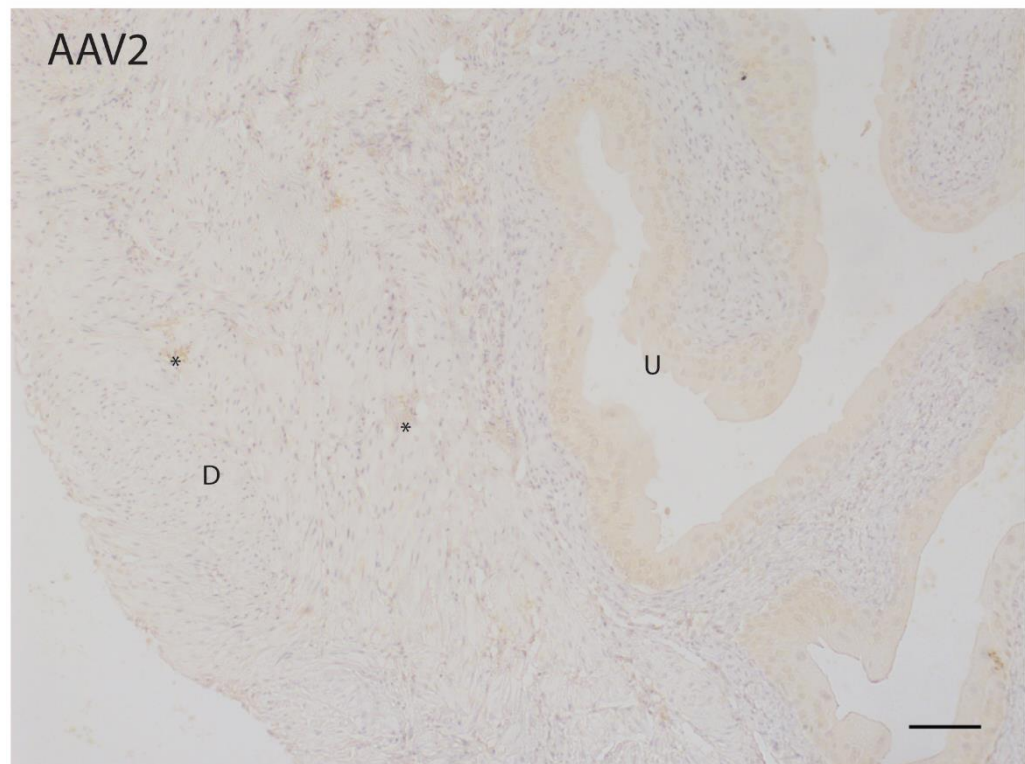
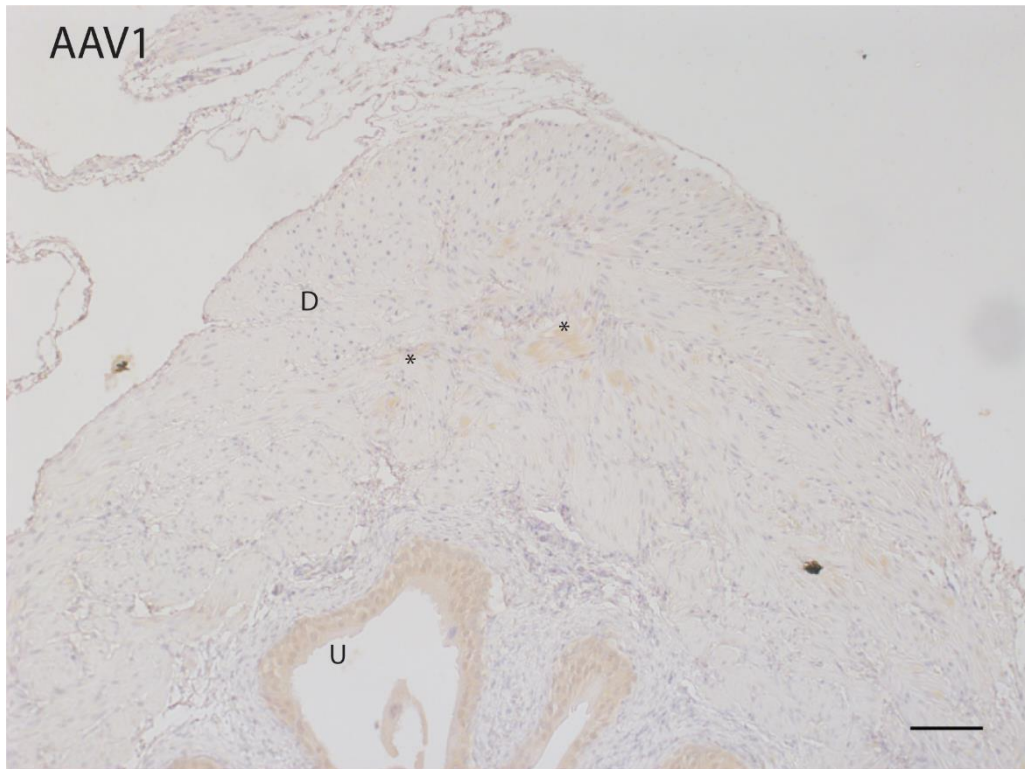


Figure 50. Biodistribution study bladders from mice injected with AAV1 and AAV2, both expressing GFP. DAB staining for GFP has been carried out. All scale bars are set to 100 μ m, areas of weakly positive GFP expression in the smooth muscle wall are marked with *. D - detrusor smooth muscle, U - urothelium. Representative examples, n=3.

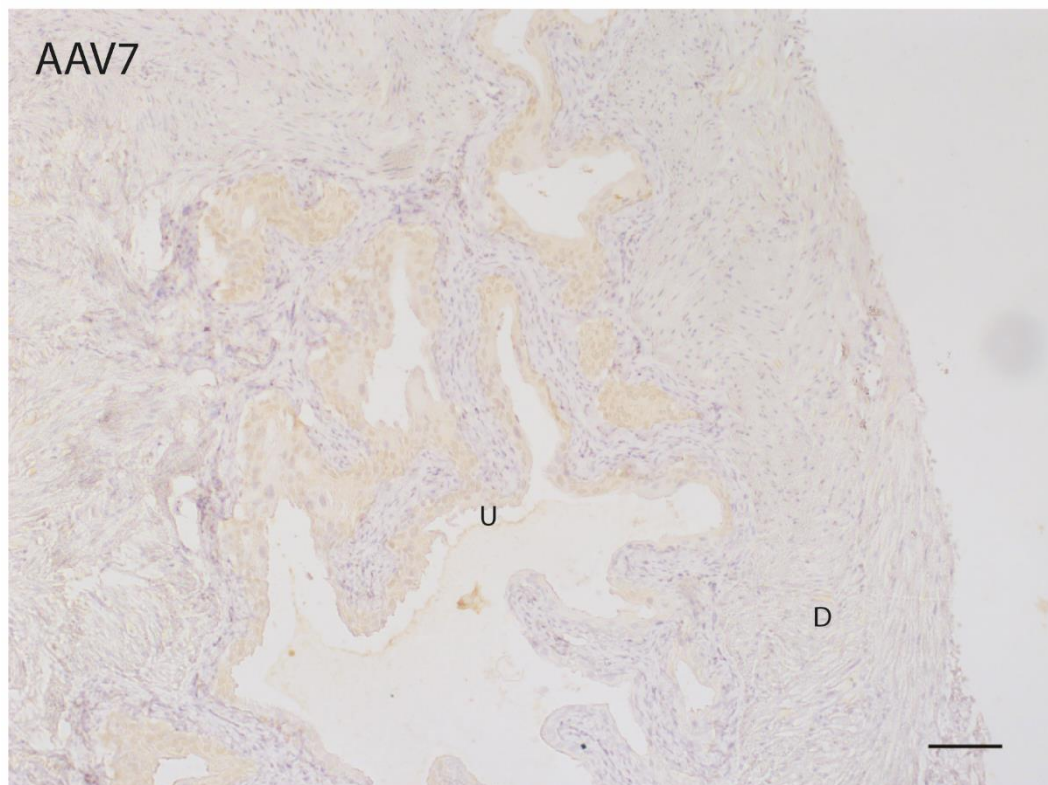
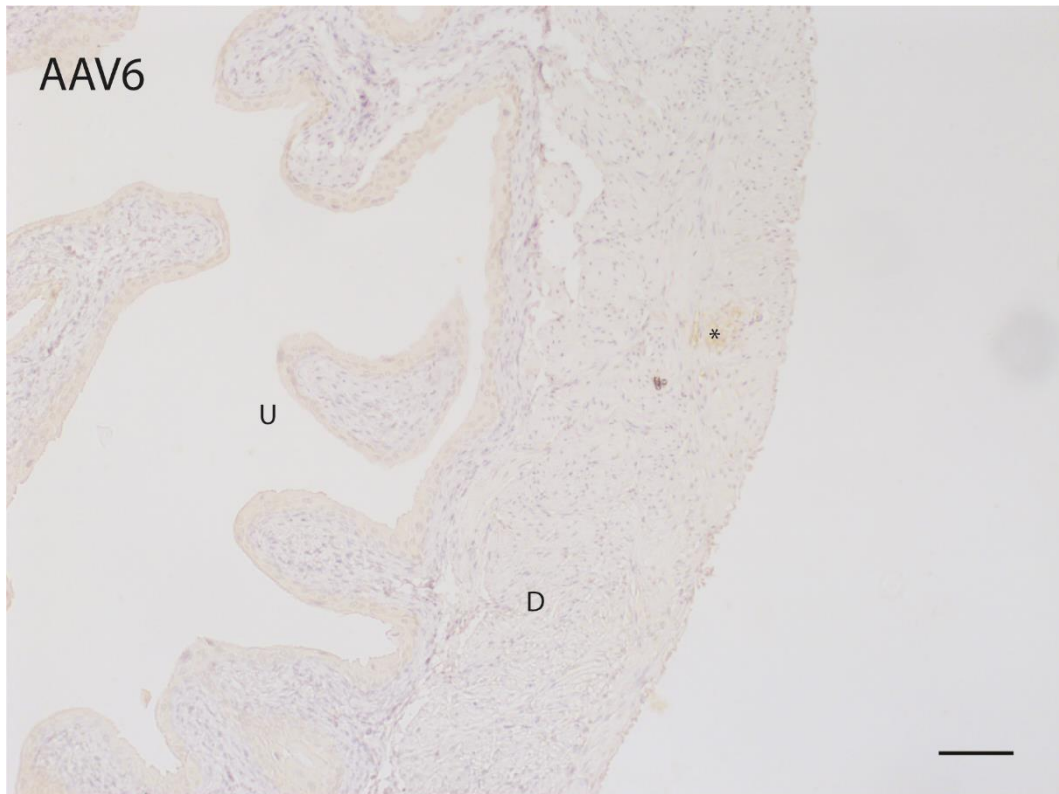


Figure 51. Biodistribution study bladders from mice injected with AAV6 and AAV7, both expressing GFP. DAB staining for GFP has been carried out. All scale bars are set to 100 μ m, areas of weakly positive GFP expression in the smooth muscle wall are marked with *. D - detrusor smooth muscle, U - urothelium. Representative examples, n=3.

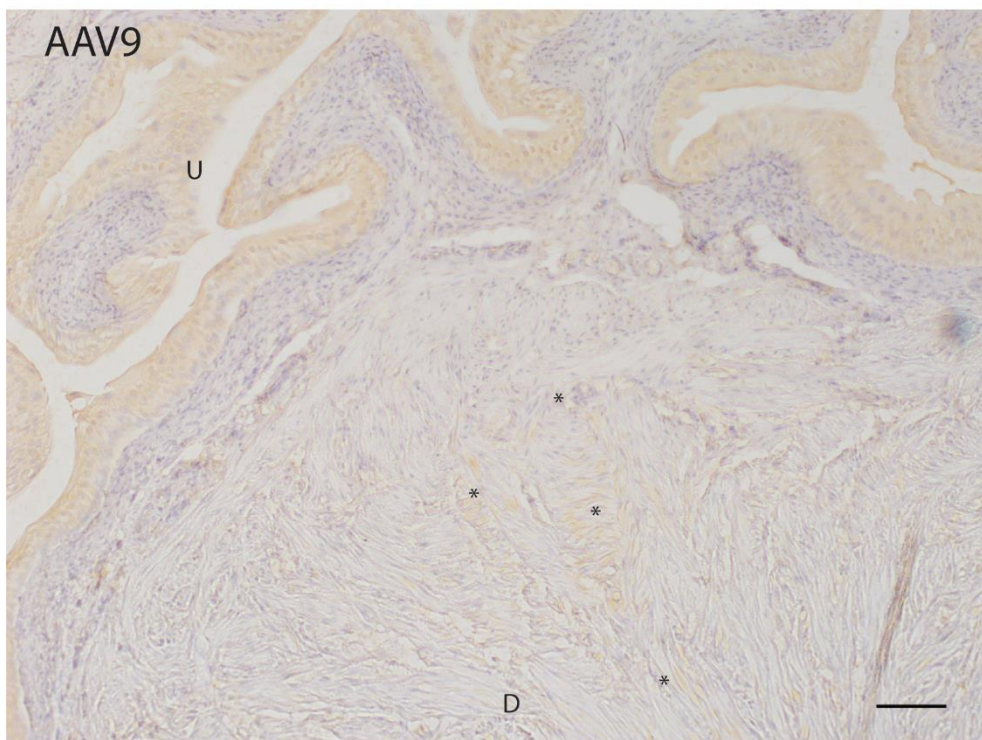
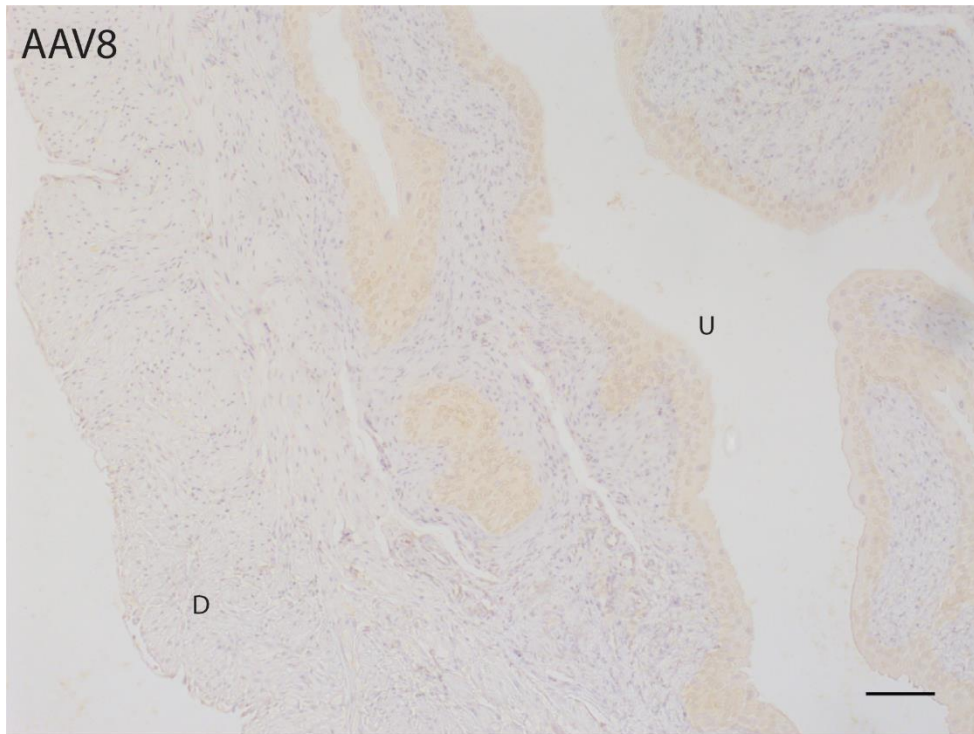


Figure 52. Biodistribution study bladders from mice injected with AAV8 and AAV9, both expressing GFP. DAB staining for GFP has been carried out. All scale bars are set to 100 μ m, areas of weakly positive GFP expression in the smooth muscle wall are marked with *. D - detrusor smooth muscle, U - urothelium. Representative examples, n=3.

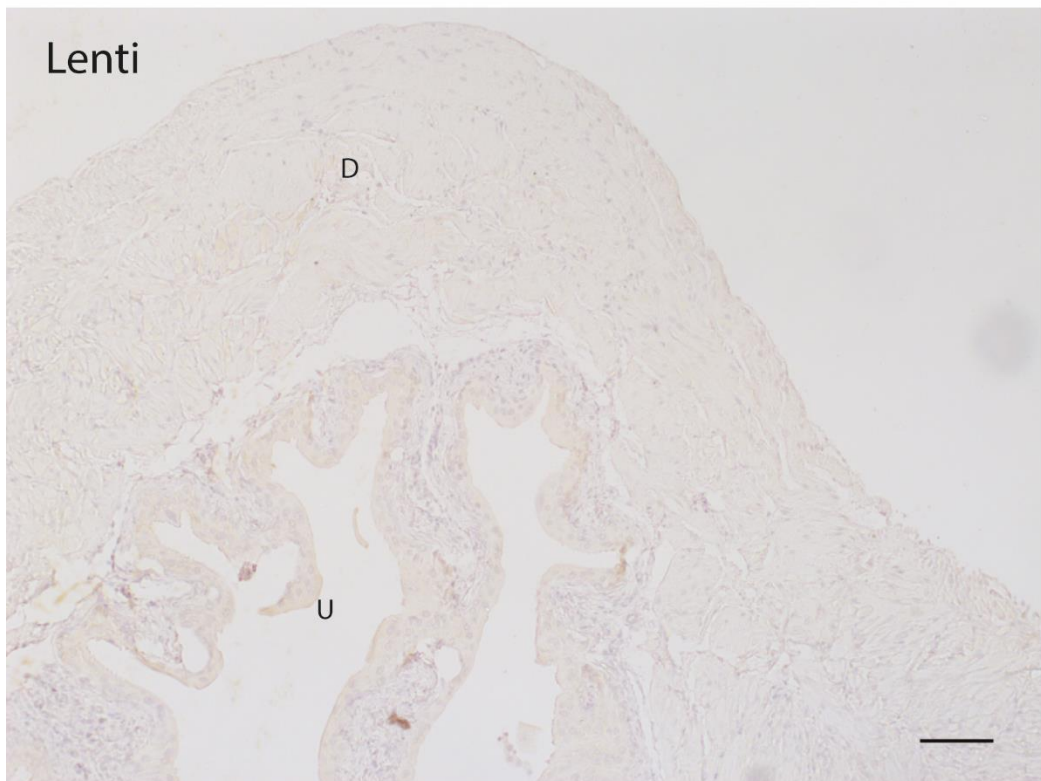
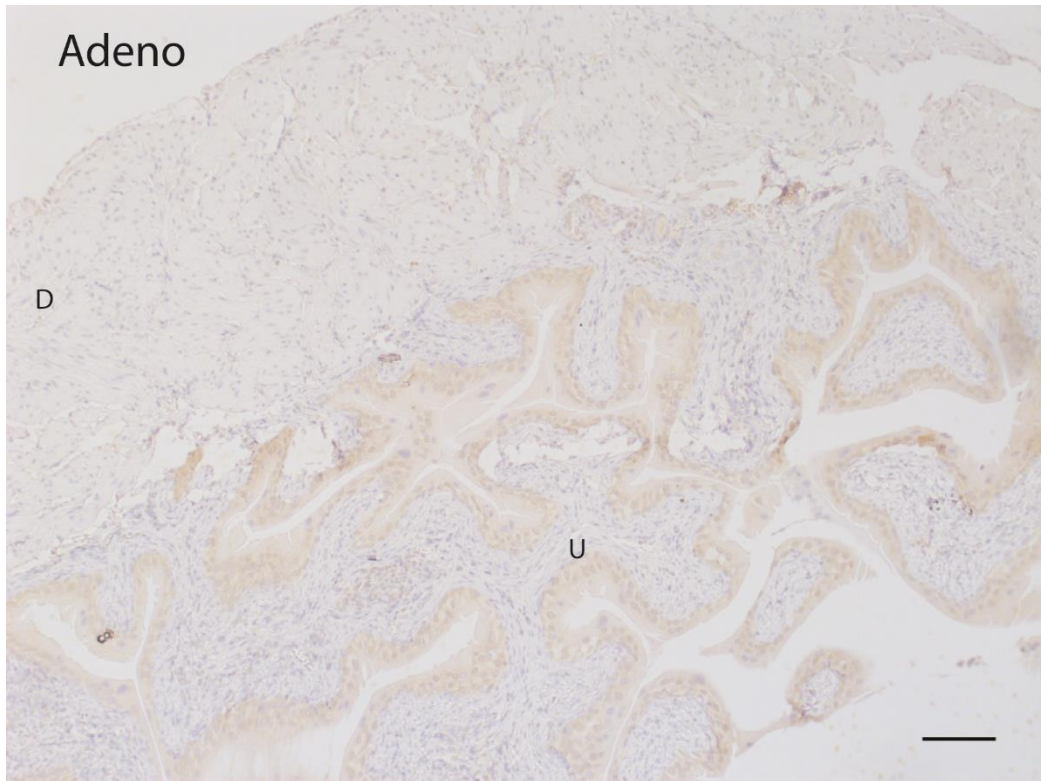


Figure 53. Biodistribution study bladders from mice injected with adeno- and lentivirus, both expressing GFP. DAB staining for GFP has been carried out. All scale bars are set to 100 μ m, neither construct worked especially well and it was difficult to find any areas of positive staining in the smooth muscle. D - detrusor smooth muscle, U - urothelium. Representative examples, n=3.

5.3.5 Summary

Experiments *in vitro* are also useful for forming pilot studies before carrying out potential therapies *in vivo*. Initially in this project whole organ culture was carried out to use as an experimental model. However, the difficulties in reproducibly delivering viral vectors inherent to the culture model meant that dissociated bladder culture of fetal bladders was used instead as a more efficient system to model changes to *Myocd* gene expression.

When culturing these cells, to investigate the effects of *Myocd*, lentiviral vectors carrying shRNA inhibiting *Myocd* expression were used to block expression of the gene. This decrease in the expression of *Myocd* resulted in decreased cell growth. This mimics the phenotype we see in the T30H mouse model, where a change to *Myocd* expression results in a lack of smooth muscle cells in the bladder.

In future, in order to rescue the phenotype, gene therapy over-expressing *Myocd* could be injected into the bladder *in utero*. Before this can be achieved a vector must be chosen to deliver the therapy. Data collected from a biodistribution study where GFP expressing vectors were injected into the orbital vein of P1 mice has shown that the vectors which best target the bladder are AAV1 and AAV9. However, this data is not conclusive because the vector delivery method differs from the planned delivery method for the T30H mice. The proposed method is ultrasound guided injection into the bladder, where the virus would have to overcome the barrier of the urothelium before being able to target the detrusor smooth muscle.

Ultrasound scans carried out show that the bladder in T30H mice is easily identifiable. T30H mouse bladders either do not empty *in utero* or empty very little; if gene therapy was then injected into the bladder of these mice there should be an ample window for the therapy to integrate within the cells of the bladder, provided the virus were able to overcome the barrier of the urothelium. If the virus successfully integrates with the detrusor smooth muscle wall this could rescue or at the least ameliorate the phenotype to restore some function to the bladder but affect other organs very little.

6 Discussion

Lower urinary tract obstructions are characterised by bladder muscle maldevelopment and reduced kidney function. They are one of the most common causes of end-stage renal failure in children, and treatment options are limited. More animal models are desperately needed in order to better characterise the genetic aetiology of lower urinary tract obstructions, and to inform future human therapies.

Regulatory pathways of muscle development during disease are poorly understood in the bladder. The T30H mouse model is an excellent model of obstructive uropathy which leads to end-stage renal failure. Here I have characterised the model using a number of different techniques and discovered the genetic location of the translocation causing the obstruction. The translocation point likely resides in a regulatory region of *Myocd*, a master regulator of smooth muscle. I have used *in vitro* techniques to further investigate the role of *Myocd* in development and disease.

6.1 Characterising the T30H Mouse Genetics

The reason that the T30H mouse has not previously been used to investigate obstructive uropathies was because of the difficulty in confirming whether a mouse was a T30H homozygote or not, especially *in utero*. The greatest barrier to overcome at the commencement of my project was finding the location of the T30H translocation points on chromosome 2 and 11. Discovering this point not only allowed genotyping to be carried out, but also allowed investigation into the genes causing the phenotype to be carried out.

Before the translocation point was found, distinguishing heterozygotes from wild-types was carried out by crossing the T30H mice with a reporter line carrying a *Gdf5* mutation causing brachypody. Beyond this method, the only way to ensure that the translocation had been lost was monitoring litter sizes and ensuring that they stayed low.

6.1.1 Chromosomal translocations – mapping the breakpoint

Chromosomal translocations are genetic anomalies where all or part of a chromosome arm breaks off and reattaches elsewhere in the genome. In individual

cells within the body these genomic rearrangements can cause cancer, but if they occur in gametes or during fertilisation they can result in various congenital defects (Roukos et al, 2014). Congenital defects caused by chromosome translocations are caused by either the creation of fusion genes if the breakpoints occur within two genes, or simply disrupt genes or their regulatory regions if the breakpoints are only within one gene or no genes at all. Translocations occur when there are double strand breaks at multiple points within the genome. This can happen by chance when there are errors in replication, or it can be due to exogenous sources (Roukos et al, 2014).

The most common forms of translocation which cause birth defects are either Robertsonian translocations or reciprocal translocations. Robertsonian translocations only occur with allocentric chromosomes, this is where the centromere of the chromosome is close to the end terminus of the chromosome arms. During a Robertsonian translocation two, usually non-homologous, allocentric chromosomes fuse. This has little impact on function due to redundancy in the genome, however, during meiosis the fusion often results in the formation of trivalent chromosomes. This creates gametes with chromosome duplications or deletions which are responsible for conditions such as Down's syndrome and Turner syndrome (Morin et al, 2017).

Reciprocal translocations are where two parts of non-homologous chromosomes are swapped over. Certain regions of the genome with repetitive sequences of DNA are at much more risk of a translocation occurring than others; these areas of DNA also make up a large portion of the genome in both humans and mice. This is because in these areas where chromosome breakpoints take place the highly homologous repeat regions can be incorporated more easily into another chromosome without being recognised as erroneous by DNA polymerases during meiosis. The translocation responsible for the T30H phenotype is a reciprocal translocation. These translocations also occur in humans, and ones which take place between the highly homologous regions are responsible for disorders such as DiGeorge syndrome (Nimmakayalu et al, 2003).

When a translocation has taken place, it is important to uncover the location of the breakpoints in order to work out which genes could be affected. Historically chromosome fluorescence in situ hybridisation (FISH) has been used to ascertain the location of translocations and duplications (Pellestor et al, 2001). However, chromosome FISH is time consuming and results do not give a great deal of specificity in terms of the location of breakpoints. It is also very technically difficult to successfully carry out chromosome precipitation in mice compared to humans, and is somewhat of a lost art. The advantage, however, is that they can be used to narrow down prospective areas for translocation points.

Whole-genome sequencing provides a method for attaining better coverage and more reliable results than chromosome FISH alone (Liang et al, 2017). Previously, relying on Sanger sequencing to screen for translocation breakpoints would have been prohibitively expensive. However, with newer sequencing by synthesis technologies sequencing is cheap enough to be able to use more routinely and has been used to map translocations in patients successfully (Chen et al, 2008).

The strategy used to map the T30H mouse translocation was next-generation sequencing. I then used Tablet software to visualise areas where translocations could be present (Milne et al, 2013), and then confirmed these locations using PCR. We then sent the amplified PCR products for sequencing in order to ascertain the precise sequence of the two translocation points.

In this case we were fortunate to find the translocation point using this technique. Uncovering translocations can be made difficult because of the propensity for translocations to take place in areas of the genome where there are repetitive elements, making it more difficult to narrow down exact translocation points (Tóth et al, 1994). If this had been the case with the T30H translocation then there are other methods aside in addition to whole-genome sequencing which I would have used, such as comparative genome hybridisation combined with fluorescence labelling.

Comparative genome hybridisation can be used in addition to fluorescence labelling to give more accurate results of the location of repeat regions (Duchon et al, 2011).

A technique called array painting can also be used. This is where a genome with a translocation between two known chromosomes is labelled fluorescently and then hybridised against a reference genome. The fluorescence ratios of probes can then be calculated to give precise breakpoint flanking regions. This technique relies on only the translocated chromosomes being hybridised to the array, which can only be achieved by flow sorting chromosomes, or through laser microdissection. Both of these techniques, however, are expensive and require specialist equipment (Obenauf et al, 2010).

6.1.2 Genetic context of the chromosome breakpoint

The T30H translocation is between chromosomes 2 and 11; on chromosome 2 the translocation point lies within the 3' end of the nonagouti gene, and on chromosome 11 the translocation point does not intersect any known genes.

Even though on chromosome 2 there is an intersection within a gene where the translocation takes place, this chromosome is the less likely to cause the phenotype. The gene which it intersects, nonagouti (*a*), codes for agouti signalling protein (ASIP) which is present in melanocytes and controls the switch between eumelanin and pheomelanin; variants of the gene result in different coat colours in rodents and lagomorphs, among other species (Fontanesi et al, 2010). Nonagouti is also expressed in the brain; when it is knocked out there is no change to the expression level of neurotransmitters in the brain, apart from a dopamine transporter gene, which affects the docility of the mice (Hirose et al, 2017). The gene has also been shown to affect the activity of the preputial gland, a sebaceous gland in the rodent urinary tract involved with secreting pheromones which affect social behaviour (Carola et al, 2014). T30H heterozygotes are relatively docile, which could be an indicator that the translocation falling within the agouti gene attenuates expression in some way. Coat colour, however, is not affected in heterozygotes and homozygotes do not survive for long enough to be able to discern either coat colour or docility.

The nonagouti gene is also involved in yellow mouse obesity syndrome, which is caused by dominant mutations to the nonagouti locus which causes it to be

expressed in tissues where it is not normally found, such as adipocytes. Specifically, there is a 170kb deletion which encompasses part of the nonagouti gene plus its upstream regulatory gene *raly*. It results in obesity and diabetes symptoms. Nonagouti and agouti-related proteins act as antagonists to central melanocortin receptor (MC4-R). Lack of MC4-R results in an inability to control appetite which causes obesity in the mice (Moussa et al, 1999). The regulatory gene which is important to yellow mouse obesity syndrome is not disrupted by the translocation, so is unlikely to affect the phenotype.

Although the nonagouti gene has never previously been reported affecting the bladder or the rest of the urinary tract, this does not rule out that the gene is not able to do so. It may be affecting the phenotype through some mechanism not previously identified or characterised, and so cannot be ruled out completely.

Also close to the chromosome 2 translocation region is the gene *AHCY*. This gene encodes S-Adenosylhomocysteine hydrolase, which is a highly conserved metabolic enzyme which hydrolyses AdoHcy (Kusakabe et al, 2015). If this does not happen then it can lead to endothelial cell damage and inflammation (Grbeša et al, 2017). If the gene is knocked out it results in embryonic lethality in mice (Miller et al, 1994), and in human cases where its expression is attenuated there are severe delays to brain development and nerve myelination, and there is also myopathy of skeletal muscle. The muscular disease in these patients is thought to be due to a lack of choline which is a metabolic side effect of the enzyme coded by *AHCY* not being transcribed. There are no mentioned differences to kidney, bladder or smooth muscle development in mice (Barić et al, 2004, Barić et al, 2005). This along with the severity of symptoms that comes with the knockout or attenuation of this gene makes it unlikely that its expression is disrupted by the T30H translocation.

Both T30H homozygotes and heterozygotes appear to show no symptoms of abnormal expression of either nonagouti or *Ahcy*. There are also no changes to the expression of nonagouti or *Ahcy* in comparison with wild-types P1 mice using RT-PCR. In a similar mouse model, the megabladder mouse, no regions of chromosome 2 are

affected in these mice. This implies that the genetic environment of chromosome 11 is more likely to be responsible for the phenotype caused.

On chromosome 11 the closest genes to the translocation point are mitogen activated protein kinase kinase 4 (*MAP2K4*) and *Myocd*. *MAP2K4* protein is a serine and threonine protein kinase. During development it has important roles in liver, brain and heart development, as well as having roles in the immune system and stem cell differentiation; knockout is embryonic lethal by the latest day 13 in mice (Haeusgen et al, 2014). Due to the severity of disrupted expression of *Map2k4* and the multiple organs it is involved in during development it is unlikely that it is responsible for the bladder defect in T30H mice.

MYOCD on the other hand has been directly implicated in both bladder and smooth muscle development. It is an important transcription factor which when heterodimerised with SRF can activate the expression of smooth muscle genes during development and maintenance of smooth muscle (Chen et al, 2002). The megabladder mouse model (Singh et al, 2007) has very similar morphology and a translocation causing a disruption of upstream regulatory elements of *Myocd*. This induces a change to the splice variants expressed in the bladder, and this has been postulated as the cause of the phenotype (Saha et al, 2009). In conditional postnatal *Myocd* knockout mice the bladder muscle wall progressively thins until the bladder phenotype is very similar to that of the T30H mouse and is no longer capable of emptying, causing hydronephrosis (Huang et al, 2015). These similar mouse models provide evidence that *Myocd* is the gene causing the phenotype in T30H mice. However, the translocation in T30H mice does not actually intersect with the transcribed sequence of *Myocd*. If *Myocd* is the responsible gene for the phenotype, the mechanism observed in T30H mice must, therefore, involve the regulatory mechanisms of *Myocd*.

A lack of other genes which appear to be involved in smooth muscle regulation surrounding the chromosome breakpoint alone does not provide enough evidence to say with certainty that *Myocd* disruption causes the phenotype in T30H mice. Other animal models which report similar phenotypes upon disruption to *Myocd*

expression also provide a supporting argument for the gene but again do not provide substantiated evidence that it is the gene causing the phenotype in T30H mice. There could be unknown functions for other genes surrounding the breakpoint region in smooth muscle expression which are unknown. There could also be an enhancer or suppressor region within the translocation point which does not affect *Myocd* expression at all, but instead affects another gene crucial to smooth muscle development.

6.1.3 Mechanisms for differential splice expression

For the majority of genes, control of expression takes place at the transcriptional level. This can be through either the regulation of the structure of the chromatin on which the gene resides, which makes it physically more or less likely to be transcribed. It can also be through the action of enhancers on regulatory sequences. The two are linked because these enhancers can affect the accessibility the chromatin region they target (Kleinjan et al, 2008).

An enhancer is a short DNA segment able to increase transcription level of a gene through binding to gene promoters, the regions of DNA that initiate transcription of a gene (Schaffner, 2015). Enhancers allow genes to be expressed in both a spatially and temporally distinct fashion; this gives rise to tissue-specific gene expression. They can be up to a megabase away from the promotor region they target and can be either up- or downstream of their target gene. The activation of a gene through enhancer activity requires chromatin remodelling so the enhancer and promotor region can physically interact. This is thought to be mediated by a class of non-coding RNAs transcribed from enhancers termed eRNAs. Alongside transcription factor binding they help to increase the stability of the promotor-enhancer complex. This complex in turn allows RNA polymerase to bind to the promotor region and initiate transcription of the target gene (Hu et al, 2017).

Enhancers can both be found, and their activity ascertained, by the acetylation and methylation of the histone profiles surrounding them. Where there are active enhancers chromatin packaging protein H3 is modified to H3K4me1 and H3K27ac, whereas inactive enhancers have H3K27me3-modified H3. Enhancers can also

occupy a third 'poised' state where they are marked by H3K27me3 as well as H3K4me1, which is where enhancer target genes are expressed at low levels but are ready for rapid upregulation once appropriate signals are expressed (Ko et al, 2017).

In cases of disease where the genetic sequence of the gene is not affected, but potential regulatory regions surrounding the gene are, then disruption of gene control mechanisms like enhancers could be the cause of the disease. There are called position effect mutations, and there are a number of diseases which are caused by mutations of this kind. One of the earliest discovered examples of a disease caused by a point mutation is Dutch and Spanish thalassemias, where the locus control region, a cis-regulatory site for β -globulin is lost to another chromosome where it can no longer be active through a translocation (Kioussis et al, 1983).

Another example of a gene where the coding sequence is not disrupted but there is still a disease phenotype caused by disruption of the regulatory region is sclerostin (*SOST*), which is a negative regulator of bone formation. Sclerosteosis is an extremely severe disease-causing bone malformation and is caused by homozygous null mutations to *SOST*. Van Buchem disease is similar but much less severe, and the coding region of *SOST* is completely intact. There is however, a deletion to the downstream regulatory region of the gene, which decreases the expression of the gene. This was found by examining conserved elements between the human and mouse genome in the area downstream of *SOST*. These conserved elements were tested using a luciferase assay in cell lines to ascertain which of the control regions could activate expression of the promoter cloned into the cell line; only one of these sites, SCR5, activated the promoter (Loots et al, 2005).

In the T30H mouse model the sequence of *Myocd* is intact, but expression is nevertheless altered. The translocation point is around 180kb pairs away from *Myocd*, which is well within the distance that enhancers are capable of acting. There is a large region of enhancers close to *Map2k4* which is 0.4Mb away from *Myocd*, and there are also enhancers within the introns of *Map2k4* which could also act on *Myocd* expression. *Myocd* has several splice variants which are tissue specific, the

expression of which could be controlled by enhancer activity (Saha et al, 2009, Imamura et al, 2010).

There are other genes in mammals which undergo tissue-specific alternative splicing in this manner. *NCAM* is a gene with 20 exons and can induce myoblasts to differentiate into skeletal muscle if the gene is expressed containing a muscle-specific domain, which is found between exons 12 and 13. There is a regulatory element in one of the introns of *NCAM* which is activated in non-myogenic cells to repress translation of exons containing muscle-specific domains (Kawahigashi et al, 1998). Organ-specific alternative splicing also takes place in non-muscle myosin heavy chain II-B (*NMHC-B*). Specific exons are only transcribed in neural cell types and are excluded from all other cells; this action is mediated by an enhancer found in an intron of the gene (Nakahata et al, 2005).

The translocation point falls upstream of *Myocd*, and it is in this area that a regulatory region controlling organ specific splicing of the gene is thought to reside in mice (Saha et al, 2009). I used a Basic Local Alignment Search Tool (BLAST) to compare a 350bp region surrounding the translocation point on chromosome 11 against the human genome using Ensembl and no matches have been found on chromosome 17, the location of *MYOCD* in humans. This does not mean that there is not a regulatory region for *MYOCD* in humans. It could mean that it is either not well conserved, or that highly conserved areas are not immediately surrounding the area of the translocation point. A genomic hybridisation study would be required in order to ascertain whether there was a conserved regulatory region upstream of *MYOCD* in humans.

6.1.4 Correcting the malformation and finding the enhancer

The most likely gene causing the T30H genotype is *Myocd*; while the coding region of *Myocd* is unchanged, disruption of gene expression could take place through knock out of the control region of *Myocd* through the translocation of cis-acting enhancer elements to chromosome 2. This would knock out tissue specific enhancers for *Myocd* expression in the bladder, while *Myocd* in other organs such as the heart and gut remains normal.

If the gene causing the mutation is known, then theoretically a rescue of the phenotype in the mouse is possible. This could be achieved through manipulation of *Myocd* expression in the muscular tissue of the bladder. Manipulation of *Myocd* in the T30H mouse model causing an improvement of the phenotype would also provide compelling evidence that *Myocd* is causing the phenotype in the first place.

6.2 Characterisation of the T30H mouse Phenotype

The most striking feature of the T30H mouse model is the almost complete lack of smooth muscle in the bladder wall. Staining with early and mature smooth muscle markers such as α SMA and calponin shows a severely reduced or complete lack of these markers in the detrusor smooth muscle wall. *Myocd* has been identified as an important gene in bladder development, but its expression in T30H mouse bladders is difficult to properly localise and validate. This is due to a combination of poor antibodies and the severe reduction in the tissue present in T30H homozygous mouse bladders compared to wild-types.

To date commercial antibodies for MYOCD are unreliable, and other methods such as in situ hybridisation, or CRISPR-Cas9-mediated epitope tagging may be required to properly ascertain MYOCD expression levels (Lyu et al, 2019).

In situ hybridisation is a technique which could be used to ascertain the expression of *Myocd* in the bladder. This technique substitutes an RNA probe in place of the antibody used in immunohistochemistry, although there are other significant differences to the in situ hybridisation protocol which make it much more complex. In situ hybridisation probes can also be designed to stain for expression of specific splice variants in the bladder. As my laboratory did not have expertise in carrying out in situ hybridisations I consulted with Kirk McHugh, whose group worked with the megabladder mouse model and had previous experience in staining for *Myocd* in the bladder using this protocol (DeSouza et al, 2013). I was advised that in situ hybridisation experiments were very difficult to optimise for *Myocd* and that due to limited mouse numbers it might be better to focus on examining *Myocd* expression using PCR.

The urothelium in T30H mouse bladder samples stains positive for Uroplakin 3a expression. This provides some evidence that the urothelium is present and still maintaining a barrier function in these mice. Further experiments staining other markers of the urothelium are required, however, to ascertain how the extreme distension of the bladder has affected the urothelium. That the cells of the urothelium in T30H mice are still able to express uroplakin 3a points towards an

undisrupted development of the urothelium. This may imply that the bladder epithelium's function as a signalling centre to induce smooth muscle expression, though factors such as sonic hedgehog, is normal, and so the disruption to the pathway is downstream of the sonic hedgehog signalling pathway. There is minimal evidence for this, however, and so further experiments would be required to prove this, either through staining for or testing for gene expression of signalling factors in the sonic hedgehog signalling pathway.

Genes in the sonic hedgehog regulatory pathway, in addition to other smooth muscle genes, are not located near the translocation point on either chromosome 2 or chromosome 11 (**Figure 54**), so are unlikely to cause the phenotype. This further promotes the hypothesis that disruptions to *Myocd* expression causes the phenotype in T30H mice, although does not prove it.

Another animal model, the megabladder mouse, helps to further the hypothesis that *Myocd* is the culpable gene. It is a similar, but less severe, model, in which some sections of multi-layered smooth muscle remain in the bladder, but the majority of the bladder is amuscular. This is the case in adult and male megabladder mice, whereas in female mice at birth there is a smooth muscle layer around the bladder, albeit a very thin one, and the megabladder phenotype still develops *in utero* (Singh et al, 2007). The T30H phenotype presents similarly, as a bladder wall almost completely devoid of any smooth muscle tissue. When it is present, it is no more than a few cells thick. The gene responsible for the megabladder mouse phenotype is also suggested to be *Myocd* (Singh et al, 2008), although the deletion which causes then phenotype is further away from *Myocd* than the T30H translocation point is (McHugh, 2013). This difference in distance from the translocation point could explain the difference in severity of the phenotype. The T30H translocation point is closer to *Myocd*, removing more of the proposed regulatory region of the gene.

Gene of interest	Mouse chromosome
Myocardin	11 (exact - 65173608)
Alpha smooth muscle actin	19
Uroplakin 3a	15
Calponin	9
Serum Response Factor	17
CDH11	8
BMP4	14
SMAD2/3	18/9
MRTFA/B	15/16
Smoothelin	11 (exact - 3517522)
Desmin	1
SMMHC	16
Transgelin	9

Figure 54. Myocardin and other genes of interest plus their location in the mouse genome. The only other gene on chromosome 11 is smoothelin, and this gene is very far away from the translocation point so is unlikely to be implicated in the phenotype.

Previous to the commencement of my project it was not possible to collect embryonic timepoints with any certainty as to their genotype. Even after the development of a genotyping PCR the scarce numbers of T30H mice meant that culling pregnant heterozygote dams was difficult to carry out without losing too many breeding females. In order to generate data from as many timepoints as possible from each pregnant heterozygote ultrasound scanning was used.

In utero, at very early stages up to E14, T30H mice are indistinguishable from their wild-type litter mates using observation from ultrasound scanning. At this stage the smooth muscle layer is not fully functional and the smooth muscle cells have not yet compacted into mature smooth muscle cells. This makes it difficult to ascertain the bladder wall tissue from surrounding tissue, however, the indiscernible difference in the morphology of the bladder implies that there is little difference in bladder structure at this stage in T30H mice.

Phenotype onset is at E15, where there is a clear and dramatic difference in the volume of the T30H mouse bladder compared to that of wild-type mice. This coincides with the first production of urine and the onset of the kidneys function as a filtration unit (Woolf et al, 2001).

The T30H phenotype is particularly striking given that the development of the smooth muscle in the gut and heart, two other smooth muscle-rich organs, appears completely normal and functional. This implies that the maintenance and/or development of smooth muscle cells in the bladder is distinct to the development and maintenance of smooth muscle cells in other organs.

When *Myocd* is totally knocked out either constitutively or conditionally, it is always lethal (Li et al, 2003). In cases of constitutive expression this is because of global organ failure, predominantly that of the heart leading to failure of the embryo to survive (Huang et al, 2015). With conditional expression there is a time gap between the initiation of knockout and the resulting lethality. The animals eventually die from myocardial infarction. This suggests that *Myocd* is not just responsible for the development of smooth muscle, as is evidenced in the literature (Zheng, 2014). There also seems to be a role for *Myocd* in the maintenance of smooth muscle cells, as

when expression is blocked there is a slow decline in the number of viable smooth muscle cells in animals where there is knock-down (Huang et al, 2015).

6.2.1 Why is the T30H mouse a valid model

The T30H mouse is a functional model of lower urinary tract obstruction. This means that there is no physical obstruction to the lower urinary tract as there is in cases of PUV or urethral atresia in humans. In these conditions the bladder wall becomes more muscular and there is increased collagen deposition (Woolf et al, 2001). In terms of morphology the T30H mouse model is most similar to cases of PBS where the bladder is non-emptying but there is no evidence of physical obstruction apart from the lack of musculature in the abdominal wall.

Irrespective of the bladder muscle wall content, the phenotype in T30H kidneys is very similar to that seen in humans with lower urinary tract obstructions. There is severe dilation of the renal pelvis from urine which is not able to enter the non-emptying bladder. This hydronephrosis also extends into the proximal and distal tubules of the kidney and into the glomerulus, with evidence of space between the glomerulus and the Bowman's capsule where urine has not been able to drain.

Oligohydramnios is present in the most severe cases of lower urinary tract obstruction. It is a secondary symptom of lower urinary tract obstruction; *in utero* the fetus is constantly taking in amniotic fluid orally, which is then filtered by the kidneys and released back into the amniotic sac via the bladder and urethra. This cannot occur in cases of obstruction and fluid remains in the urinary tract. This results in a reduction in the amount of amniotic fluid surrounding the fetus. Amniotic fluid is also important for lung development, as the fetus also takes the fluid into the lungs. This helps the lungs to distend which is essential for their development. In animal models induced oligohydramnios reduced future air space in the lungs and also changes the size and shape of epithelial lung cells, further compromising proper development (Najrana et al, 2017). This secondary effect of obstruction is often a more urgent problem *in utero*, as the mother's kidney can compensate for lack of function in the fetus.

In the T30H mouse there is no evidence for oligohydramnios: pups born do not appear to be in respiratory distress, their lungs have normal morphology in tissue sections, and they are of normal size. There could be no oligohydramnios in the mice because there is simply not enough time to develop, from when the bladder develops to birth there are only six days, whereas in humans there are still around 30 weeks of gestation left from when the bladder first starts to acquire smooth muscle at around 12 weeks of gestation (Newman et al, 1989). When obstruction takes place the rate of filtration by the kidney decreases and slows down, therefore decreasing fluid intake by the embryo. There is also no oligohydramnios or lung phenotype in any other mouse lower urinary tract obstruction models reported in the literature; and when mouse models of oligohydramnios are generated amniotic fluid is removed from the embryonic sac. One of the only genetic models of a renal malformation where the fetus develops oligohydramnios is a mouse model of complete bilateral renal agenesis (Smith et al, 2006).

6.2.1.1 Comparison with other mouse models

The most similar model to the T30H mouse is the megabladder mouse model. These mice also have a functional obstruction of the lower urinary tract, in that they also do not develop any smooth muscle in the bladder. However, the phenotype is much less severe in these mice, the females can live to breeding age, and the males live for several weeks after birth. Both male and female T30H mice have been observed, and no T30H mouse has survived more than a few days after birth (Singh et al, 2007).

There are also differences in that the megabladder mouse exhibits a one sided 'pop off' mechanism, where one of the kidneys has much worse hydronephrosis than the other, however, this acts as a protective mechanism for the function of the other kidney (McHugh, 2014). The renal pelvis of the more heavily affected kidney becomes almost a second bladder and takes on more of the urine which is unable to drain. This response is thought to take place in order to preserve some kidney function. This does not appear to take place to such a great extent with the T30H mouse and has not been observed in a quantifiable way on ultrasound. This could be because the phenotype is more severe in the T30H mouse so the damage progresses to the

kidneys too quickly for them to be able to adapt to compensate against the effects of the disease. On the other hand, the disease is so much more severe in the T30H mice that the 'pop off' mechanism could take place and then be overwhelmed if bladder function is so poor that the bladder cannot void at all *in utero*.

The primary difference between the two animal models is the severity. The proposed cause of both animal models is the disruption to the regulatory region of *Myocd*. In both cases the regulatory region has been moved to another chromosome, which means that any promoters or enhancer elements cannot interact with *Myocd* as these elements are cis acting and must be on the same chromosome (Schaffner et al, 2015). The translocation which causes the T30H mouse mutation is closer to *Myocd* than that which causes the mutation in the megabladder mouse. This could mean that more of the regulatory region is removed, making the phenotype more severe.

6.2.1.2 Humans with the phenotype

The most similar phenotype to the T30H mouse in humans is prune belly syndrome. Humans with these cases present with either a transient physical obstruction or a functional obstruction of the lower urinary tract which causes bilateral hydronephrosis and gross distension of the bladder. There is also a lack of abdominal and bladder musculature.

The lack of physical obstruction and the lack of smooth muscle in the bladder wall sets the T30H mouse apart from humans with PUV. In children with this disorder the physical obstruction is caused by improper fusion at the trigone of the bladder; it results in an increase in the smooth muscle of the bladder wall, and an increase in collagen deposition and fibrosis. However, the kidney symptoms are very similar. In both the T30H mouse and children with obstruction there is extensive hydronephrosis *in utero* and a decrease in the functional tissue of the kidney. Affected individuals die from end-stage renal failure if no intervention takes place. These are common pathways of the disease with the phenotype seen in T30H mice.

Myocd is the most likely culpable gene for the T30H phenotype. Humans have been found with changes to *MYOCD* expression and prune belly syndrome. In one of these

cases there was a heterozygous deletion to *MYOCD* and in another study four families were found with heritable changes to *MYOCD* expression with produced a prune belly syndrome phenotype (Boghossian et al, 2018, Houweling et al, 2019).

Recently a study was published where a human family presented with mutations to *MYOCD* resulting in offspring with a prune belly phenotype (Houweling et al, 2019). The parents had no defects to any organs expressing smooth muscle, including the bladder, but both were heterozygote for *MYOCD* mutations. There were two children. The girl had heart defects including patent ductus arteriosus; the boy presented with megabladder on ultrasound scanning and the pregnancy was terminated mid-way through gestation. There were also heart and gut defects.

Whole exome sequencing of both the parents and the offspring found that both children were compound heterozygotes for *MYOCD* mutations, one of which introduced a premature stop codon, and the other carried a missense mutation. Twenty-two other families with a history of prune belly syndrome were then analysed using whole exome sequencing and three other families were found carrying mutations to *MYOCD*.

A mouse line was generated by Houweling et al (2019), carrying mutations to the LZ domain of *Myocd*, similar to the missense mutation in the human cases, was used to further investigate this disease phenotype. Compound heterozygotes for megabladder mice and LZ mice produced a severe megabladder phenotype. This further strengthens the case that alterations to *MYOCD* levels during development result in bladder malformations.

No humans have been found with defects to the regulatory region postulated to be affected in T30H mice, however, studies to date have focused primarily on alterations to the gene itself and not the regulatory region. In cases where no genetic cause has been found for prune belly syndrome or other bladder defects it may be of interest to investigate this regulatory region in the future. Alternately, *MYOCD* may not be heavily involved in human disease, as research into its effects on lower urinary tract obstructions or malformations has thus far been limited to the few studies where

patients have a mutation to *MYOCD*, and where the gene itself is not involved altering expression may not improve patient symptoms.

Despite the similarities between the T30H mouse phenotype and humans with *MYOCD* mutations, there are still problems with making a direct comparison between mouse models and human disease. This is especially true of the bladder because of the differences in voiding patterns and even function between the human and the mouse bladder. After continence is gained in childhood the bladder is important in humans for the storage of urine and allowing urine voiding at socially acceptable times. In mice the bladder especially in males is used for scent marking and communication, and it can be more common for small amounts of urine to be voided regularly, in contrast to humans.

Restoration of a normal muscle phenotype may also not be that important in treating cases of lower urinary tract obstruction. In patients one of the main concerns is maintaining or restoring kidney function. While a non-functional smooth muscle wall may exacerbate the kidney phenotype, improving tissue engineering to develop bladder replacements (Atala, 2020) may remove the need to restore function to the native bladder completely.

6.3 *In Vitro* Manipulation

Whole organ culture is a useful technique which allows development and differentiation of various cell types within an organ to be studied within the closest approximation possible of their normal biological environment. Organs must be grown at the surface to air interface, as oxygen diffusion to the centre of the organoid becomes a limiting factor with the lack of circulation (Trowell 1954). Serum-free media is used with added insulin, transferrin and selenium to promote differentiation (Anver et al, 1982, Lopes et al, 2019).

Whole organ culture was initially used as a technique for growing bladders *ex vivo* for use as a model for testing future therapies. This culture system has previously been used to ascertain the effects of vascular endothelial growth factor on developing bladders, with positive results (Burgu et al, 2006). In order to use this organ culture system as a testing system for manipulating the smooth muscle defect as a trial for future *in vivo* studies, a reliable, reproducible method for quantifying both growth of the whole organ and of the smooth muscle layer was required.

Initially measuring total DNA content was suggested, as well as dissociating the whole bladder and then using flow cytometry to determine the percentage of smooth muscle cells in the bladder as a whole. These techniques were dismissed in favour of a method which would not sacrifice data showing the morphology of the bladder. Therefore, after several time points in culture bladders were fixed, embedded and then the entire bladder was sectioned through. One in every three sections was selected for staining, and then the bladders were imaged, and the bladder wall thickness of each section was calculated in four points on the bladder using ImageJ.

Using four points on the bladder wall to calculate thickness removes some of the inherent variability in the thickness of the smooth muscle wall within a bladder which is present because the muscle layer of the dome is much thicker than that of the trigone. This is also limited through the dissection technique, where the trigone is removed before the organ is put into culture.

The bladders were grown for six days in culture. This was chosen because the bladders were dissected out at E14, so another six days of culture would resemble the remaining 6 days of gestation and give a physiological time point to compare the cultured organs to. The bladders grew the most in the first three days, although continued to grow through to day six of culture. However, the differences in the mean smooth muscle wall thickness did not change after 2, 3 or 6 days in culture. It was decided not to continue to use this culture technique, this was for a number of reasons.

As the length of time in culture continued, the bladders flattened to the cell culture inserts they were growing on. This meant that their morphology started to diverge from what would be seen *in vivo*. The bladders also grow at a much lower rate once excised from the fetus – this is also recapitulated when growing fetal kidneys in culture, which only grow at half the rate of a developing kidney *in utero* (Nishinakamura, 2019). An E18 bladder dissected from a fetus is much larger than a day 4 cultured bladder. The environment the bladders are grown in does not perfectly recapitulate the environment the bladder would grow in biologically; this is because there is no urine flow in the cell culture system. The normal filling and voiding of the bladder is likely essential to the proper smooth muscle growth and innervation (Clothier et al, 2018). There are also various other factors which do not take place in organ culture which the bladder requires to grow during development, such as lack of blood supply. When the bladder is developing, once the bladder passes E14 in mice it starts to expand and contract in order to contain and excrete urine. Contraction and relaxation are physiologically required for the bladder to develop normally, but is difficult to achieve in culture with developing bladders due to the very small size (Nyirady et al, 2002). Maintaining bladders in culture with a voiding pattern is generally only done with adult bladders (Collins et al, 2013, Durnin et al, 2016).

There is also some question as to whether a viral therapy would actually enter the bladder if it was grown in a whole organ culture system. Any vector introduced into cell culture media would probably only reach the layers of the bladder in contact with

the cell culture insert, as the virus would have to be added with the cell culture media. This would not mimic very well the method for virus delivery which would be attempted in culture and would give a less accurate idea of the effects of *Myocd* knock-down in the whole bladder.

After deciding the whole organ culture would not be carried forward, two possible options were considered. The first option was dissociation of the bladder followed by pooling of cells and reaggregation. This methodology is commonly used in the kidney and gives an easy way of introducing therapies to all cells of the organ simultaneously, and the organ can then grow in culture in a way which somewhat resembles the way the cells of the organ would interact with each other during development.

This technique relies on the organ's ability to self-organise – this is well established in the kidney. And many dissociation-reaggregation studies have been pioneered in this organ (Howden et al, 2019, Kumar et al, 2019, Davies 2018). For the most part bladder organoids to date have been primarily used to model tumorigenesis or to model the effects of infection (Vasyutin et al, 2019, Horsley et al, 2018). Dissociation followed by reassociation not only allows the role of self-organisation in the bladder to be investigated, but once the organ has been dissociated, the cells can be treated with drugs or viral vectors which can easily access all cells in the organ before it is spun down to form an organoid. Organoids can also be made in this way from stem cells, these can be either induced stem cells from a tissue of interest or obtained commercially. This means that organoids can be generated quickly and at scale. Although the organoids grew, they became infected before any data could be gained from them. After these initial experiments become infected no more reassociation experiments were carried out. The technique is complicated and time consuming, and also uses a lot of bladders (between 6 and 8) to make a single organoid.

Instead dissociated culture of the bladder was used to investigate the potential effects of therapy *in vitro*, as a way of extrapolating for what potential results might be *in vivo*. The technique is relatively simple and was used as a way of obtaining results on potential therapies relatively quickly, but still maintaining some of the

physiology that would be present *in vivo* by using primary cell culture of the entire bladder instead of an immortalised cell line.

Primary bladder smooth muscle cells in culture can be identified through their spindle shaped morphology, non-contact inhibited growth and the expression of α SMA (Baskin et al, 1993). Smooth muscle cells, both *in vivo* and *in vitro*, fall into two broad categories: one is proliferative and secretes ECM, the other is not highly proliferative and has the morphology of a more mature, terminally differentiated smooth muscle cell. When culturing cells from embryological tissue a limiting factor is the low number of cells generated because of small tissue size; because of this a cell culture environment which pushed cells towards a more proliferative phenotype was chosen for growth. Whether the smooth muscle cells are highly proliferative or highly differentiated depends on the serum levels in the tissue culture media. Low serum levels create a more differentiated, less proliferative cell type, and high serum levels produce the opposite (Veber et al, 2018).

When grown in serum-rich media cells could be grown up to 5 passages, allowing enough cells to be able to generate reliable data. Cells were split into three populations after harvesting from E14 wild-type mouse fetuses. Short hairpin RNA (shRNA) packaged in a lentiviral vector was used to knock-down *Myocd* in one of the three populations; these cells exhibited reduced levels of growth compared to untreated cells. This was not due to deleterious effects of the lentivirus as a population treated with a scrambled control virus did not show a reduction in growth.

The level of *Myocd* knock-down was most efficient in the first assay of the three which were carried out. This could be because viral titre is severely impacted by freeze thawing. Although every precaution was taken to reduce the number of freeze thaw cycles the lentivirus was exposed to, for example initially splitting the virus into aliquots when it was first delivered, things like temperature fluctuations to freezers could have caused a reduction in the viral titre for the second two assays. There could also be variation in the efficiency of viral transduction for a number of other reasons, including differing levels of cell viability after dissociation, varying incubator

temperatures, or differing effects of cell viability depending on the time taken to dissect the bladders from all mice in the litter.

Myocd has diverse roles in smooth muscle cell development and disease and seems to be required for maintenance of smooth muscle cells, as when it is knocked out in adult mice smooth muscle in tissues deteriorates over time (Huang et al, 2015, Zheng, 2014).

When I knocked down *Myocd* in cultured smooth muscle cells from E14 mice there was a reduction in growth compared to untransfected controls. However, further replicates of this study need to be carried out in order to be certain of this effect because the *Myocd* knock-down was only successful in one of the replicates using data from western blotting. *Myocd* has diverse roles in smooth muscle development. This, coupled with the lack of certainty over the extent to which the gene was knocked, down means that it is difficult to tell from these experiments whether the decrease in *Myocd* in culture actually results in a decrease in the number of cells which grow. It also makes it difficult to directly relate these experiments to the phenotype seen in T30H mice. The reduction in the number of cells observed in the *Myocd* knock-down assays could be either because the cells are prevented from proliferating, or the cells undergo apoptosis. The differences between the number of cells in control populations compared to the *Myocd* knock-down population also increases with the number of passages. This could simply be due to the number of passages amplifying the effects of less 'founder' cells which either die or stop proliferating early.

This could be tested by ascertaining whether there was a difference in KI67 expression between control and transfected cell populations. Apoptosis could be tested by carrying out caspase assays using a western blot to assess the levels of pro and active caspase. Caspases are proteases which are involved with apoptosis, and so active caspase is only present where cells are undergoing apoptosis (Shalini et al, 2015). TUNEL assays can also be used to measure apoptosis. DNA condenses when apoptosis takes place, and in a TUNEL assay the 3' end of DNA fragments are stained with a fluorescent dye which can be measured.

There was also a small reduction in the level of α SMA present shown using western blot assay. This is as expected as α SMA expression is activated by *MYOCD*-mediated SRF binding to CArG boxes in the regulatory region of *α SMA*. In future other smooth muscle markers should also be tested, such as CNN, SMTN or SM22 α .

There are inherent limitations to growing cells as a dissociated culture and then using this culture method to test the effects of treatments which *in vivo* would be applied to the whole organ. Bladder cells grown in dissociated culture have no barriers to the vector being able to access the cells. This is good for ensuring that all cells are treated in the same way but at the same time does not recapitulate the conditions the cells would be under *in vivo* when the natural barrier of the urothelium would be in place potentially preventing the vector from accessing the cells of the smooth muscle wall. This underlines the importance of testing in animal models such as the T30H mouse, as modelling the actual conditions of how a gene therapy vector would be applied to the bladder *in vivo* is difficult.

The issue of the differences to therapy delivery method also applies to the biodistribution study. The mice used in this study had the vector injected into their bloodstream, whereas to treat the T30H phenotype the vector delivery would be intravesical. This means that the vectors identified as being good at targeting the bladder may not work as well or in the same way when injected intravesically *in utero*. If it were possible to breed a greater quantity of T30H mice it would be advantageous to carry out an experiment trialling different vectors for injections into the bladder to see which vectors would target the smooth muscle wall, or other components, best. However, the low litter sizes, even for T30H heterozygote mice crossed out against CD1 mice are low enough that this would be challenging.

In the future it would be of interest to knock-down only specific isoforms of *Myocd* to see whether any specific isoforms had a profound effect on smooth muscle cell proliferation or differentiation. As this would have required much larger cell numbers to carry this out simultaneously or more time to carry out more assays it was not attempted in this project. It may be more useful to carry out these experiments using

immortalised cell lines or bladder smooth muscle cells generated from iPSCs to overcome the issue of cell numbers.

It would also be interesting to ascertain the effect *Myocd* knock-down would have on cells with a contractile phenotype. When immortalised uterine smooth muscle cells are grown to confluence, they lose some of their proliferative potential and express an increased level of contractile genes (Vaes et al, 2018). This technique could be used to culture primary embryonic bladder cells and switch them to a more contractile phenotype to see how *Myocd* knock-down affects contractility in culture. *Myocd* is required for smooth muscle differentiation, but after binding to smooth muscle genes it is marked for degradation by ubiquitylation, and this step is necessary for the cells to obtain a contractile phenotype (Singh et al, 2017), and to see how specific isoforms of *Myocd* also affect this contractility.

A goal for the *in vitro* manipulation of the *Myocd* phenotype was not only to investigate the role *Myocd* plays in normal development. It was also to develop a vector delivery method for the delivery of *Myocd* as a gene therapy to restore bladder smooth muscle function in amuscular bladders like that of the T30H mouse model. However, delivery of a vector upregulating *Myocd* expression may not result in a rescue of the phenotype. The organ specific splice variant expression of *Myocd* is important for muscle growth (Saha et al, 2009), simply having upregulation of *Myocd* through a ubiquitous promoter may still result in aberrant smooth muscle growth in the bladder wall. Gene therapy delivering specific splice variants of *Myocd* may be required in order to correct the phenotype.

6.4 Future work

6.4.1 Rescue of the Phenotype

Research from my PhD project has directly resulted in the acquisition of funding from an innovation grant from the charity Kidney Research UK. In this grant we will use gene therapy to manipulate *Myocd* expression in the developing bladder in T30H mice, with a focus on rescuing the phenotype in the mouse model.

T30H pups will be identified *in utero* via ultrasound scanning; pups will then be injected intravesically, into the bladder with a human *MYOCD* over-expression AAV construct at E16 and then examined at birth for both bladder and renal histology. Empty vectors will be used as controls. Both therapy and control vectors also express green fluorescent protein (GFP) making it easier to localise areas of successful transduction. If bladder musculature is improved, then we will investigate survival and long-term bladder and kidney function. Refinements to improve success of therapy may include repeated dosing, targeted upregulation of specific *MYOCD* isoforms or use of other vector systems.

In order to better establish the role of *Myocd* in bladder muscle development the experiments knocking down *Myocd* expression in dissociated bladder cells in culture must be repeated to ascertain whether the knock-down of *Myocd* in these cells actually results in a decrease in growth or whether these results were due to some other underlying factor. This is because MYOCD protein levels were only removed in one of the three assays.

6.4.2 Development of a conditional knockout model

The T30H mouse model has provided a valuable tool for investigating the effects of obstruction on the development of the urinary system, and on understanding the role of *MYOCD* on bladder development. It has also highlighted the need for more animal models of obstructive uropathy. The T30H mouse model is an excellent model for lower urinary tract obstruction, but the mouse model also has drawbacks. The low litter sizes and inability to breed from the homozygous mice is a significant stumbling block to widespread use of the animal model. A solution to this would be

the generation of a conditional knockout for *Myocd* in the urinary system using the cre-lox system.

The cre-lox system can be used to target specific genes for upregulation or knockout (Utomo et al, 1999). This can be carried out at specific times and in specific tissues, allowing genes to be studied in distinct environments during different points in development. The cre-lox system works by excision and recombination of specific sites in the genome. In a cre mouse a cre transgene will be inserted into the genome in an area where it can be targeted by a chosen tissue-specific promoter. The transgene can then be activated under specific conditions such as dietary supplementation, providing temporal and tissue specific gene expression.

The cre mouse will then be bred with a loxP mouse which will have loxP sites flanking a gene of interest. LoxP sites contain spacer regions flanked by palindromic repeats, this allows both binding of loxP sites and recombination within the spacer sequence catalysed by cre recombinase. The progeny of these mice will then be able to initiate deletions, inversions or translocations conditionally around the loxP sites (Nagy, 2000).

The cre-lox system could be used to generate a mouse model knocking out *Myocd* in the urinary tract, creating an inducible functional obstruction. This would allow the effects of obstruction to be observable at different timepoints in development as well as reducing the problem of low litter numbers caused by the effects of unbalanced translocations. The problem with the generation of this model lies in finding a promoter for the cre recombinase transgene which is specific only to the smooth muscle of the urinary tract. Uroplakins are only expressed in the urinary tract but their expression is specific to the urothelium, and so would be unlikely to have an effect on smooth muscle development in the bladder. Many of the genes involved in bladder and kidney development and patterning, such as *OSR1*, *HOXB7*, *Pax3*, *Tbx18*, *Sox17* and *Sall1* are also involved in heart and gastrointestinal tract development and knockout of *Myocd* in these tissues would create a disease phenotype unrelated to obstruction.

Another area of difficulty in studying smooth muscle development in the bladder is the lack of good antibodies for *MYOCD*. A solution to this problem could be epitope tagging. This is a technique that can be used to tag either novel proteins or for which there are no commercial antibodies readily available; the target protein of interest is fused with a known protein, for example FLAG, which can then be targeted using antibodies. CRISPR-Cas9-mediated epitope tagging involves delivery to cells of a vector containing Cas9 and guide RNA (gRNA) specific to the gene of interest (in this case *MYOCD*). The homology directed repair (HDR) plasmid contains homology arms with the chosen selection marker incorporated (in this case FLAG). Once this has incorporated into the DNA the gene of interest can be targeted by FLAG specific antibodies (Brizzard, 2008).

In order for this technique to work in T30H mice, both the vector containing Cas9 and the HDR plasmid would need to be injected into a T30H zygote and then that zygote be implanted into a sham pregnant female. Both the timescale and the expense of this experiment are outside of the remit of this project, but the technique is an interesting one for future work, as it not only allows the transcription factor *MYOCD* to be stained, but the tagged proteins can be precipitated and then measured to ascertain the splice variants present in the tissue being tested.

6.4.3 Discovering the Myocardin Enhancer

The importance of specific expression of *MYOCD* splice variants to proper bladder development is not well understood. Going forward in order to better understand the role of *MYOCD* in bladder development and disease it would be advantageous to find the bladder-specific enhancer which causes the T30H phenotype when it is translocated. There are several different methods by which this could be done.

ATAC-seq is a method which can be used to identify potential areas of enhancer activity. It can be used to ascertain whether areas of the genome are transcriptionally active or not by identifying the chromatin accessibility of specific areas of the genome. Transcriptionally active areas will be loosely coiled, and transcriptionally inactive areas will be tightly coiled and inaccessible. ATAC-seq relies on using a transposase (specifically Tn5) that inserts into open areas of chromatin; this

transposase then excises open DNA. This can be purified, amplified and then sequenced to identify transcriptionally active areas (Buenrostro et al, 2013).

Once an area has been found where there is enhancer activity, enhancers can be identified through the histone methylation and acetylation states. The histones surrounding enhancer regions have a 'histone signature' which can be searched for in the genome *in silico*. Regions containing high levels of H3K4me1 and H3K27ac are likely to be putative enhancer regions. Their enhancer activity can then be verified by cloning the proposed enhancer region into the regulatory region of a reporter gene in a cell line specific to the activity of the gene of interest (Chiang et al, 2017).

6.5 Thesis Summary

In this thesis I have characterised the phenotype of the T30H mouse, a model of functional obstructive uropathy. Symptoms of obstruction are observable at embryonic day 15 of development. *In utero* using ultrasound scanning the bladder can be identified as being grossly distended and hydronephrosis can be identified in both kidneys. All other organs appear unaffected and develop normally until birth.

α SMA, calponin and MYOCD expression in the bladder are almost completely lacking. The smooth muscle wall of the bladder in T30H mice is reduced to only a few cells thick. Uroplakin 3a expression can be identified in the urothelium, implying that the barrier function of the bladder epithelium is maintained despite the huge increase in the size of the bladder.

I have also identified the specific location of the translocation causing the T30H mouse phenotype. It intersects the nonagouti gene on chromosome 2 and is downstream of *Myocd* on chromosome 11. *MYOCD* is a master regulator of smooth muscle expression through its cofactor SRF and regulates smooth muscle expression through expression of organ-specific splice isoforms. The splice variant profile of T30H mice is different to that of wild-type mice, indicating that the lack of smooth muscle development in the bladder is caused by bladder-specific changes to *Myocd* expression. This is most likely through an alteration to enhancer activity caused by the translocation, although further work must be carried out to categorically prove that *Myocd* is the gene causing the T30H phenotype.

In order to create a methodology for manipulating the expression of *Myocd* in the bladder, several *in vitro* methods were used. Dissociated primary culture of bladder smooth muscle cells was used over whole organ culture to ascertain the effects of knock-down of *Myocd* on bladder smooth muscle cells through treatment with a lentiviral vector. *Myocd* knock-down may have caused a decrease in the growth of cells in culture. This reiterates the phenotype observed in T30H mice but does not prove that changes to *Myocd* expression are responsible for the T30H phenotype.

As a direct result of research carried out during this PhD project an innovation grant from Kidney Research UK has been obtained. Using funding from this grant I will use ultrasound guided injection of adeno associated viral gene therapy to upregulate *Myocd* in T30H mouse bladder and attempt to rescue the phenotype.

References

Almeida-Porada G, Waddington SN, Chan JKY, Peranteau WH, MacKenzie T, Porada CD, 2019, In Utero Gene Therapy Consensus Statement from the IFeTIS, *Mol Ther*, 27(4):705-707

Anders C, Ashton N, Ranjzad P, Dilworth MR, Woolf AS, 2013, *Ex vivo* modeling of chemical synergy in prenatal kidney cystogenesis, *PLoS One*, 8(3):e57797

Andersson KE, McCloskey KD, 2014, Lamina propria: the functional center of the bladder? *Neurourol Urodyn*, 33(1):9-16

Anguela XM, High KA, 2019, Entering the Modern Era of Gene Therapy, *Annu Rev Med*, 70:273-288

Apodaca G, Balestreire E, Birder L A, 2007, The Uroepithelial-Associated Sensory Web, *Kidney Int*, 72(9): 1057-64

Atala A, 2020, Bladder Tissue Engineering: The Past and the Future, *Urology*, 145:337-338

Avner ED, Ellis D, Temple T, Jaffe R, 1982, Metanephric development in serum-free organ culture, *In Vitro*, 18(8):675-82

Bainbridge JW, Smith AJ, Barker SS, Robbie S, Henderson R, Balaggan K, Viswanathan A, Holder GE, Stockman A, Tyler N, Petersen-Jones S,

Bhattacharya SS, Thrasher AJ, Fitzke FW, Carter BJ, Rubin GS, Moore AT, Ali RR, 2008, Effect of gene therapy on visual function in Leber's congenital amaurosis, *N Engl J Med*, 358(21):2231-9

Bainbridge JW, Mehat MS, Sundaram V, Robbie SJ, Barker SE, Ripamonti C, Georgiadis A, Mowat FM, Beattie SG, Gardner PJ, Feathers KL, Luong VA, Yzer S, Balaggan K, Viswanathan A, de Ravel TJ, Casteels I, Holder GE, Tyler N, Fitzke FW, Weleber RG, Nardini M, Moore AT, Thompson DA, Petersen-Jones SM, Michaelides M, van den Born LI, Stockman A, Smith AJ, Rubin G, Ali RR, 2015, Long-term effect of gene therapy on Leber's congenital amaurosis, *N Engl J Med*, 372(20):1887-97

Baric I, Fumic K, Glenn B, Cuk M, Schulze A, Finkelstein JD, James SJ, Mejaski-Bosnjak V, Pazanin L, Pogribny IP, Rados M, Sarnavka V, Scukanec-Spoljar M, Allen RH, Stabler S, Uzelac L, Vugrek O, Wagner C, Zeisel S, Mudd SH, 2004, S-adenosylhomocysteine hydrolase deficiency in a human: a genetic disorder of methionine metabolism, *Proc Natl Acad Sci U S A*, 101(12):4234-9

Barić I, Cuk M, Fumić K, Vugrek O, Allen RH, Glenn B, Maradin M, Pazanin L, Pogribny I, Rados M, Sarnavka V, Schulze A, Stabler S, Wagner C, Zeisel SH, Mudd SH, 2005, S-Adenosylhomocysteine hydrolase deficiency: a second patient, the younger brother of the index patient, and outcomes during therapy, *J Inherit Metab Dis*, 28(6):885-902

Baskin LS, Howard PS, Duckett JW, Snyder HM, Macarak EJ, 1993, Bladder smooth muscle cells in culture: I. Identification and characterization, *J Urol*, 149(1):190-7

Becknell BF, Carpenter AR, Allen JL, Wilhide ME, Ingraham SE, Hains DS, McHugh KM, 2013, Molecular basis of renal adaptation in a murine model of congenital obstructive nephropathy, PLoS One, 4;8(9):e72762

Bentley DR, Balasubramanian S, Swerdlow HP, Smith GP, Milton J, Brown CG, Hall KP, Evers DJ, Barnes CL, Bignell HR, Boutell JM, Bryant J, Carter RJ, Keira Cheetham R, Cox AJ, Ellis DJ, Flatbush MR, Gormley NA, Humphray SJ, Irving LJ, Karbelashvili MS, Kirk SM, Li H, Liu X, Maisinger KS, Murray LJ, Obradovic B, Ost T, Parkinson ML, Pratt MR, Rasolonjatovo IM, Reed MT, Rigatti R, Rodighiero C, Ross MT, Sabot A, Sankar SV, Scally A, Schroth GP, Smith ME, Smith VP, Spiridou A, Torrance PE, Tzonev SS, Vermaas EH, Walter K, Wu X, Zhang L, Alam MD, Anastasi C, Aniebo IC, Bailey DM, Bancarz IR, Banerjee S, Barbour SG, Baybayan PA, Benoit VA, Benson KF, Bevis C, Black PJ, Boodhun A, Brennan JS, Bridgham JA, Brown RC, Brown AA, Buermann DH, Bundu AA, Burrows JC, Carter NP, Castillo N, Chiara E, Catenazzi M, Chang S, Neil Cooley R, Crake NR, Dada OO, Diakoumakos KD, Dominguez-Fernandez B, Earnshaw DJ, Egbujor UC, Elmore DW, Etchin SS, Ewan MR, Fedurco M, Fraser LJ, Fuentes Fajardo KV, Scott Furey W, George D, Gietzen KJ, Goddard CP, Golda GS, Granieri PA, Green DE, Gustafson DL, Hansen NF, Harnish K, Haudenschild CD, Heyer NI, Hims MM, Ho JT, Horgan AM, Hoschler K, Hurwitz S, Ivanov DV, Johnson MQ, James T, Huw Jones TA, Kang GD, Kerelska TH, Kersey AD, Khrebtukova I, Kindwall AP, Kingsbury Z, Kokko-Gonzales PI, Kumar A, Laurent MA, Lawley CT, Lee SE, Lee X, Liao AK, Loch JA, Lok M, Luo S, Mammen RM, Martin JW, McCauley PG, McNitt P, Mehta P, Moon KW, Mullens JW, Newington T, Ning Z, Ling Ng B, Novo SM, O'Neill MJ, Osborne MA, Osnowski A, Ostadan O, Paraschos LL, Pickering L, Pike AC, Pike AC, Chris Pinkard D, Pliskin DP, Podhasky J, Quijano VJ, Raczky C, Rae VH, Rawlings SR, Chiva Rodriguez A, Roe PM, Rogers J, Rogert Bacigalupo MC, Romanov N, Romieu A,

Roth RK, Rourke NJ, Ruediger ST, Rusman E, Sanches-Kuiper RM, Schenker MR, Seoane JM, Shaw RJ, Shiver MK, Short SW, Sizto NL, Sluis JP, Smith MA, Ernest Sohna J, Spence EJ, Stevens K, Sutton N, Szajkowski L, Tregidgo CL, Turcatti G, Vandevondele S, Verhovsky Y, Virk SM, Wakelin S, Walcott GC, Wang J, Worsley GJ, Yan J, Yau L, Zuerlein M, Rogers J, Mullikin JC, Hurles ME, McCooke NJ, West JS, Oaks FL, Lundberg PL, Klenerman D, Durbin R, Smith AJ, 2008, Accurate whole human genome sequencing using reversible terminator chemistry, *Nature*, 456(7218):53-9

Bilgutay AN, Roth DR, Gonzales ET Jr, Janzen N, Zhang W, Koh CJ, Gargollo P, Seth A, 2016, Posterior urethral valves: risk factors for progression to renal failure. *J Pediatr Urol*, 12(3):179.e1-7

Birder LA, Ruggieri M, Takeda M, van Koeveringe G, Veltkamp S, Korstanje C, Parsons B, Fry CH, 2012, How Does the Urothelium Affect Bladder Function in Health and Disease? *Neurourol Urodyn*, 31(3):293-9

Birder L, Andersson KE, Urothelial Signalling, 2013, *Physiol Rev* 93: 653–680

Boghossian NS, Sicko RJ, Giannakou A, Dimopoulos A, Caggana M, Tsai MY, Yeung EH, Pankratz N, Cole BR, Romitti PA, Browne ML, Fan R, Liu A, Kay DM, Mills JL, 2018, Rare copy number variants identified in prune belly syndrome, *Eur J Med Genet*, 61(3):145-151

Bouchard M, Souabni A, Mandler M, Neubüser A, Busslinger M, 2002, Nephric lineage specification by Pax2 and Pax8, *Genes Dev*, 15;16(22):2958-70

Bouhout S, Goulet F, Bolduc S, 2015, A Novel and Faster Method to Obtain a Differentiated 3-Dimensional Tissue Engineered Bladder, *J Urol*, 194(3):834-41

Brizzard B, 2008, Epitope tagging, *Biotechniques*, 44(5):693-5

Buenrostro JD, Giresi PG, Zaba LC, Chang HY, Greenleaf WJ, 2013, Transposition of native chromatin for fast and sensitive epigenomic profiling of open chromatin, DNA-binding proteins and nucleosome position, *Nature Methods*, 10:1213–1218

Burgu B, McCarthy LS, Shah V, Long DA, Wilcox DT, Woolf AS, 2006, Vascular endothelial growth factor stimulates embryonic urinary bladder development in organ culture, *BJU Int*, 98(1):217-25

Burgu B, Medina Ortiz WE, Pitera JE, Woolf AS, Wilcox DT, 2007, Vascular endothelial growth factor mediates hypoxic stimulated embryonic bladder growth in organ culture, *J Urol*, 177(4):1552-7

Cao M, Liu B, Cunha G, Baskin L, 2008, Urothelium patterns bladder smooth muscle location, *Pediatr Res*, 64(4):352-7

Carlson BM, 1999, *Human Embryology and Developmental Biology*, 2nd edition, Mosby, St Louis

Carola V, Perlas E, Zonfrillo F, Soini HA, Novotny MV, Gross CT, 2014, Modulation of social behavior by the agouti pigmentation gene, *Front Behav Neurosci*, 8:259

Carpenter AR, Becknell B, Hirselj DA, McHugh KM, 2012, Urinary diversion via cutaneous vesicostomy in the megabladder mouse, *Methods Mol Biol*, 886:393-402

Cattanach BM, 1957, Induction of translocations in mice by triethylenemelamine, *Nature*, 14;180(4598):1364-5

Cattanach BM, Kirk M, 1985, Differential activity of maternally and paternally derived chromosome regions in mice, *Nature*, 315(6019):496-8

Caubit X, Lye CM, Martin E, Coré N, Long DA, Vola C, Jenkins D, Garratt AN, Skaer H, Woolf AS, Fasano L, 2008, Teashirt 3 is necessary for ureteral smooth muscle differentiation downstream of SHH and BMP4, *Development*, 135(19):3301-10

Cavazzana M, Six E, Lagresle-Peyrou C, André-Schmutz I, Hacein-Bey-Abina S, 2016, Gene Therapy for X-Linked Severe Combined Immunodeficiency: Where Do We Stand? *Hum Gene Ther*, 27(2):108-16

Cavazzana-Calvo M, Payen E, Negre O, Wang G, Hehir K, Fusil F, Down J, Denaro M, Brady T, Westerman K, Cavallesco R, Gillet-Legrand B, Caccavelli L, Sgarra R, Maouche-Chrétien L, Bernaudin F, Girot R, Dorazio R, Mulder GJ, Polack A, Bank A, Soulier J, Larghero J, Kabbara N, Dalle B, Gourmel B, Socie G, Chrétien S, Cartier N, Aubourg P, Fischer A, Cornetta K, Galacteros F, Beuzard Y, Gluckman E, Bushman F, Hacein-Bey-Abina S, Leboulch P, 2010, Transfusion independence and HMGA2 activation after gene therapy of human β -thalassaemia, *Nature*, 467(7313):318-22 Chang DF, Belaguli NS, Iyer D, Roberts

WB, Wu SP, Dong XR, Marx JG, Moore MS, Beckerle MC, Majesky MW, Schwartz RJ, 2003, Cysteine-rich LIM-only proteins CRP1 and CRP2 are potent smooth muscle differentiation cofactors, *Dev Cell*, 4(1):107-18

Chauhan DP, Srivastava AS, Moustafa ME, Shenouda S, Carrier E, 2004, In utero gene therapy: prospect and future, *Curr Pharm Des*, 10(29):3663-72

Chen J, Kitchen CM, Streb JW, Miano JM, 2002, Myocardin: a component of a molecular switch for smooth muscle differentiation, *J Mol Cell Cardiol*, 34(10):1345-56

Chen W, Kalscheuer V, Tzschach A, Menzel C, Ullmann R, Schulz MH, Erdogan F, Li N, Kijas Z, Arkesteijn G, Pajares IL, Goetz-Sothmann M, Heinrich U, Rost I, Dufke A, Grasshoff U, Glaeser B, Vingron M, Ropers HH, 2008, Mapping translocation breakpoints by next-generation sequencing, *Genome Res*, 18(7):1143-9

Chiang C, Litingtung Y, Lee E, Young KE, Corden JL, Westphal H, Beachy PA, 1996, Cyclopia and defective axial patterning in mice lacking Sonic hedgehog gene function. *Nature* 383:407–413

Chiang IK, Fritzsche M, Pichol-Thievend C, Neal A, Holmes K, Lagendijk A, Overman J, D'Angelo D, Omini A, Hermkens D, Lesieur E, Liu K, Ratnayaka I, Corada M, Bou-Gharios G, Carroll J, Dejana E, Schulte-Merker S, Hogan B, Beltrame M, De Val S, Francois M, 2017, SoxF factors induce Notch1 expression via direct transcriptional regulation during early arterial development, *Development*, 144(14):2629-2639

Chiaromonte C, Bommarito D, Zambaiti E, Antona V, Li Voti G, 2015, Genetic Basis of Posterior Urethral Valves Inheritance, *Urology*, 95:175-9

Churchill BM, Gilmour RF, Williot P, 1987, Urodynamics, *Pediatr Clin North Am*, 34(5):1133-57

Clark TJ, Martin WL, Divakaran TG, Whittle MJ, Kilby MD, Khan KS, 2003, Prenatal bladder drainage in the management of fetal lower urinary tract obstruction: a systematic review and meta-analysis. *Obstet Gynecol*, 102:367e82

Clothier JC, Wright AJ, 2018, Dysfunctional voiding: the importance of non-invasive urodynamics in diagnosis and treatment, *Pediatr Nephrol*, 33(3):381-394

Collins VM, Daly DM, Liaskos M, McKay NG, Sellers D, Chapple C, Grundy D, 2013, OnabotulinumtoxinA significantly attenuates bladder afferent nerve firing and inhibits ATP release from the urothelium, *BJU Int*, 112(7):1018-26

Costamagna D, Mommaerts H, Sampaolesi M, Tylzanowski P, 2016, Noggin inactivation affects the number and differentiation potential of muscle progenitor cells *in vivo*, *Sci Rep*, 30;6:31949

Coutelle C, Douar AM, Colledge WH, Froster U, 1995, The challenge of fetal gene therapy, *Nat Med*, 1(9):864-6

Creemers EE, Sutherland LB, Oh J, Barbosa AC, Olson EN, 2006, Coactivation of MEF2 by the SAP domain proteins myocardin and MASTR. *Mol Cell*, 23: 83.

Cross WR, Eardley I, Leese HJ, Southgate J, 2005, A biomimetic tissue from cultured normal human urothelial cells: analysis of physiological function, *Am J Physiol Renal Physiol*, 289(2):F459-68

Crystal RG, 2014, Adenovirus: the first effective in vivo gene delivery vector, *Hum Gene Ther*, 25(1):3-11

Danesh SM, Villasenor A, Chong D, Soukup C, Cleaver O, 2009, BMP and BMP receptor expression during murine organogenesis, *Gene Expr Patterns*, 9(5):255-65.

Davies JA, 2018, Adaptive self-organization in the embryo: its importance to adult anatomy and to tissue engineering, *J Anat.* 2018, 232(4):524-533

De Jonge BW, Wolffenbuttel KP, Scheepe JR, Kok DJ, 2008, The detrusor glycogen content of a de-obstructed bladder reflects the functional history of that bladder during PBOO, *Neurourol Urodyn*, 27(5):454-60

De Sasso JM, 1995, Anatomical relationships of urinary bladders compared: Their potential role in the development of bladder tumours in humans and rats, *Food Chem Toxicol*, 33(9):705-14

Deng M, Mohanan S, Polyak E, Chacko S, 2007, Caldesmon is necessary for maintaining the actin and intermediate filaments in cultured bladder smooth muscle cells. *Cell Motil. Cytoskeleton* 64, 951–965

DeSouza KR, Saha M, Carpenter AR, Scott M, McHugh KM, 2013, Analysis of the Sonic Hedgehog signaling pathway in normal and abnormal bladder development, *PLoS One*, 8(1):e53675

DiSandro MJ, Li Y, Baskin LS, Hayward S, Cunha G, 1998, Mesenchymal-epithelial interactions in bladder smooth muscle development: epithelial specificity, *J Urol*, 160(3 Pt 2):1040-6

Du KL, Ip HS, Li J, Chen M, Dandre F, Yu W, Lu MM, Owens GK, Parmacek MS, 2003, Myocardin is a critical serum response factor cofactor in the transcriptional program regulating smooth muscle cell differentiation, *Mol Cell Biol*, 23(7):2425-37

Duchon A, Raveau M, Chevalier C, Nalesso V, Sharp AJ, Herault Y, 2011, Identification of the translocation breakpoints in the Ts65Dn and Ts1Cje mouse lines: relevance for modeling down syndrome, *Mamm Genome*, 22(11-12): 674–684

Durnin L, Hayoz S, Corrigan RD, Yanez A, Koh SD, Mutafova-Yambolieva VN, 2016, Urothelial purine release during filling of murine and primate bladders, *Am J Physiol Renal Physiol*, 1;311(4):F708-F716

Michael J Eblan 1, Ozlem Goker-Alpan, Ellen Sidransky, 2005, Perinatal lethal Gaucher disease: a distinct phenotype along the neuronopathic continuum, *Fetal Pediatr Pathol*, 24(4-5):205-22

Eckoldt F1, Heling KS, Woderich R, Wolke S, 2004, Posterior urethral valves: prenatal diagnostic signs and outcome, *Urol Int*, 73(4):296-301.

Ericson J, Muhr J, Jessell TM, Edlund T, 1995, Sonic hedgehog: a common signal for ventral patterning along the rostrocaudal axis of the neural tube. *Int J Dev Biol* 39:809 – 816

Estrada CR, Salanga M, Bielenberg DR, Harrell WB, Zurakowski D, Zhu X, Palmer MR, Freeman MR, Adam RM, 2006, Behavioral profiling of human transitional cell carcinoma ex vivo, *Cancer Res*, 66(6):3078-8

Farrugia MK, Long DA, Godley ML, Peebles DM, Fry CH, Cuckow PM, Woolf AS, 2006, Experimental short-term fetal bladder outflow obstruction: I. Morphology and cell biology associated with urinary flow impairment, *J Pediatr Urol*, 2(4):243-53

Flake AW, Roncarolo MG, Puck JM, Almeida-Porada G, Evans MI, Johnson MP, Abella EM, Harrison DD, Zanjani ED, 1996, Treatment of X-linked severe combined immunodeficiency by in utero transplantation of paternal bone marrow, *N Engl J Med*, 335(24):1806-10

Fontanesi L, Forestier L, Allain D, Scotti E, Beretti F, Deretz-Picoulet S, Pecchioli E, Vernesi C, Robinson TJ, Malaney JL, Russo V, Oulmouden A, 2010,

Characterization of the rabbit agouti signaling protein (ASIP) gene: transcripts and phylogenetic analyses and identification of the causative mutation of the nonagouti black coat colour, *Genomics*, 95(3):166-75

Freedman, A. L., Johnson, M. P., Smith, C. A, 1999 Long-term outcome in children after antenatal intervention for obstructive uropathies. *Lancet*, 354: 374

Fry CH, Skennerton D, Wood D, Wu C, 2002, The cellular basis of contraction in human detrusor smooth muscle from patients with stable and unstable bladders, *Urology*, 59(5 Suppl 1):3-12

Fry CH, 2004, Experimental models to study the physiology, pathophysiology, and pharmacology of the lower urinary tract, *J Pharmacol Toxicol Methods*, 49(3):201-10

Gevaert T, Neuhaus J, Vanstreels E, Daelemans D, Everaerts W, Der Aa FV, Timmermans JP, Roskams T, Steiner C, Pintelon I, De Ridder D, 2017, Comparative study of the organisation and phenotypes of bladder interstitial cells in human, mouse and rat, *Cell Tissue Res*, 370(3):403-416

Georgas KM, Armstrong J, Keast JR, Larkins CE, McHugh KM, Southard-Smith EM, Cohn MJ, Batourina E, Dan H, Schneider K, Buehler DP, Wiese CB, Brennan J, Davies JA, Harding SD, Baldock RA, Little MH, Vezina CM, Mendelsohn C, 2015, An illustrated anatomical ontology of the developing mouse lower urogenital tract, *Development*, 15;142(10):1893-908

Glick PL, Harrison MR, Noall RA, Villa RL, 1983, Correction of congenital hydronephrosis *in utero* III. Early mid-trimester ureteral obstruction produces renal dysplasia, *J Pediatr Surg*, 18(6):681-7

González R, De Filippo R, Jednak R, Barthold JS, 2001, Urethral atresia: long-term outcome in 6 children who survived the neonatal period, *J Urol*, 165(6 Pt 2):2241-4

Gosling JA, Dixon JS, 1974, Sensory nerves in the mammalian urinary tract. An evaluation using light and electron microscopy, *J Anat*, 117(Pt 1): 133–144

Granberg CF, Harrison SM, Dajusta D, Zhang S, Hajarnis S, Igarashi P, Baker LA, 2012, Genetic basis of prune belly syndrome: screening for HNF1 β gene, *J Urol*, 187(1):272-8

Grbeša I, Kalo A, Belužić R, Kovačević L, Lepur A, Rokić F, Hochberg H, Kanter I, Simunović V, Muñoz-Torres PM, Shav-Tal Y, Vugrek O, 2017, Mutations in S-adenosylhomocysteine hydrolase (AHCY) affect its nucleocytoplasmic distribution and capability to interact with S-adenosylhomocysteine hydrolase-like 1 protein, *Eur J Cell Biol*, 96(6):579-590

Haeusgen W, Tueffers L, Herdegen T, Waetzig V, 2014, Map2k4 δ - identification and functional characterization of a novel Map2k4 splice variant, *Biochim Biophys Acta*, 1843(5):875-84

Haraguchi R, Motoyama J, Sasaki H, Satoh Y, Miyagawa S, Nakagata N, Moon A, Yamada G, 2007, Molecular analysis of coordinated bladder and urogenital organ formation by Hedgehog signalling, *Development*, 134(3):525-33

Harrison MR, Nakayama DK, Noall R, de Lorimier AA, 1982, Correction of congenital hydronephrosis *in utero* II. Decompression reverses the effects of obstruction on the fetal lung and urinary tract, *J Pediatr Surg*, 17(6):965-74

Harrison MR, Ross N, Noall R, de Lorimier AA, 1983, Correction of congenital hydronephrosis *in utero*. I. The model: fetal urethral obstruction produces hydronephrosis and pulmonary hypoplasia in fetal lambs, *J Pediatr Surg*, 18(3):247-56

Hashemi Gheinani A, Burkhard FC, Rehauer H, Aquino Fournier C, Monastyrskaya K, 2015, MicroRNA MiR-199a-5p regulates smooth muscle cell proliferation and morphology by targeting WNT2 signaling pathway, *J Biol Chem*, 290(11):7067-86

Hicks RM, 1975, The mammalian urinary bladder: an accommodating organ, *Biol Rev Camb Philos Soc*, 50(2):215-46

Hill WG, Zeidel ML, Bjorling DE, Vezina CM, 2018, Void spot assay: recommendations on the use of a simple micturition assay for mice, *Am J Physiol Renal Physiol*, 315(5):F1422-F1429

Hirose M, Hasegawa A, Mochida K, Matoba S, Hatanaka Y, Inoue K, Goto T, Kaneda H, Yamada I, Furuse T, Abe K, Uenoyama Y, Tsukamura H, Wakana S,

Honda A, Ogura A, 2017, CRISPR/Cas9-mediated genome editing in wild-derived mice: generation of tamed wild-derived strains by mutation of the a (nonagouti) gene, *Sci Rep*, 7:42476

Holmdahl G, Hanson E, Hanson M, 1998, Four-hour voiding observation in young boys with posterior urethral valves. *J Urol* 160: 1477–1481.

Holmes N, Harrison MR, Baskin LS, 2001, Fetal surgery for posterior urethral valves: Long-term postnatal outcomes. *Pediatrics* 108: 1–7.

Hoofnagle MH, Nepl RL, Berzin EL, Teg Pipes GC, Olson EN, Wamhoff BW, Somlyo AV, Owens GK, 2011, Myocardin is differentially required for the development of smooth muscle cells and cardiomyocytes, *Am J Physiol Heart Circ Physiol*, 300(5):H1707-21

Horsley H, Dharmasena D, Malone-Lee J, Rohn JL, 2018, A urine-dependent human urothelial organoid offers a potential alternative to rodent models of infection, *Sci Rep*, 8(1):1238

Hossler FE, Lametschwandtner A, Kao R, Finsterbusch F, 2013, Microvascular architecture of mouse urinary bladder described with vascular corrosion casting, light microscopy, SEM, and TEM, *Microsc Microanal*, 19(6):1428-35

Houweling AC, Beaman GM, Postma AV, Gainous TB, Lichtenbelt KD, Brancati F, Lopes FM, van der Made I, Polstra AM, Robinson ML, Wright KD, Ellingford JM, Jackson AR, Overwater E, Genesio R, Romano S, Camerota L, D'Angelo E, Meijers-Heijboer EJ, Christoffels VM, McHugh KM, Black BL, Newman WG,

Woolf AS, Creemers EE, 2019, Loss-of-function variants in myocardin cause congenital megabladder in humans and mice, *J Clin Invest*, pii: 128545

Howden SE, Vanslambrouck JM, Wilson SB, Tan KS, Little MH, 2019, Reporter-based fate mapping in human kidney organoids confirms nephron lineage relationships and reveals synchronous nephron formation, *EMBO Rep*, pii: e47483

Hu Z, Tee WW, 2017, Enhancers and chromatin structures: regulatory hubs in gene expression and diseases, *Biosci Rep*, 37(2), pii: BSR20160183

Huang J, Cheng L, Li J, Chen M, Zhou D, Lu MM, Proweller A, Epstein JA, Parmacek MS, 2008, Myocardin regulates expression of contractile genes in smooth muscle cells and is required for closure of the ductus arteriosus in mice, *J Clin Invest*, 118(2):515-25

Huang J, Wang T, Wright AC, Yang J, Zhou S, Li L, Yang J, Small A, Parmacek MS, 2015, Myocardin is required for maintenance of vascular and visceral smooth muscle homeostasis during postnatal development, *Proc Natl Acad Sci U S A*, 112(14):4447-52

Iguchi N, Malykhina AP, Wilcox DT, 2016, Inhibition of HIF Reduces Bladder Hypertrophy and Improves Bladder Function in Murine Model of Partial Bladder Outlet Obstruction, *J Urol*, 195(4 Pt 2):1250-6

Ikeda Y, Zabbarova I, Schaefer CM, Bushnell D, De Groat WC, Kanai A, Bates CM, 2017, Fgfr2 is integral for bladder mesenchyme patterning and function, *Am J Physiol Renal Physiol*, 1; 312(4): F607–F618

Ilagan RM, Genheimer CW, Quinlan SF, Guthrie KI, Sangha N, Ramachandrannair S, Kelley RW, Presnell SC, Basu J, Ludlow JW, 2011, Smooth muscle phenotypic diversity is mediated through alterations in myocardin gene splicing, *J Cell Physiol*, 226(10):2702-11

Imamura M, Long X, Nanda V, Miano JM, 2010, Expression and functional activity of four myocardin isoforms, *Gene*, 464(1-2):1-10

Imamura M, Sugino Y, Long X, Slivano OJ, Nishikawa N, Yoshimura N, Miano JM, 2013, Myocardin and microRNA-1 modulate bladder activity through connexin 43 expression during post-natal development, *J Cell Physiol*, 228(9):1819-26

Ingraham SE, Saha M, Carpenter AR, Robinson M, Ismail I, Singh S, Hains D, Robinson ML, Hirselj DA, Koff SA, Bates CM, McHugh KM, 2010, Pathogenesis of renal injury in the megabladder mouse: a genetic model of congenital obstructive nephropathy, *Pediatr Res*, 68(6):500-7

Jackson AR, Li B, Cohen SH, Ching CB, McHugh KM, Becknell B, 2018, The uroplakin plaque promotes renal structural integrity during congenital and acquired urinary tract obstruction, *Am J Physiol Renal Physiol*, 315(4):F1019-F1031

Kanematsu A, Ramachandran A, Adam RM, 2007, GATA-6 mediates human bladder smooth muscle differentiation: involvement of a novel enhancer element in regulating alpha-smooth muscle actin gene expression, *Am J Physiol Cell Physiol*, 293(3):C1093-102

Karda R, Buckley SM, Mattar CN, Ng J, Massaro G, Hughes MP, Kurian MA, Baruteau J, Gissen P, Chan JK, Bacchelli C, Waddington SN, Rahim AA, 2014, Perinatal systemic gene delivery using adeno-associated viral vectors, *Front Mol Neurosci*, 7:89

Kasai F, Pereira JC, Kohara A, Ferguson-Smith MA, 2018, Homologue-specific chromosome sequencing characterizes translocation junctions and permits allelic assignment, *DNA Res*, 1;25(4):353-360

Kattenhorn LM, Tipper CH, Stoica L, Geraghty DS, Wright TL, Clark KR, Wadsworth SC, 2016, Adeno-Associated Virus Gene Therapy for Liver Disease, *Hum Gene Ther*, 27(12):947-961

Kaufmann KB, Büning H, Galy A, Schambach A, Grez M, 2013, Gene therapy on the move, *EMBO Mol Med*, 5(11):1642-61

Kawahigashi H, Harada Y, Asano A, Nakamura M, 1998, A cis-acting regulatory element that affects the alternative splicing of a muscle-specific exon in the mouse NCAM gene, *Biochim Biophys Acta*, 1397(3):305-15

Khandelwal P, Abraham SN, Apodaca G, 2009, Cell biology and physiology of the uroepithelium, *Am J Physiol Renal Physiol*, 297(6): F1477–F1501

Kimura Y, Morita T, Hayashi K, Miki T, Sobue K, 2010, Myocardin functions as an effective inducer of growth arrest and differentiation in human uterine leiomyosarcoma cells, *Cancer Res* 70:501–511

Kioussis D, Vanin E, deLange T, Flavell RA, Grosveld FG, 1983, Beta-globin gene inactivation by DNA translocation in gamma beta-thalassaemia, *Nature*, 306(5944):662-6

Kitta T, Kanno Y, Chiba H, Higuchi M, Ouchi M, Togo M, Moriya K, Shinohara N, 2018, Benefits and limitations of animal models in partial bladder outlet obstruction for translational research, *Int J Urol*, 25(1):36-44

Klebig ML, Wilkinson JE, Geisler JG, Woychik RP, 1995, Ectopic expression of the agouti gene in transgenic mice causes obesity, features of type II diabetes, and yellow fur, *Proc Natl Acad Sci U S A*, 92(11):4728-32

Kleinjan DA, Lettice LA, 2008, Long-range gene control and genetic disease, *Adv Genet*, 61:339-88

Knowles MA, Hicks RM, Berry RJ, Milroy E, 1980, Organ Culture of Normal Human Bladder: Choice of Starting Material and Culture Characteristics, Chapter 12, *Methods in Cell Biology*, 21B: 257-285

Krishnan, A. de Souza, R. Konijeti, L.S. Baskin, 2006, The anatomy and embryology of posterior urethral valves, *J Urol*, 175:.1214-1220

Kumar SV, Er PX, Lawlor KT, Motazedian A, Scurr M, Ghobrial I, Combes AN, Zappia L, Oshlack A, Stanley EG, Little MH, 2019, Kidney micro-organoids in suspension culture as a scalable source of human pluripotent stem cell-derived kidney cells, *Development*, 146(5)

Kusakabe Y, Ishihara M, Umeda T, Kuroda D, Nakanishi M, Kitade Y, Gouda H, Nakamura KT, Tanaka N, 2015, Structural insights into the reaction mechanism of S-adenosyl-L-homocysteine hydrolase, *Sci Rep*, 5:16641

Lam P, Khan G, Stripecke R, Hui KM, Kasahara N, Peng KW, Guinn BA, 2013, The innovative evolution of cancer gene and cellular therapies, *Cancer Gene Ther*, 20(3):141-9

Lee G, Uroplakins in the lower urinary tract, 2011, *Int Neurourol J*, 15(1):4-12

Lee SH, Hu W, Matulay JT, Silva MV, Owczarek TB, Kim K, Chua CW, Barlow LJ, Kandoth C, Williams AB, Bergren SK, Pietzak EJ, Anderson CB, Benson MC, Coleman JA, Taylor BS, Abate-Shen C, McKiernan JM, Al-Ahmadie H, Solit DB, Shen MM, 2018, Tumor Evolution and Drug Response in Patient-Derived Organoid Models of Bladder Cancer, *Cell*, 173(2):515-528.e17

Li J, Shiroyanagi Y, Lin G, Haqq C, Lin CS, Lue TF, Willingham E, Baskin LS, 2005, Serum response factor, its cofactors, and epithelial-mesenchymal signaling in urinary bladder smooth muscle formation, *Differentiation*, 74(1):30-9

Li M, Li S, Rao Y, Cui S, Gou K, 2018, Loss of smooth muscle myosin heavy chain results in the bladder and stomach developing lesion during foetal development in mice, *J Genet*, 97(2):469-475

Li S, Wang DZ, Wang Z, Richardson JA, Olson EN, 2003, The serum response factor coactivator myocardin is required for vascular smooth muscle development, *Proc Natl Acad Sci U S A*, 100(16):9366-70

Liang D, Wang Y, Ji X, Hu H, Zhang J, Meng L, Lin Y, Ma D, Jiang T, Jiang H, Asan, Song L, Guo J, Hu P, Xu Z, 2017, Clinical application of whole-genome low-coverage next-generation sequencing to detect and characterize balanced chromosomal translocations, *Clin Genet*, 91(4):605-610

Liang FX, Riedel I, Deng FM, Zhou G, Xu C, Wu XR, Kong XP, Moll R, Sun TT, 2001, Organization of uroplakin subunits: transmembrane topology, pair formation and plaque composition, *Biochem J*, 355(Pt 1):13-8

Liaw A, Cunha GR, Shen J, Cao M, Liu G, Sinclair A, Baskin L, 2018, Development of the human bladder and ureterovesical junction, *Differentiation*, 103:66-73

Liyanaige M, Coleman A, du Manoir S, Veldman T, McCormack S, Dickson RB, Barlow C, Wynshaw-Boris A, Janz S, Wienberg J, Ferguson-Smith MA, Schröck E, Ried T, 1996, Multicolour spectral karyotyping of mouse chromosomes, *Nat Genet*, 14(3):312-5

Longley JB, Fisher ER, 1954, Alkaline phosphatase and the periodic acid Schiff reaction in the proximal tubule of the vertebrate kidney; a study in segmental

differentiation, *Anat Rec*, 120(1):1-21
Loots GG, Kneissel M, Keller H, Baptist M, Chang J, Collette NM, Ovcharenko D, Plajzer-Frick I, Rubin EM, 2005, Genomic deletion of a long-range bone enhancer misregulates sclerostin in Van Buchem disease, *Genome Res*, 15(7):928-35

Lopes FM, Woolf AS, 2019, Serum-Free Organ Culture of the Embryonic Mouse Ureter, *Methods Mol Biol*, 1926:31-38

Lyu Q, Dhagia V, Han Y, Guo B, Wines-Samuels ME, Christie CK, Yin Q, Slivano OJ, Herring P, Long X, Gupte SA, Miano J, 2018, CRISPR-Cas9-Mediated Epitope Tagging Provides Accurate and Versatile Assessment of Myocardin-Brief Report, *Arterioscler Thromb Vasc Biol*, 38(9):2184-2190

Malysz J, Afeli SA, Provence A, Petkov GV, 2014, Ethanol-mediated relaxation of guinea pig urinary bladder smooth muscle: involvement of BK and L-type Ca²⁺ channels, *Am J Physiol Cell Physiol*, 306(1):C45-58

Massaro G, Mattar CNZ, Wong AMS, Sirka E, Buckley SMK, Herbert BR, Karlsson S, Perocheau DP, Burke D, Heales S, Richard-Londt A, Brandner S, Huebecker M, Priestman DA, Platt FM, Mills K, Biswas A, Cooper JD, Chan JKY, Cheng SH, Waddington SN, Rahim AA, 2018, Fetal gene therapy for neurodegenerative disease of infants, *Nat Med*, 24(9):1317-1323

Matkar PN, Leong-Poi H, Singh KK, 2016, Cardiac gene therapy: are we there yet? *Gene Ther*, 23(8-9):635-48

Mattar CN, Wong AM, Hoefer K, Alonso-Ferrero ME, Buckley SM, Howe SJ, Cooper JD, Waddington SN, Chan JK, Rahim AA, 2015, Systemic gene delivery following intravenous administration of AAV9 to fetal and neonatal mice and late-gestation nonhuman primates, *FASEB J*, 29(9):3876-88

Matuszewski MA, Tupikowski K, Dołowy Ł, Szymańska B, Dembowski J, Zdrojowy R, 2016, Uroplakins and their potential applications in urology, *Cent European J Urol*, 69(3):252-257

McHugh KM, 2014, Megabladder mouse model of congenital obstructive nephropathy: genetic etiology and renal adaptation, *Pediatr Nephrol*, 29(4):645-50

McLorie G, Farhat W, Khouri A, Geary D, Ryan G, 2001, Outcome analysis of vesicoamniotic shunting in a comprehensive population. *J Urol*, 166: 1036–1040

Mendell JR, Al-Zaidy S, Shell R, Arnold WD, Rodino-Klapac LR, Prior TW, Lowes L, Alfano L, Berry K, Church K, Kissel JT, Nagendran S, L'Italien J, Sproule DM, Wells C, Cardenas JA, Heitzer MD, Kaspar A, Corcoran S, Braun L, Likhite S, Miranda C, Meyer K, Foust KD, Burghes AHM, Kaspar BK, 2017, Single-Dose Gene-Replacement Therapy for Spinal Muscular Atrophy, *N Engl J Med*, 377(18):1713-1722

Miano JM, Cserjesi P, Ligon KL, Periasamy M, Olson EN, 1994, Smooth muscle myosin heavy chain exclusively marks the smooth muscle lineage during mouse embryogenesis. *Circ. Res.* 75, 803–812

Michel MC, 2016, Cellular basis of detrusor smooth muscle contraction, *BJU Int*, 117(1):177-8

Michishita M, Tomita K, Yano K, Kasahara K, 2015, Mast Cell Accumulation and Degranulation in Rat Bladder with Partial Outlet Obstruction, *Adv Ther*, 32 Suppl 1:16-28

Miller MW, Duhl DM, Winkes BM, Arredondo-Vega F, Saxon PJ, Wolff GL, Epstein CJ, Hershfield MS, Barsh GS, 1994, The mouse lethal nonagouti (a(x)) mutation deletes the S-adenosylhomocysteine hydrolase (AHCY) gene, *EMBO J*, 13(8):1806-16

Milne I, Stephen G, Bayer M, Cock PJA, Pritchard L, Cardle L, Shaw PD and Marshall D. 2013. Using Tablet for visual exploration of second-generation sequencing data. *Briefings in Bioinformatics* 14(2), 193-202

Miyahara J, Yamamoto M, Motoshige K, Fujita N, Ohki S, 2016, Survival of a very low-birthweight infant with Potter sequence on long-term hemodialysis, *Pediatr Int*, 58(7):604-6

Morales AV, Espeso-Gil S, Ocaña I, Nieto-Lopez F, Calleja E, Bovolenta P, Lewandoski M, Diez Del Corral R, 2016, FGF signaling enhances a sonic hedgehog negative feedback loop at the initiation of spinal cord ventral patterning, *Dev Neurobiol*, 76(9):956-71

Morin SJ, Eccles J, Iturriaga A, Zimmerman RS, 2017, Translocations, inversions and other chromosome rearrangements, *Fertil Steril*, 107(1):19-26

Morrissey EE, Ip HS, Lu MM, Parmacek MS, 1996, GATA-6: a zinc finger transcription factor that is expressed in multiple cell lineages derived from lateral mesoderm, *Dev Biol*, 10;177(1):309-22

Moussa NM, Claycombe KJ, 1999, The yellow mouse obesity syndrome and mechanisms of agouti-induced obesity, *Obes Res*, 7(5):506-14

Mullenders J, de Jongh E, Brousalı A, Roosen M, Blom JPA, Begthel H, Korving J, Jonges T, Kranenburg O, Meijer R, Clevers HC, 2019, Mouse and human urothelial cancer organoids: A tool for bladder cancer research, *Proc Natl Acad Sci U S A*, 116(10):4567-4574.

Nagy A, 2000, Cre recombinase: the universal reagent for genome tailoring, *Genesis*, 26(2):99-109

Najrana T, Ramos LM, Abu Eid R, Sanchez-Esteban J, 2017, Oligohydramnios compromises lung cells size and interferes with epithelial-endothelial development, *Pediatr Pulmonol*, 52(6):746-756

Nakahata S, Kawamoto S, 2005, Tissue-dependent isoforms of mammalian Fox-1 homologs are associated with tissue-specific splicing activities, *Nucleic Acids Res*, 33(7):2078-89

Naso MF, Tomkowicz B, Perry WL 3rd, Strohl WR, 2017, Adeno-Associated Virus (AAV) as a Vector for Gene Therapy, *BioDrugs*, 31(4):317-334

Newman J, Antonakopoulos GN, 1989, The fine structure of the human fetal urinary bladder. Development and maturation. A light, transmission and scanning electron microscopic study, *J Anat*, 166: 135–150

Nicolaou N, Renkema KY, Bongers EM, Giles RH, Knoers NV, 2015, Genetic, environmental, and epigenetic factors involved in CAKUT, *Nat Rev Nephrol*, 11(12):720-31

Nimmakayalu MA, Gotter AL, Shaikh TH, Emanuel BS, 2003, A novel sequence-based approach to localize translocation breakpoints identifies the molecular basis of a t(4;22), *Hum Mol Genet*, 12(21):2817-25

Nishinakamura R, 2019, Human kidney organoids: progress and remaining challenges, *Nat Rev Nephrol*, 15(10):613-624

Nyirady P, Thiruchelvam N, Fry CH, Godley ML, Winyard PJ, Peebles DM, Woolf AS, Cuckow PM, 2002, Effects of in utero bladder outflow obstruction on fetal sheep detrusor contractility, compliance and innervation, *J Urol*, 168(4 Pt 1):1615-20

Obenauf AC, Schwarzbraun T, Auer M, Hoffmann EM, Waldispuehl-Geigl J, Ulz P, Günther B, Duba HC, Speicher MR, Geigl JB, 2010, Mapping of balanced chromosome translocation breakpoints to the basepair level from microdissected chromosomes, *J Cell Mol Med*, 14(8):2078-84

Owens GK, Kumar MS, Wamhoff BR, 2004, Molecular regulation of vascular smooth muscle cell differentiation in development and disease, *Physiol Rev*, 84(3):767-801

Oxburgh L, Carroll TJ, Cleaver O, Gossett DR, Hoshizaki DK, Hubbell JA, Humphreys BD, Jain S, Jensen J, Kaplan DL, Kesselman C, Ketchum CJ, Little MH, McMahon AP, Shankland SJ, Spence JR, Valerius MT, Wertheim JA, Wessely O, Zheng Y, Drummond IA, 2017, (Re)Building a Kidney, *J Am Soc Nephrol*, 28(5):1370-1378

Paner GP, Ro JY, Wojcik EM, Venkataraman G, Datta MW, Amin MB, 2007, Further characterization of the muscle layers and lamina propria of the urinary bladder by systematic histologic mapping: implications for pathologic staging of invasive urothelial carcinoma, *Am J Surg Pathol*, 31(9):1420-9

Pearson EG, Flake AW, 2013, Stem cell and genetic therapies for the fetus, *Semin Pediatr Surg*, 22(1):56-61

Pellestor F, Imbert I, Andréo B, Lefort G, 2001, Study of the occurrence of interchromosomal effect in spermatozoa of chromosomal rearrangement carriers by fluorescence in-situ hybridization and primed in-situ labelling techniques, *Hum Reprod*, 16(6):1155-64

Perlman RL, 2016, Mouse models of human disease: An evolutionary perspective, *Evol Med Public Health*, 2016(1):170-6

Pfeifer A, Kessler T, Yang M, Baranov E, Kootstra N, Cheresh DA, Hoffman RM, Verma IM, 2001, Transduction of liver cells by lentiviral vectors: analysis in living animals by fluorescence imaging, *Mol Ther*, 3(3):319-22

Price KL, Woolf AS, Long DA, 2009, Unraveling the genetic landscape of bladder development in mice, *J Urol*, 181(5):2366-74

Rabie N, Magann E, Steelman S, Ounpraseuth S, 2017, Oligohydramnios in complicated and uncomplicated pregnancy: a systematic review and meta-analysis, *Ultrasound Obstet Gynecol*, 49(4):442-449

Rasouly HM, Lu W, 2013, Lower urinary tract development and disease, *Wiley Interdiscip Rev Syst Biol Med*, 5(3):307-42

Reay DP, Bilbao R, Koppanati BM, Cai L, O'Day TL, Jiang Z, Zheng H, Watchko JF, Clemens PR, 2008, Full-length dystrophin gene transfer to the mdx mouse in utero, *Gene Ther*, 15(7):531-6

Rittenberg MH, Hulbert WC, Snyder HM 3rd, Duckett JW, 1988, Protective factors in posterior urethral valves, *J Urol*, 140(5):993-6

Roukos V, Misteli T, 2014, The biogenesis of chromosome translocations, *Nat Cell Biol*, 16(4):293-300

Row S, Liu Y, Alimperti S, Agarwal SK, Andreadis ST, 2016, Cadherin-11 is a novel regulator of extracellular matrix synthesis and tissue mechanics, *J Cell Sci*, 1;129(15):2950-61

Saha M, Ingraham SE, Carpenter A, Robinson M, McHugh KE, Singh S, Robinson ML, McHugh KM, 2009, Identification of distinct myocardin splice variants in the bladder, *J Urol*, 182(2):766-75

Samal SK, Rathod S, 2015, Prune Belly syndrome: A rare case report, *J Nat Sci Biol Med*, 6(1):255-7

Schäfer FM, Algarrahi K, Savarino A, Yang X, Seager C, Franck D, Costa K, Liu S, Logvinenko T, Adam R, Mauney JR, 2017, Mode of Surgical Injury Influences the Source of Urothelial Progenitors during Bladder Defect Repair, *Stem Cell Reports*, 12;9(6):2005-2017

Schaffner W, 2015, Enhancers, enhancers - from their discovery to today's universe of transcription enhancers, *Biol Chem*, 396(4):311-27

Seidel NE, Arlen AM, Smith EA, Kirsch AJ, 2015, Clinical manifestations and management of prune-belly syndrome in a large contemporary pediatric population, *Urology*, 85(1):211-5

Shalini S, Dorstyn L, Dawar S, Kumar S, 2015, Old, new and emerging functions of caspases, *Cell Death Differ*, 22(4):526-39

Shapiro E, Huang, HY, Wu, XR, 2000, Uroplakin and androgen receptor expression in the human fetal genital tract: insights into the development of the vagina. *J. Urol.* 164, 1048-1051

Sharif W, Sharif Z, 2017, Leber's congenital amaurosis and the role of gene therapy in congenital retinal disorders, *Int J Ophthalmol*, 10(3):480-484

Shiroyanagi Y, Liu B, Cao M, Agras K, Li J, Hsieh MH, Willingham EJ, Baskin LS, 2007, Urothelial sonic hedgehog signalling plays an important role in bladder smooth muscle formation, *Differentiation*, 75(10):968-77

Singh P, Li D, Gui Y, Zheng XL, 2017, Atrogin-1 Increases Smooth Muscle Contractility Through Myocardin Degradation, *J Cell Physiol*, 232(4):806-817

Singh S, Robinson M, Nahi F, Coley B, Robinson ML, Bates CM, Kornacker K, McHugh KM, 2007, Identification of a unique transgenic mouse line that develops megabladder, obstructive uropathy, and renal dysfunction, *J Am Soc Nephrol*, 18(2):461-71

Singh S, Robinson M, Ismail I, Saha M, Auer H, Kornacker K, Robinson ML, Bates CM, McHugh KM, 2008, Transcriptional profiling of the megabladder mouse: a unique model of bladder dysmorphogenesis, *Dev Dyn*, 237(1):170-86

Smith NP, Losty PD, Connell MG, Mayer U, Jesudason EC, 2006, Abnormal lung development precedes oligohydramnios in a transgenic murine model of renal dysgenesis, *J Urol*, 175(2):783-6

Stephens FD, 1955 Urethral obstruction in childhood; the use of urethrography in diagnosis. *Aust NZ J Surg*, 25: 89

Stiber J, Hawkins A, Zhang ZS, Wang S, Burch J, Graham V, Ward CC, Seth M, Finch E, Malouf N, Williams RS, Eu JP, Rosenberg P, 2008, STIM1 signalling controls store-operated calcium entry required for development and contractile function in skeletal muscle, *Nat Cell Biol*, 10(6):688-97

Straub S, Spranger J, 1981, Etiology and pathogenesis of the prune belly syndrome, *Kidney Int.*, 20, pp. 695-699

Sun KH, Chang Y, Reed NI, Sheppard D, 2016, α -Smooth muscle actin is an inconsistent marker of fibroblasts responsible for force-dependent TGF β activation or collagen production across multiple models of organ fibrosis, *Am J Physiol Lung Cell Mol Physiol*, 310(9):L824-36

Tanago EA, 1972, Surgically induced partial urinary obstruction in the fetal lamb. III. Ureteral obstruction. *Invest Urol* 10(1):35-52

Tasian G, Cunha G, Baskin L, 2010, Smooth muscle differentiation and patterning in the urinary bladder, *Differentiation*, 80(2-3):106-17

Thiruchelvam N, Nyirady P, Peebles DM, Fry CH, Cuckow PM, Woolf AS, 2003, Urinary outflow obstruction increases apoptosis and deregulates Bcl-2 and Bax expression in the fetal ovine bladder, *Am J Pathol*, 162(4):1271-82

Tóth G, Jurka J, 1994, Repetitive DNA in and around translocation breakpoints of the Philadelphia chromosome, *Gene*, 140(2):285-8

Trowell OA, 1954, A modified technique for organ culture *in vitro*, *Exp Cell Res*, 6(1):246-8

Truschel ST, Wang E, Ruiz WG, Leung SM, Rojas R, Lavelle J, Zeidel M, Stoffer D, Apodaca G, 2002, Stretch-regulated exocytosis/endocytosis in bladder umbrella cells, *Mol Biol Cell*, 13(3):830-46

Turner AM, Subramaniam R, Thomas DF, Southgate J, 2008, Generation of a functional, differentiated porcine urothelial tissue *in vitro*, *Eur Urol*, 54(6):1423-32

Unbekandt M, Davies JA, 2010, Dissociation of embryonic kidneys followed by reaggregation allows the formation of renal tissues, *Kidney Int*, 77(5):407-16

Utomo AR, Nikitin AY, Lee WH, 1999, Temporal, spatial, and cell type-specific control of Cre-mediated DNA recombination in transgenic mice, *Nat Biotechnol*, 17(11):1091-6

Uvelius B, 1980. Relation between mechanical and morphological characteristics in urinary bladder smooth muscle. *Acta Physiol. Scand. Suppl.* 483, 1–51

Vaes RDW, van den Berk L, Boonen B, van Dijk DPJ, Olde Damink SWM, Rensen SS, 2018, A novel human cell culture model to study visceral smooth muscle phenotypic modulation in health and disease, *Am J Physiol Cell Physiol*, 315(4):C598-C607

Vandekerckhove J, Weber K, 1978, At least six different actins are expressed in a higher mammal: an analysis based on the amino acid sequence of the amino-terminal tryptic peptide, *J Mol Biol*, 126: 783

Vasconcelos MA, Simões E Silva AC, Dias CS, Gomes IR, Carvalho RA, Figueiredo SV, Dumont TR, Oliveira MCL, Pinheiro SV, Mak RH, Oliveira EA, 2018, Posterior urethral valves: comparison of clinical outcomes between postnatal and antenatal cohorts, *J Pediatr Urol*, pii: S1477-5131(18)30429-7

Vasyutin I, Zerihun L, Ivan C, Atala A, 2019, Bladder Organoids and Spheroids: Potential Tools for Normal and Diseased Tissue Modelling, *Anticancer Res*, 39(3):1105-1118

Veber M, Dolivo D, Rolle M, Dominko T, 2018, Pro-myogenic and low-oxygen culture increases expression of contractile smooth muscle markers in human fibroblasts, *J Tissue Eng Regen Med*, 12(3):572-582

Waddington SN, Nivsarkar MS, Mistry AR, Buckley SM, Kemball-Cook G, Mosley KL, Mitrophanous K, Radcliffe P, Holder MV, Brittan M, Georgiadis A, Al-Allaf F, Bigger BW, Gregory LG, Cook HT, Ali RR, Thrasher A, Tuddenham EG, Themis M, Coutelle C, 2004, Permanent phenotypic correction of hemophilia B in immunocompetent mice by prenatal gene therapy, *Blood*, 104(9):2714-21

Wang D, Chang PS, Wang Z, Sutherland L, Richardson JA, Small E, Krieg PA, Olson EN, 2001, Activation of cardiac gene expression by myocardin, a transcriptional cofactor for serum response factor, *Cell*, 105(7):851-62

Wang D, Zhong L, Nahid MA, Gao G, 2014, The potential of adeno-associated viral vectors for gene delivery to muscle tissue, *Expert Opin Drug Deliv*, 11(3):345-364

Wang T, Kendig DM, Chang S, Trappanese DM, Chacko S, Moreland RS, 2012, Bladder smooth muscle organ culture preparation maintains the contractile phenotype, *Am J Physiol Renal Physiol*, 303(9):F1382-97

Weber S, Mir S, Schlingmann KP, Nürnberg G, Becker C, Kara PE, Ozkayin N, Konrad M, Nürnberg P, Schaefer F, 2005, Gene locus ambiguity in posterior urethral valves/prune-belly syndrome, *Pediatr Nephrol*, 20(8):1036-42

Weninger WJ, Maurer-Gesek B, Reissig LF, Prin F, Wilson R, Galli A, Adams DJ, White JK, Mohun TJ, Geyer SH, 2018, Visualising the Cardiovascular System of Embryos of Biomedical Model Organisms with High Resolution Episcopic Microscopy (HREM), *J Cardiovasc Dev Dis*, 5(4):58

Wilhide ME, Feller JD, Li B, Mohamed AZ, Becknell B, Jackson AR, McHugh KM, Ingraham SE, 2016, Renal epithelial miR-205 expression correlates with disease severity in a mouse model of congenital obstructive nephropathy, *Pediatr Res*, 80(4):602-9

Williams JH, Turner WH, Sainsbury GM, Brading AF, 1993, Experimental model of bladder outflow tract obstruction in the guinea-pig, *Br J Urol*, 71(5):543-54

Witt R, MacKenzie TC, Peranteau WH, 2017, Fetal stem cell and gene therapy, *Semin Fetal Neonatal Med*, 22(6):410-414

Woodard JR, 1985, Prune Belly syndrome, *Clinical Pediatric Urology*, p. 805-24

Woolf AS, Thiruchelvam N, 2001, Congenital obstructive uropathy: its origin and contribution to end-stage renal disease in children, *Adv Ren Replace Ther*, 8(3):157-63

Woolf AS, Lopes FM, Ranjzad P, Roberts NA, 2019, Congenital Disorders of the Human Urinary Tract: Recent Insights From Genetic and Molecular Studies, *Front Pediatr*, 7:136

Wu XR, Kong XP, Pellicer A, Kreibich G, Sun TT, 2009, Uroplakins in urothelial biology, function, and disease, *Kidney Int*, 75(11):1153-1165

Yan Z, McCray PB Jr, Engelhardt JF, 2019, Advances in gene therapy for cystic fibrosis lung disease, *Hum Mol Genet*, 28(R1):R88-R94

Yang PJ, Pham J, Choo J, Hu DL, 2014, Duration of urination does not change with body size, *Proc Natl Acad Sci U S A*, 111(33):11932-7

Yen TT, Gill AM, Frigeri LG, Barsh GS, Wolff GL, 1994, Obesity, diabetes, and neoplasia in yellow *A(vy)/-* mice: ectopic expression of the agouti gene, *FASEB J*, 8(8):479-88

Yoshida T, Sinha S, Dandré F, Wamhoff BR, Hoofnagle MH, Kremer BE, Wang DZ, Olson EN, Owens GK, 2003, Myocardin is a key regulator of CArG-dependent transcription of multiple smooth muscle marker genes, *Circ Res*, 2;92(8):856-64

Yoshida T, Singh AK, Bishai WR, McConkey DJ, Bivalacqua TJ, 2018, Organoid culture of bladder cancer cells, *Investig Clin Urol*, 59(3):149-151

Yoshimura N, Chancellor MB, 2003, Neurophysiology of Lower Urinary Tract Function and Dysfunction, *Rev Urol*, 5(8): S3–S10

Yu Z, Liao J, Chen Y, Zou C, Zhang H, Cheng J, Liu D, Li T, Zhang Q, Li J, Yang X, Ye Y, Huang Z, Long X, Yang R, Mo Z, 2019, Single-Cell Transcriptomic Map of the Human and Mouse Bladders, *J Am Soc Nephrol*, 30(11):2159-2176

Yucel S, Liu W, Cordero D, Donjacour A, Cunha G, Baskin LS, 2004, Anatomical studies of the fibroblast growth factor-10 mutant, Sonic Hedge Hog mutant and androgen receptor mutant mouse genital tubercle. *Adv Exp Med Biol* 545:123–148

Yue F, Cheng Y, Breschi A, Vierstra J, Wu W, Ryba T, Sandstrom R, Ma Z, Davis C, Pope BD, Shen Y, Pervouchine DD, Djebali S, Thurman RE, Kaul R, Rynes E, Kirilusha A, Marinov GK, Williams BA, Trout D, Amrhein H, Fisher-Aylor K, Antoshechkin I, DeSalvo G, See LH, Fastuca M, Drenkow J, Zaleski C, Dobin A, Prieto P, Lagarde J, Bussotti G, Tanzer A, Denas O, Li K, Bender MA, Zhang M, Byron R, Groudine MT, McCleary D, Pham L, Ye Z, Kuan S, Edsall L, Wu YC, Rasmussen MD, Bansal MS, Kellis M, Keller CA, Morrissey CS, Mishra T, Jain D, Dogan N, Harris RS, Cayting P, Kawli T, Boyle AP, Euskirchen G, Kundaje A, Lin S, Lin Y, Jansen C, Malladi VS, Cline MS, Erickson DT, Kirkup VM, Learned K, Sloan CA, Rosenbloom KR, Lacerda de Sousa B, Beal K, Pignatelli M, Flicek P, Lian J, Kahveci T, Lee D, Kent WJ, Ramalho Santos M, Herrero J, Notredame C, Johnson A, Vong S, Lee K, Bates D, Neri F, Diegel M, Canfield T, Sabo PJ, Wilken MS, Reh TA, Giste E, Shafer A, Kutayavin T, Haugen E, Dunn D, Reynolds AP,

Neph S, Humbert R, Hansen RS, De Bruijn M, Selleri L, Rudensky A, Josefowicz S, Samstein R, Eichler EE, Orkin SH, Levasseur D, Papayannopoulou T, Chang KH, Skoultchi A, Gosh S, Disteché C, Treuting P, Wang Y, Weiss MJ, Blobel GA, Cao X, Zhong S, Wang T, Good PJ, Lowdon RF, Adams LB, Zhou XQ, Pazin MJ, Feingold EA, Wold B, Taylor J, Mortazavi A, Weissman SM, Stamatoyannopoulos JA, Snyder MP, Guigo R, Gingeras TR, Gilbert DM, Hardison RC, Beer MA, Ren B; Mouse ENCODE Consortium, 2014, A comparative encyclopedia of DNA elements in the mouse genome, *Nature*, 515(7527):355-64

Zeng J, Ekman M, Jiang C, Uvelius B, Swärd K, 2015, Non-uniform changes in membrane receptors in the rat urinary bladder following outlet obstruction, *Eur J Pharmacol*, 762:82-8

Zheng XL, 2014, Myocardin and smooth muscle differentiation, *Arch Biochem Biophys*, 543:48-56

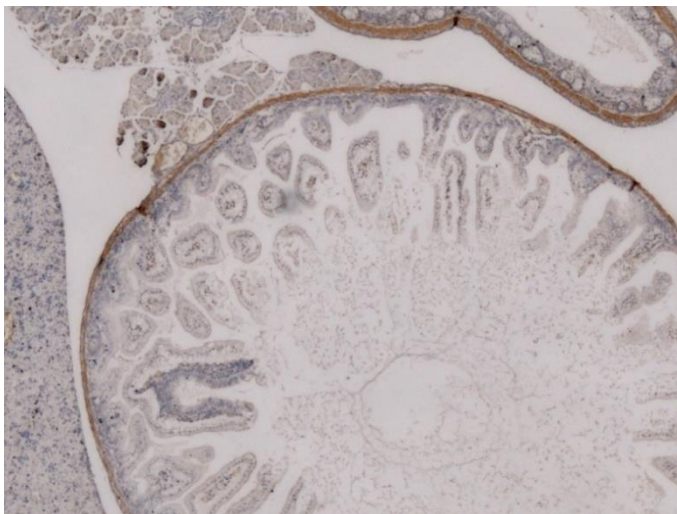
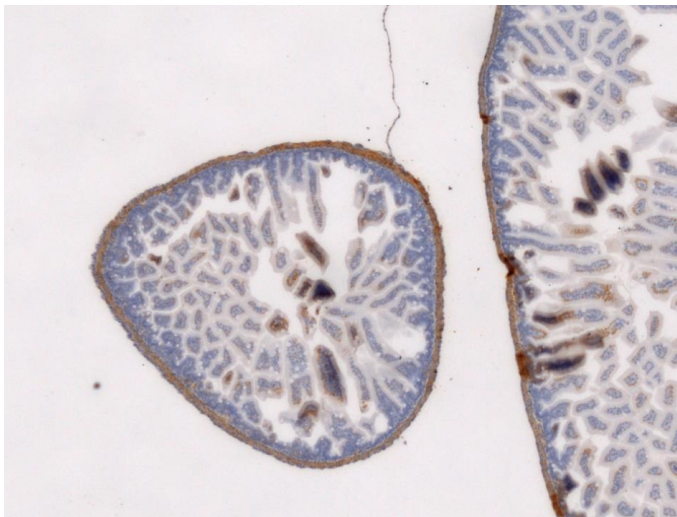
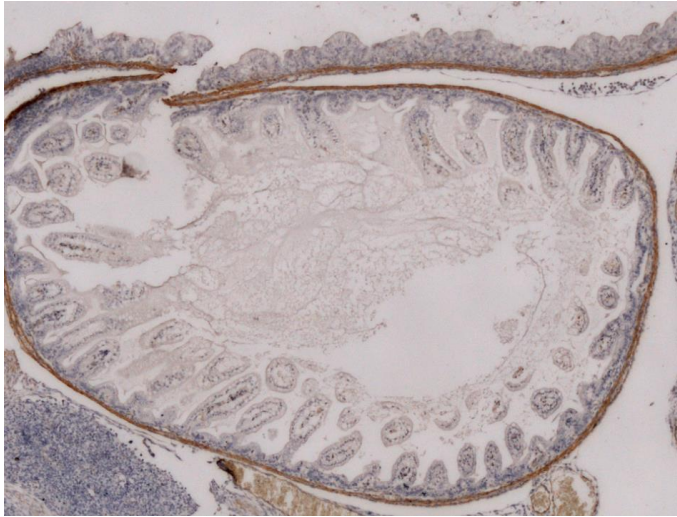
Zhou H, Liu Y, He F, Mo L, Sun TT, Wu XR, 2010, Temporally and spatially controllable gene expression and knockout in mouse urothelium, *Am J Physiol Renal Physiol*, 299(2):F387-95

Zimmerman RA, Tomasek JJ, McRae J, Haaksma CJ, Schwartz RJ, Lin HK, Cowan RL, Jones AN, Kropp BP, 2004, Decreased expression of smooth muscle alpha-actin results in decreased contractile function of the mouse bladder, *J Urol*, 172(4 Pt 2):1667-72

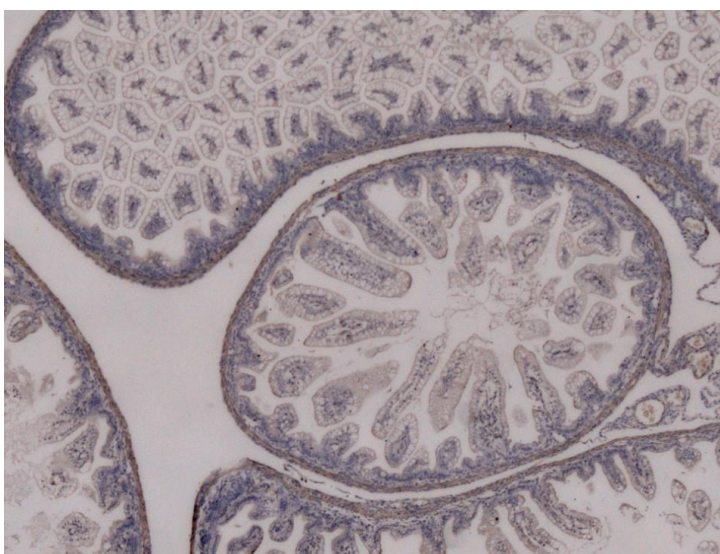
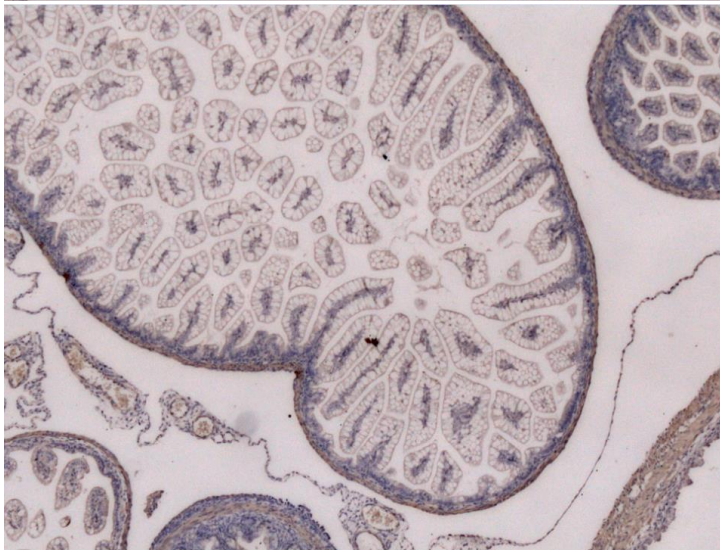
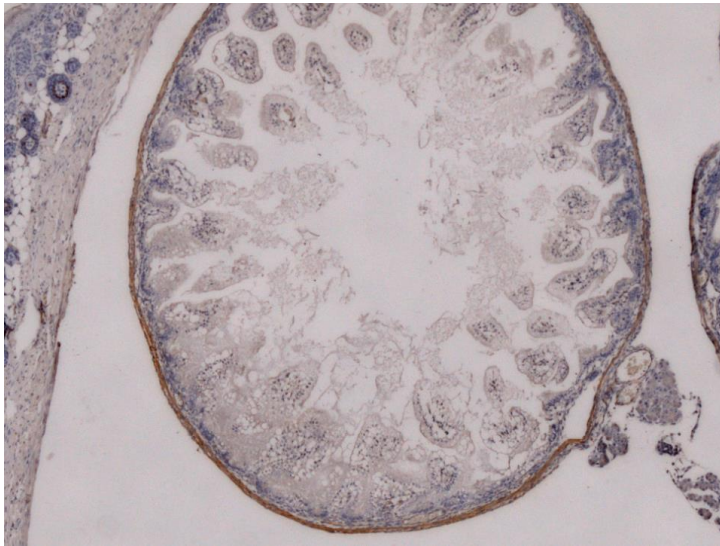
Zylberberg C, Gaskill K, Pasley S, Matosevic S, 2017, Engineering liposomal nanoparticles for targeted gene therapy, *Gene Ther*, 24(8):441-452

Appendix

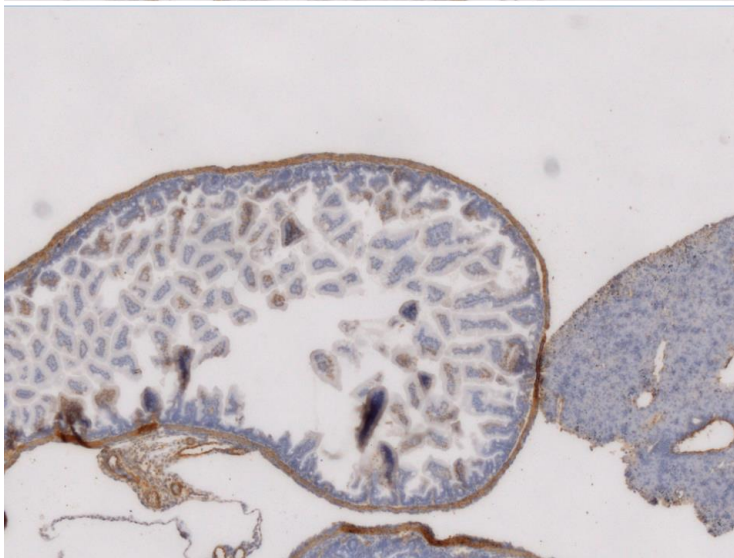
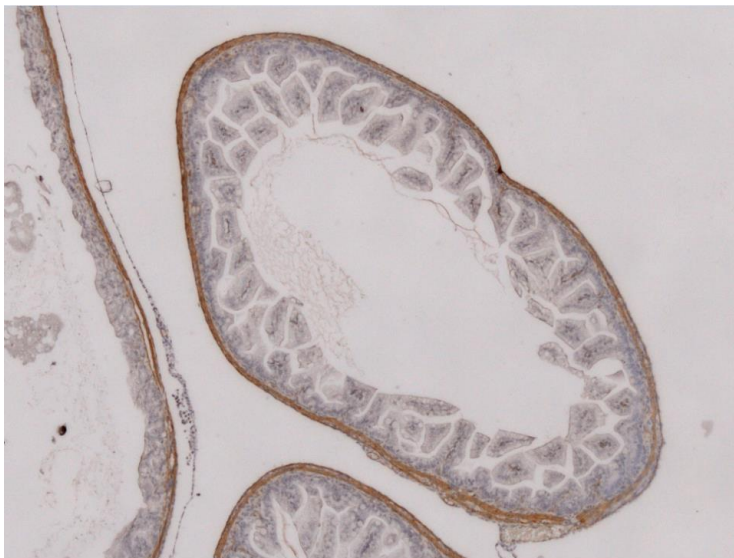
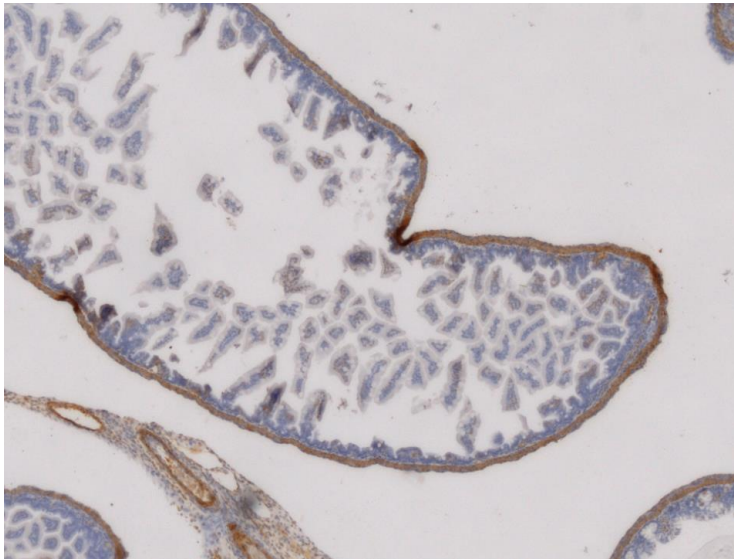
Mouse 1



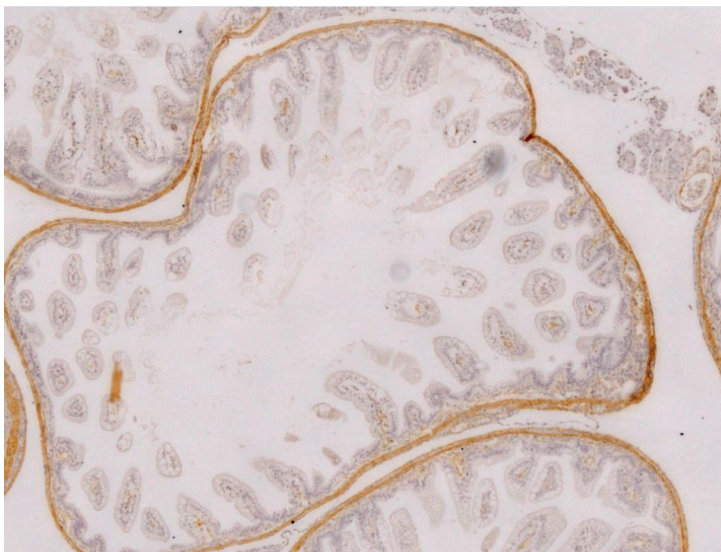
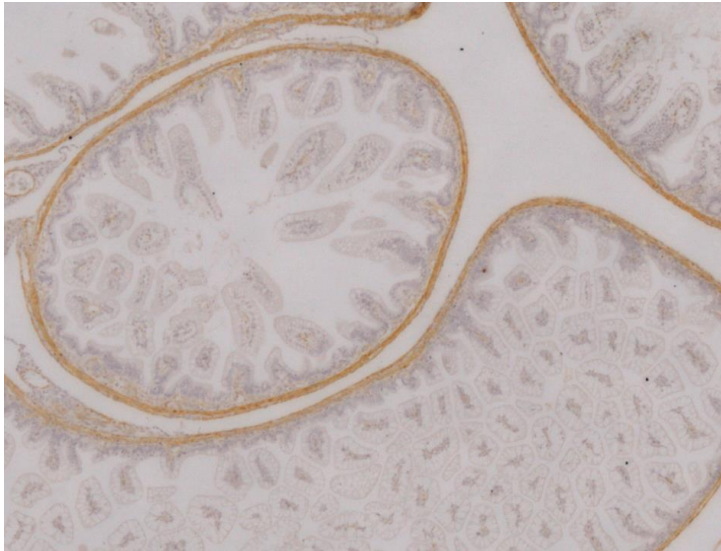
Mouse 2



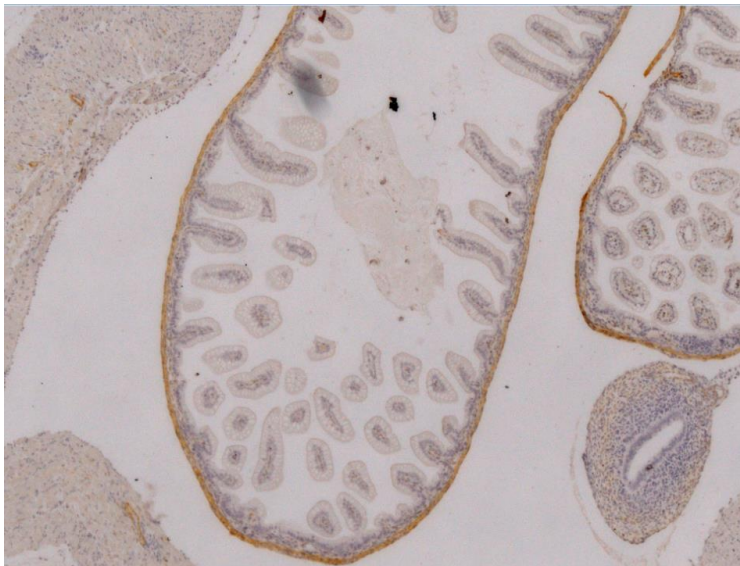
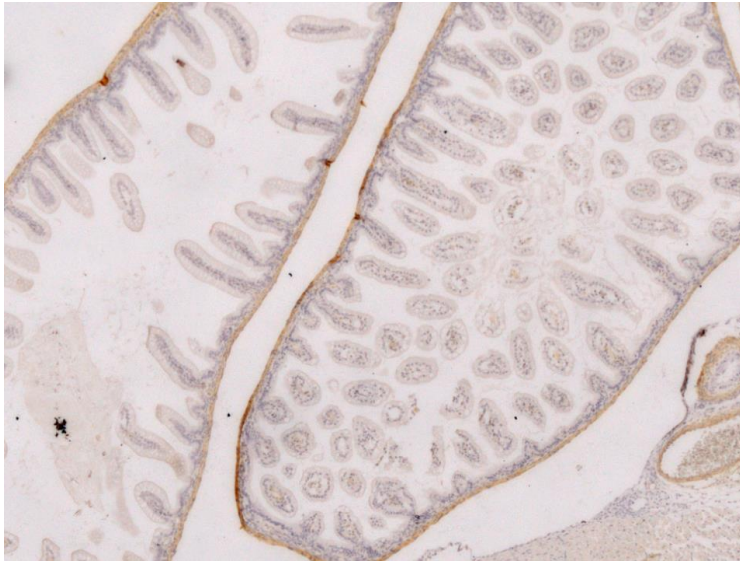
Mouse 3



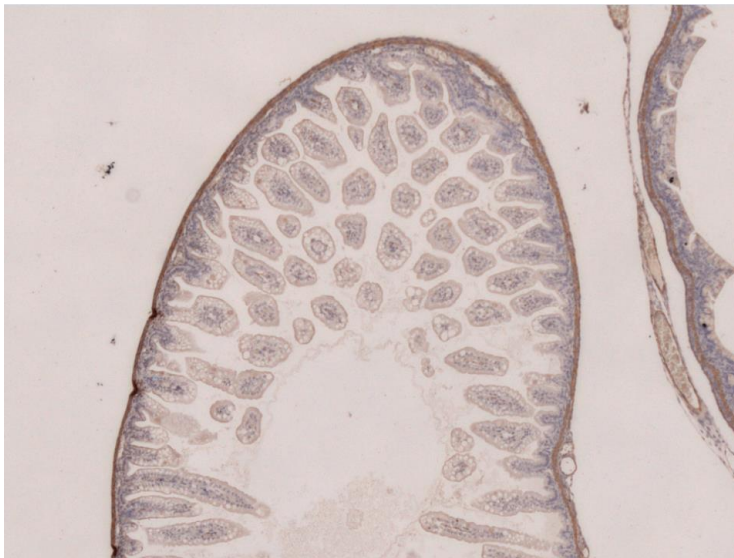
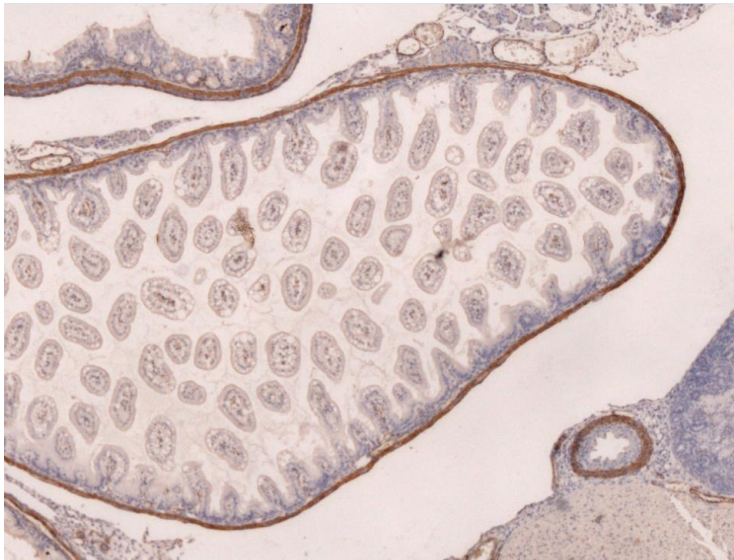
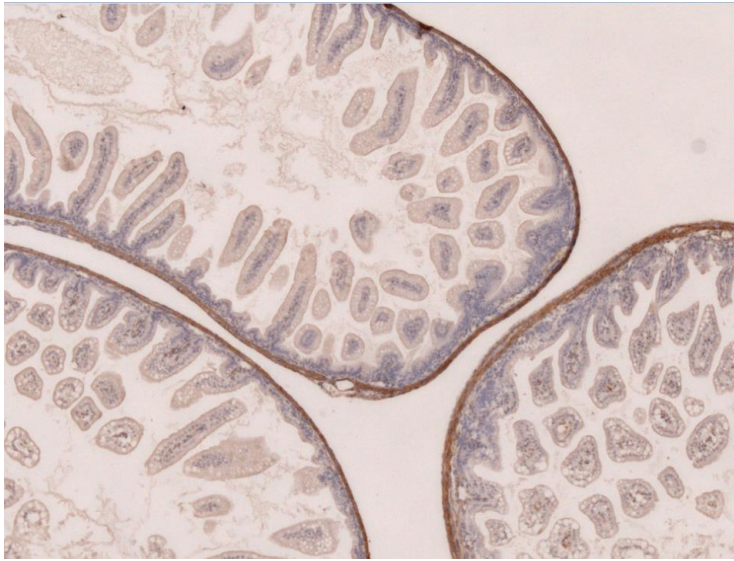
Mouse 4



Mouse 5



Mouse 6



Samples from all six mice show three representative sample images from the gut. Mouse 6 is a WT mouse, all other samples are either T30H or WT.

Looking at the morphology of the gut samples do mice 1 – 5 look different from WT mouse 6? Intensity of staining is variable due to variation in time given for the DAB stain to develop and Dako no longer stocking DAB EnVision. Try to assess slides on morphology alone not staining intensity. Highlight your answer by changing the font colour in the box you select.

Mouse 1

<input type="checkbox"/> The same as WT	<input type="checkbox"/> Not sure	<input type="checkbox"/> Different to WT
---	-----------------------------------	--

Mouse 2

<input type="checkbox"/> The same as WT	<input type="checkbox"/> Not sure	<input type="checkbox"/> Different to WT
---	-----------------------------------	--

Mouse 3

<input type="checkbox"/> The same as WT	<input type="checkbox"/> Not sure	<input type="checkbox"/> Different to WT
---	-----------------------------------	--

Mouse 4

<input type="checkbox"/> The same as WT	<input type="checkbox"/> Not sure	<input type="checkbox"/> Different to WT
---	-----------------------------------	--

Mouse 5

<input type="checkbox"/> The same as WT	<input type="checkbox"/> Not sure	<input type="checkbox"/> Different to WT
---	-----------------------------------	--